STUDIES OF TRANSITION METAL

THIOETHER MACROCYCLIC COMPLEXES

by

Anne Taylor

Doctor of Philosophy

University of Edinburgh

1991

To my Mum and Dad

Philip and Alan

Declaration

Except where specific reference is made to other sources, the work presented in this thesis is the original work of the author. It has not been submitted, in whole or in part, for any other degree. Certain of the results have already been published.

Acknowledgements

I wish to express my gratitude to those who have assisted me throughout the course of this work. I would like to begin by thanking Dr. Martin Schröder for his invaluable guidance and encouragement during the past three years.

I am also very grateful to Dr. A.J. Blake for his help and patience whilst guiding me through the labyrinth of X-ray crystallography.

I am also indebted to Dr. D. Collison for carrying out the e.p.r. spectroscopic simulations and for many informative discussions. I wish to acknowledge Dr. R.V. Parish for collecting and interpreting the Mössbauer spectra presented in this thesis.

I would also like to thank Mr. J.R.A. Millar and Miss H. Grant for recording the n.m.r. spectra, Mr. A.T. Taylor for collecting the mass spectral data and Mrs E. MacDougall for performing the microanalytical measurements.

I am very grateful to Dr. Gill Reid, Andy Atkins, Malcolm Halcrow and the other members of the 'Schröder Group' for their help and humour throughout my time in lab. 94. I also wish to express my appreciation to Mrs G.A. Taylor for typing this thesis.

My thanks must also go to Dr. L.J. Yellowlees and her group for their advice on the kinetics experiments, in particular to Alan Brown for supplying the 'magic anion'- $[Li(B(C_6F_5)_4]$.

Finally, I would like to thank my Mum and Dad and my friends for all their support, tolerance and encouragement during both the good and bad times.

Abstract

Chapter 1 : A general discussion of macrocyclic co-ordination chemistry is given, with particular emphasis on the biological and catalytic relevance of macrocyclic systems. The binding modes of various thioether macrocycles are also summarised.

Chapter 2 : Reproducible high-yield syntheses of $[Au([9]aneS_3)_2](PF_6)$ and $[Au([9]aneS_3)_2](BF_4)_2$ have been established. Electrochemical and spectroscopic studies of these complexes were undertaken. $[Au([9]aneS_3)_2]^{2+}$ undergoes a one-electron oxidation to Au(III) at $E_{1/2}$ = +0.44V and an irreversible reduction to Au(I) at E_{pc} = +0.15V (Fc/Fc^+). The solution e.p.r. spectrum of $[Au([9]aneS_3)_2]^{2+}$ shows an isotropic signal, g_{iso} = 2.016 and hyperfine coupling to ^{197}Au (I = 3/2, 100%), A_{iso} = 44.3G. The frozen glass e.p.r. spectrum depicts a complicated anisotropic signal. Attempted e.p.r. spectrum simulation on the basis of the g and A tensors only suggested that the quadrupole and nuclear Zeeman interactions are significant in $[Au([9]aneS_3)_2]^{2+}$. This is consistent with the ^{197}Au Mössbauer data recorded for Au(II) complex. The stable Au(I) complex, $[Au(PPh_3)([9]aneS_3)](PF_6)$ was also prepared.

Chapter 3 : The ability of $[18]aneS_6$ to stabilise Au(I), Au(II) and Au(III) was examined. $[Au([18]aneS_6)](PF_6)$ was isolated and structurally characterised; $[18]aneS_6$ binds the Au(I) centre in a [2+2] distorted tetrahedral co-ordination, Au - S = 2.321(3), 2.320(4)Å, Au...S = 2.870(4), 2.856(4)Å. This complex exhibits two quasi-reversible oxidations at $E_{1/2}$ = +0.36V, +0.56V (vs Fc/Fc^+). These oxidations were assigned as being largely metal-based

processes by e.p.r. spectroscopy. Electrogenerations of the Au(II) and Au(III) species were monitored by electronic absorption spectroscopy, which demonstrated the absence of any transient intermediates. The electron-transfer rate constant determined for the $[Au([18]aneS_6)]^{+/2+}$ couple ($k_s = 26.8 \times 10^{-3}$ cms^{-1}) indicates that a large stereochemical change accompanies the oxidation of Au(I) to Au(II). Direct synthesis of $[Au([18]aneS_6)](PF_6)_2$ was carried out. The solution e.p.r. spectrum of $[Au([18]aneS_6)](PF_6)_2$ in $MeNO_2$, at 293 K shows an isotropic signal ($g_{iso} = 2.026$, $A_{iso} = 45.6$G); a complicated anisotropic signal is observed at 77 K. The comparable e.p.r. and electronic absorption spectra observed for $[Au([18]aneS_6)]^{2+}$ and $[Au([9]aneS_3)_2]^{2+}$ suggest that the co-ordination spheres about the Au(II) centres are similar; hence, the geometry of $[Au([18]aneS_6)]^{2+}$ was proposed to be distorted octahedral.

Chapter 4 : The Au(I) complex of $[15]aneS_5$ was isolated. $[Au([15]aneS_5)](B(C_6F_5)_4)$ is **dimeric** in the solid-state, the Au(I) centres are in [2+2] distorted tetrahedral stereochemistries (Au - S = 2.3001(13), 2.2927(13)Å, Au...S = 3.2008(14), 3.1055(13)Å) and bound in an exocyclic manner between the two facial macrocycles. A similar structure was found for the PF_6^- salt, although the Au...S interactions are more prenounced at 2.887(6) and 2.992(6)Å. $[Au([15]aneS_5)]^{2+}$ exhibits two solvent dependent quasi-reversible oxidations at $E_{1/2} = +0.36$, +0.54 V (in MeCN vs Fc/Fc^+), which were assigned as largely metal-based processes using e.p.r. spectroscopy. The electron-transfer rate constant, k_s, for the first oxidation was determined ($k_s = 2.7 \times 10^{-3}$ cms^{-1}). Electrogeneration of the Au(II) and Au(III) species were monitored using the O.T.E. technique. $[Au([15]aneS_5)](PF_6)_2$ was synthesised and found to be a 2:1 electrolyte in

$MeNO_2$, $[Au([15]aneS_5)]^{2+}$ is therefore **monomeric** in solution. An isotropic e.p.r. spectrum was observed for $[Au([15]aneS_5)]^{2+}$ in $MeNO_2$ solution ($g_{iso} = 2.014$, $A_{iso} = 43.4G$). A solvent independent rhombic signal was recorded at 77 K ($g_1 = 2.040$, $A_1 = 66.0G$; $g_2 = 2.022$, $A_2 = 60.8G$; $g_3 = 2.009$, $A_3 = 67.0G$); this suggested that the d^9 centre is in an unsymmetrical enviroment and the Au(II) species is not solvent-adduct. The dimeric $[Au([15]aneS_5)]^+$ solid must either immediately dissociate on solvation, or prior to or on oxidation to $[Au([15]aneS_5)]^{2+}$. A solution pre-equilibrium between monomer and dimer was proposed.

Chapter 5 : $[Au([18]aneN_2S_4)](PF_6)$ and $[Au(Me_2[18]aneN_2S_4)](PF_6)$ were isolated. $Me_2[18]aneN_2S_4$ binds Au(I) in a [2+1] co-ordination, (Au - S = 2.3043(15), 2.3138(14)Å, Au...S = 2.8883(15)Å). $[Au(Me_2[18]aneN_2S_4)](PF_6)$ exhibits two quasi-reversible oxidations at $E_{1/2}$ = +0.14, +0.43 V (vs Fc/Fc^+), these are presumed to be largely metal-based processes. $[Au([18]aneN_2S_4)](PF_6)$ undergoes an ireversible oxidation at E_{pa} = +0.88V (vs Fc/Fc^+). It would appear that $Me_2[18]aneN_2S_4$ can stabilise Au(I), Au(II) and Au(III), whereas $[18]aneN_2S_4$ can not stabilise the intermediate oxidation state. The synthesis of a binucleating face - to - face ligand, together with its successful complexation of Pd(II) and Au(I) were carried out.

Chapter 6 : The large cavity sizes and octadentate binding of $[24]aneS_8$ and $[28]aneS_8$ were exploited in the formation of binuclear Cu(I) and Ag(I) complexes. Structural characterisation of $[Cu_2(L)]^{2+}$ (L = $[24]aneS_8$, $[28]aneS_8$) showed that the Cu(I) centres are encapsulated within the macrocyclic framework in distorted tetrahedral stereochemistries. The

separation between the Cu(I) ions is clearly indicative of non-interacting centres (Cu...Cu (L = [24]aneS$_8$) 5.172(3)Å, (L = [28]aneS$_8$) 6.454(3)Å). Both Cu(I) complexes show two-electron irreversible oxidations producing Cu(II) species; these electrogenerations were monitored by electronic absorption spectroscopy. The analogous Ag(I) compounds can be chemically oxidised to generate purple Ag(II) species.

Chapter 7 : Complexation of Au(I) using the tetrathia ligands, [12]aneS$_4$, [14]aneS$_4$ and [16]aneS$_4$ was examined. [Au([16]aneS$_4$)](PF$_6$) undergoes a two-electron oxidation at $E_{1/2}$ = +0.14 V; this oxidation from Au(I) to Au(III) proceeds through a transient intermediate. The progression of the oxidation was monitored by e.p.r. and electronic absorption spectroscopies. [Au$_2$([28]aneS$_8$)](PF$_6$)$_2$ was isolated, the Au(I) centres are in [2+2] distorted tetrahedral stereochemistries within the ring . This compound experiences a four-electron oxidation at $E_{1/2}$ = +0.55 V (vs Fc/Fc$^+$) to afford a binuclear Au(III) species, this process involves an e.p.r. active intermediate similar in behaviour to the Au(II) species observed during the oxidation of [Au([16]aneS$_4$)]$^+$. [Au$_2$([24]aneS$_8$)](PF$_6$)$_2$ was also synthesised.

Chapter 8 : A new oxidation product of [9]aneS$_3$ was isolated. Structural characterisation showed it to be a bicyclic sulphonium salt, [C$_3$H$_{11}$S$_3$]$^+$ incorporating fused four- and five-membered rings. Electrochemical and chemical oxidation of [9]aneS$_3$ produced e.p.r. active species, assigned as thioether-radical cations and dications.

Chapter 9 : The conclusions drawn from the studies of gold thioether macrocyclic complexes are presented.

CONTENTS

List of Figures and Tables

CHAPTER 1

Introduction

1.1 GENERAL MACROCYCLIC CHEMISTRY

The development and diversity of macrocyclic co-ordination chemistry has escalated in the past 25 years.[1,2] This growth has been due mainly to improved synthetic routes of numerous macrocyclic ligands and exploitation of their metal binding properties. Central to this area of co-ordination chemistry is the kinetic inertness and thermodynamic stability of macrocyclic complexes. This enhanced stability of macrocyclic complexes relative to the analogous non-macrocyclic systems was first discussed by Cabbiness and Margerum[3], and was entitled the "macrocyclic effect". The magnitude of the "macrocyclic effect" is dependent on the particular metal-ligand-solvent system being considered.

The "Macrocyclic Effect"

(a) Thermodynamic origins

In general terms, the "macrocyclic effect" refers to the decrease in Gibbs free energy ($\Delta G_f = \Delta H_f - T\Delta S_f$) for the metathesis reaction (1)

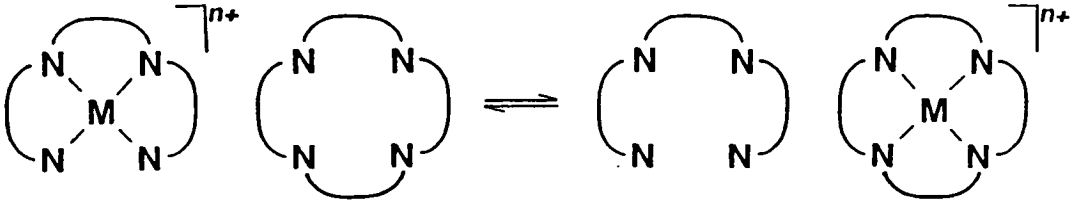

(1)

Considerable attention has been directed toward separating ΔG_f into its enthalpic and entropic components in order to understand the thermodynamic origins of this effect.[4-9]

Consider the entropy of reaction (1). In the metal complexes (i) and (iv) the bound cyclic and non-cyclic ligands have limited flexibility and hence similar entropies. The free macrocycle (ii) has fewer internal degrees of freedom than its open-chain analogue (iii). Therefore the entropic component will usually be favourable for macrocyclic complexation due to the increase in configurational entropy when the open-chain ligand is released into solution

Exact assessment of the enthalpic component is more difficult. The enthalpy of reaction (1) is influenced by the relative solvation energies of the free ligands (i) and (ii). The more compact macrocyclic ligand is generally less solvated than its open-chain counterpart. The overall solvation energies for reaction (1) may produce a favourable or unfavourable enthalpic contribution to the "macrocyclic effect".

(b) Kinetic considerations

Macrocyclic complexes also display an enhanced kinetic inertness, with respect to either their formation or decomposition.[11] This has been well established for various tetraaza[11] and tetrathia[12] systems. The kinetic studies of two Cu(II)-tetraaza complexes have shown that the formation and dissociation rate constants are smaller for the macrocyclic complex, $[Cu([14]aneN_4)]^{2+}$, than the open-chain species, $[Cu(2,3,2\text{-tet})]^{2+}$.[11]

Busch[13] proposed that the rate of dissociation of the ligand from the metal centre was significantly reduced in the macrocyclic complex since the initial M-L bond cleavage would cause unfavourable distortion and strain in the macrocyclic ring. The open-chain ligand, however can be removed from the

metal co-ordination sphere without imposing this distortion by "unzipping" the ligand from one end to the other (2).[13]

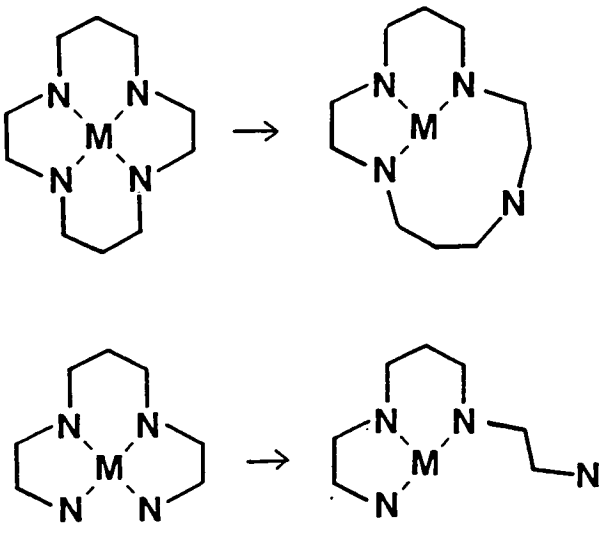

(2)

For any complexation :-

$$M^{n+} + L \underset{k_d}{\overset{k_f}{\rightleftharpoons}} ML^{n+}$$

with the stability constant of the complex being given by:-

$$K_{ML}{}^{n+} = k_f/k_d$$

Therefore, $K_{ML}{}^{n+}$ depends on k_f/k_d.[4] Hence the kinetic inertness is reflected in the enhanced thermodynamic stability.

(c) Ligand pre-organisation

Both the thermodynamic and kinetic properties of macrocyclic complexes can be affected by any ligand re-arrangement required for metal ion complexation.[14] The solid-state structures of [12]aneS$_3$,[15] [12]aneS$_4$,[16] [14]aneS$_4$,[17] [16]aneS$_4$,[82] [15]aneS$_5$[78] and [18]aneS$_6$ [78,18] show that the majority of the S-donors are exodentate, i.e. the S-lone pairs are directed

away from the ligand cavity. Therefore, if the solid-state structure is retained in solution, an energetically unfavourable ligand re-arrangement is required prior to the encapsulation of the metal centre (3).

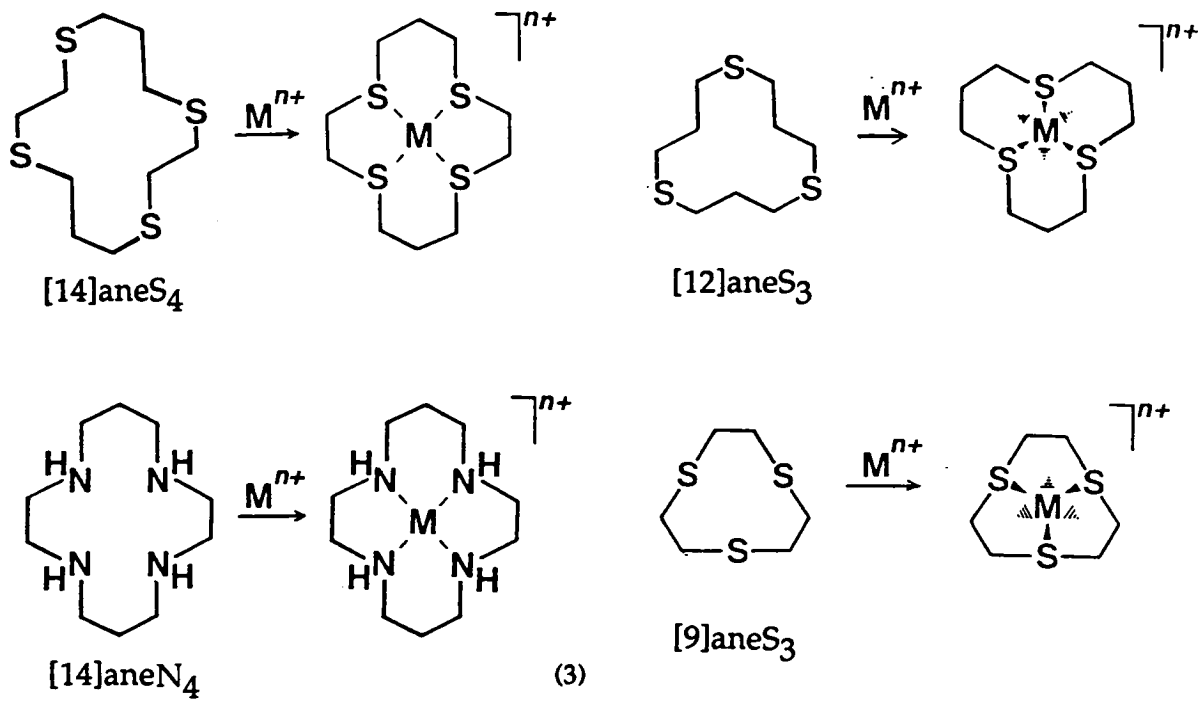

(3)

In contrast, the lone pairs of the donor atoms in [9]aneS$_3$[19] and [14]aneN$_4$[20] are endodentate. Consequently these ligands are considered to be pre-organised for metal complexation; [9]aneS$_3$ in a facial manner and [14]aneN$_4$ in a facial or inclusion manner depending on the metal ion size. This ligand pre-organisation contributes to the enhanced "macrocyclic effect" exhibited by [9]aneS$_3$ and various polyaza ligands,[10] in comparison to the larger polythia systems. [12]

(d) Ligand-metal compatibility

The compatibility of the metal ion with the complexing macrocyclic ligand influences the stability and properties of the resultant complex.[14] This important factor can be exploited to its two extremes.

Compatible ligand-metal systems: When the cavity size and donor set of the macrocycle present a suitable co-ordination sphere for metal ion binding, a stable, rigid complex is formed. The redox and magnetic properties of the metal centre are regulated by the ligand system. Effectively the macrocycle is acting as a protecting group enabling the activation of the metal centre, e.g. $[Ni([14]aneN_4)]^{2+}$. [21b]

Incompatible ligand-metal systems: Creating an inherent mis-match between the metal ion and the ligand cavity size or donor set, can result in a complex which exhibits a strained stereochemistry (e.g. $[Cu([12]aneN_4)]^{2+}$)[22] or unusual redox behaviour (e.g. $[Pd([18]aneN_2S_4)]^{2+}$ [23]).

Utilisation of this compatibilty feature of macrocyclic co-ordination chemistry has been the key to the majority of the work carried out in Edinburgh.[23-27]

1.2 BIOLOGICAL ASPECTS

Regulation of the steroechemical, electronic and redox properties of a metal centre is required in the function of numerous metalloproteins.[28-31] The macrocyclic moiety - the tetrapyrrolic unit is used for Fe, Mg and Co ion control in haemoglobin (4)[32] and cytochromes,[35] chlorophyll (5)[33] and vitamin B_{12} (6)[29,34] respectively. In these systems the macrocyclic unit co-ordinates the four equatorial sites leaving the two axial positions available for binding and activation of small substrate molecules, e.g. O_2 in haemoglobin.[32]

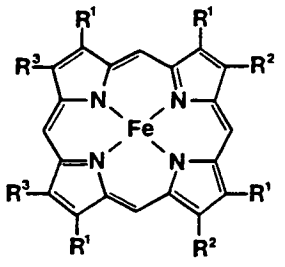

R^1=Me
R^2=CH=CH_2
R^3=$(CH_2)_2CO_2H$

(4) Protoporphyrin IX

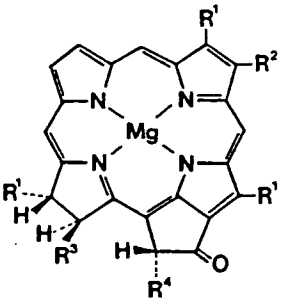

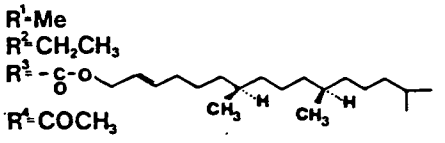

(5) Chlorophyll

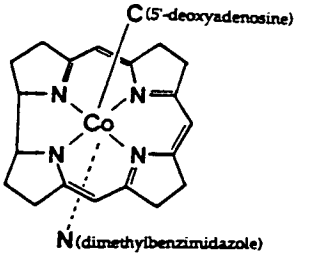

(6) Vitamin B_{12} (core structure)

Elucidation of the exact processes occurring at the active sites of metalloproteins has led to the synthesis of numerous model compounds.[20] The function of these simple models is to mimic the behaviour of the more complicated natural systems, and by virtue of their simplicity be easier to handle and study. These models have been designated as either "speculative" or "corroborative" depending on whether the structure of the active site is known.[36] Synthetic porphyrin and tetraaza macrocyclic complexes have been used to model porphyrinoid species e.g. Fe-porphyrin and "picket-fence" models for haeme protein oxygen carriers.[37] Macrocyclic model compounds have also been used to mimic the behaviour of non-porphyrinoid biological systems, e.g. haemocyanin (7),[35] haemerythin (8).[39]

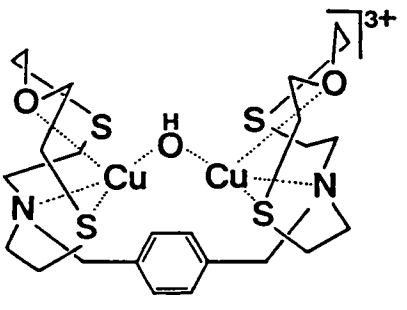

(7)

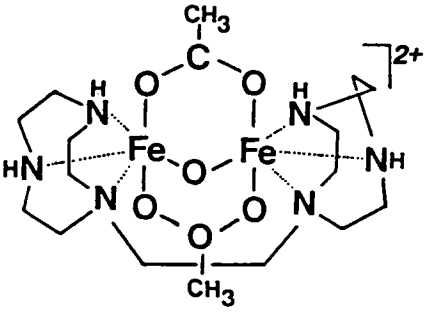

(8)

Using the potentially restrictive stereochemical nature of a macrocyclic ring, it may be possible to create model systems for binuclear metalloproteins such as haemocyanin, tyrosinase (discussed further in Chapter 6) and haemerythin. The modelling of important bio-inorganic systems is a rapidly expanding area.[40-42] The desire for new and more precise models has generated the need for specialised ligands which not only impose a certain co-ordination sphere upon a metal centre, but also regulated its properties specifically. Derivitised macrocycles will continue to be an important source of such ligands.

1.3 CATALYTIC ASPECTS

For a metal complex to have the potential to be catalytically active certain design features are required. Particular co-ordination sites of the metal centre must be protected or blocked whilst additional specific labile positions must remain available for substrate binding. Porphyrins and macrocycles can act as protecting groups to transition metal centres and stabilise a wide range of metal oxidation states in reversible multi-redox processes. Consequently, considerable attention has been focussed on this type of metal complex regarding their ability to activate small molecule substrates such as CO, CO_2, NO, NO_3^-, O_2, N_2, and H_2.[43-54]

The catalytic conversion of O_2 to H_2O is important in fuel cells.[55] Certain metalloproteins are able to mediate electrocatalytic reactions.[56] The four-electron reduction of O_2 to H_2O using a cobalt cofacial porphyrin dimer (9) has been reported.[51]

(9)

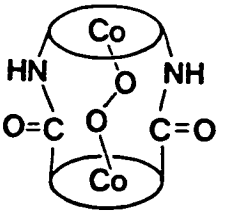

The iridium monomer [Ir(OEP)H] can exhibit a similar catalytic reduction, (Scheme 10).[49] The iridium monomeric unit dimerises and encapsulates the dioxygen molecule to facilitate the reduction without the formation of H_2O_2.

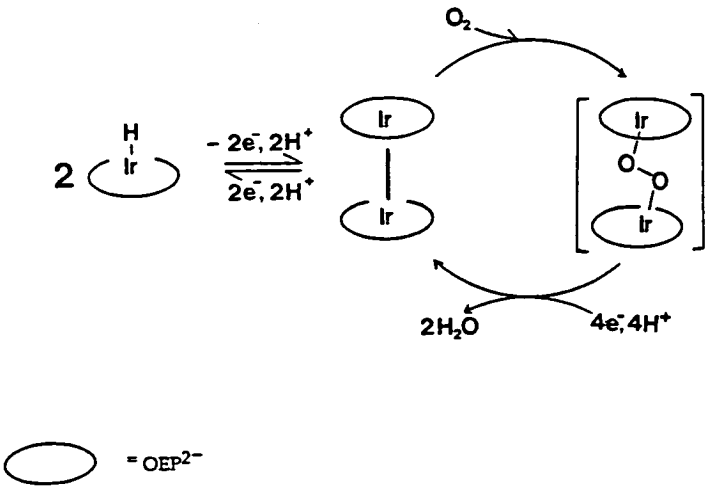

(10)

The ability of cytochrome P_{450} to activate oxygen for the oxidation of hydrocarbons[56] has inspired studies that utilise metalloproteins as potential catalysts for the oxidation of alkanes and alkenes.[57-60] Renewed interest has prompted reports on the use of Fe(III)-porphyrin complexes to facilitate the oxidation of aldehydes,[61] sulphides,[62] sulphur dioxide[63] and alkyl aromatic compounds.[64]

By utilising the macrocycle/porphyrin as a metal protecting group, it is possible to carry out oxidative addition reactions on the low valent, electron rich Rh(I) and Ni(I) centres, e.g. oxidative addition of a alkyl halide on an "out of plane" Rh(I) complex, resulting in the formation of alkyl and acyl species (11).[65]

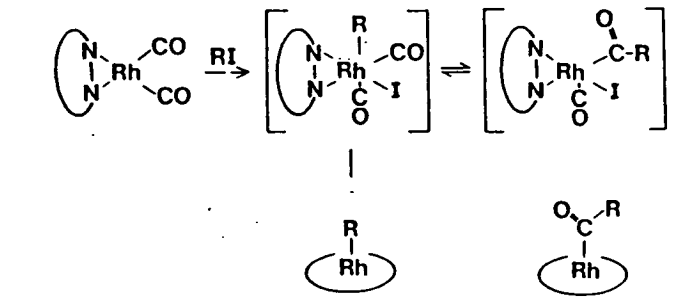

(11)

Rh(I) complexes of L^1 (12) and L^2 (13), and the Ni(I) complex of L^3 (14) can undergo oxidative addition reactions to give $[Rh(L^1)(C_6H_5CO)Cl]^+$, $[Rh(L^2)(C_3H_6Br)I]$ and $[Ni(L^3)CH_3]^+$ species respectively, under particular conditions.[67-69]

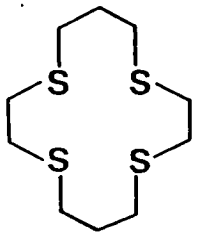

(12)

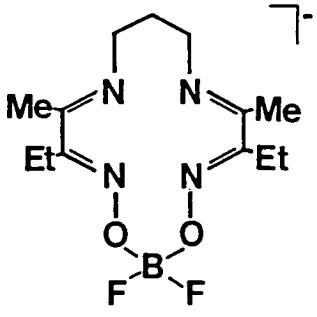

(13)

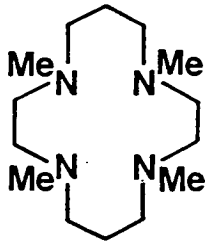

(14)

1.4 THIOETHER MACROCYCLIC LIGANDS

Traditionally acyclic thioethers are considered to be weak ligands for transition metals in comparison to amine and phosphine ligands.[70] However incorporation into a macrocyclic ring enhances the binding of the S-donors. Three factors contribute to this greater stability (i) chelate effect (ii) macrocyclic effect (iii) reduction of the steric repulsions between the thioether alkyl substituents. The nature of the metal-sulphur bonding in thioether complexes is not clear-cut. The two S-lone pairs can be involved in

σ-bonding and π-donating interactions (shown below), however, the empty π-accepting d-orbitals on the S-donor atom must also be considered. Therefore it is feasible that the thioether ligands can be π-donors or π-acceptors (15-16).[70]

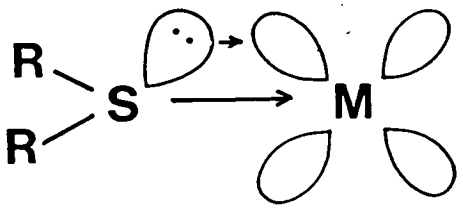

(15) σ-donor / π-donor

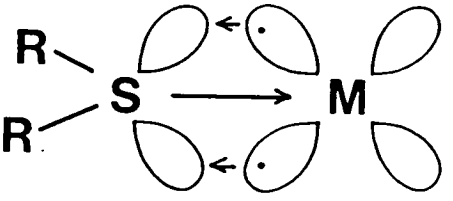

(16) σ - donor / π acceptor

The chemistry of thioether macrocyclic ligands has been reviewed by Murray and Hartley,[70] Kwehn and Isied,[71] Cooper,[72] Schröder,[73] Muller and Dyemann[74] and most comprehensively by Blake and Schröder in 1990.[26] The aim of this section is to present a brief insight into the binding modes of the thioether ligands used in this work.

Ligand synthesis: The progress of metal complexation of the thioether macrocycles was hindered by difficult, low yield ligand syntheses. Until 1980 when Buter and Kellogg reported large scale, high yield routes to the larger polythia ligands.[75,76] Using a combination of methods reported by Ochrymowycz and high dilution Cs_2CO_3 mediated cyclisation techniques, they were able to produce these ligands in good yields.[75-78]

The synthesis of [9]aneS_3 has received much attention; beginning with the first reported synthesis by Ochrymowycz in 1977.[79] The reaction of the dithiolate species (A) with 1,2, dibromoethane (B) under high dilution conditions afforded [9]aneS_3 in low yield, a significant quantity of the [2+2] addition product, [18]aneS_6, was also formed (17).

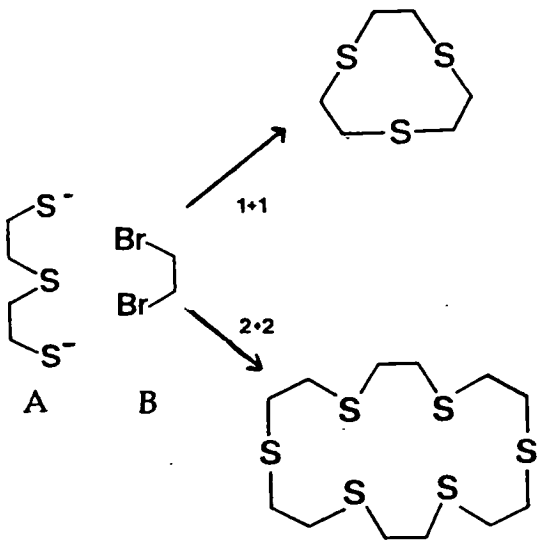

(17)

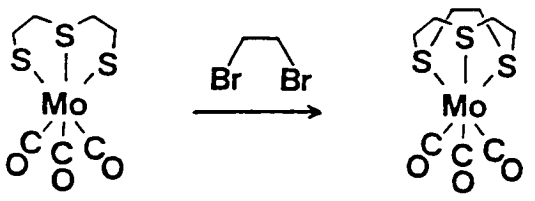

(18)

A template synthetic route (18) was reported in 1984 using a $Mo(CO)_3$ fragment; this gave a high yield of the desired [9]aneS_3.[80] This route requires thiolate co-ordination to the Mo centre, consquently the formation of the [2+2] by-product is inhibited. A high yield synthesis based on the Buter and Kellogg method[75,76] was reported by Blower and Cooper in 1987.[81]

Free ligands: In the solid-state structure, [9]aneS_3 adopts an *endo* conformation, the lone pairs of the S atoms are directed toward the macrocyclic cavity.[19]. As discussed in Section 1.1.c., [9]aneS_3 is pre-organised for facial co-ordination to a metal centre. The larger ring polythia ligands [12]aneS_3,[15] [12]aneS_4,[16] [14]aneS_4,[17] [16]aneS_4,[82] [15]aneS_5[78] and [18]aneS_6.[78,18] adopt conformations in which the lone pairs of the S atoms are directed out of the ring. The formation of *endo* complexes of these polythia ligands therefore requires re-organisation of the ligand from an *exo* to an *endo* conformation.

[9]aneS$_3$: Due to the pre-organisation of [9]aneS$_3$ for facial co-ordination, complexes of [9]aneS$_3$ are generally more stable than their [12]aneS$_3$ analogues.[83] The compact facial binding of [9]aneS$_3$ facilitates octahedral co-ordination of a metal centre, e.g. [Ru([9]aneS$_3$)$_2$]$^{2+}$,[83] [Os([9]aneS$_3$)$_2$]$^{2+}$,[84] [Rh([9]aneS$_3$)$_2$]$^{3+}$,[86,87] [Ni([9]aneS$_3$)$_2$]$^{2+}$.[88] The tighter fit of [9]aneS$_3$ over [12]aneS$_3$ is reflected in the shorter M-S bond lengths in the [9]aneS$_3$ complex e.g. [Ru([n]aneS$_3$)$_2$]$^{3+}$ Ru-S (n = 9) 2.3272(14), 2.3357(14), 2.3331(14)Å [83]; (n = 12) 2.3676(4), 2.3772(4), 2.3736(4)Å.[84,85] When required [9]aneS$_3$ can also bind less symmetrically to satisfy tetragonally elongated (e.g. [Cu([9]aneS$_3$)$_2$]$^{2+}$ [89]) and tetragonally compressed (e.g. [Co([9]aneS$_3$)$_2$]$^{2+}$ [88]) stereochemistries. Although considered to be pre-organised for facial co-ordination the trithia ligand is still sufficiently flexible to alter its co-ordination mode, e.g. [Pt([9]aneS$_3$)$_2$]$^{2+}$ (19),[90] [Ag$_3$([9]aneS$_3$)$_3$]$^{3+}$ (20).[91]

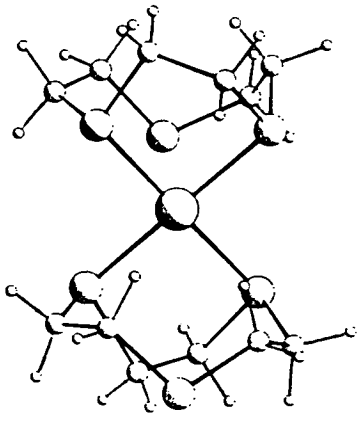

(19) [Pt([9]aneS$_3$)$_2$]$^{2+}$

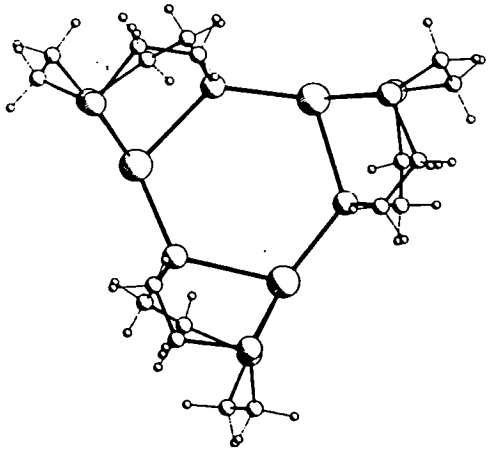

(20) [Ag$_3$([9]aneS$_3$)$_3$]$^{3+}$

This stereochemical and electronic flexibility is reflected in the ability of [9]aneS$_3$ to stabilise a wide range of metal oxidation states, e.g. stabilisation of Rh(I)/(II)/(III),[86,87] Ir(II)/(III),[93-95] Pd(II)/(III) (21-22),[93-91] and Pt(II)/(III)/IV).[90,73]

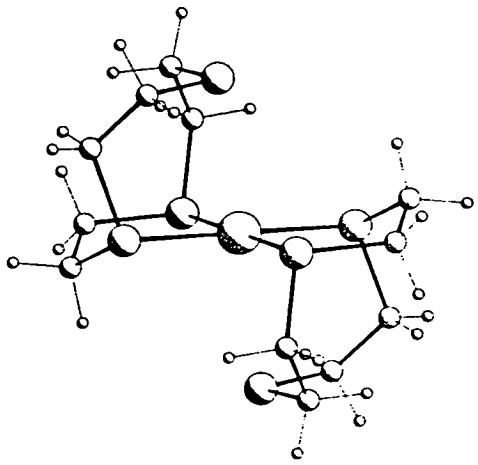

(21) $[Pd([9]aneS_3)_2]^{2+}$

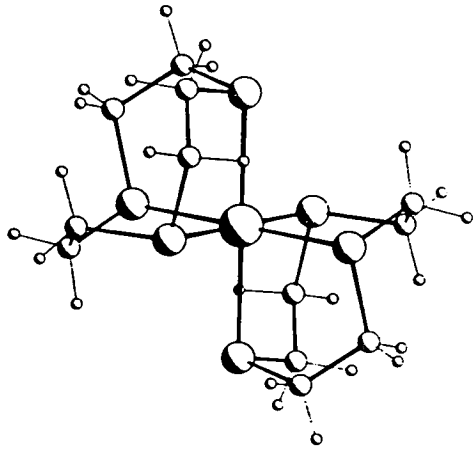

(22) $[Pd([9]aneS_3)_2]^{3+}$

In the structure of $[Pd([9]aneS_3)_2]^{2+}$ (21), the Pd (II) centre is bound in a [4+2] co-ordination, a compromise between the facial binding of [9]$aneS_3$ and the preference for Pd (II) to be square planar.[93,94] The $[Pd([9]aneS_3)_2]^{3+}$ cation shows a tetragonally distorted stereochemistry.[95] On oxidation from Pd(II) to Pd(III) the interaction of the apical S-donors shortens from 2.952(4) to 2.5448(15)Å, consistent with the preferred geometry of d^7 metal ions and the increase in nuclear charge at the metal centre.

The complexes of $[M([9]aneS_3)_2]^{3+}$ (M = Co, Rh, Ir) can undergo pH controlled reactions.[229] Under certain conditions one of the bound [9]$aneS_3$ ligands experiences a ring-opening reaction via C-S bond cleavage to afford a co-ordinated vinyl thioether moiety with a terminal thiolate donor. This deprotonation reaction was studied by n.m.r. spectroscopy. X-ray crystallography confirmed the structure of the deprotonated $[Rh([9]aneS_3)_2]^{3+}$ species, $[Rh([9]aneS_3)(S(CH_2)_2S(CH_2)_2SCH{=}CH_2)]^{2+}$ (22b).[229] Scheme (22c) gives the proposed mechanism for the formation of this species.[26] The first step involves deprotonation at an α-methylene carbon centre. This type of reactivity seems general for other thioether

ligands, since the complexes $[M([9]aneS_3)_2]^{2+}$ (M = Pd, Pt). and $[M([18]aneS_6)]^{n+}$ (M = Co, Rh, n = 3; M = Pd, Pt, n = 2) react similarly.[229]

(22b)

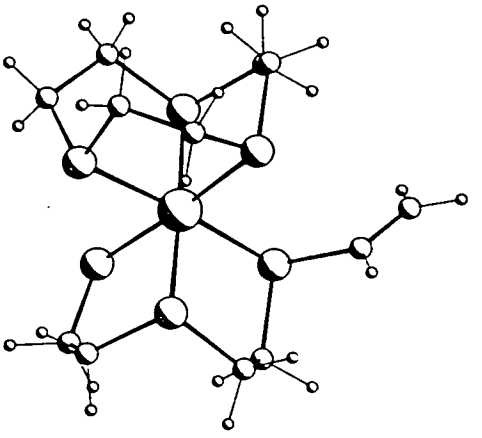

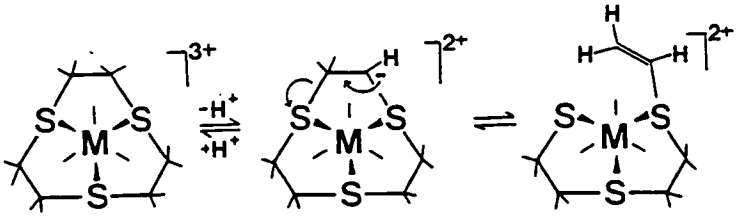

(22c)

A number of half-sandwich $[9]aneS_3$ complexes have been synthesised.[82,96,336] The $[Ni([9]anes_3)(PP)]^{2+}$ (PP = bidentate phosphine) cations are 5 co-ordinate species, with $[9]aneS_3$ bound facially.[82] $[Pd([9]aneS_3)X_2]$ ($X = Cl^-$, Br^-, PPh_3, ½bipy, ½phen) cations show [4+1] co-ordination at the metal centre, with $[9]aneS_3$ bound through two S-donors with the third S-donor involved in long-range apical interaction. [96]

Tetrathia ligands: The compatibility of the ligand cavity size and the metal ion radius is critical in determining the mode of co-ordination of $[12]aneS_4$, $[14]aneS_4$ and $[16]aneS_4$.

In [12]aneS$_4$ the ligand cavity is too small to encapsulate a metal centre, consequently the ligand tends to bind in an exocyclic manner, either in a tridentate (e.g. [Re(CO)$_3$([12]aneS$_4$)]$^+$ (23)[97]) or tetradentate fashion (e.g. cis - [RhCl$_2$(PEt$_2$Ph)([12]aneS$_4$)]$^{2+}$ [98]). This ligand has also been seen to bind in a monodentate mode in [Al(CH$_3$)([12]aneS$_4$)] (24).[99]

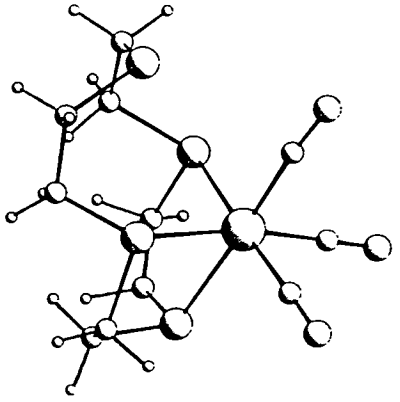

(23) [Re(CO)$_3$([12]aneS$_4$)]$^+$

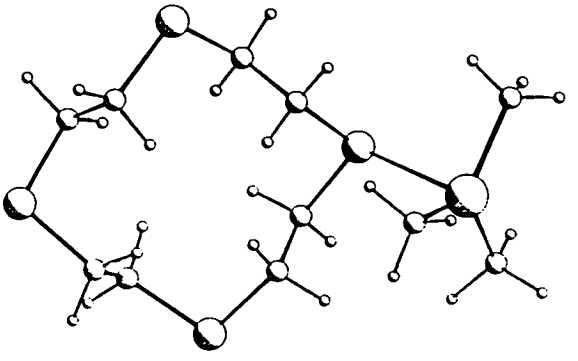

(24) [Al(CH$_3$)$_3$([12]aneS$_4$)]

[14]aneS$_4$ can bind metal centres in either an exocyclic (e.g. *cis*- [RuCl$_2$([14]aneS$_4$)] (25)[100]) or endocyclic way (e.g. [Ni([14]aneS$_4$)]$^{2+}$ (26)[101]), through all four S-donors. [14]aneS$_4$ can also bind in a bidentate mode to one metal centre (e.g. [ReBr(CO)$_3$([14]aneS$_4$)] [97]) or two metal centres (e.g. [NbCl$_5$][[14]aneS$_4$] [102]).

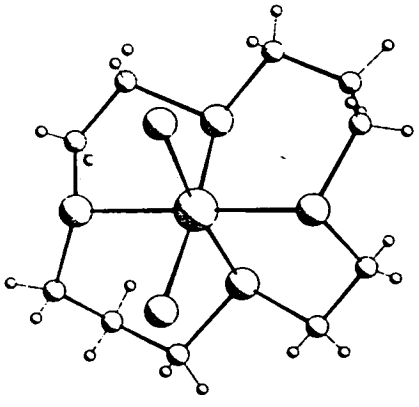

(25) *cis*-[RuCl$_2$([14]aneS$_4$)]

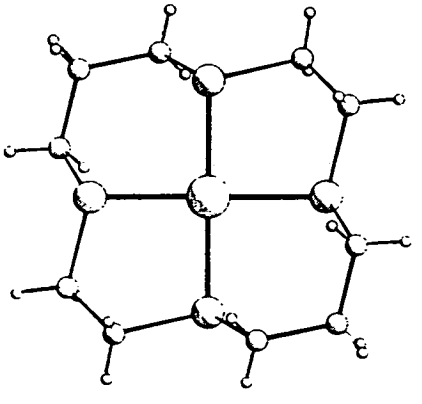

(26) [Ni([14]aneS$_4$)]$^{2+}$

The ligand cavity size of [16]aneS$_4$ is sufficiently large to include a metal centre within the macrocyclic framework (e.g. [Pd([16]aneS$_4$)]$^{2+}$ (27),[24] *trans* - [RhCl$_2$([16]aneS$_4$)]$^+$(28).[103] This ligand does not bind exclusively in this manner; [16]aneS$_4$ binds the Ni(II) ions in an exocyclic fashion in [NiCl$_2$([16]aneS$_4$)$_2$]$^{2+}$.[82]

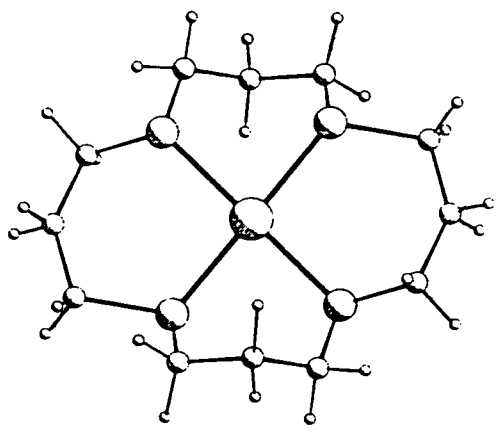

(27) [Pd([16]aneS$_4$)]$^{2+}$

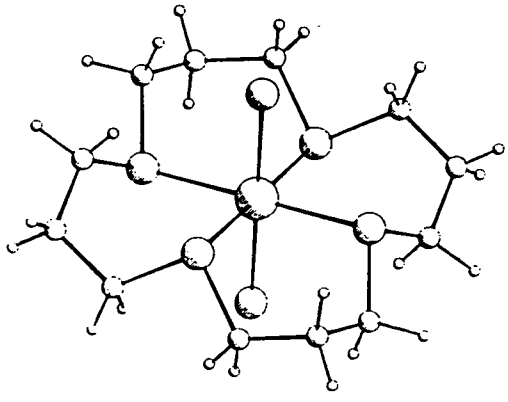

(28) *trans* - [RhCl$_2$([16]aneS$_4$)]$^+$

Pentathia ligands: Relatively few complexes of [15]aneS$_5$ are known. In [Pd([15]aneS$_5$)]$^{2+}$ and [Pt([15]aneS$_5$)]$^{2+}$ the metal ions are 5 co-ordinate.[104,105] The Pd(II) ion has a distorted trigonal bipyramindal stereochemistry unlike the Pt(II) analogue, the stereochemistry of which is closer to square-based pyramindal. [15]aneS$_5$ is known to bind in a bidentate mode in [Re(CO$_3$)Br([15]aneS$_5$)].[97] The pentathia ligand can stabilise the Cu(I) and Cu(II) species.[108-110] (discussed further in Chapter 4). The analogous Ag(I) complex is not isostructural, in fact different cation structures were obtained for various anions.[106,107] Polymeric, dimeric and monomeric structures were determined for the PF_6^-, BPh_4^- and $B(C_6F_5)_4^-$ salts respectively. The Ag(I) ion is [4+1] co-ordinate in the PF_6^- salt (29) and [4+1] co-ordinate in the $B(C_6F_5)_4^-$ salt (31). In the dimeric species, the BPh_4^-

salt, the Ag(I) ions have different geometries, they are [3+1] and [4+1] co-ordinate with an asymmetrically bridging [15]aneS$_5$ ligands (31). These structures are discussed further in Chapter 4. All of these complexes afford Ag(II) species on electrochemical or chemical oxidation.[107] This series of complexes highlights the flexibility of the co-ordination mode of [15]aneS$_5$.

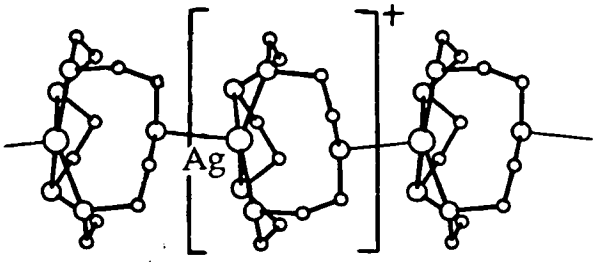

(29) [Ag([15]aneS$_5$)]$^+$ as the (a) (PF_6^-) salt

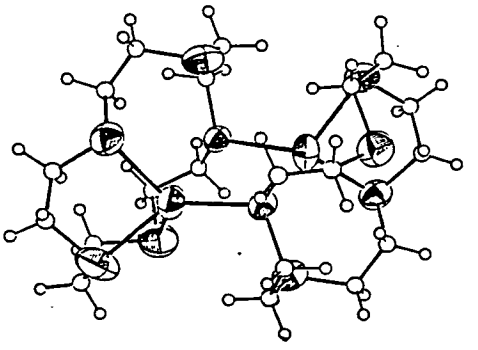

(30) (b) (BPh_4^-) salt

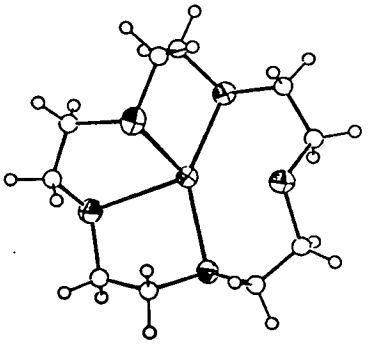

(31) (c) ($B(C_6F_5)_4^-$) salt

Hexathia ligands : The hexadentate ligand [18]aneS$_6$ can bind metal ions in a *meso* configuration, to give symmetrical octahedral stereochemistries e.g. [Ru([18]aneS$_6$)]$^{2+}$ (32)[111], [Ni([18]aneS$_6$)]$^{2+}$ [112,113]. The geometrical flexiblity of [18]aneS$_6$ enables the extension of the axial interaction in tetragonally elongated stereochemistries, e.g. [Pd([18]aneS$_6$)]$^{3+}$ Pd...S$_{ap}$ = 2.5229(24)Å,[119] [Pd([18]aneS$_6$)]$^{2+}$ (as PF_6^- salt) Pd...S$_{ap}$ = 3.0154(25)Å,[115] [Pd([18]aneS$_6$)]$^{2+}$ (as BPh_4^- salt) Pd...S$_{ap}$ = 3.2730(7)Å,[115] [Pt([18]aneS$_6$)]$^{2+}$ Pt...S$_{ap}$ = 3.380(3)Å.[116]

The binding of all six S- donors is not always required. In [Cu([18]aneS$_6$)]$^+$ four S-donors are bound to the Cu(I) centre in a distorted tetrahedral

stereochemistry[117] (discussed in Chapter 3). [18]aneS$_6$ can satisfy restricted electronic and stereochemical demands, enabling the stabilisation of certain ranges of metal oxidation states, e.g. Co(II)/(III),[118,119] Pd(II)/(III),[114,115] Cu(I)/(II)[117] and Ag(I)/(II).[120] Various binuclear [18]aneS$_6$ species are known, e.g. $[Cu_2(NCMe)_2([18]aneS_6)]^{2+}$ [121] and $[Rh_2(C_5Me_5)_2Cl_2([18]aneS_6)]^{2+}$.[122]

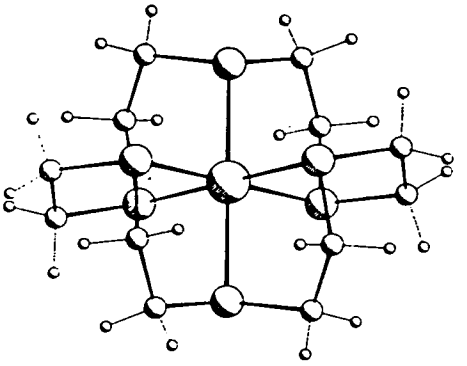

(32) $[Ru([18]aneS_6)]^{2+}$

Octathia ligands: [24]aneS$_8$ and [28]aneS$_8$ are [2+2] by-products from the [12]aneS$_4$ and [14]aneS$_4$ syntheses.[123-125] The donor sets of these ligands can be viewed as two sets of four S-donors within one ligand framework, presenting the possibility of encapsulation of two metal centres. However, the metal complexation of these ligands is limited. Products incorporating Nb(V),[89] Ni(II),[125] Pd(II),[125] Cu(II),[124] Ag(I).[126,127] and Hg(II)[126] have been reported, although no conclusive characterisation is available. Pd(II) and Pt(II) binuclear complexes have been synthesised in Edinburgh.[24] It is likely that the two d^8 metal centres adopt a square planar co-ordination within the macrocyclic cavity; although, this structure has not been confirmed by X-ray crystallography

1.5 OBJECTIVES OF THIS WORK.

The 'soft' cyclic thioether ligands have an affinity for 'soft' transition metal ions.[26] Many of the late second- and third-row metal ions form very stable complexes with a range of thioether crowns.[73] Extending the range of thioether macrocyclic complexes to include gold species is an obvious progression, since gold centres are known to exhibit a preference for S-donating ligands,[128] (Section 2.1.). The objective of the work presented in this thesis was to synthesise and study a range of gold thioether macrocyclic complexes. By exploiting the compatibility of the gold centre with various thioether ligands it may be possible to invoke stable complexes which exhibit facile redox behaviour. Alternatively, by imposing an inherent mis-match between the gold centre and the ligand donor set or cavity, the resultant complex may have a strained stereochemistry or display unusual redox behaviour.

Figure 1.1 : The macrocyclic ligands used in this work

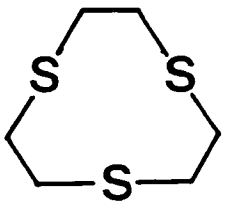

[9]aneS$_3$

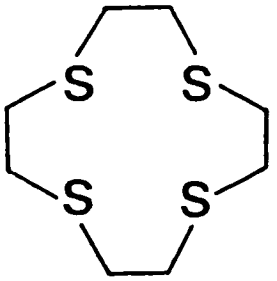

[12]aneS$_4$

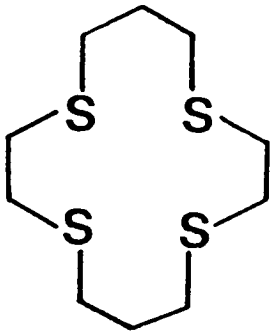

[14]aneS$_4$

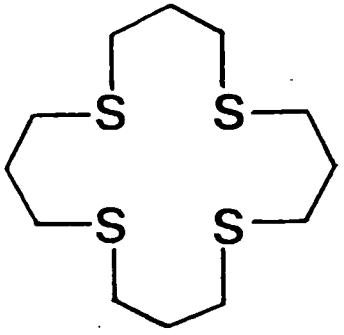

[16]aneS$_4$

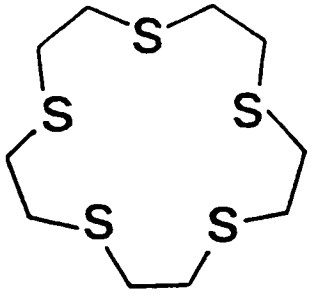

[15]aneS$_5$

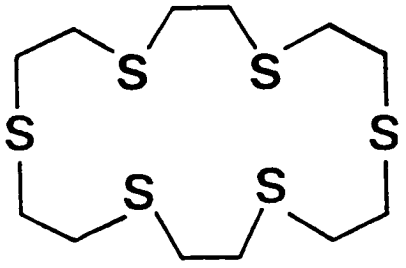

[18]aneS$_6$

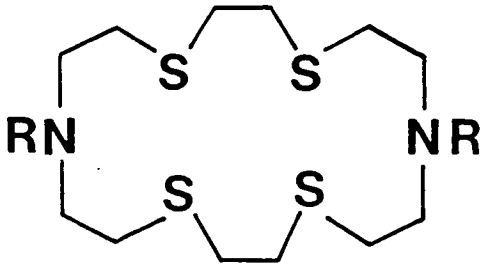

R=H [18]aneN$_2$S$_4$

R=Me Me$_2$[18]aneN$_2$S$_4$

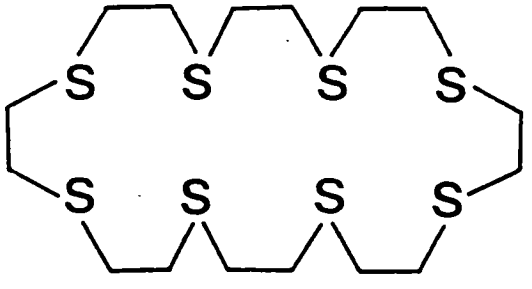

[24]aneS$_8$

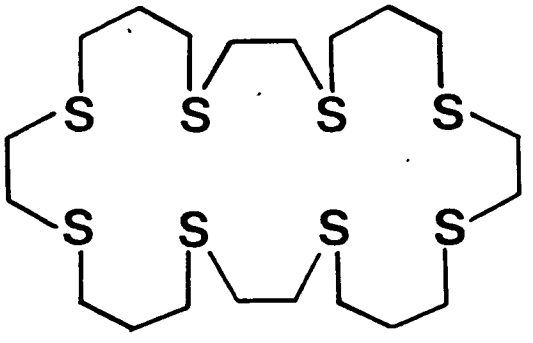

[28]aneS$_8$

CHAPTER 2

Gold complexes of [9]aneS$_3$

2.1 INTRODUCTION

2.1.1 Co-ordination chemistry of gold

Current interests in the co-ordination chemistry of gold are diverse. These areas include bio-inorganic,[133-135] cluster and organometallic chemistries[129-131,136,137] and the study of novel species with unusual metal oxidation states and geometries.[130,132] A summary of the gold chemistry relevant to the work presented in this thesis will be given as an introduction.

The general bonding of gold is influenced by relativistic effects.[138] These effects cause the contraction and stabilisation of the 6s level, with the 6p orbitals being stabilised but to a lesser extent. The 5d orbitals expand radially and are destabilised energetically; also these orbitals undergo spin-orbit splitting.[138] The alteration of the relative energies of the 6s, 6p and 5s levels affects the chemistry of gold in a number of ways:- (i) The contraction of the 6s orbital explains the stronger and shorter covalent bonding, the larger electron affinity and first ionisation energy exhibited by gold in comparison to silver.[138] (ii) The relative stabilisation of the 6s and destabilisation of the 5d levels leads to low 5d-6s separation and making 5d orbitals of suitable energy for bonding. (iii) The low-lying 5d orbitals are helpful in stabilising the higher oxidation states of gold with respect to copper and silver.[138]

The chemistry of gold is dominated by complexes in the oxidation states +1 and +3.[128,129,131]

Bonding in Au(I) complexes: Hybridisation involving the 5d orbitals in Au(I) is considered to be a major cause of the high tendency of Au(I) to form linear complexes.[131] The current explanation for linear bonding in gold is that the closely spaced 6s and $5dz^2$ orbitals mix to give orbitals ψ_1 and ψ_2 (Scheme 2.1). The electron pair then occupies ψ_1, where the lobes are situated in the xy plane. Further hybridisation of ψ_2 and $6p_z$ give two orbitals ψ_3 and ψ_4 with lobes pointing along the z axis, suitable for accepting electrons from two ligands, resulting in linear co-ordination.[139]

Scheme 2.1

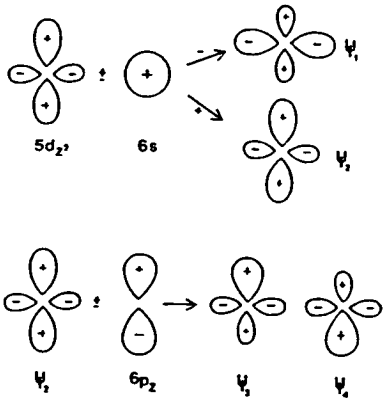

Bonding in Au(III) complexes: For square planar Au(III) complexes valence bond theory predicts that Au(III) will have the $5d^8$ configuration and that σ-bonds will be formed using four $5dx^2\text{-}y^2$ 6s $6p_x$ $6p_y$ hybrid orbitals.[129] Calculations support this prediction.[140-142]

2.1.2 Complexes of Au(I)

Au(I) complexes of the form $[AuX_2]^-$ (X = Cl^-, Br^-, I^-, N_3^-, SCN^-) are all linear species in the solid-state.[129] Complexes of the type [AuX(L)] (X = halide, pseudo-halide, RS, Me; L = PR_3. AsR_3, SbR_3, SR_2) are also linear.

The synthetic route to $[AuX(PR_3)]$ involves the reaction of $[AuCl_4]^-$ with two equivalents of tertiary phosphine. The phosphine acts as both a reducing agent and a ligand. In aprotic solvents the reaction proceeds as shown (1)[143] (R = Ph, Et, Me) :

(1) $HAuCl_4 + 2\,PR_3 \longrightarrow [AuCl(PR_3)] + PR_3Cl_2 + HCl$

Introduction of an anionic bidentate ligand as in $[Au(O_2CMe)PPh_3]^+$ still results in the linear co-ordination at Au(I) being maintained.[144] However, an additional weak interaction to Au(I) from a second donor of a bidentate ligand is possible, e.g. (2)-(3). Au(I) in complexes (2) and (3) can be considered to have [2+1] co-ordination.

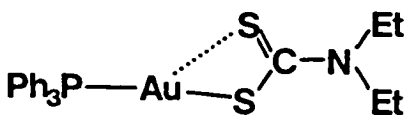

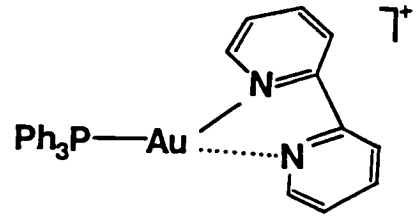

(2) $[(Ph_3P)Au(S_2(NEt_2)]$[145] (3) $[(Ph_3P)Au(bipy)]^+$ [131]

The compounds $[AuX(PR_3)]$ can react with excess PR_3 (R = Ph, Et, Me) to give complexes of the form $[AuX(PR_3)_2]$, $[AuX(PR_3)_3]$ and $[AuX(PR_3)_4]$.[147-150] In $[AuCl(PPh_3)_2]$ and $[AuCl(PPh_3)_3]$ the chloride ion is co-ordinated to give distorted trigonal planar and tetrahedral stereochemistries, respectively.[151-152] When the anion is non co-ordinating (e.g. $[BPh_4^-]$) the complexes $[AuX(PR_3)_3]$ have trigonal planar geometries, (e.g. $[Au(PPh_3)_3][BPh_4]$). The compounds containing four tertiary

phosphines, $[Au(PR_3)_4]^+$, have regular or distorted tetrahedral stereochemistries, e.g. $[Au(PMePh_2)_4](PF_6)$, $[Au(SbPh_3)_4][Au(C_6F_5)_2]$.[153-155]

The complexes [Au(Cl)L] (L = thioether ligand e.g. Me_2S, Et_2S, $(HOCH_2CH_2)_2S$, or tetrahydrothiophene) are useful preparative intermediates because R_2S can be easily displaced by other neutral or anionic groups.[156-158] The complexes $[AuX(SR_2)]$ are prepared by route (4) :

(4) $HAuCl_4 + 2R_2S + H_2O \longrightarrow [AuCl(SR_2)] + R_2SO + 3HCl$

The co-ordinated chloride in $[AuCl(SR_2)]$ can be removed by a halide abstractor in the presence of the thioether ligand to give complexes of the type $[Au(SR_2)_2]X$ ($X = PF_6^-, BF_4^-, ClO_4^-$) (5) :

(5) $[AuCl(SR_2)] + SR_2 + AgPF_6 \longrightarrow [Au(SR_2)_2]PF_6 + AgCl$

The cation $[Au(tht)_2]^+$ (tht = tetrahydrothiophene) is an excellent preparative source of free Au(I) ions, since both the thioether ligands can be easily displaced by a variety of ligands, e.g. PPh_3, $AsPh_3$, $SbPh_3$, bipy, phen, pyridine.[159]

Binuclear Au(I) complexes can be prepared using chelating phosphines and thiolates. Bidentate phosphines can bridge between two Au(I) centres to form "A-frame" compounds of the type shown in (6).[160-162]

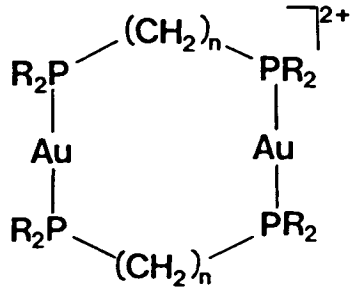

(6) n = 1, 2, 3
R = Me, Et, Ph

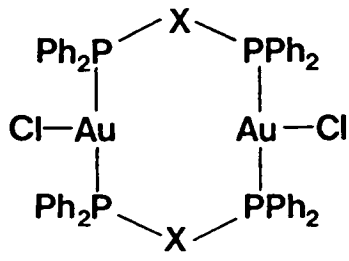

(7a) X = CH_2
(7b) X = NH

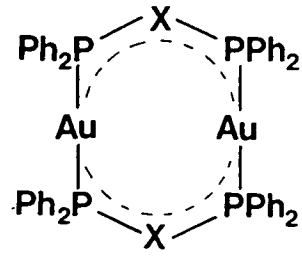

(8a) X = CH
(8b) X = N

Three co-ordinate Au(I) centres can be obtained by co-ordinating Cl^- to the metal centres in particular "A-frame" species (7).[163] Complexes (7a) and (7b) can be deprotonated with strong bases to give bis(diphenylphosphino)-methanide (8a) or -amide (8b) derivatives.[164-165] Bridged thiolate complexes incorporating tertiary phosphine groups have also been synthesised, e.g. (9), (10).[131,166] The oxidative addition reactions of binuclear Au "A-frame" complexes have been studied extensively by Schmidbauer[192] and Fackler.[190-191] (These reactions are discussed further in Section 2.1.4).

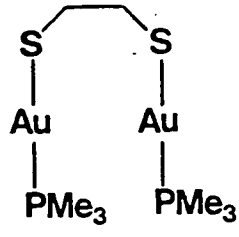

(9)

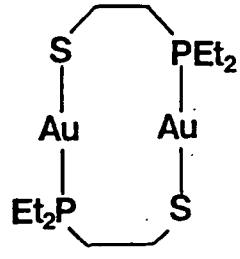

(10)

Complexes of Au(I) with nitrogen donor ligands mainly consist of anionic and neutral heterocyclic ligated species,[128,129,131] e.g. $([Ph_3P)Au(bipy)]^+$ (2), (11), (12).[131]

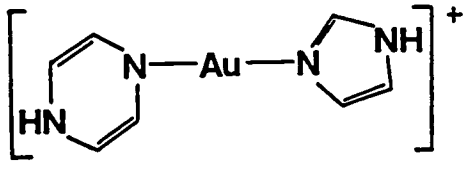

(11)

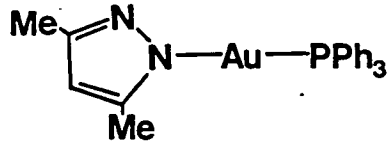

(12)

2.1.3 Complexes of Au(III)

The chemistry of Au(III) complexes is as extensive as that of Au(I).[129] However, whereas Au(I) chemistry is dominated by complexes with 'soft' ligands (e.g. PR_3), Au(III) chemistry is not.[131] As predicted from the higher oxidation state, Au(III) can be considered to be a harder Lewis acid than Au(I), therefore, complexes of Au(III) incorporate both 'soft' and 'hard' ligands. All known Au(III) complexes are diamagnetic and the vast majority are square planar,[129,131] [e.g. (13),[167] (14),[131] (15),[168] (20),[177] (22).[178]]

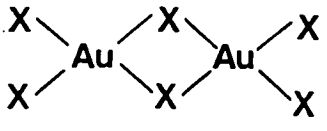

X = Cl^-, Br^-

(13)

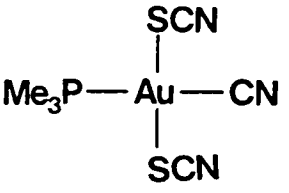

(14)

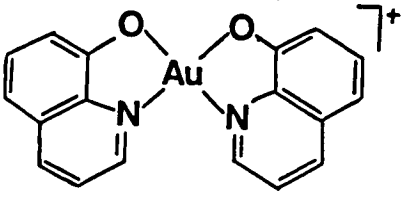

(15)

Five co-ordinate Au(III) species are also known, in complexes (16) and (17) the 2,2' biquinolyl and 2,9-dimethyl-1,1,10-phenanthroline ligands are incapable of forming square planar complexes due to steric effects. The resultant complexes show distorted square-pyramindal stereochemistries.[169-171] However, with more flexible chelate ligands (18-19) the strong affinity of Au(III) for square planar co-ordination dominates.[172-173]

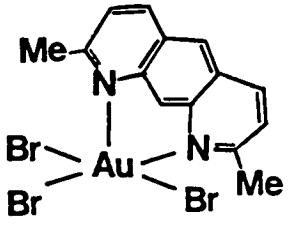

(16)

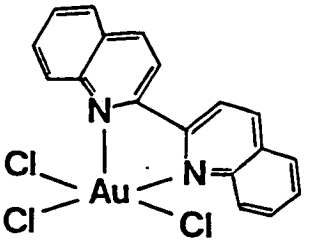

(17)

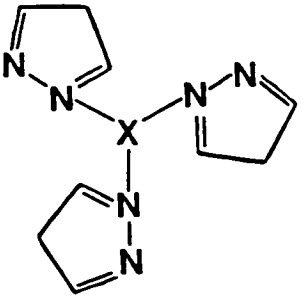

(18) X = BH

(19) X = CH

Many neutral complexes of Au(III) can be obtained as simple adducts of R_3Y (Y = P, As, Sb) with AuX_3 (X = Cl^-, Br^- CN^-, SCN^-),[131] e.g. Et_3PAuCl_3, $Et_3PAu(CN_3)$.[174-175] Similarly numerous thioether complexes of the form $AuX_3(SR_2)$ are known.[131,176] Bidentate thioether ligand compounds have also been synthesised, e.g. (20),[177] (21).[162]

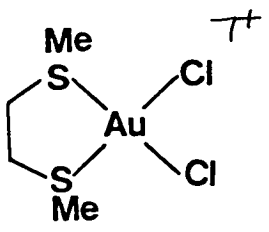

(20)

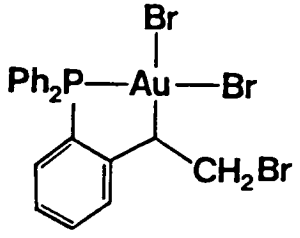

(21)

Au(III) complexes incorporating thioketones, thioamides, thioacids and thiourea are known,[178] e.g. (22), (23).[131]

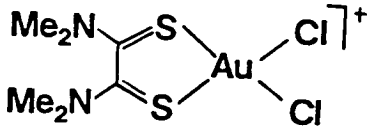

(22)

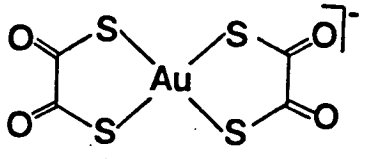

(23)

Dithiolate and dithiocarbamate complexes of Au(III) are very stable and have been studied extensively.[131] The most common are the bis-ligand species e.g. (24),[179] (25),[180] although complexes incorporating only one dithiolate ligand have also been prepared, e.g. (26).[181]

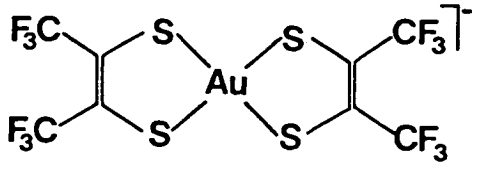

(24)

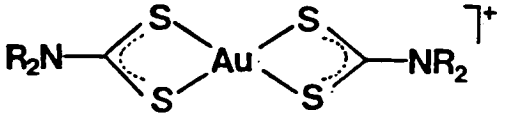

(25)

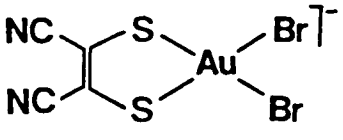

(26)

Au(III) complexes incorporating nitrogen donor ligands include the cationic complexes $[Au(NH_3)_4]^{3+}$, [182] $[Au(py)_2Cl_2]^+$ [183] and $[Au(dien)Cl]^{2+}$. [184] In the solid-state $[AuCl_2(en)_2]^{2+}$ has a distorted octahedral stereochemistry, which is rare for Au(III) complexes.[129]

Macrocyclic complexes of Au(III) are limited to phthalocyanine and tetraaza ligated species e.g. (27),[185] (28),[186] (29),[187a] (30).[187b] Compounds containing gold in a higher oxidation state (e.g. Au(V)) are restricted to the gold-containing fluoranions (e.g. AuF_6^-) and gold pentafluoride (AuF_5).[130]

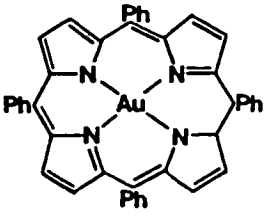

(27)

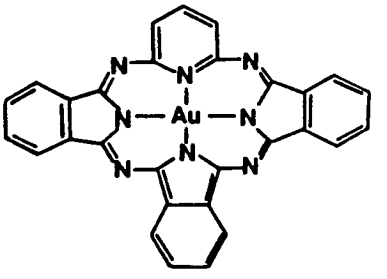

(28)

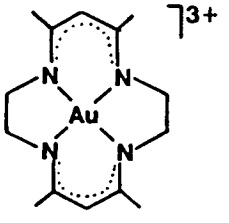

(29)

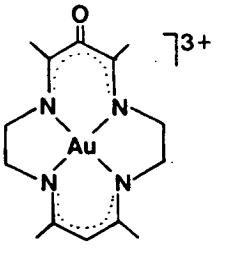

(30)

2.1.4 Complexes of Au(II)

As mentioned earlier, the chemistry of gold is dominated by the +1 and +3 oxidation states. The chemistry of the intermediate oxidation state Au(II) is very limited.[129-131] Ionisation energies show that it is more difficult to obtain Au(II) than either Cu(II) or Ag(II), but easier to obtain Au(III) than Cu(III) or Ag(III). Hence genuine Au(II) complexes are rare because Au(II)

displays a strong tendency for disproportionation to give Au(I) and Au(III) species. Mononuclear Au(II) complexes should be paramagnetic and identifiable by e.p.r. spectroscopy: however, many compounds which, from their empirical formulae appear to be Au(II) species are not paramagnetic.[129,130] Some of these complexes are in fact mixed oxidation state Au(I)-Au(III) compounds, e.g. Au_4Cl_8 (31).[189]

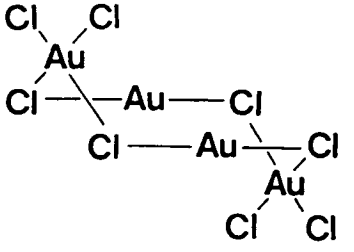

(31)

Many binuclear Au(II) "A-frame" complexes contain Au-Au bonds and consequently are diamagnetic.[129,130,190-196] These species are obtained by oxidative addition reactions of binuclear Au(I) phosphine ylide complexes (e.g. Scheme 2.2).[190-196]

Scheme 2.2

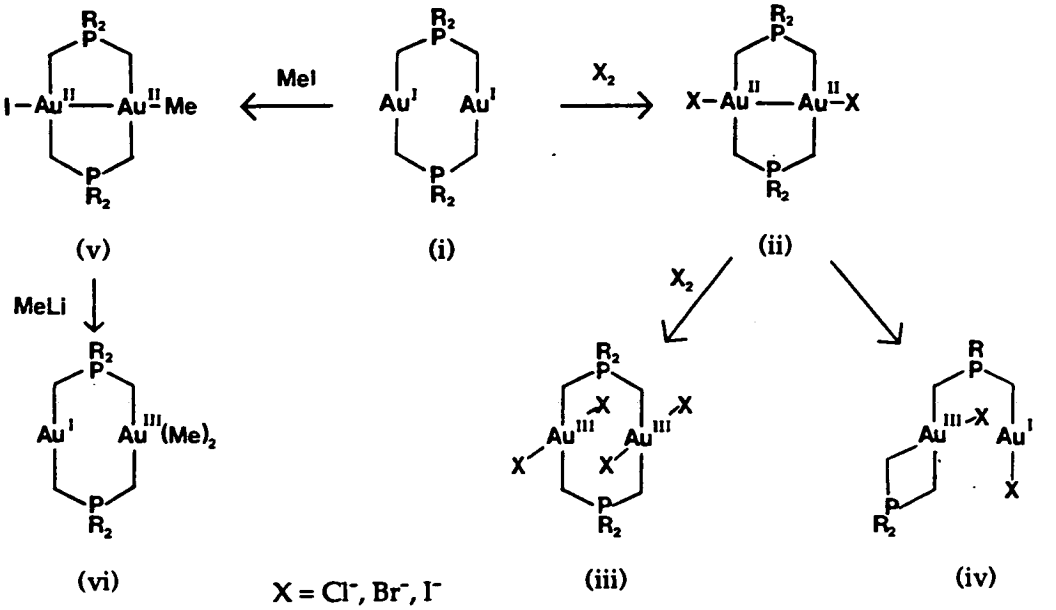

(v) (i) (ii) (vi) (iii) (iv)

These Au(II)-Au(II) species, (e.g. (ii) and (v)) have limited stability. In some cases the oxidative-addition reactions are reversible (e.g. (ii) back to (i)), and in other examples the Au(II)-Au(II) pair undergoes ligand migration to give a Au(I)-Au(III) unit, [190] (e.g. (ii) to (iv)). Also the oxidative addition to give Au(II)-Au(II) complexes can rapidly proceed further to give a Au(III)-Au(III) species,[192] (e.g. (i) to (ii) to (iii)). Some further examples in which binuclear Au(I) complexes can be oxidised to give Au(II)-Au(II) species are given in (32) and (33).[197,180]

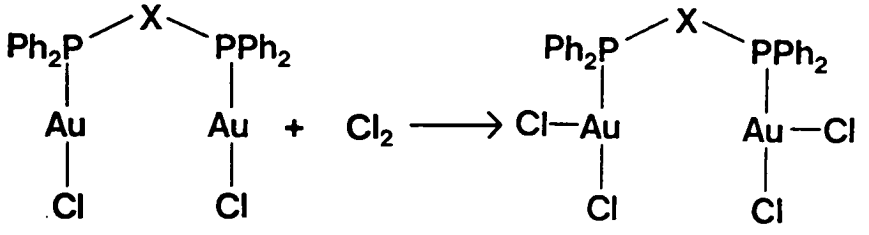

(32)

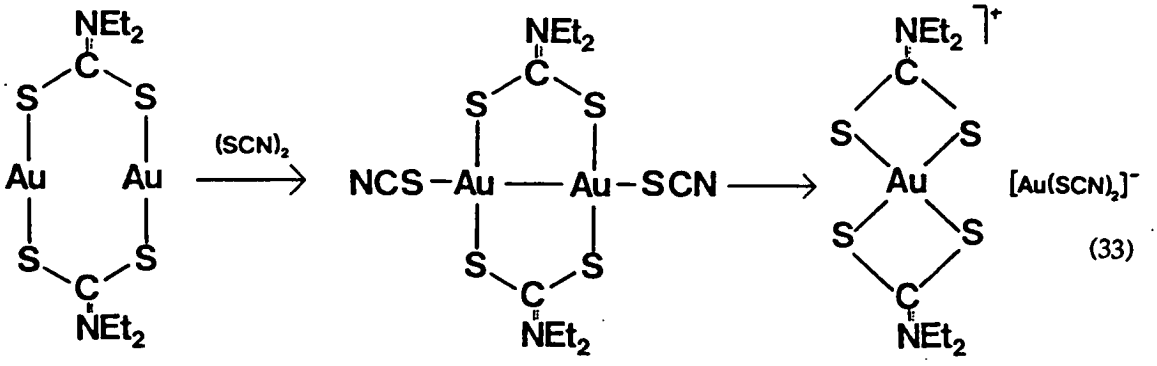

(33)

In reaction (33) the binuclear Au(I) species is oxidised to give the binuclear Au(II) species, which disproportionates to form a mixed-valence salt.[180] Further experiments on this system produced a mononuclear paramagnetic intermediate.[198] This result led to subsequent attempts to isolate genuine mononuclear Au(II) species.[130] A similar reaction to (29) using the

n-Bu_2NCS_2 ligand was studied.[199] The presence of a paramagnetic species was confirmed by e.p.r. spectroscopy.

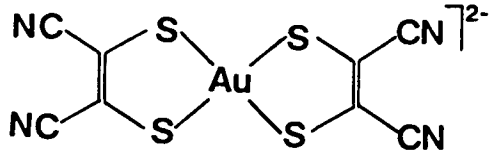

(34)

Water and Gray prepared the mononuclear, paramagnetic Au(II) species (34), by the borohydride reduction of the corresponding Au(III) complex.[200] This complex is stable in the solid state in the presence of air for short periods but in solution it is easily oxidised. This square planar complex (34) can be prepared by an alternative route (35)[210]

(35) $[Au(mnt)_2]^{3-} + [Au(mnt)_2]^{-} \longrightarrow 2[Au(mnt)_2]^{2-}$

Detailed single crystal e.p.r. spectroscopic studies on $[Au(mnt)_2]^{2-}$ diluted in $[n\text{-}Bu_4N]_2[Ni(mnt)_2]$ showed that the unpaired electron is significantly delocalised over the mnt^{2-} ligand, i.e. the electron is in a largely ligand-based molecular orbital.[202-204] In fact the paramagnetic gold dithiocarbamate and 1,2-dithiolate complexes are best described as Au(III) complexes incorporating a radical-anion ligand.[130]

There are two other reported examples of mononuclear Au(II) complexes. The first example of a paramagnetic gold (II) species was reported in 1965 by MacCragh and Koski.[205] They isolated a Au(II) phthalocyanine complex which was found to be e.p.r. active. In 1968 Warren and Hawthorne reported a Au(II) carborane species $(Et_4N)[Au(B_9C_2H_{11})_2]$.[206] This blue-green solid

was found to have a magnetic moment μ_{eff} = 1.79BM, consistent with a Au(II) complex; however, e.p.r. spectroscopic data was not reported.

Koley and co-workers have synthesised and characterised the dimeric Au(II) complexes (36) and(37).[207] These complexes are paramagnetic, the solution e.p.r. spectra showing a seven-line isotropic signal, assigned to two interacting Au(II) centres. However, the hyperfine coupling to the ^{197}Au nuclei is very small (A_{iso} = 4.25G) suggesting very low metal character for the molecular orbital occupied by the unpaired electrons, i.e. the unpaired electron is probably delocalised over the ligand π-system.

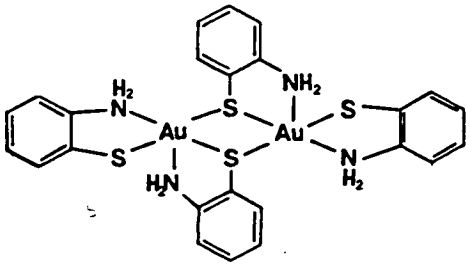

(36)

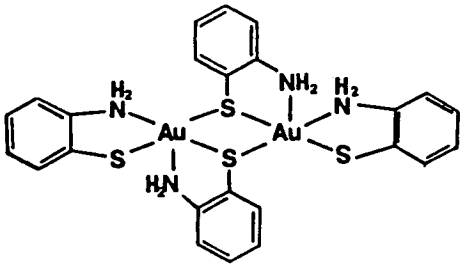

(37)

2.1.5 Cluster and organometallic gold chemistry

Gold cluster and organogold chemistries are growing areas, and have been reviewed extensively. [131,139,208] The work on gold cluster complexes centres mainly on the reduction of [Au(X)PR_3] compounds.[128] In one example, B_2H_6 was used to reduce [Au(Cl)PPh_3] resulting in the formation of $Au_{55}(PPh_3)_{12}Cl_6$ [209]; smaller clusters of Au_n (n = 4, 5, 6, 8, 9, 11, 13) are also known. Mixed metal clusters are numerous and many exploit the assumption that the AuL unit is approximately isolobal with the H atom.[131]

Alkyl derivatives of both Au(I) and Au(III) are known in organogold chemistry, but will not be discussed.[137,210]

2.1.6 Applications of gold chemistry

Au(I) thiolates have important applications in the deposition of gold films and in the treatment of rheumatoid arthritis.[129] They exist as linear and cyclic oligomeric or polymeric species.[211] The polymeric Au(I) thiolates may be insoluble solids or liquids. These latter "liquid golds" may be painted onto ceramics and then pyrolyzed to give decorative gold films.

Chemotherapeutic applications of gold compounds have been studied.[133-135] Au(I) compounds such as (38)-(40) are administered intramuscularly and are effective drugs for the treatment of rheumatoid arthritis, although toxic side-effects are a significant problem.[134] The tertiary phosphine complex (40) has various advantages over (38) and (39), (i) it is administered orally, (ii) it has enhanced lipid solubility which facilitates its absorption and distribution of gold throughout the body, (iii) there are reduced harmful effects, especially for the kidneys, due to its different solubility.[135] The effectiveness of this complex (40) has lead to a new generation of gold phosphine anti-arthritic compounds.

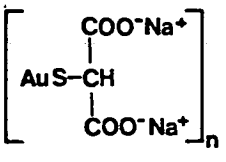

(38) Myocrisin

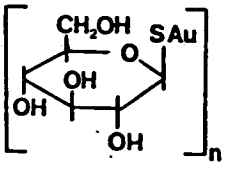

(39) Solganol

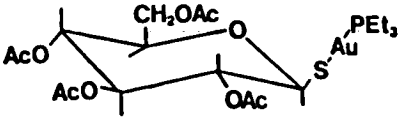

(40) Auranofin

Although the mechanism of the action of gold drugs is still unclear, it is believed that the interaction of Au(I) centres with thiol groups of proteins and enzymes is of key significance.[133] The general toxicity of gold may in part be due to reactions with cysteine disulphide groups in proteins.[135]

The binding of gold species to DNA has shown that Au(I) and Au(III) complexes can produce inter-strand crosslinks and single-strand breaks which are potential anti-cancer properties.[212-214] Also (2-hydroethylpyridine)-trichloro-gold is known to inhibit DNA replication.[215]. Auranofin (40) is extremely cytotoxic to tumour cells in cell culture experiments, which evokes the possibility of its use as an anti-cancer agent.[216] Some Au(I) thiolate complexes (e.g. Au(I)-thioglucose) have been found to be effective inhibitors of human immunodeficiency virus (HIV) reverse transcriptase.[135] Therefore complexes related to gold thioglucose may be beneficial anti-viral agents, if mobilisation of the active species into the cells can be achieved.

2.1.7 Aims of this work

The gold-sulphur interaction dominates the biological applications of gold chemistry.[133-135] The specific nature of this interaction and the reactions of the redox-active gold centres still remain unclear. Hence, the synthesis of gold-sulphur based complexes with the potential to exhibit facile redox behaviour was pursued.

Previous studies have demonstrated that the macrocycle [9]aneS$_3$ can impose a specific co-ordination sphere about a second- or third row transition metal centre,[73] producing unusual stereochemistries and the stabilisation of rare oxidation states, e.g. [Pd([9]aneS$_3$)$_2$]$^{n+}$ (n = 2,3,4),[93-95] [Rh([9]aneS$_3$)$_2$]$^{m+}$ (m = 1,2,3).[86-87]

Complexation of gold in the +1, +2 and +3 oxidation states using [9]aneS$_3$ has been achieved by the Edinburgh group.[97,217,218] However, at the onset of this work only structural characterisation of these species had been carried out due to the low-yield synthetic routes to these complexes. The structures of the [Au(9]aneS$_3$)$_2$]$^{n+}$ (n = 1,2,3) cations will be discussed within the context of this work. The initial aims of the work described in this Chapter were to establish reproducible high-yield syntheses of [Au(9]aneS$_3$)$_2$]$^{n+}$ (n = 1, 2, 3) complexes and characterise them fully using electrochemical and e.p.r. spectroscopic techniques. Secondly the synthesis and characterisation of [Au([9]aneS3)PPh$_3$]$^+$ was undertaken.

2.2 RESULTS AND DISCUSSION

2.2.1 Synthesis and characterisation of $[Au([9]aneS_3)_2](PF_6)$

The synthesis of $[Au([9]aneS_3)_2](PF_6)$ has previously been reported; however, only structural characterisation was obtained due to the very low yield (5%) of the product.[217] Therefore, an alternative higher-yield synthetic route was urgently required.

The reported synthesis of $[Au([9]aneS_3)_2]^+$ used $KAuCl_4$ as a starting material to produce a yellow complex with $[9]aneS_3$, assigned as $[AuCl_3[9]aneS_3)]$. Further reaction of this complex with one equivalent of $[9]aneS_3$ under reducing conditions (MeOH) afforded $[Au([9]aneS_3)_2]^+$, which was isolated as the PF_6^- salt.[217] The very low yield of this product may have been due to the sensitivity of the reduction step. By avoiding Au(III) starting materials this reduction step would be eliminated. Therefore, a suitable Au(I) starting material was required. Removing the phosphine group from Au(I) phosphine species can be exceptionally difficult; hence,the synthesis of a homoleptic Au(I) complex using this route was not feasible. The species $[Au(SR_2)_2]^+$ are known to be good precursors for the synthesis of Au(I) complexes[159] (see Section 2.1.2a). Therefore, the complex $[Au(tht)_2](PF_6)$ was used in the synthesis of $[Au([9]aneS_3)_2](PF_6)$.

The reaction of $[Au(tht)_2](PF_6)$ with two molar equivalents of $[9]aneS_3$ in stirring, degassed CH_2Cl_2 at 0°C afforded, on the addition of Et_2O, a white precipitate. This product was obtained in 76% yield and shows f.a.b. mass spectral peaks at $M^+ =$ 557, 377 assigned to $[^{197}Au([9]aneS_3)_2]^+$, $[^{197}Au([9]aneS_3)]^+$ respectively. On the basis of this evidence together with

microanalytical and i.r. spectroscopic data, the product was assigned as $[Au([9]aneS_3)_2](PF_6)$. Full experimental details are given in Section 2.4.2. This complex decomposes in CH_2Cl_2, MeCN, $MeNO_2$, Me_2CO, MeOH within ~30 mins., to give metallic and/or colloidal gold. Consequently, due to decomposition and limited solubility n.m.r. studies were unsuccessful.

The structural determination of $[Au([9]aneS_3)_2]^+$ carried by A.J. Blake *et. al.*[217] shows a distorted tetrahedral stereochemistry at the d^{10} Au(I) centre with one $[9]aneS_3$ macrocycle bound asymmetrically through three S-donors, Au-S(14) = 2.825(8), Au-S(11) = 2.350(11), Au-S(17) = 2.733(8)Å and the other ligand bound through one S-donor, in a monodentate fashion, Au-S(21) = 2.302(6)Å (Figure 2.1). The $[Au([9]aneS_3)_2]^+$ cation is not isostructural with the Ag(I) congener. The structure of $[Ag([9]aneS_3)_2]^+$ shows the Ag(I) centre bound to six S-donors in an octahedral arrangement, with Ag-S(1) = 2.6665(12), Ag-S(4) = 2.7813(10)Å.[91,219] Therefore the [2+2] co-ordination at the Au(I) centre can be considered as compromise between the preferred facial binding of $[9]aneS_3$ and the tendency of Au(I) for linear co-ordination. The largest angle at the Au(I) centre is distorted from linearity, S(11)-Au-S(21) being 153.98(23)°.

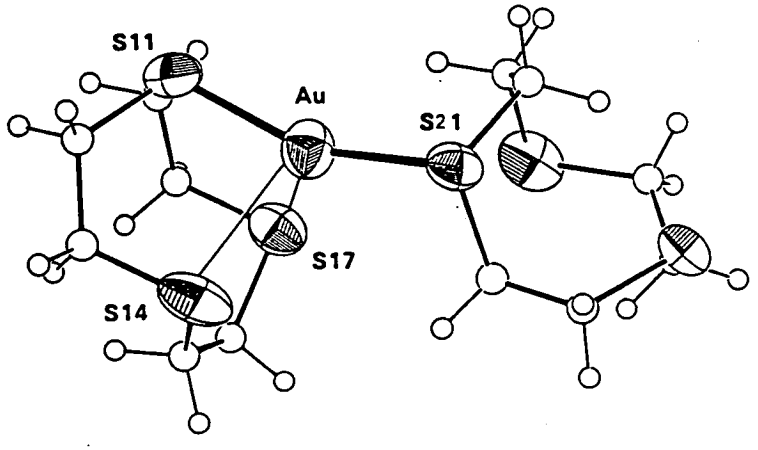

Figure 2.1: Single crystal structure of $[Au([9]aneS_3)_2](PF_6)$

Subsequent to the publication of $[Au([9]aneS_3)_2]^{+/3+}$ by the Edinburgh group,[217] the Au(I) thioether macrocyclic complex $[AuCl[9]aneS_3)]$ was reported by Parker.[227] In this complex $[9]aneS_3$ is bound in a monodentate fashion to Au(I), Au-S = 2.270(3), Au-Cl = 2.267(3)Å, with the angle S(1)-Au-Cl being 176.31(1)° (41). The Au atom is also weakly co-ordinated to two adjacent Au atoms, (Au-Au = 3.3095(4)Å) producing an almost linear chain of Au atoms. The strained solid-state conformation of $[9]aneS_3$ in this species is similar to the conformation of the monodentate $[9]aneS_3$ in $[Au([9]aneS_3)_2]^+$.[217] N.m.r. studies on $[AuCl([9]aneS_3)]$ suggest that the S-donors are equivalent in solution and involved in a rapid intramolecular exchange process.[227] This is the only other reported Au(I) macrocyclic complex apart from $[Au([9]aneS_3)_2]^+$.

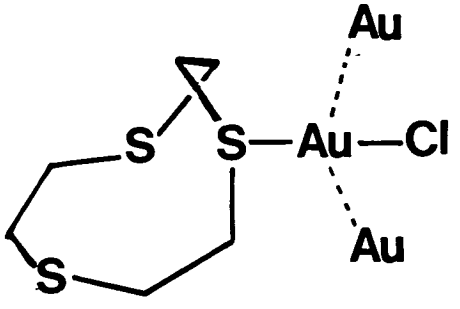

(41) $[AuCl([9]aneS_3)]$

2.2.2 ^{197}Au Mössbauer spectroscopic data for $[Au([9]aneS_3)_2](PF_6)$

All the ^{197}Au Mössbauer spectroscopic data was collected and interpretated in collaboration with Dr. R.V. Parish. The ^{197}Au Mössbauer spectrum of $[Au([9]aneS_3)_2](PF_6)$ shows a simple doublet (Figure 2.2) with isomer shift (I.S.) = -0.1(5) mms^{-1} and the quadrupole splitting (Q.S.) = 4.00(8) mms^{-1}, consistent with four co-ordination at the Au(I) centre.[220] These results are consistent with the known structure previously determined by X-ray crystallography. (Section 2.1.1)

Figure 2.2: ^{197}Au Mössbauer spectrum for [Au([9]aneS$_3$)$_2$](PF$_6$)

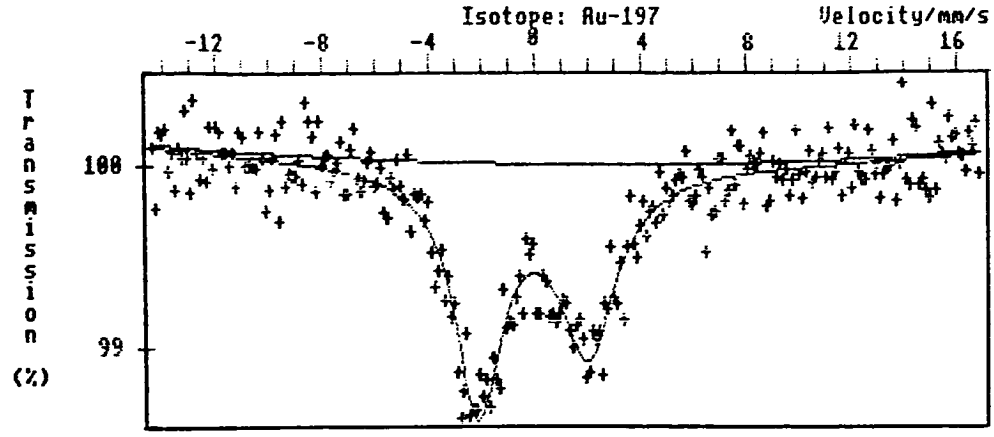

2.2.3 Characterisation of [Au([9]aneS$_3$)$_2$]$^{3+}$

[Au([9]aneS$_3$)$_2$]$^{3+}$ species could not be synthesised under ambient conditions due to the reduction of the Au(III) centre. However, chemical oxidation of [Au([9]aneS$_3$)]$^+$ using 98% $HClO_4$ afforded red crystals of the d^8 Au(III) complex.[217] The structure determination carried out by A.J. Blake *et. al.*[217] shows that [Au([9]aneS$_3$)$_2$]$^{3+}$ cation shows a tetragonally elongated octahedral stereochemistry at the Au(III) centre (Figure 2.3). Four Au-S bonds define a square plane, Au-S(4) = 2.348(4), Au-S(7) = 2.354(4)Å, while the two remaining two donors participate in long range apical interactions, Au...S(1) = 2.926(4)Å. The stereochemistry at the d^8 Au(III) centre is similar to that adopted at the d^8 Pd(II) centre in the analogous [Pd([9]aneS$_3$)$_2$]$^{2+}$ complex.[93,94]

Figure 2.3: Single crystal X-ray structure of [Au([9]aneS$_3$)$_2$]$^{3+}$

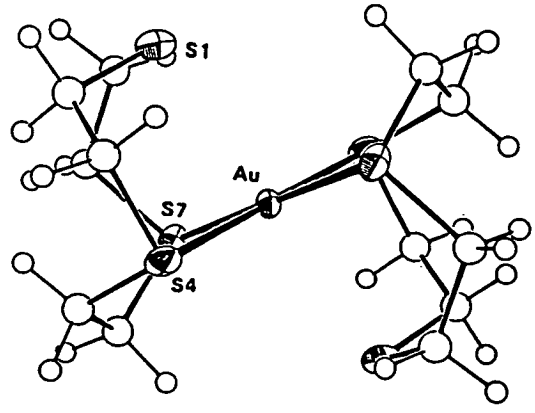

Under acidic conditions [Au([9]aneS$_3$)$_2$]$^{3+}$ does not undergo the ring-opening mechanism proposed for [9]aneS$_3$ bound to an electropositive

centre[229] (discussed in Section 1.4); although the potential ring-opening reaction may contribute to the unsuccessful synthesis of $[Au([9]aneS_3)_2]^{3+}$ under ambient conditions. Au(III) is considered to be a 'harder' Lewis acid than Au(I) hence the affinity for 'soft' S-donors is reduced for Au(III) compared to Au(I).[129] The mis-match of Au(III) with the S-donors along with the potential ring-opening reaction may explain the diminished stability of $[Au([9]aneS_3)_2]^{3+}$.

2.2.4 Synthesis and characterisation of $[Au([9]aneS_3)_2](BF_4)_2$

$[Au([9]aneS_3)_2](BF_4)_2$ can be synthesised in good yield using a modified synthetic route first outlined by A.J. Holder.[228]

Refluxing $HAuCl_4$ with 2 molar equivalents of $[9]aneS_3$ in 40%aq. HBF_4 produces a brown solution. To the resultant mixture $MeNO_2$ was added, followed by H_2O to facilitate the extraction of the complex into the organic solvent. The combined extracts were reduced in volume and the resultant brown oil was taken up in MeCN. Bulk vapour diffusion with Et_2O yielded an orange-brown microcrystalline product. A white, non-metal containing contaminant was isolated at this stage; full characterisation has shown the product to be a bicyclic sulphonium salt of $[9]aneS_3$ (see Chapter 8). The synthesis of $[Au([9]aneS_3)_2]^{2+}$ involves reduction of the Au(III) starting material with the excess $[9]aneS_3$ being oxidised.

The orange-brown microcrystalline compound, the major product, shows f.a.b. mass spectral peaks at $M^+ = 645$, 577 assigned to $[^{197}Au([9]aneS_3)_2BF_4]^+$ and $[^{197}Au([9]aneS_3)_2]^+$ respectively. The product was assigned as $[Au([9]aneS_3)_2](BF_4)_2$, on the basis of this evidence and

additional data from microanalyses and i.r. spectroscopy. Full experimental details are given in Section 2.4.3. The complex dissolves in MeCN to give an orange solution, the electronic spectrum of which shows two bands at λ_{max} = 402 nm (ε_{max} = 8100 $M^{-1}cm^{-1}$), 234 (14700). The band at 234 nm is probably due to a ligand to metal charge-transfer transition. Assignment of the band at 402 nm is more difficult, as the extinction coefficient is high for a pure d-d transition yet low for a charge-transfer transition.

The structural determination of $[Au([9]aneS_3)_2](BF_4)_2$ carried out by A.J. Blake *et. al.*, shows that in the centrosymmetric $[Au([9]aneS_3)_2]^{2+}$ cation the Au(II) centre is bound to six thioether donors in a tetragonally elongated stereochemistry, Au-S(1) = 2.839(5), Au-S(4) = 2.462(5), Au-S(7) = 2.452(5)Å.[218] (Figure 2.4) The two $[9]aneS_3$ macrocycles therefore encapsulate the genuine d^9 Au(II) centre to give a Jahn-Teller distorted octahedral stereochemistry.

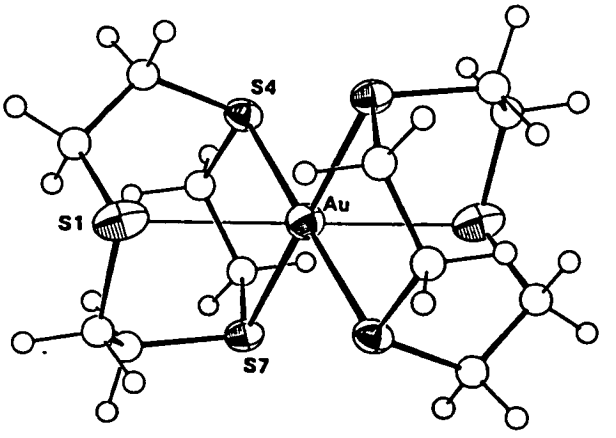

Figure 2.4: Single crystal X-ray structure of $[Au([9]aneS_3)_2](BF_4)_2$

$[Au([9]aneS_3)_2](BF_4)_2$ is an air-stable solid and shows no appreciable degradation over several months. As discussed in Section 2.1.4 mononuclear Au(II) species are exceptionally rare, due to the tendency for disproportionation to the more stable Au(I) and Au(III) ions.[129-131] $[Au([9]aneS_3)_2]^{2+}$ does not disproportionate under ambient conditions and is the first structurally characterised mononuclear Au(II) species.

2.2.5 ^{197}Au Mössbauer spectroscopic data for $[Au([9]aneS_3)_2](BF_4)_2$

The ^{197}Au Mössbauer spectrum for $[Au([9]aneS_3)_2](BF_4)_2$ has a non-standard shape. To interpret this spectrum magnetic ordering at the Au nucleus was assumed. A first-order treatment of simultaneous splitting/ modification of the nuclear energy levels by a magnetic field and a quadrupole interaction were the basis of the model used.[224] It was possible to fit the data to this model (Figure 2.5). This gave values of I.S. = 0.78(3) mms^{-1}, Q.S. = +3.1(5) mms^{-1} and B = 21(5)T.

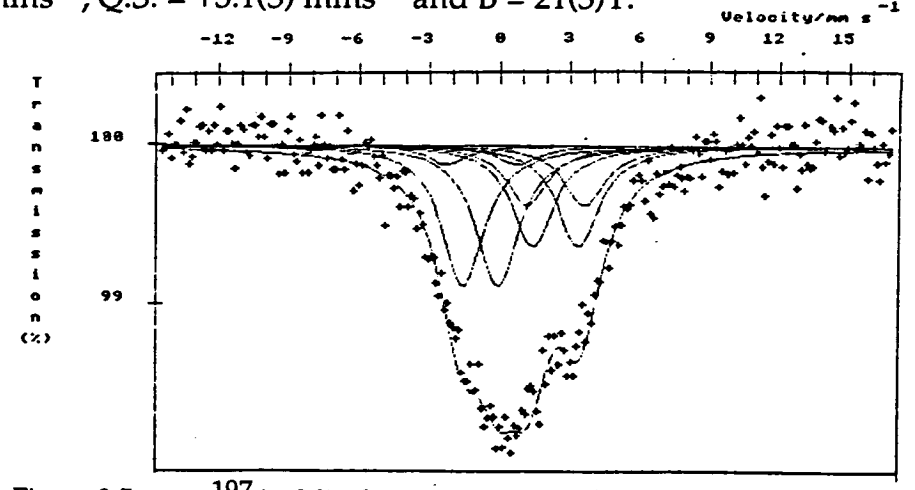

Figure 2.5: ^{197}Au Mössbauer spectrum of $[Au([9]aneS_3)_2](BF_4)_2$

2.2.6 E.p.r. studies of $[Au([9]aneS_3)_2]^{2+}$

The fluid solution e.p.r. spectrum of $[Au([9]aneS_3)_2](BF_4)_2$ in $MeNO_2$, at 293K, shows an isotropic signal with g_{iso} = 2.016 and hyperfine coupling to ^{197}Au (I = 3/2, 100%) producing a quartet with A_{iso} = 44.3G, (Figure 2.6).

The X-band spectrum of $[Au([9]aneS_3)_2](BF_4)_2$ in MeCN as a frozen glass at 77K shows a broad, ill-resolved anisotropic signal (Figure 2.7). However, on the addition of a 100-fold excess of $^{n}Bu_4NPF_6$ to the sample a better resolved signal is obtained (Figure 2.8). The $^{n}Bu_4NPF_6$ proved to be a good diamagnetic, inert dilutant, (presumably disrupting the ion pairings of

$[Au([9]aneS_3)_2]^{2+}$) minimising the spin-spin relaxation of the Au(II) centres which probably caused the line broadening. The resultant spectrum was initially assigned as a simple rhrombic signal with $g_1 = 2.018$ ($A_1 = 17.3G$), $g_2 = 2.023$ ($A_2 = 56.9G$), $g_3 = 2.007$ ($A_3 = 58.7G$), with all the rhombic components showing hyperfine coupling to the ^{197}Au nucleus. Attempted simulation of this spectrum using g and A tensor parameters only did not reproduce the experimental spectrum (Figure 2.9).[226] The effects of the quadrupole (P) and nuclear Zeeman (g_w) interactions are likely to be significant in this complex and related systems (see also Sections 3.2.9, 4.2.12) for the following reasons: (i) The overall appearance of the spectra is not readily recognisable as deriving from a rhombic (or axial) system for which I = 3/2. (ii) Attempts at simulating the spectra using g and A tensors only were unsuccessful. (iii) $[Au(mnt)_2]^{2-}$ displays a substantial quadrupole coupling interaction; this contributes to the weak (forbidden) transitions appearing outside the central region of the spectrum.[204] Similar features are seen in the X-band spectrum of $[Au([9]aneS_3)_2]^{2+}$ (Figure 2.8 marked by *).

The effects of nuclear quadrupole and nuclear Zeeman interactions have made full assignment of the anisotropic signal recorded for $[Au([9]aneS_3)_2]^{2+}$ difficult. However, the estimated initial g values from the X-band spectra indicate some covalent character of the Au-S bonds. This is consistent with the π-accepting S-donors removing electron density from the Au nucleus, consequently reducing the spin-orbit coupling. To quantify the s/d character of the unpaired electron, exact g values, hyperfine and quadrupole constants are required. Obtaining these values requires computer simulation incorporating the extra terms in the spin-Hamiltonian. This is beyond the scope of this work.

Figure 2.6: X-band solution e.p.r. spectrum of $[Au([9]aneS_3)_2](BF_4)_2$

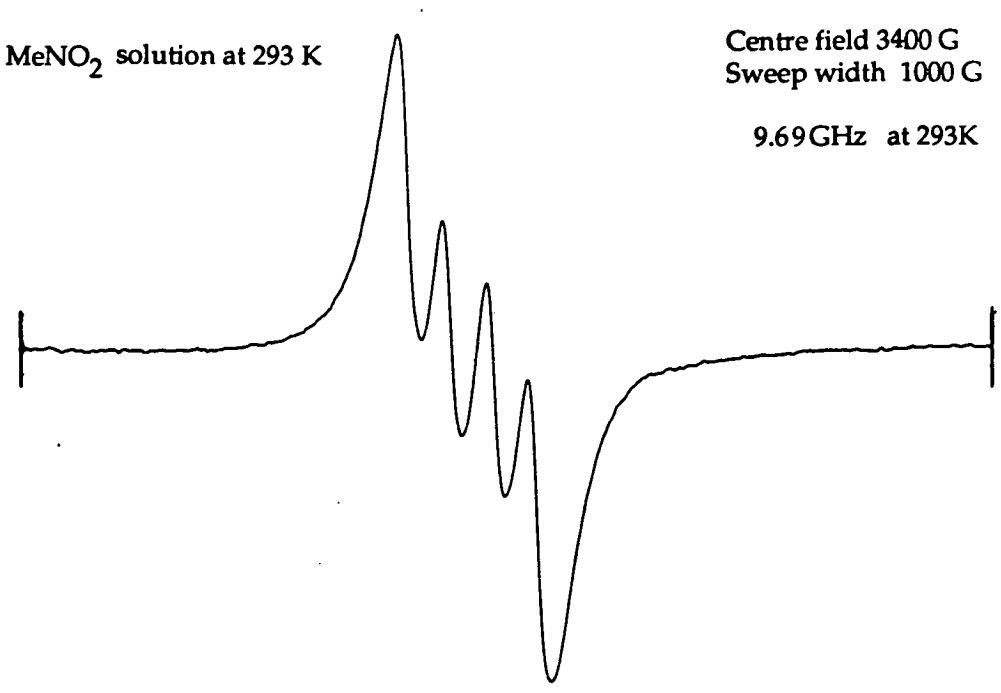

Figure 2.7: X-band frozen glass e.p.r. spectrum of $[Au([9]aneS_3)_2](BF_4)_2$

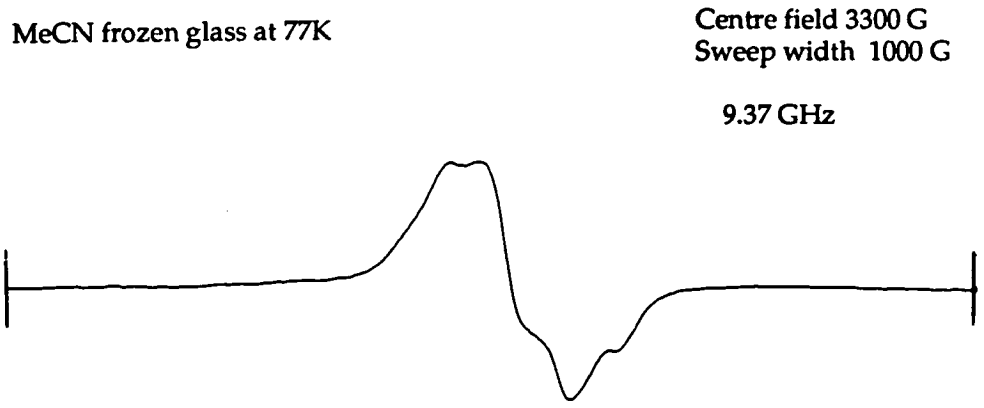

Figure 2.8: X-band frozen glass e.p.r. spectrum of $[Au([9]aneS_3)_2](BF_4)_2$ with $^nBu_4NPF_6$

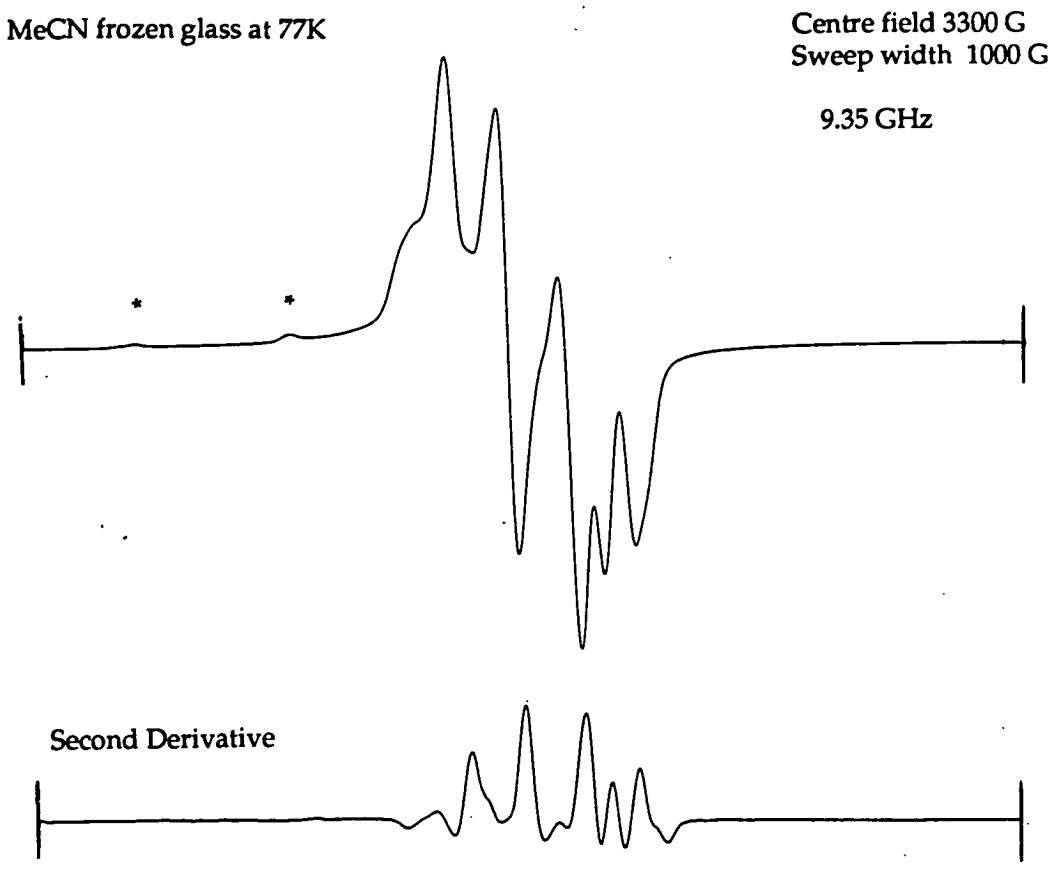

Figure 2.9: Simulated e.p.r. spectrum of $[Au([9]aneS_3)_2](BF_4)_2$

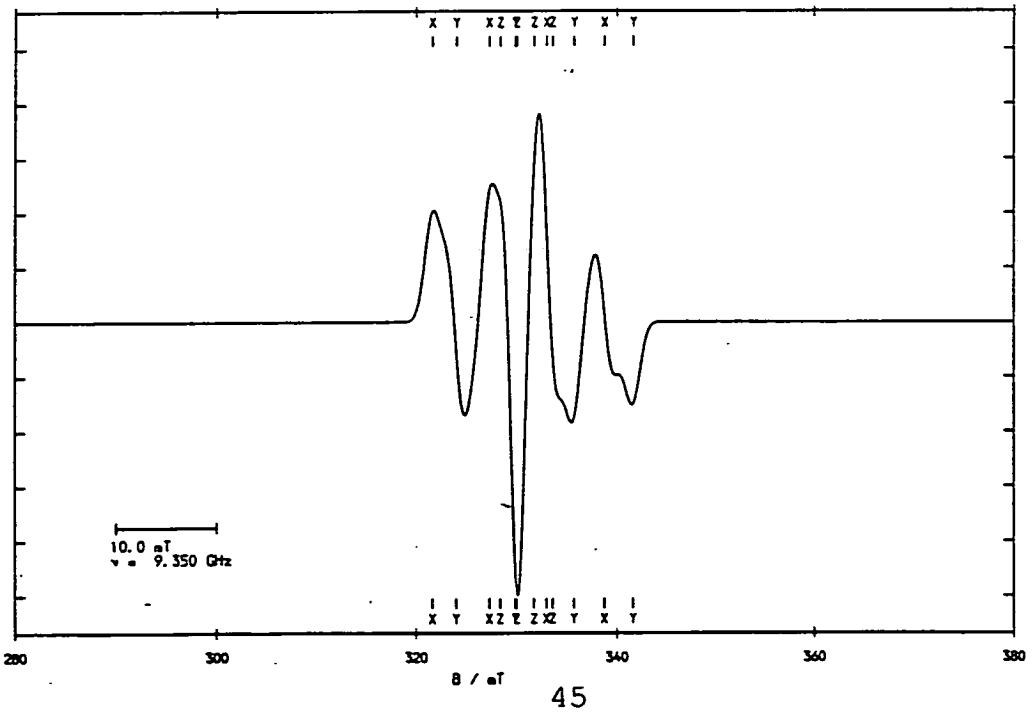

Solution e.p.r. spectral data for some known paramagnetic mononuclear gold species are listed in Table 2.1.

Table 2.1: Solution e.p.r. data for some paramagnetic gold species

	g	$A(^{197}Au)/cm^{-1}$	Ref
[Au(phthalocyanine)]	2.065	$61.0X10^{-4}$	*205*
$[Au(S_2CNEt_2)_2]$	2.040	$28.0X10^{-4}$	*139*
$[Au(Se_2CNEt_2)_2]$	2.013	$28.9x10^{-4}$	*139*
$[Au(S_2CN^iPr_2)_2]$	2.040	$28.0x10^{-4}$	*198*
$[Au(S_2CNBu_2)_2]$	2.039	$26.2x10^{-4}$	*199*
$[Au(mnt)^*_2](NBu_4)_2$	2.009	$27.6x10^{-4}$	*200*
$[Au([9]aneS_3)_2](BF_4)_2$	2.016	$42.0x10^{-4}$	this work

(*mnt = maleonitriledithiolate: $[S_2C_2(CN)_2]^{2-}$)

$[Au(mnt)_2]^{2-}$ has been co-crystallised with its Ni(II), Pd(II) or Pt(II) analogue and studied by single crystal e.p.r. techniques.[205,204] These revealed that the unpaired electron is in a largely ligand-based molecular orbital and that the quadrupole effects are significant.

$[Au([9]aneS_3)_2]^{2+}$ exhibits a greater hyperfine coupling constant in the solution spectrum than the 1,1-dithiolate and 1,2-dithiolate complexes, suggesting greater metal-based character of the unpaired electron. This is not surprising, since unlike the dithiolates thioether macrocycles do not tend to stabilise bound ligand-radical species.[26]

Preliminary work towards a single crystal e.p.r. study of $[Au([9]aneS_3)2]^{2+}$ was undertaken. Magnetically dilute single crystals of a diamagnetic host doped with $[Au([9]aneS_3)_2](BF_4)_2$ are required for this type of e.p.r. study. $[Pd([9]aneS_3)_2](BF_4)_2$ was selected as the diamagnetic host based on the identical nuclear charge and the near iso-structural stereochemistry of the Pd(II) cation in comparison with the Au(II) cation.

$[Pd([9]aneS_3)_2](BF_4)_2$ (prepared as outlined in ref. *93,94*) was dissolved in dry MeCN and 0.1 molar equivalent of $[Au([9]aneS_3)_2](BF_4)_2$ was added. The resultant solution was stirred then filtered into Et_2O to afford a blue-green precipitate. The blue-green solid was re-dissolved in dry MeCN and yielded a green microcrystalline solid after slow evaporation of the solvent.

The e.p.r. powder spectrum, of the doped sample at 290K, shows an anisotropic signal (Figure 2.10) similar to the frozen glass e.p.r. spectrum of $[Au([9]aneS_3)_2]^{2+}$ in the presence of $^nBu_4NPF_6$ (Figure 2.8). The resolution of the doped powder spectrum is not as good as the frozen glass spectrum, however, it is greatly improved over the powder e.p.r. spectrum of pure $[Au([9]aneS_3)_2](BF_4)_2$ (Figure 2.11), which shows a broad isotropic signal.

Figure 2.10: The e.p.r. powder spectrum of $[Pd([9]aneS_3)_2](BF_4)_2$ doped with 10% $[Au([9]aneS_3)_2](BF_4)_2$ at 293K

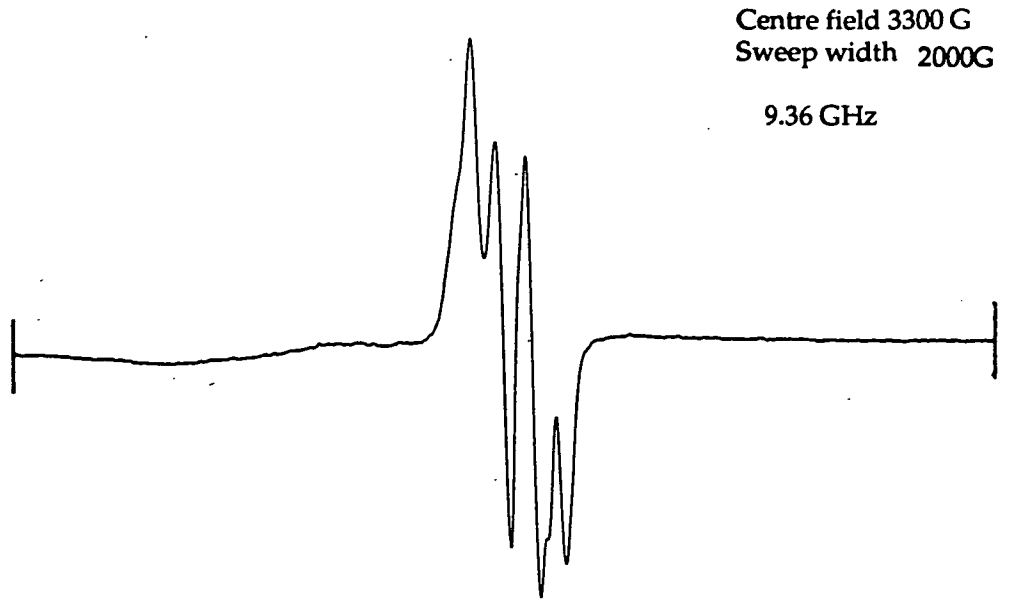

Figure 2.11: The e.p.r. powder spectrum of $[Au([9]aneS_3)_2](BF_4)_2$ at 293K

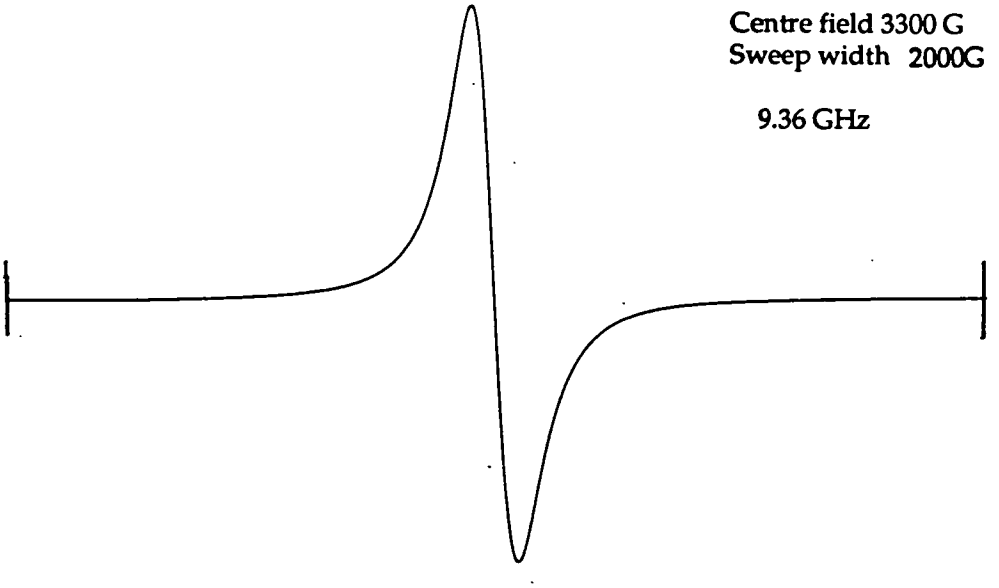

Therefore, it can be deduced that the concentration of $[Au([9]aneS_3)_2](BF_4)_2$ in the doped sample was too high. The control of the concentration of $[Au([9]aneS_3)_2](BF_4)_2$ within the host proved difficult, due to the gradual degradation of the Au(II) species during the synthesis of the doped complex. The growth of doped single crystals sufficiently magnetically dilute may be possible under different solvent and temperature conditions, however time did not allow this to be carried out successfully.

2.2.7 Electrochemical study of $[Au([9]aneS_3)_2]^{n+}$

Due to the relative instability of $[Au([9]aneS_3)_2](PF_6)$ in solution the electrochemical study was carried out on the Au(II) complex $[Au([9]aneS_3)_2](BF_4)_2$. Cyclic voltammetry of $[Au([9]aneS_3)_2](BF_4)_2$ at platinum electrodes in MeCN (0.1M $^nBu_4NBF_4$) shows a quasi-reversible oxidation at $E_{1/2}$ = +0.44V (ΔE_p = 80mV) and two irreversible reductions at E_{pc}^1 = +0.15V, and E_{pc}^2 =-0.58V vs Fc/Fc^+ at a scan rate of 200 mVs^{-1} (Figure 2.12).

Figure 2.12: Cyclic voltammogram of $[Au([9]aneS_3)_2](BF_4)_2$

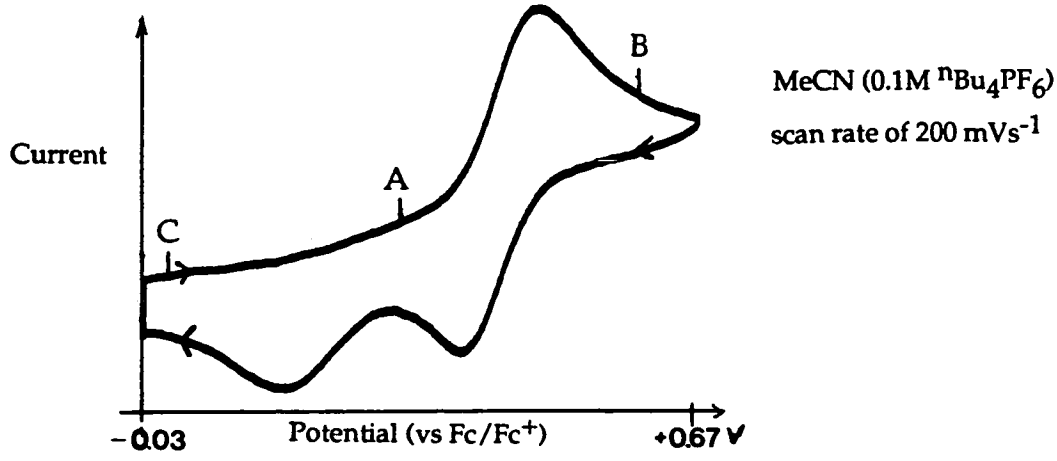

Coulometric measurements confirmed a one-electron oxidation step on the applied potential from +0.30V (A) to +0.60V (B), producing a e.p.r. silent

solution consistent with the oxidation of the initial Au(II) to a d^8 Au(III) species. This process is chemically reversible. $[Au([9]aneS_3)_2]^{2+}$ also undergoes a one-electron reduction at an applied potential of 0.0V(C) to give a colourless, diamagnetic solution consistent with a d^{10} Au(I) species, although this process is only partially reversible due to decomposition. The remaining reduction at E_{pc}^2 = 0.58V is assigned as a Au(I)/(0) couple.

The Au(I) complex $[Au([9]aneS_3)_2](PF_6)$ is sufficently stable in CH_2Cl_2 to be studied by cyclic voltammetry. The redox behaviour of $[Au([9]aneS_3)_2](PF_6)$ at platinum electrodes in CH_2Cl_2 (0.4M $^nBu_4NPF_6$) is identical to that exhibited by the Au(II) complex in MeCN (Figure 2.12).

The absence of the initial anodic peak on the cyclic voltammetric time-scale is due to the very slow electron transfer, indicative of a stereochemical change occurring on the oxidation of d^{10} Au(I) to d^9 Au(II).

2.2.8 Spectroelectrochemical study of $[Au([9]aneS_3)_2](BF_4)_2$

The redox behaviour of $[Au([9]aneS_3)_2](BF_4)_2$ can be monitored by UV/Vis spectroscopy using the *in situ* electrogeneration O.T.E. technique (discussed in Appendix A). $[Au([9]aneS_3)_2](BF_4)_2$ shows characteristic absorption bands at λ_{max} = 402 nm (ε_{max} = 8100 $M^{-1}cm^{-1}$), 234 (14700). Conversion of Au(II) to Au(III) at +0.73V (vs Fc/Fc^+ at 253K) shifts the absorption bands to λ_{max} = 334 nm (ε_{max} = 17075 $M^{-1}cm^{-1}$), 248 (15290) with isobestic points at λ_{iso} = 360, 208 nm (Figure 2.13). The presence of isosbestic points indicates that there are no apparent transient intermediates occurring during the redox process.

Figure 2.13: Spectroelectrochemical study of $[Au([9]aneS_3)_2](BF_4)_2$ (oxidation of $[Au([9]aneS_3)_2]^{2+}$ to $[Au([9]aneS_3)_2]^{3+}$)

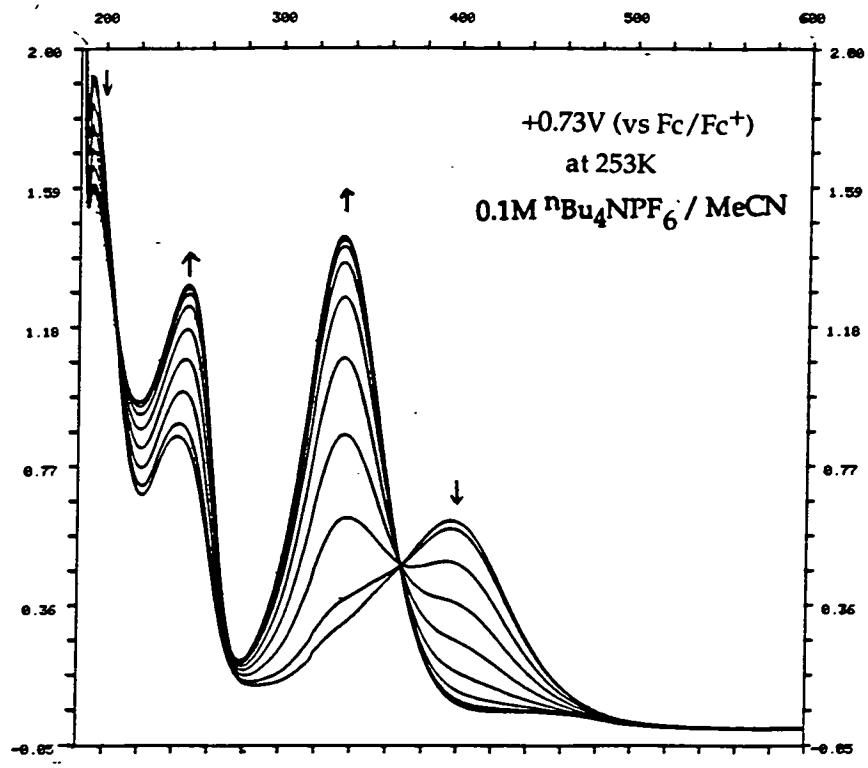

Figure 2.14: Spectroelectrochemical study of $[Au([9]aneS_3)_2](BF_4)_2$ (reduction of $[Au([9]aneS_3)_2]^{2+}$ to $[Au([9]aneS_3)_2]^{+}$)

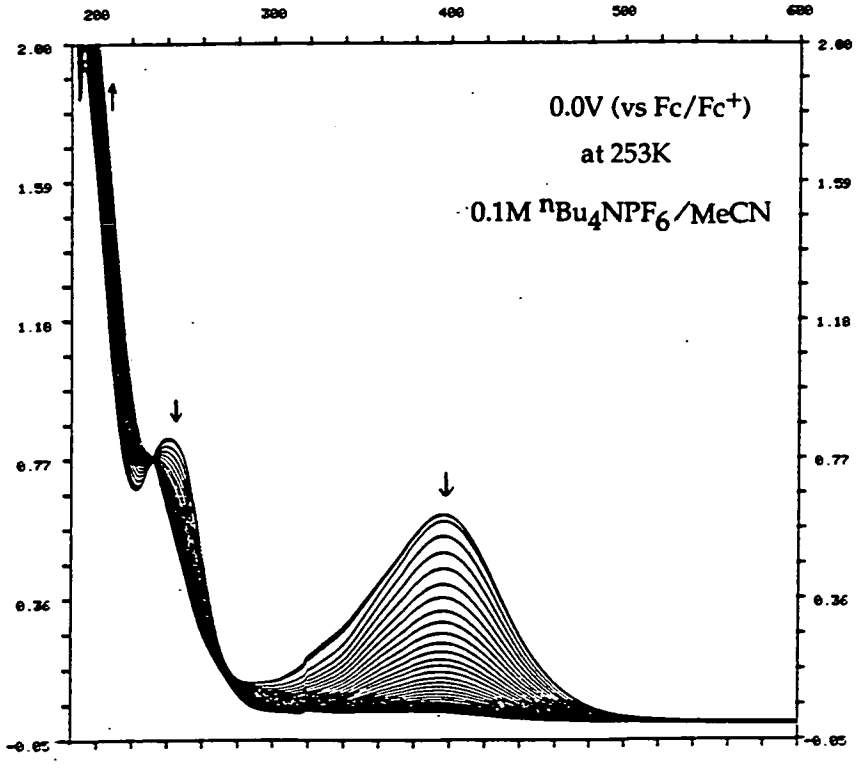

The oxidation to Au(III) is fully chemically reversible with reduction to the original Au(II) species occurring at an applied potential of +0.30V (vs Fc/Fc^+). The reduction of $[Au([9]aneS_3)_2]^{2+}$ to $[Au([9]aneS_3)_2]^+$ at 0.0V shows the collapse of all the absorption bands (Figure 2.14). The resultant featureless spectrum is consistent with a d^{10} species. Partial return to $[Au([9]aneS_3)_2]^{2+}$ from $[Au([9]aneS_3)_2]^+$ can be obtained at +0.30V and at an elevated temperature (293K).

2.2.9 Summary of $[Au([9]aneS_3)_2]^{n+}$ chemistry

High-yield synthetic routes to $[Au([9]aneS_3)_2](PF_6)$ and $[Au([9]aneS_3)_2](BF_4)_2$ have been established. The electrochemical studies have confirmed that $[9]aneS_3$ can stabilise Au(I), Au(II) and Au(III). The e.p.r. behaviour of the Au(II) species is consistent with the metal centre being in a distorted octahedral stereochemistry, as confirmed in the solid-state structure of $[Au([9]aneS_3)_2](BF_4)_2$. The $[Au([9]aneS_3)_2]^+$ species is prone to decomposition probably via the loss of the terminally bound monodentate thioether ligand. The stabilisation of the Au(I) centre using PPh_3 was also examined.

2.2.10 Synthesis and characterisation of $[Au(PPh_3)([9]aneS_3)](PF_6)$

The reaction of $[Au(PPh_3)Cl]$ with one molar equivalent of $[9]aneS_3$ in a 3:5 v/v MeCN: $MeNO_2$ mixture under reflux gave a colourless solution. Addition of NH_4PF_6 gave a white solid in good yield which was re-crystallised from $MeNO_2$ and Et_2O. The product shows f.a.b. mass spectral peaks at $M^+ = 638, 459$ assigned to $[^{197}Au(PPh_3)([9]aneS_3)]^+$ and $[^{197}Au(PPh_3)]^+$ respectively. On the basis of this evidence together with

microanalytical and i.r. spectroscopic data, the product was assigned as $[Au(PPh_3)([9]aneS_3)](PF_6)$. This complex is stable in the solid-state.

The ^1H n.m.r. spectrum of $[Au(PPh_3)([9]aneS_3)](PF_6)$ in CD_3NO_2 shows two broad resonances at δ = 2.87 - 3.18 ppm and δ = 7.55 - 7.65 ppm due to the macrocyclic and aromatic protons respectively. This spectrum is similar to the ^1H n.m.r. spectrum reported for $[Cu(PPh_3)([9]aneS_3)](ClO_4)$ in CD_3NO_2.[37]

The ^{13}C n.m.r. spectrum of $[Au(PPh_3)([9]aneS_3)](PF_6)$ shows three resonances due to the aromatic carbons at δ = 127.41, 129.63, 131.87 ppm, and a single methylene resonance at δ = 28.01 ppm due to the macrocyclic carbons. The appearance of the single macrocyclic resonance may be due to the bound $[9]aneS_3$ undergoing a rapid intramolecular exchange process in solution. Lowering the temperature may affect such a process. Unfortunately attempts to obtain n.m.r. spectra of $[Au(PPh_3)([9]aneS_3](PF_6)$ at 253K resulted in the precipitation of the complex from solution. Therefore unambiguous information on the binding of $[9]aneS_3$ to the Au(I) centre could not be obtained from the n.m.r. studies.

Attempts to grow single crystals of $[Au(PPh_3)[9]aneS_3)](PF_6)$ by vapour diffusion and hexane layering methods produced white films and powders. The structure of the $[Cu(AsPh_3)([9]aneS_3)]^+$ cation is known (Figure 2.15). The $[9]aneS_3$ ligand is bound facially to the Cu(I) centre, with the $AsPh_3$ ligand completing the distorted tetrahedral stereochemistry at the metal centre.

Figure 2.15: Structure of $[Cu(AsPh_3)([9]aneS_3)]^+$

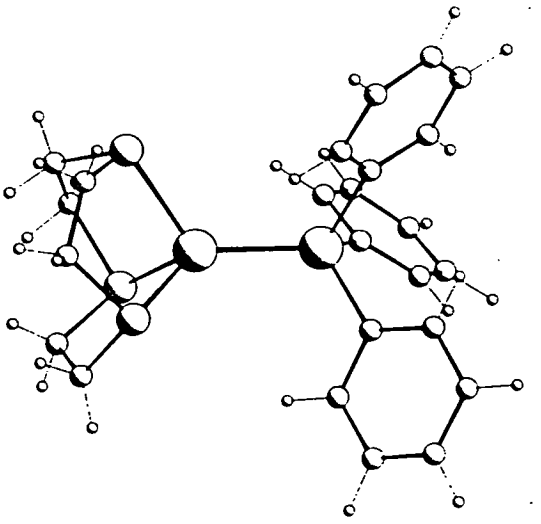

$[9]aneS_3$ can bind to Au(I) in a facial or monodentate fashion as seen in $[Au([9]aneS_3)_2]^+$. If the Au(I) centre in $[Au(PPh_3)([9]aneS_3)]^+$ were linear, the $[9]aneS_3$ ligand would have to bound through only one S- donor, which may be relatively insecure. The $[Au(PPh_3)([9]aneS_3)](PF_6)$ complex is very stable suggesting a more stable binding mode of $[9]aneS_3$, i.e. facial co-ordination (Figure 2.16).

Figure 2.16: Proposed structure of $[Au(PPh_3)([9]aneS_3)]^+$

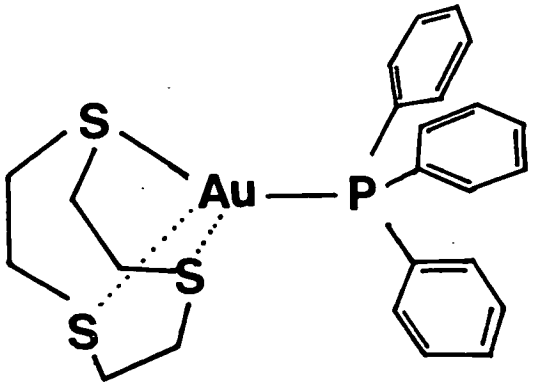

$[Au(PPh_3)[9]aneS_3)](PF_6)$ is redox inactive at platinum electrodes in MeCN (0.1M $^nBu_4NPF_6$) in the potential range of +1.2V to -2.2V vs Fc/Fc^+.

2.3. CONCLUSIONS

The stabilisation of $[Au([9]aneS_3)_2]^{n+}$ (n = 1,2,3) species reflects the ability of $[9]aneS_3$ to act as a formal 2, 4 and 6 electron donor. The isolation and characterisation of the mononuclear $[Au([9]aneS_3)_2]^{2+}$ complex has presented a rare opportunity for the study of this unusual oxidation state of gold under ambient conditions.

The probable loss of the monodentate $[9]aneS_3$ in $[Au([9]aneS_3)_2]^{+}$ accounts for the relative instability of this species. The stability of $[Au([9]aneS_3)_2]^{3+}$ under ambient conditions is affected by the mis-match of Au(III) centre with the 'soft' S-donors of $[9]aneS_3$, together with the potential for ring-opening reactions.[26] The relative instability of the $[Au([9]aneS_3)_2]^{+}$ and $[Au([9]aneS_3)_2]^{3+}$ species undoubtedly enhances the stability of the intermediate Au(II) complex.

Interestingly, by using a facially capping trithia macrocycle, Au(I) and Au(III) (the normal oxidation states for Au) have been relatively destabilised, while Au(II) (the 'rare' oxidation state) has been stabilised.

Replacement of one $[9]aneS_3$ ligand in $[Au([9]aneS_3)_2]^{+}$ with a tertiary phosphine, PPh_3 produces a stable Au(I) complex. The phosphine ligand stabilises the Au(I) centre so well, that the redox behaviour of $[Au(PPh_3)([9]aneS_3)](PF_6)$ is limited.

2.4 EXPERIMENTAL SECTION

2.4.1 Synthesis of [Au(tht)Cl]

$HAuCl_4$ (340 mg, 1.0 mmol) in dry ethanol was added to a stirring solution of tetrahydrothiophene (tht) (1 cm^3) in ethanol (10 cm^3), a white precipitate was formed immediately. The suspension was stirred for 30 mins. at room temperature, then stored at -20°C overnight. The product was collected and washed with ethanol, dried *in vacuo* and stored at -20°C. (Yield 266 mg, 83%). M.Wt = 320.63. I.r. spectrum (KBr disc): 2950w, 2920, 2880, 1435, 1425, 1380w, 1310, 1265, 1255, 1195w, 1080w, 1040w, 950, 900w, 740w, 760w, 340 and 330 cm^{-1}.

2.4.2 Synthesis of $[Au(tht)_2](PF_6)$

Method as in ref *159*. The white product was dried *in vacuo* and stored at -20°C. (Yield 373 mg, 72%). M.Wt = 518.27. I.r. spectrum (KBr disc): 2950, 2920, 2850, 1435, 1425, 1310, 1265, 1235, 1195w, 900, 840-820, and 560 cm^{-1}. F.a.b mass spectrum (3-NOBA matrix): found $M^+ = 373$. Calc. for $[^{197}Au(C_4H_8S)_2]^+$: $M^+ = 373$, with fragmentation products at 345, 331, 317, 285. Calc. for $[M^+ - (CH_2)_2] = 345$, $[M^+ - (CH_2)_3] = 331$, $[M^+ - (CH_2)_4] = 317$, $[M^+ - (CH_2)_4S] = 285$.

2.4.2 Synthesis of $[Au([9]aneS_3)_2](PF_6)$

Reaction of $[9]aneS_3$ (40 mg, 0.222 mmol) with $[Au(tht)_2](PF_6)$ (61 mg, 0.117 mmol) in stirring CH_2Cl_2 (10 cm^3) for 15 mins in the dark at 0°C gives a colourless solution. Filtration into Et_2O (30 cm^3) afforded a white precipitate which collected and washed with Et_2O. The white solid was dried *in vacuo*, stored at -20°C. (Yield 119 mg, 76%) M.Wt. = 702.64. Elemental analyses: found C = 18.0, H = 2.97%. Calc. for $C_{12}H_{24}S_6Au_1P_1F_6$: C = 20.5, H = 3.44%. I.r. spectrum (KBr disc): 2900, 1450, 1440, 1410, 1310, 1280, 1210, 1190, 1150, 940, 920, 840-820 and 560 cm^{-1}. F.a.b. mass spectrum (3-NOBA matrix) : found M^+ = 557, 337. Calc. for $[^{19}Au([9]aneS_3)_2]^+$: M^+ = 557; $[^{197}Au([9]aneS_3)]^+$: M^+ = 377, with correct isotopic distributions.

2.4.3 Synthesis of $[Au([9]aneS_3)_2](BF_4)_2$

To a stirring suspension of $[9]aneS_3$ (70 mg, 0.388 mmol) in 40%aq. HBF_4(15 cm^3), $HAuCl_4$ (66 mg, 0.194 mmol) was added. The mixture was refluxed for 15 mins. To the resultant brown solution $MeNO_2$ (40 cm^3) was added, followed by H_2O (80 cm^3) to facilitate the extraction of the complex in the organic solvent. Additional washing of the aqueous layer using $MeNO_2$ (4 x 10 cm^3) gave combined extracts, from which the solvent was removed *in vacuo*. The brown oil was washed with CH_2Cl_2 (5 cm^3), and the residue taken up in MeCN (10 cm^3). Bulk vapour diffusion with Et_2O into the MeCN solution over 18hrs. under pressure, yielded an orange-brown microcrystalline product on filtration and washing with Et_2O. Dried *in vacuo*. (Yield 107mg, 75%). M.Wt. = 731.57. Elemental analyses:

found C = 19.2, H = 3.20, N = 0.06%. Calc. for $C_{12}H_{24}S_6Au_1B_2F_8$: C = 19.7, H = 3.28%. I.r. spectrum (KBr disc): 2940, 2900, 1440, 1420, 1405, 1295, 1290, 1285, 1080-1030, 940, 920, 965w, 880, 825, 810, 530 and 520 cm^{-1}. F.a.b. mass spectrum (3-NOBA matrix): found M^+ = 645, 577. Calc. for $[^{197}Au([9]aneS_3)_2BF_4]^+$: M^+ = 645; $[^{197}Au([9]aneS_3)_2]^+$: M^+ = 577, with correct isotopic distributions. UV/Vis spectrum (MeCN) : λ = 402 nm (ε_{max} = 8100 $M^{-1}cm^{-1}$), 234 (14700).

2.4.4 Synthesis of $[Au(PPh_3)([9]aneS_3)](PF_6)$

$[Au(PPh_3)Cl]$ (55 mg, 0.11 mmol) with $[9]aneS_3$ (20 mg. 0.11 mmol) were refluxed for 3 hrs. in MeCN: $MeNO_2$ (3 cm^3: 5 cm^3) mixture: on the addition of NH_4PF_6 a white precipitate was formed, and filtered off. The resultant colourless solution afforded a white precipitate on the addition of Et_2O. The white product was recrystallised from $MeNO_2$ and Et_2O. (Yield 50 mg,58%). M.Wt. = 784.28. Elemental analyses : found C = 36.4, H = 3.48% Calc for $C_{24}H_{27}S_3Au_1P_2F_6$: C = 36.8, H = 3.47%. I.r. spectrum (KBr disc): 3140, 3040, 2980, 2960w, 1960w 1905w, 1890w, 1770w, 1665w, 1580w, 1550w, 1480, 1435, 1400, 1330, 1300, 1280, 1250, 1180, 1160w, 1100, 1025, 1000, 990w, 925, 875, 855, 840, 810, 750, 710, 690, 560, 535, 500, 440 and 430 cm^{-1}. F.a.b. mass spectrum (3-NOBA matrix) found M^+ = 638, 459. Calc. for $[^{197}Au(PPh_3)([9]aneS_3)]^+$: M^+ = 638; $[^{197}Au(PPh_3)]^+$: M^+ = 459, with correct isotropic distributions. ^1H n.m.r. (CD_3NO_2, 298K, 200. 13MHz) : δ = 2.87 - 3.18 , 7.55 - 7.65 ppm. ^{13}C n.m.r. (CD_3NO_2, 298K, 50.32 MHz) : δ = 127.41, 129.63, 131.87 ppm (CH), δ = 28.01 ppm (CH_2).

CHAPTER 3

Gold complexes of [18]aneS$_6$

3.1 INTRODUCTION

The work discussed in this Chapter extends directly from the chemistry examined in Chapter 2. The ligand [9]aneS$_3$ can stabilise a gold centre in the +1, +2 and +3 oxidation states. However, the [Au([9]aneS$_3$)$_2$]$^+$ species is inclined to decompose, probably via the loss of the monodentate ligand. Pursuit of a more stable Au(I) complex, still with the potential to stabilise the higher oxidation states (+2,+3) led us to the use of the hexadentate thioether macrocycle [18]aneS$_6$. Encapsulation of the gold centre within one ring eliminates the route to decomposition via the loss of a terminally bound ligand.

3.2 RESULTS AND DISCUSSION

3.2.1 Synthesis and characterisation of [Au([18]aneS$_6$)](PF$_6$)

The reaction of [18]aneS$_6$ with one molar equivalent of [Au(tht)$_2$](PF$_6$) in stirring, degassed MeCN affords a white precipitate on addition of Et$_2$O. The isolated white micro-crystalline solid shows a f.a.b. mass spectral peak at M^+ = 557 assigned to [^{197}Au([18]aneS$_6$)]$^+$. On the basis of this evidence together with microanalyses and i.r. spectroscopic data, the product was assigned as [Au([18]aneS$_6$)](PF$_6$). Full experimental details are given in Section 3.4.1. The ^{1}H n.m.r. spectra of [Au([18]aneS$_6$)](PF$_6$) in CD$_3$CN, at 298 and 223 K both show a broad resonance at δ = 2.91-3.01 p.p.m., assigned to the macrocyclic protons. The ^{13}C n.m.r. spectrum at 223 K shows a single

resonance at δ = 30.09 p.p.m. The n.m.r. studies indicate that the macrocycle is involved in an intra-molecular averaging process in solution.

In order to establish the co-ordination at the Au(I) centre and the conformation of the ligand, a single crystal X-ray structure determination was carried out.

3.2.2 Structure determination of [Au([18]aneS$_6$)](PF$_6$)

A single crystal X-ray structure determination on [Au([18]aneS$_6$)](PF$_6$) shows the Au(I) centre co-ordinated to two S-donors at Au - S(1) = 2.321(3), Au - S(10) = 2.320(4)Å (Figure 3.1). The co-ordination of the Au(I) centre is distorted from a linear conformation, the angle at S(1) - Au - S(10) = 155.93(12)°. Additional longer interactions to another two S-donors, Au...S(4) = 2.870(4), Au...S(7) = 2.856(4)Å create a distorted tetrahedral co-ordination geometry around the metal centre. Full details of the solution and refinement of the structure are given in Section 3.4.2. Selected bonds, angles and torsions are given in Table 3.1. There are two apparent conformations in a section of the unco-ordinated macrocycle from C(12) to C(14), involving the 'up' and 'down' orientation of the S(13) donor. This is most clearly seen in the two orthogonal views of the cation (Figure 3.2(a) and (b)).

Figure 3.1: Single X-ray crystal structure of $[Au([18]aneS_6)]^+$ ('up'conformation)

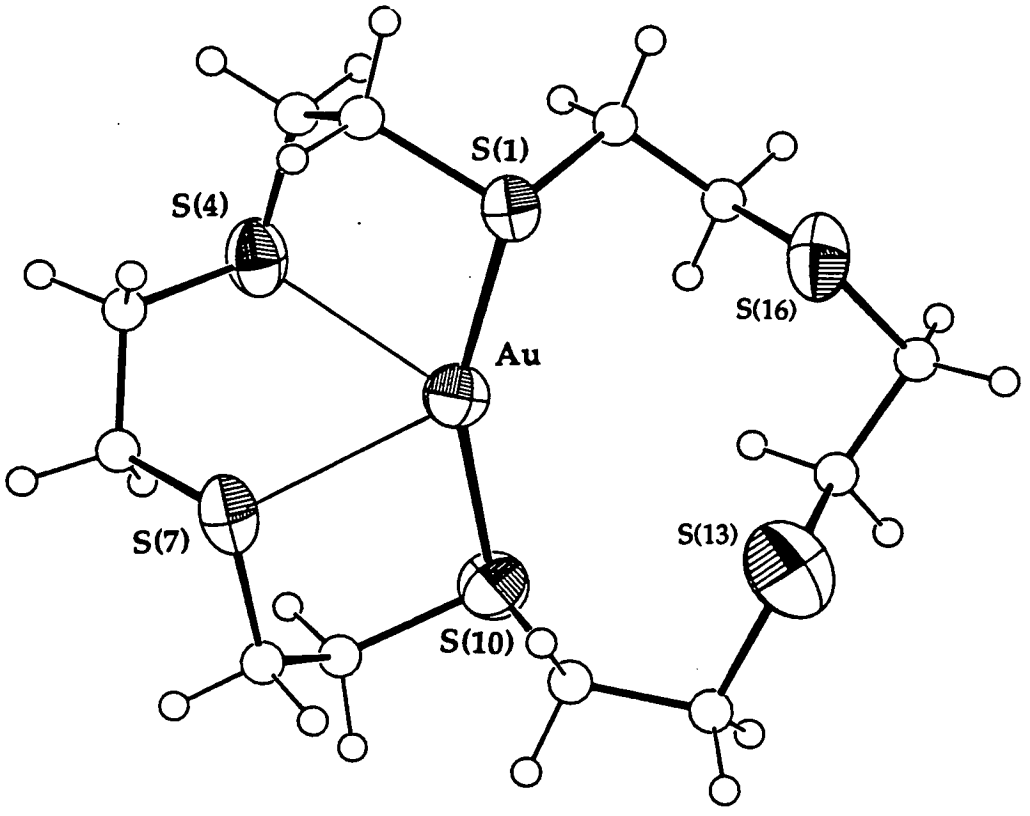

Figure 3.2: Orthogonal views of $[Au([18]aneS_6)]^+$
(a) 'up' conformation, (b) 'down' conformation

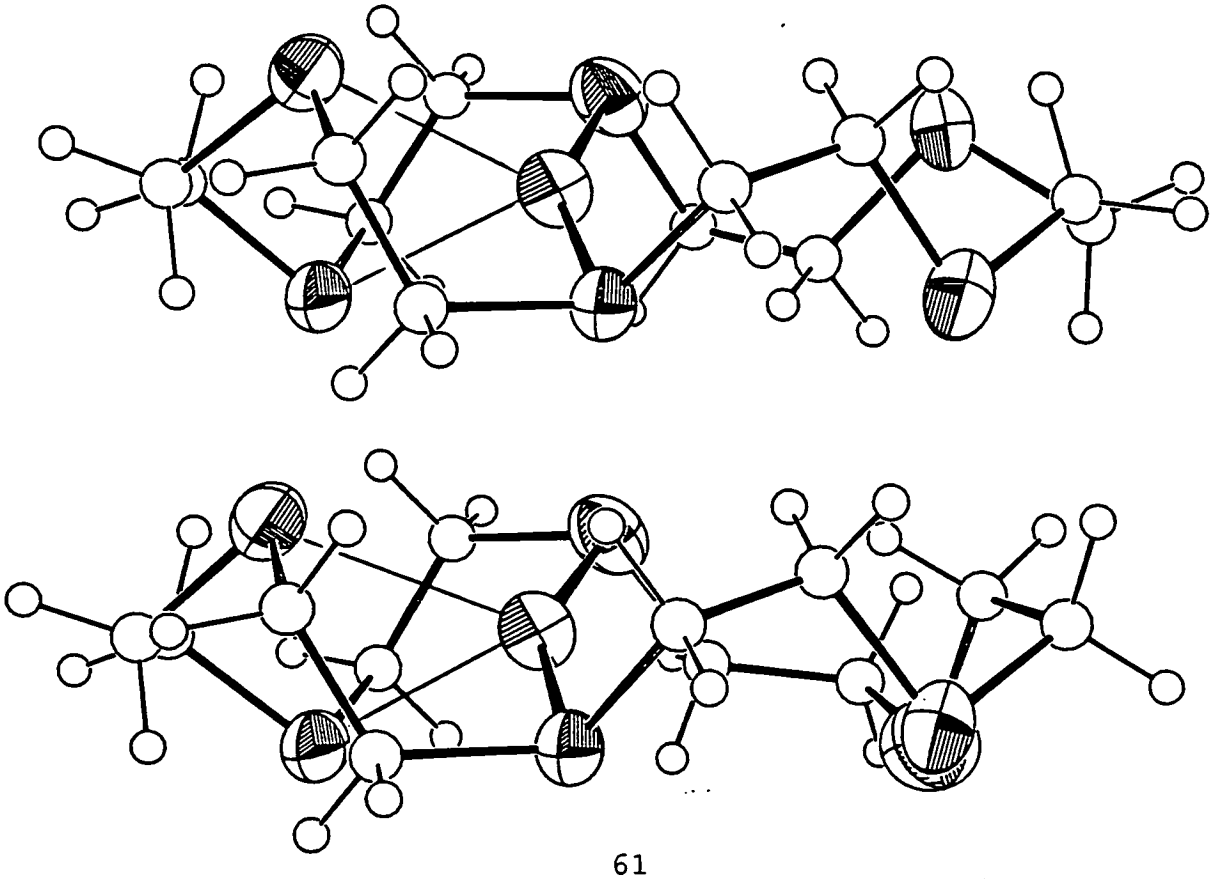

Table 3.1: Selected bonds, angles and torsions for $[Au([18]aneS_6)]^+$

Au	- S(1)	2.321(3)	C(5)	- C(6)	1.533(22)
Au	- S(4)	2.870(4)	C(6)	- S(7)	1.802(16)
Au	- S(7)	2.856(4)	S(7)	- C(8)	1.808(15)
Au	-S(10)	2.320(4)	C(8)	- C(9)	1.497(22)
S(1)	- C(2)	1.815(14)	C(9)	-S(10)	1.816(17)
S(1)	-C(18)	1.812(14)	S(10)	-C(11)	1.824(19)
C(2)	- C(3)	1.515(20)	C(15)	-S(16)	1.783(21)
C(3)	- S(4)	1.798(16)	S(16)	-C(17)	1.815(17)
S(4)	- C(5)	1.801(16)	C(17)	-C(18)	1.487(21)

S(1)	- Au	- S(4)	83.40(11)	S(7)	- C(8) - C(9)	116.3(11)
S(1)	- Au	- S(7)	113.75(11)	C(8)	- C(9) -S(10)	116.8(11)
S(1)	- Au	-S(10)	155.93(12)	Au	-S(10) - C(9)	103.7(5)
S(4)	- Au	- S(7)	75.94(11)	Au	-S(10) -C(11)	106.2(6)
S(4)	- Au	-S(10)	117.88(12)	C(9)	-S(10) -C(11)	100.4(8)
S(7)	- Au	-S(10)	84.06(12)	S(10)	-C(11) -C(12)	129.8(15)
Au	- S(1)	- C(2)	105.0(4)	C(11)	-C(12) -S(13)	107.0(16)
Au	- S(1)	-C(18)	109.6(4)	C(12)	-S(13) -C(14)	109.6(12)
C(2)	- S(1)	-C(18)	103.5(6)	S(13)	-C(14) -C(15)	118.0(17)
S(1)	- C(2)	- C(3)	116.2(10)	C(14)	-C(15) -S(16)	104.8(15)
C(2)	- C(3)	- S(4)	116.3(10)	S(10)	-C(11) -C(12')	103.2(13)
Au	- S(4)	- C(3)	95.8(5)	C(11)	-C(12')-S(13')	121.5(14)
Au	- S(4)	- C(5)	100.0(5)	C(12')	-S(13')-C(14')	105.0(14)
C(3)	- S(4)	- C(5)	102.6(7)	S(13')	-C(14')-C(15)	103.1(21)
S(4)	- C(5)	- C(6)	110.9(11)	C(14')	-C(15) -S(16)	127.6(19)
C(5)	- C(6)	- S(7)	109.6(11)	C(15)	-S(16) -C(17)	98.8(9)
Au	- S(7)	- C(6)	99.8(5)	S(16)	-C(17) -C(18)	112.1(11)
Au	- S(7)	- C(8)	95.2(5)	S(1)	-C(18) -C(17)	111.1(10)
C(6)	- S(7)	- C(8)	101.9(7)			

C(18)	- S(1)	- C(2)	- C(3)	64.4(11)	C(11)	-C(12)	-S(13) -C(14)	-89.7(18)
C(2)	- S(1)	-C(18)	-C(17)	-164.4(10)	C(12)	-S(13)	-C(14) -C(15)	-173.1(17)
S(1)	- C(2)	- C(3)	- S(4)	57.1(13)	S(13)	-C(14)	-C(15) -S(16)	-63.5(19)
C(2)	- C(3)	- S(4)	- C(5)	72.1(12)	C(14)	-C(15)	-S(16) -C(17)	-80.4(15)
C(3)	- S(4)	- C(5)	- C(6)	-150.3(11)	C(9)	-S(10)	-C(11) -C(12')	-166.9(12)
S(4)	- C(5)	- C(6)	- S(7)	79.7(12)	S(10)	-C(11)	-C(12')-S(13')	-55.6(17)
C(5)	- C(6)	- S(7)	- C(8)	-153.2(11)	C(11)	-C(12')	-S(13')-C(14')	-172.8(18)
C(6)	- S(7)	- C(8)	- C(9)	72.1(12)	C(12')	-S(13')	-C(14')-C(15)	-101.3(20)
S(7)	- C(8)	- C(9)	-S(10)	57.8(15)	S(13')	-C(14')	-C(15) -S(16)	80.5(25)
C(8)	- C(9)	-S(10)	-C(11)	58.2(13)	C(14')	-C(15)	-S(16) -C(17)	-124.8(23)
C(9)	-S(10)	-C(11)	-C(12)	154.0(19)	C(15)	-S(16)	-C(17) -C(18)	171.4(12)
S(10)	-C(11)	-C(12)	-S(13)	72.5(22)	S(16)	-C(17)	-C(18) - S(1)	-56.2(13)

The [2+2] co-ordination environment at the Au(I) centre is similar to that observed for the Au(I) ion in the analogous $[Au([9]aneS_3)_2]^{2+}$ cation, which also exhibits this unusual distorted tetrahedral geometry, with comparable bond lengths and angles (Section 2.2.1). The structure of $[Au(18)aneS_6)]^+$ however, differs markedly from that of its Ag(I) congener. In $[Ag([18]aneS_6)]^+$ the Ag(I) ion is bound to all six S-donors in a tetragonally compressed stereochemistry, Ag - S = 2.665(12), 2.7813(10)Å (Figure 3.3).[120] The [2+4] co-ordination reflects the tendency of d^{10} Ag(I) to increase its co-ordination number with soft donor ligands.[221]. Evidently d^{10} Au(I) does not wish to do this to the same degree. Interestingly, $[Au([18]aneS_6)]^+$ is similar to its Cu(I) congener.

Figure 3.3: Structure of $[Ag([18]aneS_6)]^+$

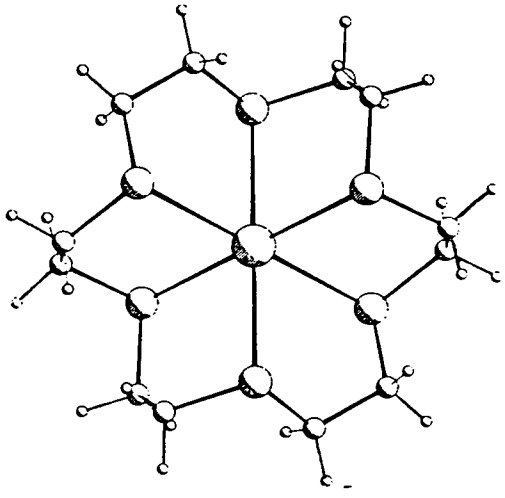

Figure 3.4: Structure of $[Cu([18]aneS_6)]^+$

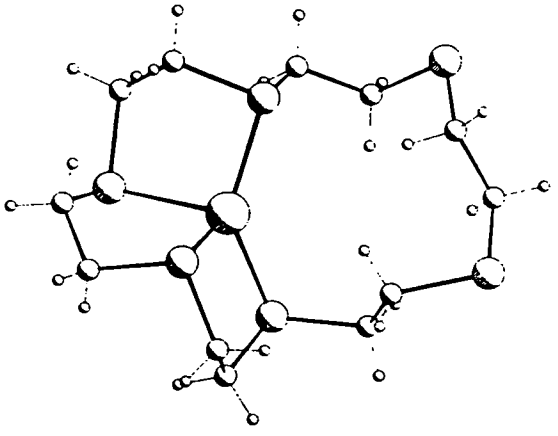

In $[Cu([18]aneS_6)]^+$ the Cu(I) ion adopts a distorted tetrahedral geometry with Cu - S(1) = 2.253(2), Cu - S(10) = 2.245(2), Cu - S(4) = 2.3620(2), Cu - S(7) = 2.358(2)Å, with the S(1)-Cu-S(10) angle being 138.4(1)° (Figure 3.4).[117] In both the Cu(I) and Au(I) structures the metal centre is bound in a [2+2] co-ordination geometry. However, the preference of Au(I) for linear co-ordination distorts the tetrahedral geometry even further than in the Cu(I) cation. This is exemplified by the increase of the S(1) - M - S(10) from 138.4(1)° at Cu(I), to 155.93(12)° at Au(I).

3.2.3 ^{197}Au Mössbauer spectroscopic data for [Au([18]aneS$_6$)](PF$_6$)

The ^{197}Au Mössbauer spectrum for [Au([18]aneS$_6$)](PF$_6$) shows a doublet with I.S. = 1.06(4) mms^{-1} and Q.S. = 5.33(8) mms^{-1} (Figure 3.5). These results imply four co-ordination at the Au(I) centre.[224] These results are consistent with the known structure determined by X-ray crystallography (Section 3.2.2).

Figure 3.5: ^{197}Au Mössbauer spectrum for [Au([18]aneS$_6$)](PF$_6$)

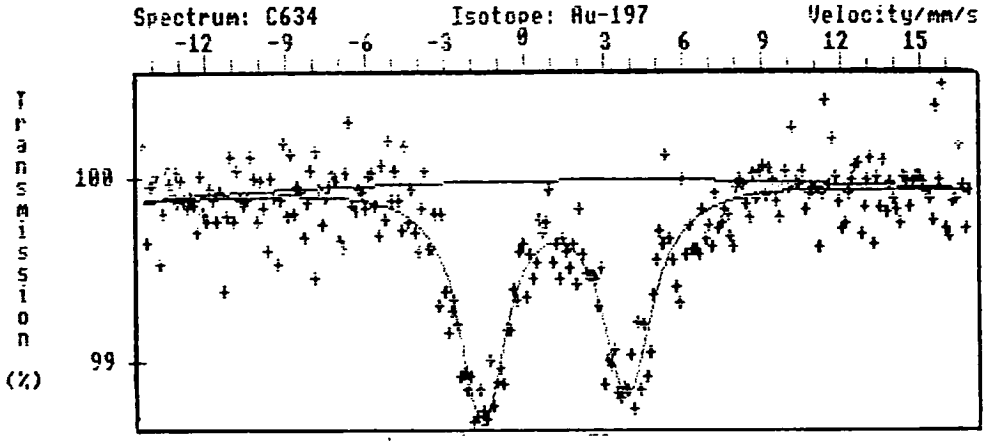

3.2.4 Electrochemical and e.p.r. studies of [Au([18]aneS$_6$)](PF$_6$)

Cyclic voltammetry of [Au([18]aneS$_6$)](PF$_6$) at platinum electrodes in MeCN (0.1M ^{n}Bu$_4$NPF$_6$) shows two quasi-reversible oxidations at $E^1_{1/2}$ = +0.36V (ΔE_p = 150 mV) and $E^2_{1/2}$ = +0.56V (ΔE_p = 60mV) (Figure 3.6) and an irreversible reduction at E_{pc} = -0.56V vs Fc/Fc$^+$ at a scan rate of 100mVs^{-1}. Coulometric measurements confirmed each process to be a one-electron transfer step.

Figure 3.6: Cyclic voltammogram of $[Au([18]aneS_6)](PF_6)$

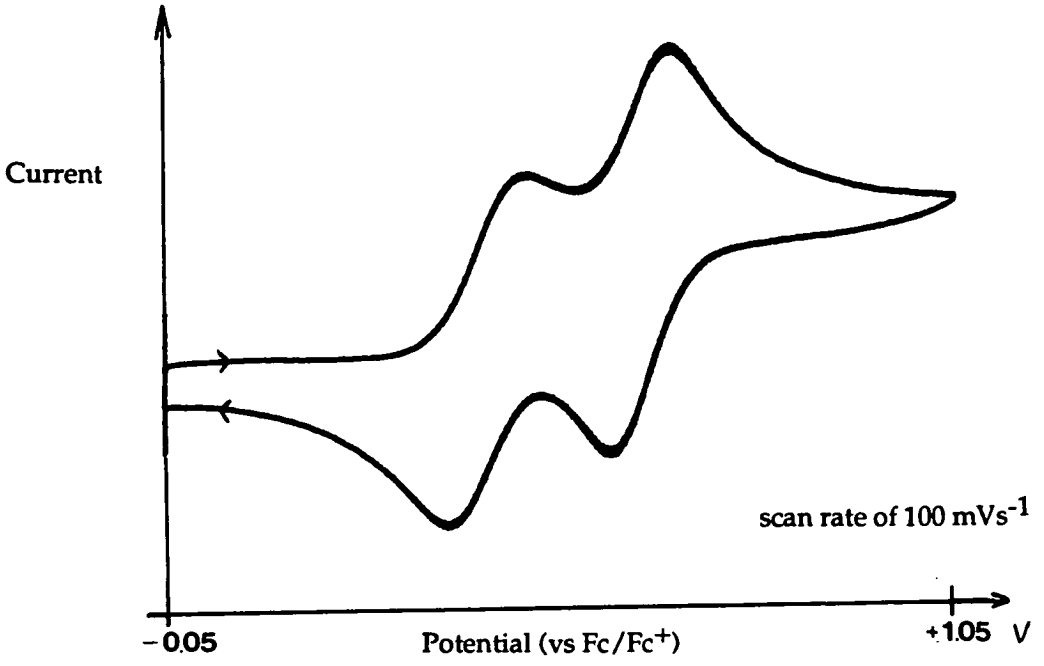

Electrogeneration of the first oxidation product at +0.45V vs Fc/Fc^+ affords a brown, e.p.r. active species. The frozen glass e.p.r. spectrum of the first oxidation product shows a strong anisotropic rhombic signal with g_1 = unresolved, $g_2 = 2.030$ ($A_2 = 62.3G$), $g_3 = 2.015$ ($A_3 = 62.3G$) (Figure 3.7). The signal is consistent with a distorted octahedral d^9 centre and is very similar to the signal obtained from $[Au([9]aneS_3)_2]^{2+}$ (Figure 2.8). Further spectral analysis is discussed in Section 3.2.9. The e.p.r. spectrum confirms that the first oxidation is largely metal-based producing a Au(II) species. Further oxidation of the Au(II) species at +0.65V produces an olive green, e.p.r. silent species, consistent with the second oxidation being metal-based, affording a Au(III) species. The irreversible reduction is assigned as a Au(I)/(0) couple. $[Au([18]aneS_6)]^+$ is very stable and exhibits facile redox behaviour.

Figure 3.7: X-band frozen glass e.p.r. spectrum of the first oxidation product of [Au([18]aneS$_6$)](PF$_6$)

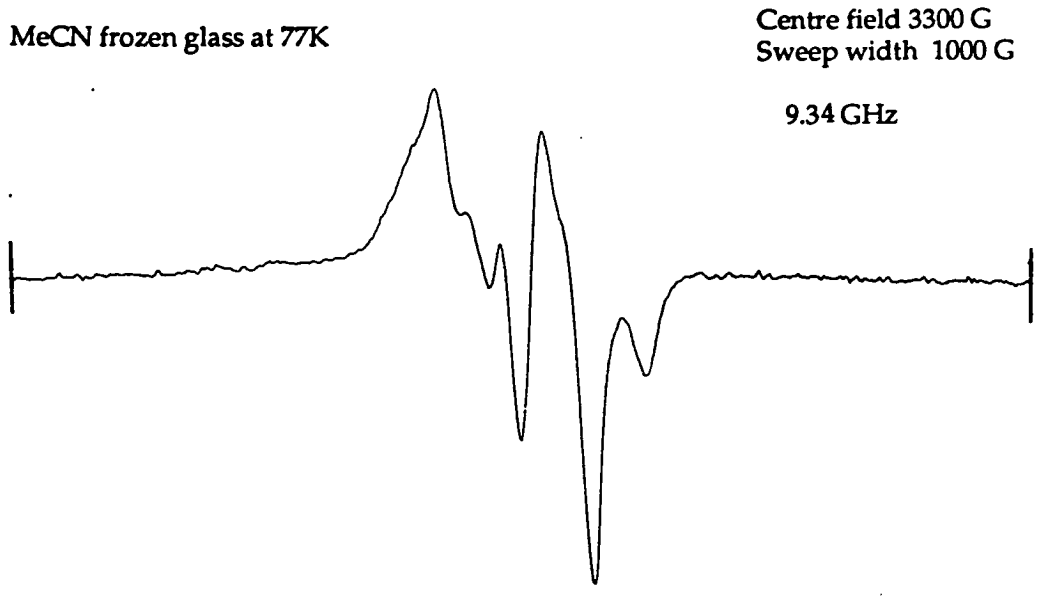

3.2.5 Spectroelectrochemical study of [Au([18]aneS$_6$)](PF$_6$)

The electrogeneration of the oxidation products of [Au([18]aneS$_6$)](PF$_6$) can be monitored by UV/Vis spectroscopy. The UV/Vis spectrum of [Au([18]aneS$_6$)]$^+$ in MeCN, at 253K is featureless. On the oxidation of Au(I) at +0.46V (vs Fc/Fc$^+$) a clear conversion to Au(II) (λ_{max} = 401 nm (ε_{max} = 7305 M^{-1}cm^{-1})) is observed (Figure 3.8). This oxidation occurs with isosbestic points at λ_{iso} = 263, 244, 205 nm, indicating the absence of any intermediate species. The Au(II) species can be further oxidised to a Au(III) product, λ_{max} = 341 nm (ε_{max} = 16740 M^{-1}cm^{-1}), 233 (13040), by increasing the applied potential to +0.78V (λ_{iso} = 524, 376, 207 nm) (Figure 3.9). Both of these oxidations are fully chemically reversible on this extended timescale.

Figure 3.8: Spectroelectrochemical study of $[Au([18]aneS_6)](PF_6)$ (oxidation of $[Au([18]aneS_6)]^{+}$ to $[Au([18]aneS_6)]^{2+}$)

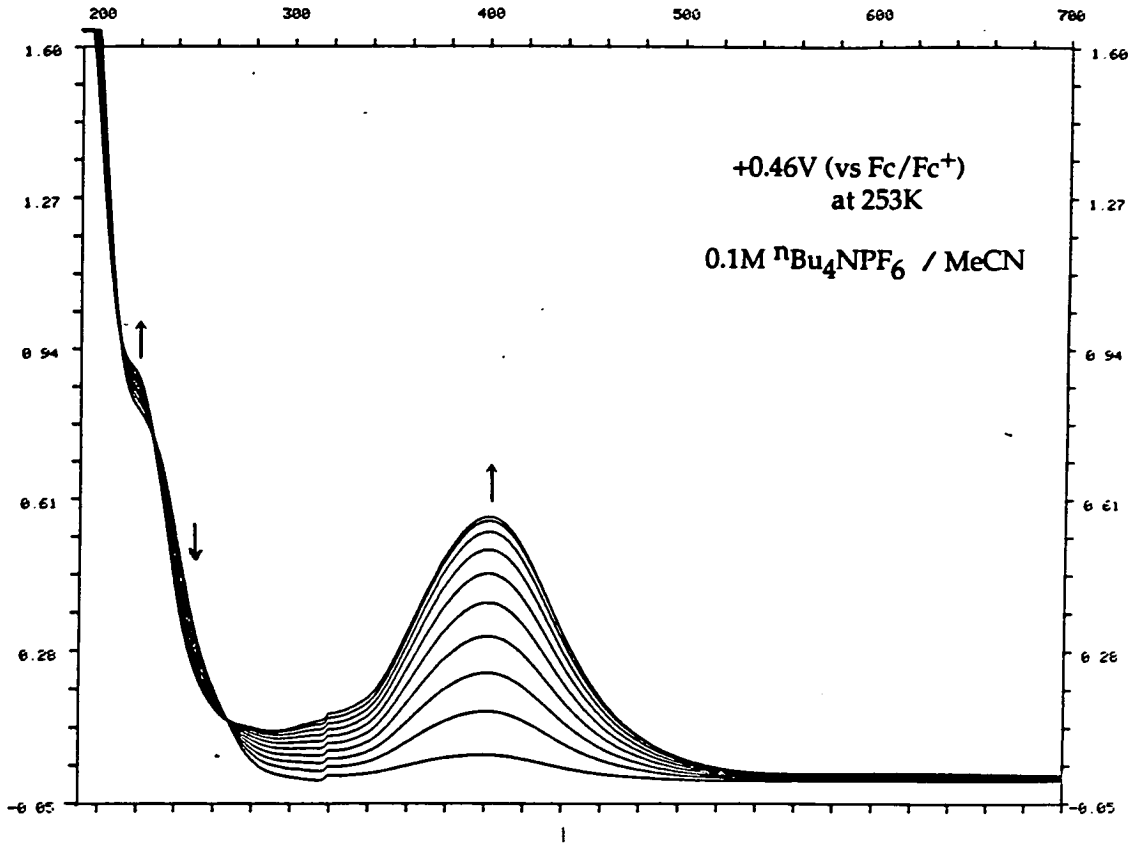

Figure 3.9: Spectroelectrochemical study of $[Au([18]aneS_6)](PF_6)$ (oxidation of $[Au([18]aneS_6)]^{2+}$ to $[Au([18]aneS_6)]^{3+}$)

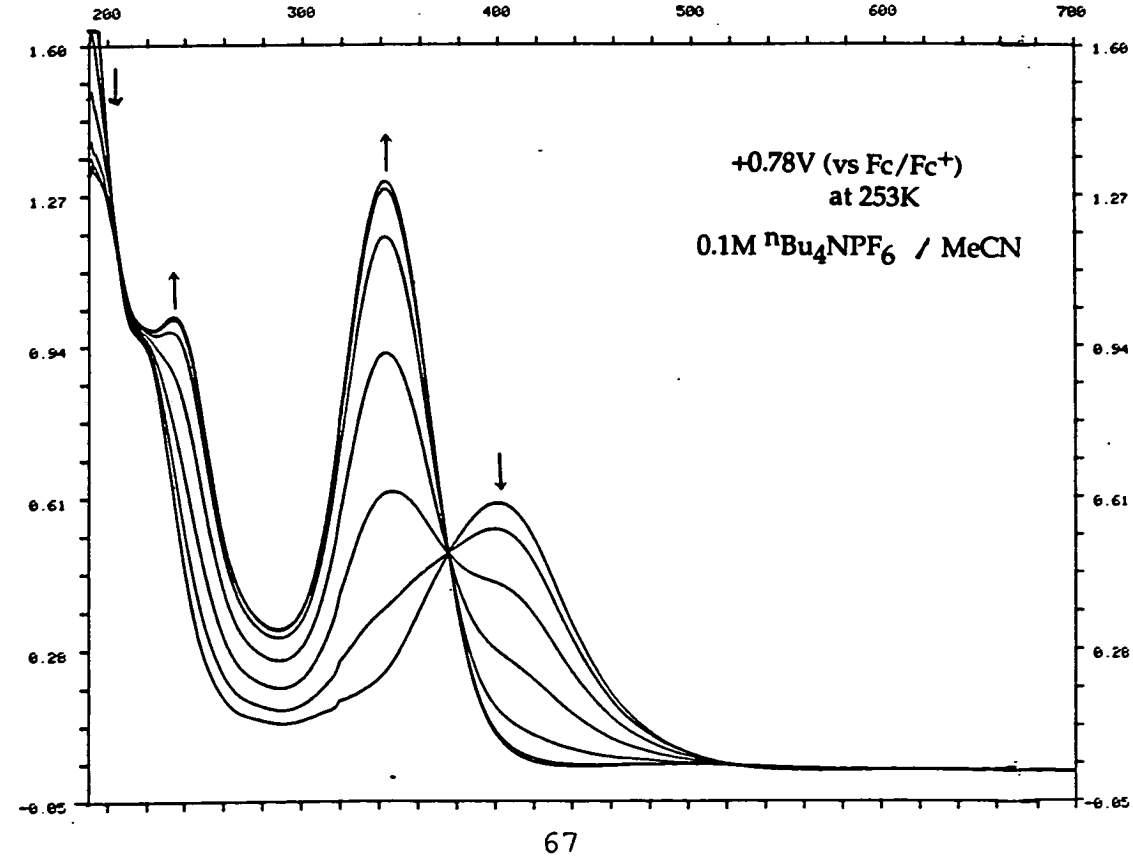

3.2.6 Kinetic study - Determination of the heterogeneous electron-transfer rate constant, k_s, for the $[Au([18]aneS_6)]^{+/2+}$ couple

(i) Introduction

For a given redox couple, the heterogeneous electron-transfer rate constant, k_s, describes the rate of the electron-transfer step for a simple electrode process, such as in (1)

$$O + ne^- \underset{}{\overset{k_s}{\rightleftharpoons}} R \qquad (1)$$

The degree of departure from the equilibrium situation observed in any electrochemical measurement of the redox couple depends on the time-scale of the measuring experiment. If the time-scale of the electron-transfer is very much shorter than the time-scale of the measuring technique, then the electrochemical equilibrium is maintained at the electrode surface. Such a process is regarded as being electrochemically reversible. If, however, the time-scale of the electron-transfer is greater than the time-scale of the measuring technique, then the redox process will exhibit significant kinetic behaviour, even if the redox process is chemically reversible. Such a process is regarded as being quasi-reversible.

Using cyclic voltammetry the kinetic behaviour of a quasi-reversible process can be studied applying the method reported by Nicholson.[222] The peak potential separation is measured as a function of scan rate, and the hetereogeneous electron-transfer rate constant, k_s can be calculated using equation (2):

$$k_s = \frac{\psi (\pi a Do)^{1/2}}{\gamma^{\alpha}} \qquad (2)$$

where $a = nF\nu / RT$

n = number of electrons

F = Faraday constant (96487 $Cmol^{-1}$)

ν = scan rate in Vs^{-1}

R = Universal gas constant (8.314 $CVK^{-1}mol^{-1}$)

T = temperature in K

D_o = diffusion coefficient in cm^2s^{-1}

$\gamma^{\alpha} = 1$

The value of ψ is obtained from the curve shown in Figure 3.10 and is dependent on the scan rate and is measured for a particular ΔE_p value.[222] The diffusion coefficient, D_o, is required for the particular system being studied. D_o is determined from the Levich equation (3), using a rotating disc electrode experiment.

$$i_l = 0.620\, nFAD_o^{2/3}\, \omega^{1/2}\, \varphi^{-1/6}\, C_o^{*} \qquad (3)$$

where i_l = limiting current

n = number of electrons

F = Faraday constant (96487 $Cmol^{-1}$)

A = area of electrode in cm^2

ω = angular frequency of rotation in s^{-1} (2π x rotation rate)

φ = kinematic viscosity in cm^2s^{-1} (absolute viscosity/density)

C_o^{*} = bulk concentration in $molcm^{-3}$

Figure 3.10: Graph of $\log_{10} \psi$ vs ΔE_p

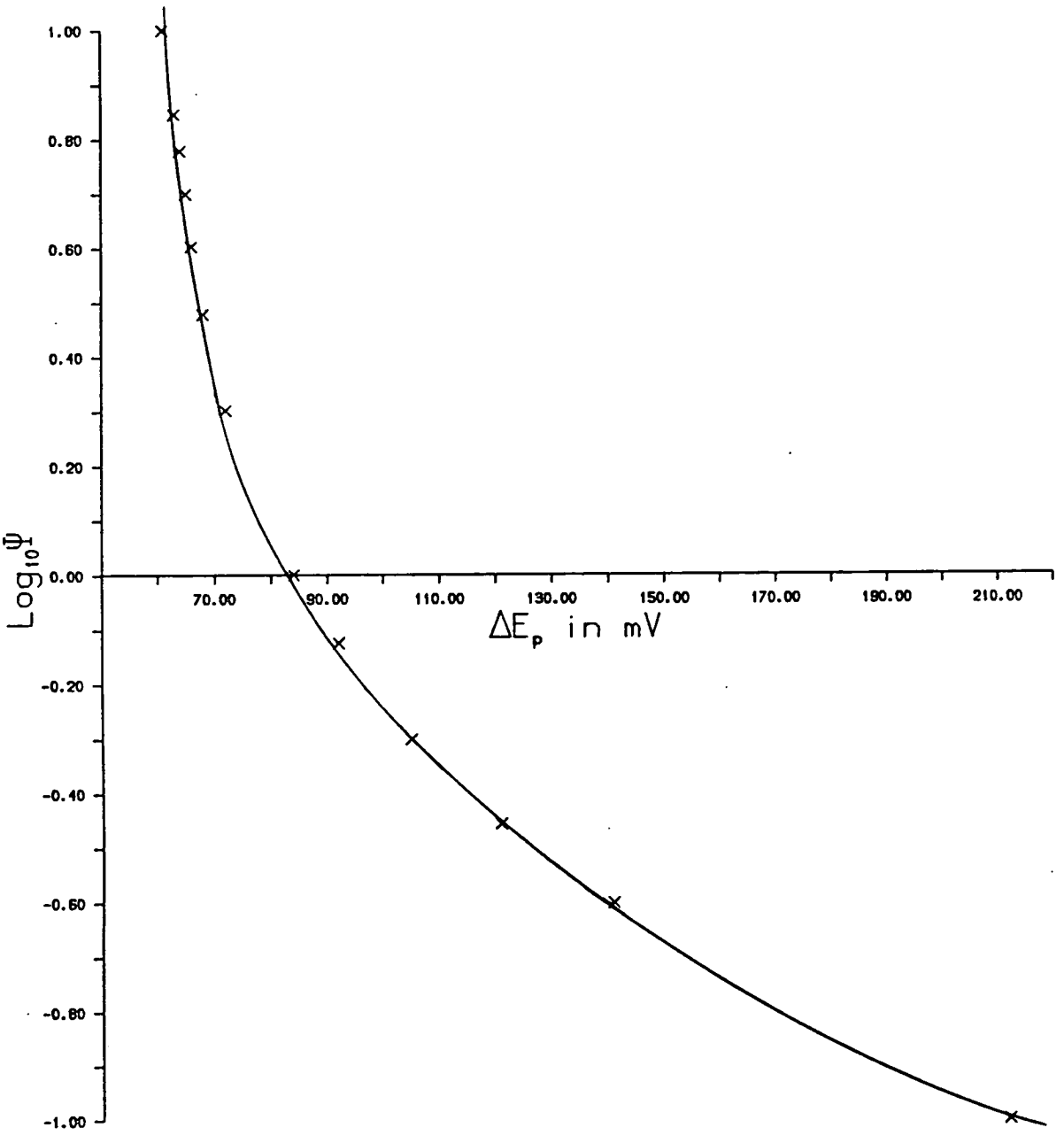

The value of D_O can be calculated from a graph in i_l vs $\omega^{1/2}$. Hence, the value of k_S for the particular redox process can be determined from a graph of ψ vs $\nu^{-1/2}$ (where ν = scan rate in Vs^{-1}).

(ii) Kinetic data for the [Au([18]aneS$_6$)]$^{+/2+}$ redox process

Cyclic voltammetric measurements on [Au([18]aneS$_6$)](PF$_6$) were carried out at platinum electrodes, in MeCN (0.1M $^nBu_4NPF_6$) at 283.0 K. Numerous scans were recorded over the potential range of +0.4V to +0.95V (vs Ag/AgCl), at various scan rates (ν = 10-400mVs^{-1}). These scans showed a variation of the peak separation for the Au(I)/Au(II) oxidation couple with scan rate. The internal resistance of the experimental set up must be compensated for, in order to obtain truly kinetically controlled variations in the peak separation. Therefore, a series of cyclic voltammetric measurements on [Fe(Cp)$_2$] were carried out using the identical solvent, temperature and electrode system. From these scans the required internal resistance compensation was evaluated, and then imposed upon the data recorded for the [Au([18]aneS$_6$)]$^{+/2+}$ couple. Using the method outlined in part (i) the value of k_S for the [Au([18]aneS$_6$)]$^{+/2+}$ process was determined.

Using the experimental (i.r. compensated) ΔE_p values, the values of ψ were obtained from the graph of $\log_{10}\psi$ vs ΔE_p shown in Figure 3.10.

The diffusion coefficient, D_O, for [Au([18]aneS$_6$)](PF$_6$) was calculated from the Levich equation (3) using the rotating disc electrode on the same solvent system. Plotting i_l vs $\omega^{1/2}$ (Figure 3.11a) for the first oxidation process gave a straight line with a slope of $(4.35 \pm 0.10) \times 10^{-5}$ corresponding to:-

$$\frac{i_l}{\omega^{1/2}} = 0.62\, nFAD_o^{2/3}\, \varphi^{-1/6}\, C_o^*$$

where $n = 1$

$F = 96487\ Cmol^{-1}$

$A = 0.385\ cm^2$

$\varphi = 4.4 \times 10^{-3}\ cm^2 s^{-1}$

$C_o^* = 1.85 \times 10^{-6}\ molcm^{-3}$

Therefore, the diffusion coefficient for $[Au([18]aneS_6)]^{+/2+}$ was calculated.

$$D_o = (8.4 \pm 0.3) \times 10^{-6}\ cm^2 s^{-1}$$

The graph of $\nu^{-1/2}$ vs ψ gave a straight line plot with a slope of 1.972 ± 0.033 (Figure 3.11b). The gradient equals:-

$$\frac{\nu^{-1/2}}{\psi} = \left\{\frac{\pi\, n\, F\, D_o}{RT}\right\}^{1/2} . k_s^{-1}$$

where $n = 1$

$F = 96487\ Cmol^{-1}$

$R = 8.314\ CV\ K^{-1}mol^{-1}$

$T = 283.0\ K$

$D_o = (8.4 \pm 0.3) \times 10^{-5}\ cm^2 s^{-1}$

$\Rightarrow \quad k_s = (26.8 \pm 1.0) \times 10^{-3}\ cms^{-1}$

Figure 3.11a: Graph of i vs $\omega^{1/2}$ for the [Au([18]aneS$_6$)]$^{+/2+}$ couple

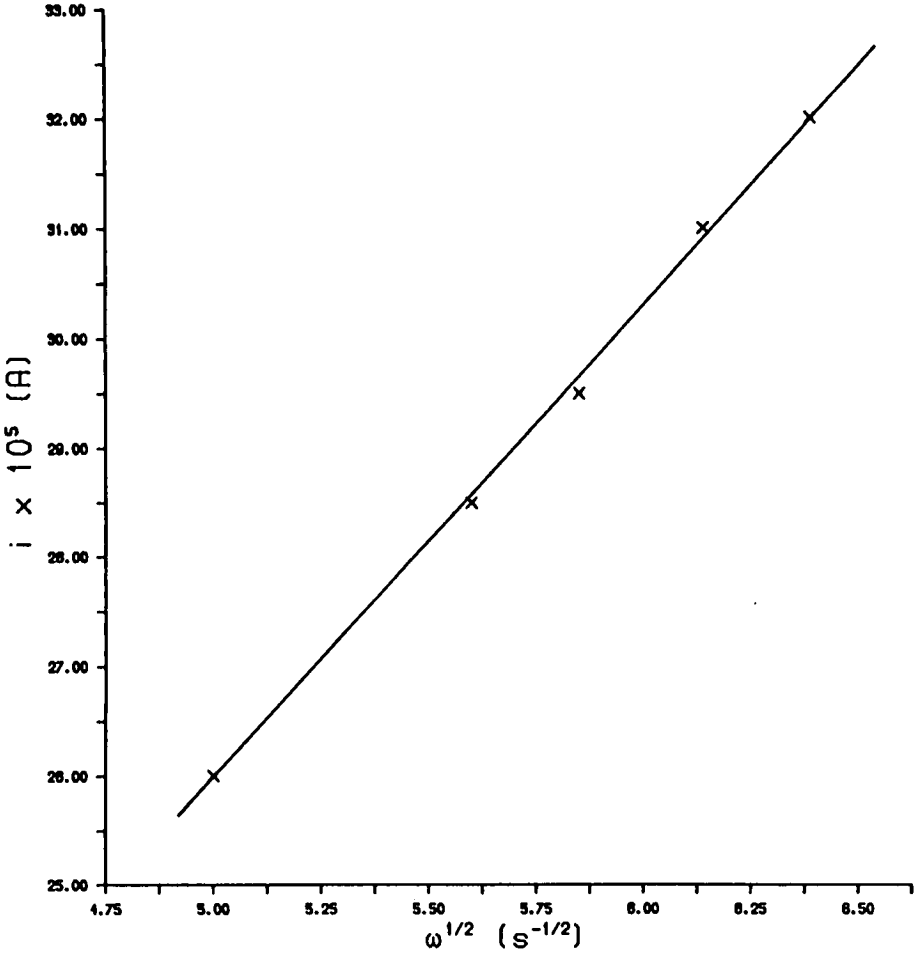

Figure 3.11b: Graph of $\nu^{1/2}$ vs ψ for the [Au([18]aneS$_6$)]$^{+/2+}$ couple

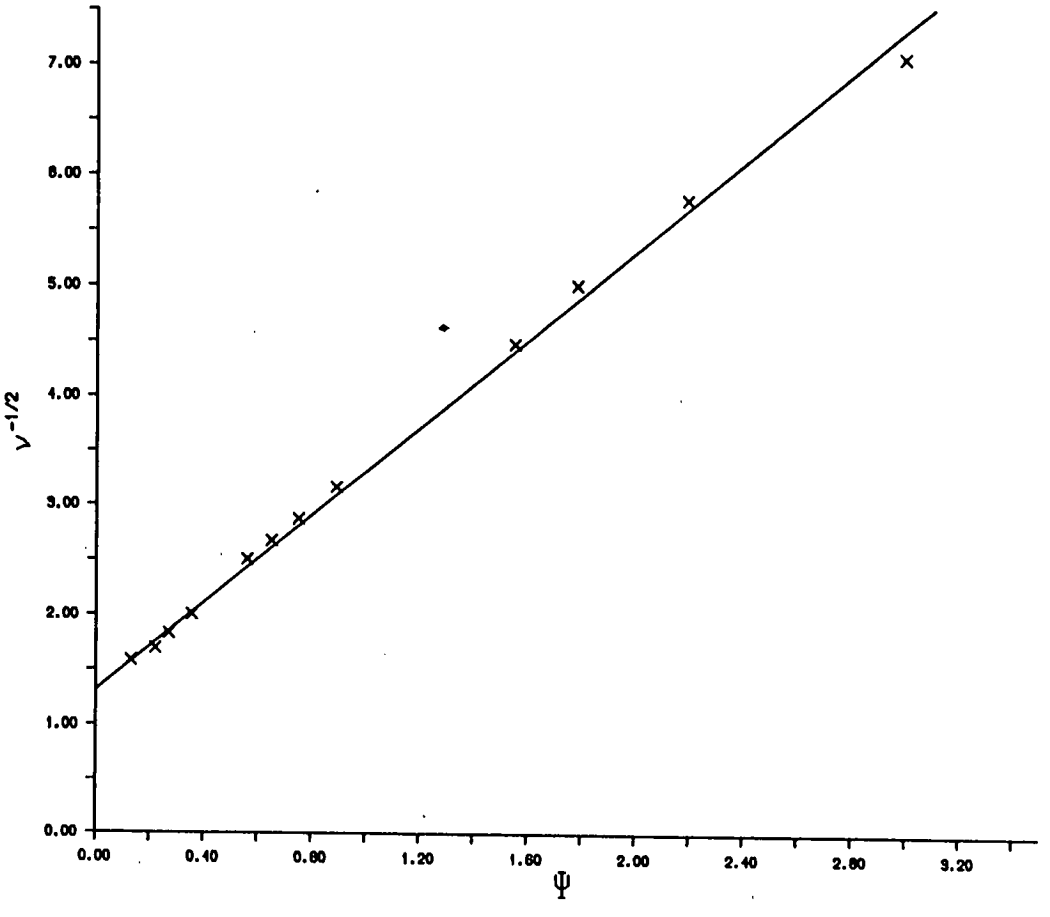

(ii) Conclusion

The fact that k_s, the heterogeneous electron-transfer rate constant, is measurable on the cyclic voltammetric time-scale indicates that the kinetic behaviour of the first oxidation process, the $[Au([18]aneS_6)]^{+/2+}$ couple, is significant. This is consistent with the occurrence of a gross stereochemical change which influences the rate of electron transfer.[223] A large stereochemical rearrangement of $[18]aneS_6$ is likely on the oxidation of Au(I) to Au(II), so that the structural and electronic preferences of both the d^{10} and d^9 ions can be satisfied.

The value of k_s for the second oxidation was not quantified due to the close proximity of the two oxidation potentials.

The kinetic behaviour observed for the first oxidation process, is consistent with the distorted tetrahedral Au(I) ion being oxidised to the expected distorted octahedral Au(II) (Figure 3.12). $[18]aneS_6$ is sufficiently flexible to exist in these co-ordination modes. In $[Au([18]aneS_6)]^+$ and $[Cu([18]aneS_6)]^{2+}$ distorted tetrahedral and tetragonally elongated octahedral[34] geometries are contained within $[18]aneS_6$. In order to confirm the co-ordination of the Au(II) ion, the $[Au([18]aneS_6)]^{2+}$ species was synthesised.

Figure 3.12: Proposed structure of $[Au([18]aneS_6)]^{2+}$

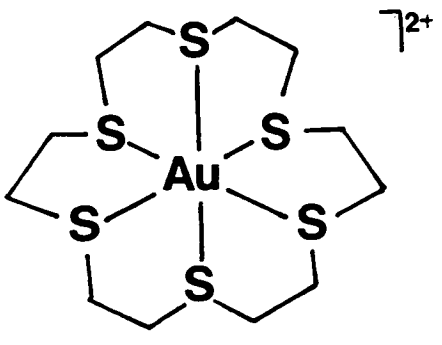

3.2.7 Synthesis and characterisation of $[Au([18]aneS_6)](PF_6)_2$

The reaction of $[18]aneS_6$ with one molar equivalent of $HAuCl_4$ in $MeNO_2$ gave a red solution. Addition of NH_4PF_6 produced a brown mixture containing a white precipitate of NH_4Cl. The filtered brown solution afforded an orange-brown precipitate on addition of Et_2O. The orange-brown solid was isolated and stored at -20°C. The f.a.b. mass spectrum of the complex shows peaks at $M^+ = 702$, 577 corresponding to $[^{197}Au([18]aneS_6)PF_6]^+$ and $[^{197}Au([18]aneS_6)]^+$ respectively. I.r. spectral and micro-analytical data were consistent with the formulation $[Au([18]aneS_6)](PF_6)_2$. Full experimental details are given in Section 3.4.3. The complex dissolves in MeCN to give a golden brown solution; the electronic spectrum shows a band at $\lambda_{max} = 401$ nm ($\varepsilon_{max} = 7300\ M^{-1}cm^{-1}$) similar to the spectrum obtained for the first oxidation product of $[Au([18]aneS_6)]^+$.

Numerous attempts to grow single crystals suitable for an X-ray crystallographic structure determination were unsuccessful. Using Et_2O vapour diffusion and hexane layering methods on solutions (e.g. MeCN, $MeNO_2$, Me_2CO) of the compound, both at ambient and lower temperatures lead to decomposition to Au(I) or metallic or colloidal gold. Stabilisation of the Au(II) complex in various dilute acids or the HBF_4-Et_2O solution lead to decomposition or polymeric materials. Therefore, other techniques were employed to elucidate the co-ordination of the Au(II) centre within the $[18]aneS_6$ ligand framework.

3.2.8 ^{197}Au Mössbauer spectroscopic data for [Au([18]aneS$_6$)](PF$_6$)$_2$

The ^{197}Au Mössbauer spectrum for [Au([18]aneS$_6$)](PF$_6$)$_2$ is similar in shape to that obtained for [Au([9]aneS$_3$)$_2$](BF$_4$)$_2$. The same model was used to fit the data (Figure 3.13). Unfortunately, there was a Au(I) impurity in the sample used in the experiment due to degradation of the [Au([18]aneS$_6$)](PF$_6$)$_2$ complex. The model fitting gave values of I.S. = 0(0.3) mms^{-1}, Q.S. = +1.0 (0.4)mms^{-1} and B = 10(5)T. Due to the lack of comparable Au(II) Mössbauer data, it was difficult to interpret these values.

Figure 3.13: ^{197}Au Mössbauer spectrum for [Au([18]aneS$_6$)](PF$_6$)$_2$

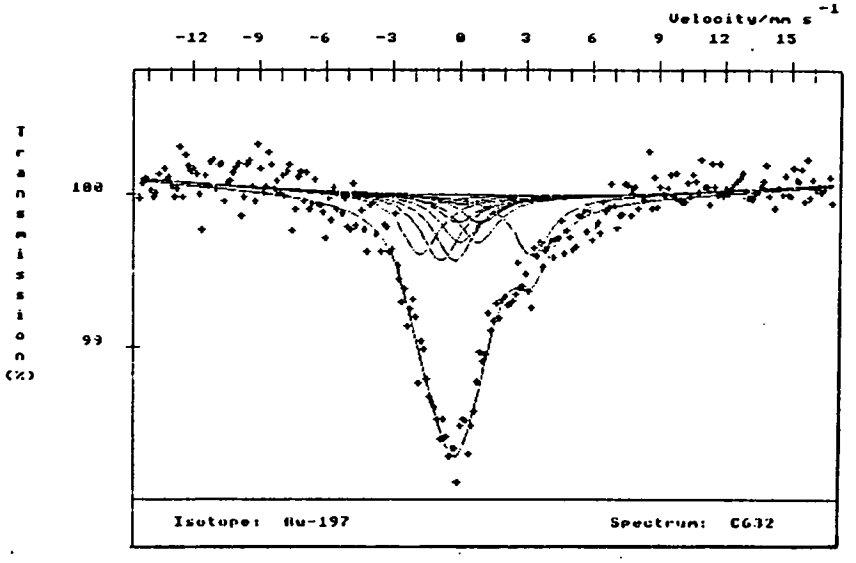

3.2.9 E.p.r. studies of [Au([18]aneS$_6$)]$^{2+}$

[Au([18]aneS$_6$)]$^{2+}$ is e.p.r. active and gives spectra similar to those recorded for [Au([9]aneS$_3$)$_2$]$^{2+}$. The solution e.p.r. spectrum of [Au([18]aneS$_6$)]$^{2+}$ in $MeNO_2$ at 293 K shows an isotropic signal with g_{iso} = 2.026 with hyperfine coupling to ^{197}Au (I = 3/2, 100%) producing a four-line signal with A_{iso} = 45.6G (Figure 3.14).

Figure 3.14: X-band solution e.p.r. spectrum of [Au([18]aneS$_6$)](PF$_6$)$_2$

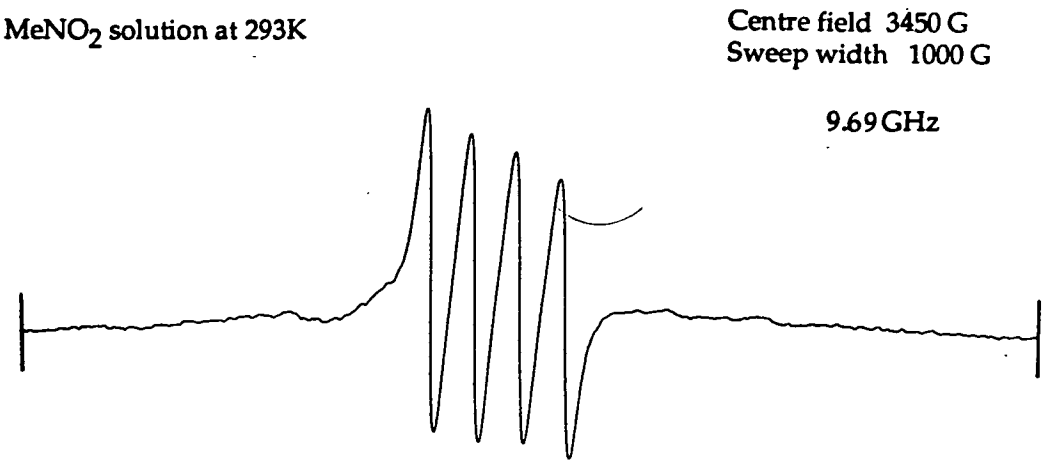

The X-band frozen glass e.p.r. spectrum of [Au([18]aneS$_6$)]$^{2+}$ in MeCN, with a ^{n}Bu$_4$NPF$_6$ dilutant, at 77K shows an anisotropic signal (Figure 3.15). The spectrum was initially assigned using the second derivative as a simple rhombic signal with $g_1 = 2.033$ ($A_1 = 12.0$G), $g_2 = 2.030$ ($A_2 = 62.3$G), $g_3 = 2.015$ ($A_3 = 62.3$G). Attempted simulation, using g and A tensor parameters only, did not reproduce the experimental spectrum (Figure 3.16). Clearly, as for [Au(9]aneS$_3$)$_2$]$^{2+}$, the effects of the quadrupole and nuclear Zeeman interactions are significant in the [Au([18]aneS$_6$)]$^{2+}$ species. Therefore complete assignment of the anisotropic signal was not possible at this stage.

The resemblance of the [Au([18]aneS$_6$)]$^{2+}$ spectrum to that obtained for [Au([9]aneS$_3$)$_2$]$^{2+}$ implies similar co-ordination at the Au(II) centres. The minimal shift of the g values from g_e indicates covalent character of the Au-S bonds as discussed in Section 2.2.6.

Figure 3.15: X-band frozen glass e.p.r. spectrum of [Au([18]aneS$_6$)](PF$_6$)$_2$ with $^nBu_4NPF_6$

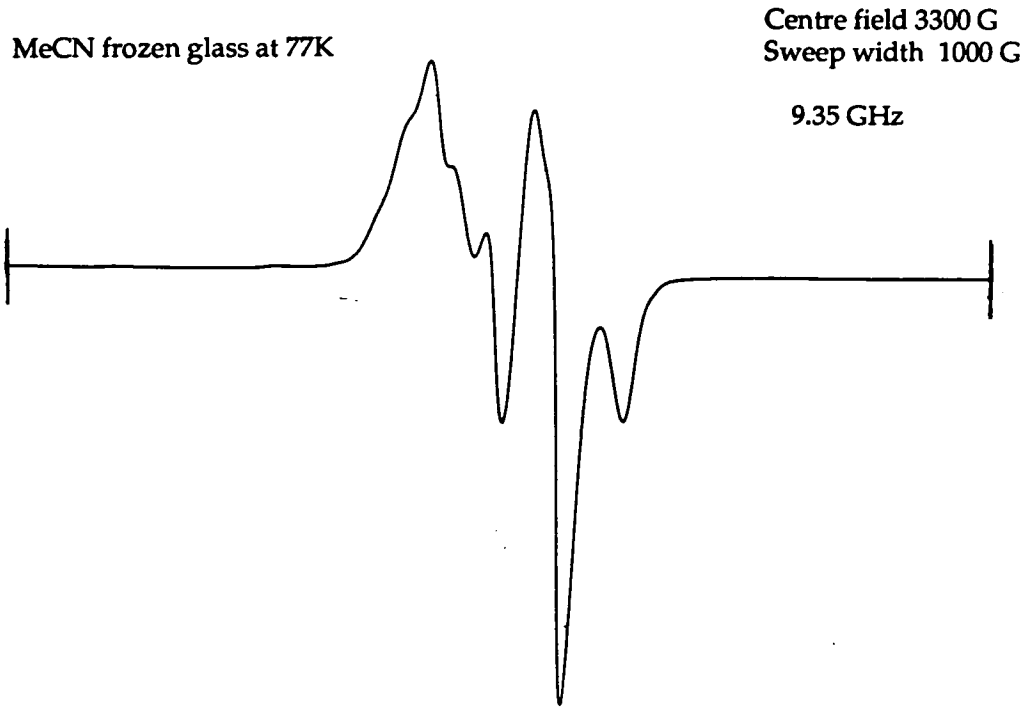

Figure 3.16: Simulated e.p.r. spectrum for [Au([18]aneS$_6$)](PF$_6$)$_2$

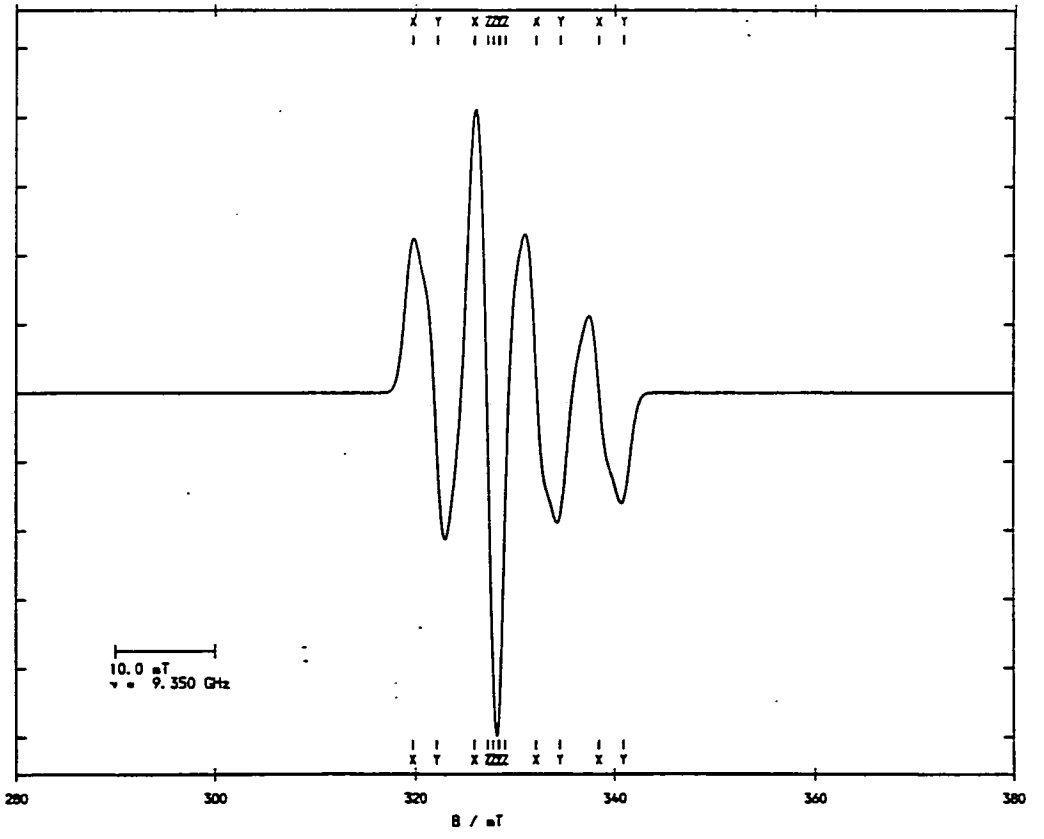

3.3 CONCLUSIONS

The hexadentate thioether macrocycle [18]aneS_6 can stabilise Au(I)/Au(II)/Au(III) centres. This ligand binds Au(I) in a distorted tetrahedral geometry to form a stable mononuclear product. The stable mononuclear Au(II) complex, [Au([18]aneS_6)]$(PF_6)_2$, was isolated. Comparison of the electronic and e.p.r. spectroscopic data imply similar co-ordination spheres about the Au(II) centres in $[Au([18]aneS_6)]^{2+}$ and $[Au([9]aneS_3)_2]^{2+}$. The proposed distorted octahedral geometry of $[Au([18]aneS_6)]^{2+}$ is substantiated by the kinetic study, which indicated that a gross stereochemical change is occurring on the oxidation of Au(I) to Au(II).

The redox behaviour of [Au([18]aneS_6)](PF_6) reflects the dexterity of [18]aneS_6, enabling the successful accommodation of the various structural and electronic preferences of the d^8, d^9 and d^{10} metal centres.

The relative stabilities of $[Au([18]aneS_6)]^{n+}$ differ from those of $[Au([9]aneS_3)_2]^{n+}$ (n = 1,2,3). In $[Au([18]aneS_6)]^{+}$, the encapsulation of Au(I) within the macrocycle enhances the protection of the metal centre; hence the increased stability of $[Au([18]aneS_6)]^{+}$ in comparison to $[Au([9]aneS_3)_2]^{+}$.

$[Au([18]aneS_6)]^{2+}$ is less stable than its [9]aneS_3 analogue; suggesting that the co-ordination environment about the Au(II) centre is more strained in $[Au([18]aneS_6)]^{2+}$ than in $[Au([9]aneS_3)_2]^{2+}$.

The greater stability of $[Au([9]aneS_3)_2]^{3+}$ in comparison to $[Au([18]aneS_6)]^{3+}$ is reflected in the Au(II)/(III) oxidation potentials for the two complexes, $E_{1/2}$ = +0.44V, +0.56V respectively. The enhanced stabilisation of Au(III) by $[9]aneS_3$ may be due to a greater interaction of the ligating S-donors in a less strained geometry than is available in $[18]aneS_6$.

3.4 EXPERIMENTAL SECTION

3.4.1 Synthesis of $[Au([18]aneS_6)](PF_6)$

Reaction of $[18]aneS_6$ (40 mg, 0.111 mmol) with $[Au(tht)_2](PF_6)$ (57.5 mg, 0.111 mmol) in stirring MeCN (7 cm^3) for 2hrs., in the dark gives a colourless solution. Filtration into ice-cold Et_2O (40 cm^3) afforded a white precipitate on cooling to -20°C. The product was filtered and washed with Et_2O and CH_2Cl_2 yielding a crystalline white solid. Dried *in vacuo*, stored at -20°C. (Yield 63 mg, 81%). M.Wt. = 702.64. Elemental analyses: found C = 20.5, H = 3.37, S = 27.9%. Calc. for $C_{12}H_{24}S_6Au_1P_1F_6$: C = 20.5, H = 3.44, S = 27.4%. I.r. spectrum (KBr disc): 2950, 2910, 2850, 1430, 1415, 1300, 1290, 1260, 1200, 1190, 1180, 1150, 1120, 1020w, 930, 920, 880, 840, 740w, 690w, 630w and 560 cm^{-1}. F.a.b. mass spectrum (3-NOBA matrix) : found M^+ = 557. Calc. for $[^{197}Au([18]aneS_6)]^+$: M^+ = 557, with correct isotopic distribution. ^1H n.m.r. (CD_3CN, 298K, 80.13 MHz): δ = 2.91-3.01 ppm.; (CD_3CN, 223K, 200.13 MHz): δ = 2.91-3.01 ppm.. ^{13}C n.m.r. (CD_3CN, 223K, 50.32MHz): δ = 30.094 p.p.m..

3.4.2 Single crystal structure determination of [Au([18]aneS$_6$)](PF$_6$)

A colourless plate (0.50 x 0.30 x 0.05 mm) suitable for X-ray analysis was obtained by vapour diffusion of Et_2O into a solution of the complex in MeCN.

Crystal data:

$[C_{12}H_{24}S_6Au]^+ (PF_6)^-$, M.Wt. = 702.56, triclinic, space group $P\bar{1}$, a = 9.7537(15), b = 11.0127(17), c = 11.2005(21)Å, α = 79.235(9), β = 75.344(8), γ = 75.582(9)°, U = 1117.4 Å^3 [from 2θ values of 36 reflections measured at ± ω (26< 2θ < 30°, λ = 0.71073Å)] Z = 2, D_c = 2.088 gcm^{-3}, T = 298 K, μ = 7.226 mm^{-1}, F (000) = 680.

Data collection and processing:

Stoë STADI-4 four circle diffractometer, graphite-monochromated Mo-K_α X-radiation, T = 298 K, ω - 2θ scans with ω scan width (0.80 + 0.347 tan θ)°, 2845 data measured ($2\theta_{max}$ 45°, h -9→10, k -11→11, l 0→12, giving 2536 with $F \geq 6\ \sigma(F)$ for use in all calculations. Initial absorption corrections were made using ψ scans (maximum transmission factor = 0.2490, minimum = 0.0722).

Structure solution and refinement:

A Patterson synthesis located the Au atom and iterative cycles of least-squares refinement and difference Fourier synthesis located the remaining non-hydrogen atoms. At isotropic convergence, corrections (min 0.582, max 1.496) for absorption were applied using DIFABS.[308] Disorder in a part of the unco-ordinated section of the macrocycle was modelled by half occupancy of two conformations, with the C-C bond lengths fixed. Refinement (by least-squares on F[309]) with anisotropic thermal parameters for all ordered non-hydrogen atoms and with hydrogen atoms in fixed,

calculated positions converged at R, R_w = 0.0547, 0.0697 respectively, S = 0.991 for 243 refined parameters, and the final ΔF synthesis showed no feature above 1.39eÅ^{-3}. The weighting scheme, $w^{-1} = \sigma^2(F) + 0.000229F^2$, gave satisfactory agreement analyses and in the final cycle $(\Delta/\sigma)_{max}$ was 0.026.

Atomic scattering factors were inlaid[310] except for gold,[311] molecular geometry calulations utilised CALC[312] and figures were produced by ORTEPII.[313]

3.4.3 Synthesis of [Au([18]aneS$_6$)](PF$_6$)$_2$

To a stirring degassed solution of [18]aneS$_6$ (80 mg, 0.222 mmol) in $MeNO_2$ (7 cm^3), a $MeNO_2$ solution of $HAuCl_4$ (75.5 mg, 0.222 mmol) was added. Resultant red solution turned brown on the addition of excess of NH_4PF_6. Schlenk filtration of the mixture produced a clear brown filtrate, which afforded an orange-brown precipitate on the addition of degassed Et_2O (30 cm^3). Schlenk filtration gave the desired product, which was stored at -20°C. (Yield 98 mg, 52%). M.Wt. = 847.61. Elemental analyses: found C = 17.2, H = 2.90, N = 0.2%. Calc. for $C_{12}H_{24}S_6Au_1P_2F_{12}$: C = 17.0, H = 2.83% I.r. spectrum (KBr disc): 2980, 2915, 1550, 1425, 1400, 1375, 1290, 1260, 1205, 1140, 1110w, 1030, 935, 840 820, 740w, 690w, 660, 560 and 485 cm^{-1}. F.a.b. mass spectrum (3-NOBA matrix) : found M^+ = 702, 577. Calc. for [^{197}Au([18]aneS$_6$)]$^+$: M^+ = 577. UV/Vis spectrum (MeCN) : λ = 403.2 nm (ε_{max} = 7205 M^{-1}cm^{-1}).

CHAPTER 4

Gold complexes of [15]aneS$_5$

4.1 INTRODUCTION

Stabilisation of gold centres in the +1, +2, and +3 oxidation states can be achieved when sufficient S-donors are available to satisfy the electronic and stereochemical demands of the d^{10}, d^9 and d^8 ions. (Chapters 2 and 3) In general, if a ligand donor set cannot fulfil the precise stereochemical preferences of a metal centre, the resultant complex may exhibit a strained stereochemistry and / or unusual redox behaviour.[14] (see Section 1.1.(d))

The aim of the work discussed in this Chapter was to synthesise gold complexes of [15]aneS_5, with a view to examining how the binding of a macrocycle with fewer S-donors and a smaller cavity affects the co-ordination at the gold centre. The redox behaviour was studied to establish if [15]aneS_5 could stabilise Au(II) and Au(III) centres.

4.2 RESULTS AND DISCUSSION

4.2.1 Synthesis and characterisation of [Au([15]aneS_5)](X)

{X = PF_6^-, ($B(C_6F_5)_4^-$)}

Reaction of [Au(tht)$_2$](PF_6) with one molar equivalent of [15]aneS_5 in stirring, degassed CH_2Cl_2 affords a colourless solution. Filtration into Et_2O yields a white precipitate. The isolated solid was recrystallised from MeCN and Et_2O. The product gave a f.a.b. mass spectral peak at $M^+ = 497$, corresponding to $[^{197}Au([15]aneS_5)]^+$. On the basis of this evidence together with i.r. spectroscopic and microanalytical data the product was

assigned as [Au([15]aneS$_5$)](PF$_6$). Full experimental details are given in Section 4.4.1.

The [BPh$_4^-$] salt could not be isolated due to the reductive nature of [BPh$_4^-$], (Cyclic voltammetry of NaBPh$_4$ shows an accessible irreversible oxidation at E_{pc} = +0.54V vs Fc/Fc$^+$) this causes the reduction of Au(I) to colloidal gold. However, the related [B(C$_6$F$_5$)$_4^-$] anion shows no accessible oxidation. [Au([15]aneS$_5$)](PF$_6$) was redissolved in CH_2Cl_2, and Li(B(C$_6$F$_5$)$_4$) added. The solution was stirred for 15 mins. and filtration into hexane produced a dense white suspension. The white product was isolated after centrifugation and any excess Li(B(C$_6$F$_5$)$_4$) removed by washing with H_2O. The product shows f.a.b. mass spectral peaks at M^+ = 693, 497 corresponding to [^{197}Au$_2$([15]aneS$_5$-H)]$^+$ and [^{197}Au([15]aneS$_5$)]$^+$ respectively. On this basis, together with i.r. spectroscopic and microanalytical data the empirical formula of the product was assigned as [Au([15]aneS$_5$)](B(C$_6$F$_5$)$_4$). Full experimental details are given in Section 4.4.3.

Initially it was believed that the mononuclear [Au([15]aneS$_5$)]$^+$ cation would have a [2+2] distorted tetrahedral geometry at Au(I), similar to the co-ordination at Au(I) in [Au([18]aneS$_6$)]$^+$ (Section 3.2.2). However due to the smaller ring size of [15]aneS$_5$ compared to [18]aneS$_6$ the distortion at Au(I) in [Au([15]aneS$_5$)]$^+$ was expected to be greater than in the [18]aneS$_6$ analogue. To establish the stereochemistry and ascertain the extent of the distortion at Au(I), an X-ray structure determination was required. Repeated attempts to grow single crystals of [Au([15]aneS$_5$)](PF$_6$), using vapour diffusion methods, generally produced colloidal gold and a green solution. Interestingly, it appeared the disproportionation of Au(I) was occurring.

Eventually, single crystals of the $[B(C_6F_5)_4^-]$ salt were obtained by hexane layering on to a CH_2Cl_2 solution of the complex.

4.2.2 Structure determination of $[Au([15]aneS_5)](B(C_6F_5)_4)$

A single crystal X-ray determination on $[Au([15]aneS_5)](B(C_6F_5)_4)$ was carried out. Full details of the solution and refinement of the structure are given in Section 4.4.4. The crystal structure shows the complex is actually a **dimeric** species in the solid-state. The two monomeric units are related by a crystallographic inversion centre. Each Au(I) centre is bound to both $[15]aneS_5$ ligands through one S-donor, Au - S(1) = 2.3001(13), Au - S(10') = 2.2927(13)Å but the Au(I) is encapsulated by neither ring. In fact the ligands are sandwiching the metal ions in a facial manner. Free $[15]aneS_5$ adopts an *exo* conformation in the solid-state.[78] Despite co-ordinating the Au(I) centre in an exocyclic manner, the bound $[15]aneS_5$ adopts an *endo* conformation with the S-donors orientated towards the centre of the dication (Figure 4.1). The two nearest S-donors (excluding those involved in the primary co-ordination) to the Au(I) centre are S(4) and S(13) at 3.2088(14) and 3.1055(13)Å respectively. Selected bonds, angles and torsions are given in Table 4.1. The Au...Au separation is 5.694(8)Å suggesting that the metal centres are non-interacting. The major angle at the metal centre, S(1) - Au - S(10'), is 169.90(5)Å, indicating that these additional S-donors are interacting weakly, causing the deviation from linearity at Au(I). By considering these additional S-donors as being involved in long-range Au...S interactions, [2+2] distorted tetrahedral co-ordination at the Au(I) centre is completed. However, it is apparent that their contribution to the co-ordination sphere about the Au(I) is significantly reduced in comparison

Figure 4.1: Single crystal X-ray structure of [Au([15]aneS$_5$)](B(C$_6$F$_5$)$_4$)

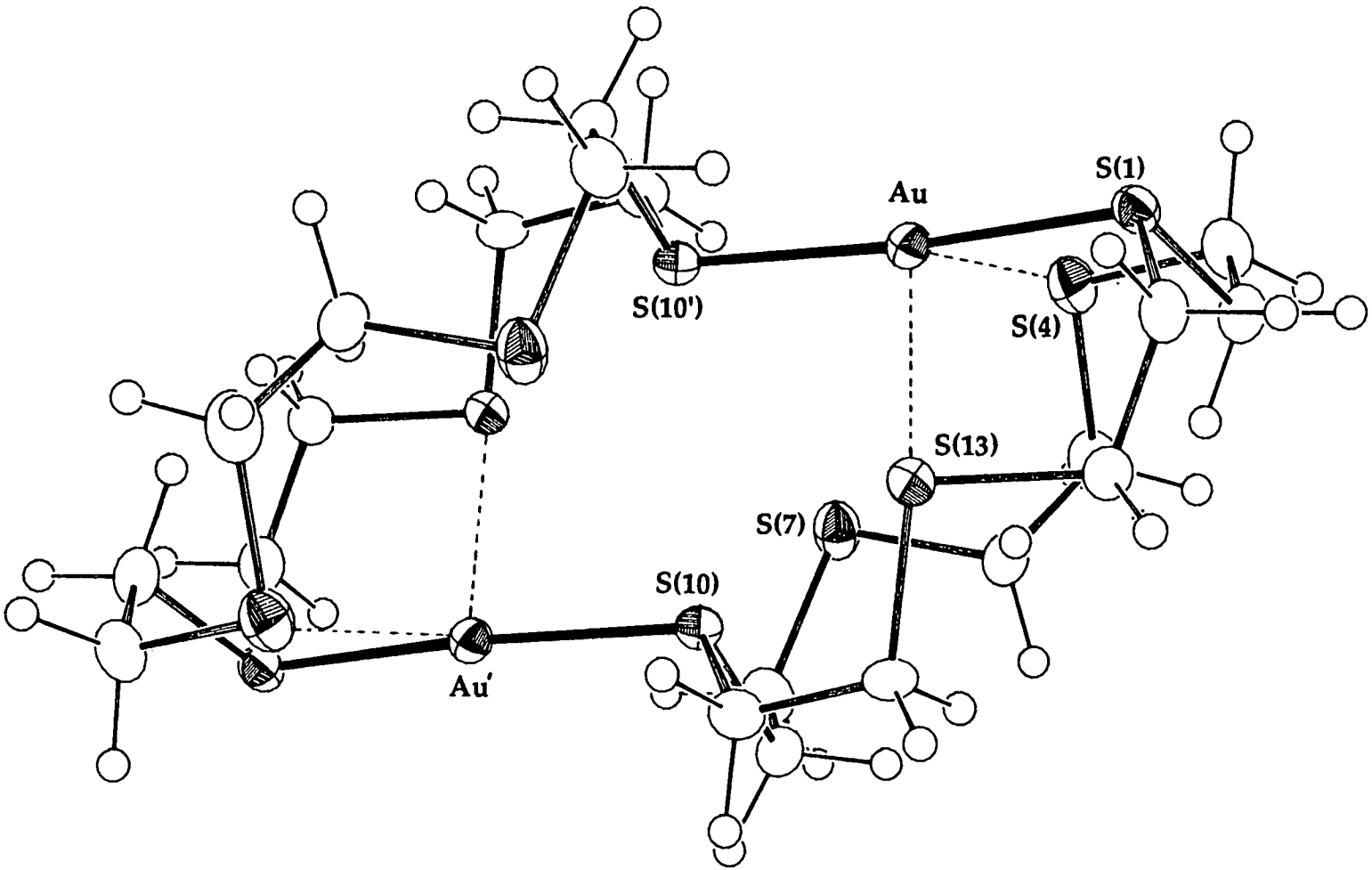

Table 4.1: Selected bonds, angles and torsions for [Au([15]aneS$_5$)](B(C$_6$F$_5$)$_4$)

Au	- S(1)	2.3001(13)	C(6)	- S(7)	1.809(6)
Au	- S(4)	3.2088(14)	S(7)	- C(8)	1.818(5)
Au	-S(13)	3.1055(13)	C(8)	- C(9)	1.524(7)
Au	-S(10')	2.2927(13)	C(9)	-S(10)	1.824(5)
S(1)	- C(2)	1.822(5)	S(10)	-C(11)	1.824(5)
S(1)	-C(15)	1.812(5)	C(11)	-C(12)	1.523(7)
C(2)	- C(3)	1.520(7)	C(12)	-S(13)	1.822(5)
C(3)	- S(4)	1.814(5)	S(13)	-C(14)	1.808(5)
S(4)	- C(5)	1.818(6)	C(14)	-C(15)	1.531(7)Å
C(5)	- C(6)	1.520(8)			

S(1)	- Au -	S(4) 78.66(4)	C(5)	- C(6) - S(7)	110.1(4)
S(1)	- Au -S(13)	81.67(4)	Au	- S(7) - C(6)	73.62(18)
S(1)	- Au -S(10')	169.90(5)	Au	- S(7) - C(8)	122.55(18)
S(4)	- Au -S(13)	122.46(4)	C(6)	- S(7) - C(8)	99.8(3)
S(4)	- Au -S(10')	111.04(4)	S(7)	- C(8) - C(9)	114.2(4)
S(10)	- Au -S(13)	53.24(3)	C(8)	- C(9) -S(10)	109.3(3)
S(13)	- Au -S(10')	94.79(4)	Au	-S(10) - C(9)	113.29(16)
Au	- S(1) - C(2)	106.20(17)	Au	-S(10) -C(11)	102.98(16)
Au	- S(1) -C(15)	107.41(18)	C(9)	-S(10) -C(11)	99.88(23)
C(2)	- S(1) -C(15)	101.47(24)	S(10)	-C(11) -C(12)	109.8(3)
S(1)	- C(2) - C(3)	109.2(4)	C(11)	-C(12) -S(13)	111.1(3)
C(2)	- C(3) - S(4)	115.5(4)	Au	-S(13) -C(12)	125.42(17)
Au	- S(4) - C(3)	88.03(18)	Au	-S(13) -C(14)	89.73(17)
Au	- S(4) - C(5)	111.06(20)	C(12)	-S(13) -C(14)	98.85(23)
C(3)	- S(4) - C(5)	100.4(3)	S(13)	-C(14) -C(15)	112.1(3)
S(4)	- C(5) - C(6)	113.5(4)	S(1)	-C(15) -C(14)	117.4(4)°

C(15)	- S(1) - C(2) - C(3)	-178.5(4)	S(7)	- C(8) - C(9) -S(10)	-56.2(4)
C(2)	- S(1) -C(15) -C(14)	64.2(4)	C(8)	- C(9) -S(10) -C(11)	176.5(4)
S(1)	- C(2) - C(3) - S(4)	75.8(4)	C(9)	-S(10) -C(11) -C(12)	-80.8(4)
C(2)	- C(3) - S(4) - C(5)	71.5(4)	S(10)	-C(11) -C(12) -S(13)	-66.2(4)
C(3)	- S(4) - C(5) - C(6)	-108.9(4)	C(11)	-C(12) -S(13) -C(14)	168.6(3)
S(4)	- C(5) - C(6) - S(7)	-66.6(5)	C(12)	-S(13) -C(14) -C(15)	-171.1(4)
C(5)	- C(6) - S(7) - C(8)	-153.6(4)	S(13)	-C(14) -C(15) - S(1)	70.5(4)°
C(6)	- S(7) - C(8) - C(9)	-57.1(4)			

Table 4.2: Comparison of [2+2] co-ordination at Au(I) for selected thioether macrocyclic structures.

	S(1) -Au-S(10)	Au-S bonds		Au...S interactions	
$[Au([9]aneS_3)_2]^+$	153.98(23)	2.302(6)	2.350(9)	2.733(8)	2.825(8)Å
$[Au([18]aneS_6)]^+$	155.93(12)	2.320(4)	2.321(3)	2.870(3)	2.856(4)Å
$[Au([15]aneS_5)](B(C_6F_5)_4)$	169.90 (5)	2.2927(13)	2.300(13)	3.1055(13)	3.2088(14)Å
$[Au([15]aneS_5)](PF_6)$ (Major)	158.82(22)°	2.223(5)	2.345(7)	2.887(6)	2.992(6)Å

to the [2+2] distorted tetrahedral geometries previously seen in $[Au([9]aneS_3)_2]^+$ and $[Au([18]aneS_6)]^+$ (see Table 4.2).

The structure of $[Au([15]aneS_5)]^+$ is very different from its Cu(I) and Ag(I) congeners. In the structure of $[Cu(15]aneS_5)](BF_4)$ the Cu(I) centre is encapsulated within the ligand framework and has a distorted tetrahedral geometry, Cu-S = 2.243(5), 2.245(3), 2.317(5), 2.338(5)Å; the fifth S-donor is non-bonding and is disordered over two sites, Cu...S = 3.442(12) and 3.560(11)Å (Figure 4.2).

Figure 4.2: Structure of $[Cu([15]aneS_5)]^+$

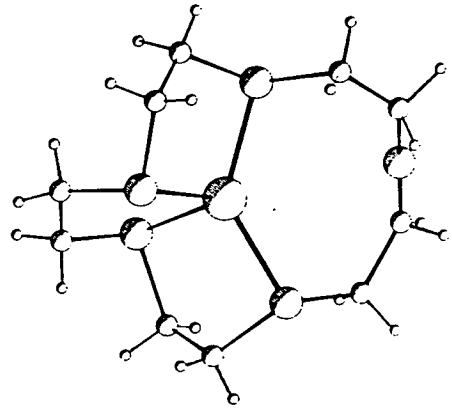

During the course of this work a series of $[Ag([15]aneS_5)]^+$ structures have been determined in Edinburgh for three different counter-anions, $[B(C_6F_5)_4^-]$,[107] $[BPh_4^-]$[106] and $[PF_6^-]$.[107] The structure of $[Ag([15]aneS_5)](B(C_6F_5)_4)$ shows that the Ag(I) ion is encapsulated within the ligand in a [4+1] co-ordination, Ag-S = 2.4712(19), 2.5261(19), 2.7262(20), 2.6847(21); Ag...S = 2.8813(19)Å (Figure 4.3a).[107] $[Ag([15]aneS_5)]$ (BPh_4), however, is dimeric in the solid-state. The two Ag(I) centres take [4+1] and [3+1] co-ordination, with asymmetrically bridging S-donors from both $[15]aneS_5$ ligands,[106] (Ag-S = 2.486(3) to 2.623(5)Å, Ag...S = 2.907(3), 3.131(3)Å) (Figure 4.3b).[106] The structure of $[Ag([15]aneS_5)](PF_6)$ is

different again. The cations form a linear-chain polymeric structure, with the Ag(I) ions in severly distorted octahedral geometries; the metal centres are bound through a [3+2] thioether donor set of one [15]aneS$_5$ (Ag - S = 2.659(5), 2.651(6), 2.564(6)Å; Ag...S = 3.219(5), 3.075(7)Å), with an additional bond to one S-donor from the next macrocycle creating the infinite chain (Ag - S = 2.742(5)Å) (Figure 4.3c).[107] A second independent chain runs anti-parallel to the one shown in Figure 4.3c, similar [4+2] co-ordination at Ag(I) is present in this array.[107]

Figure 4.3: Structures of [Ag([15]aneS$_5$)]$^+$ as (a) [B(C$_6$F$_5$)$_4^-$] (b) [BPh$_4^-$] (c) [PF$_6^-$] salts

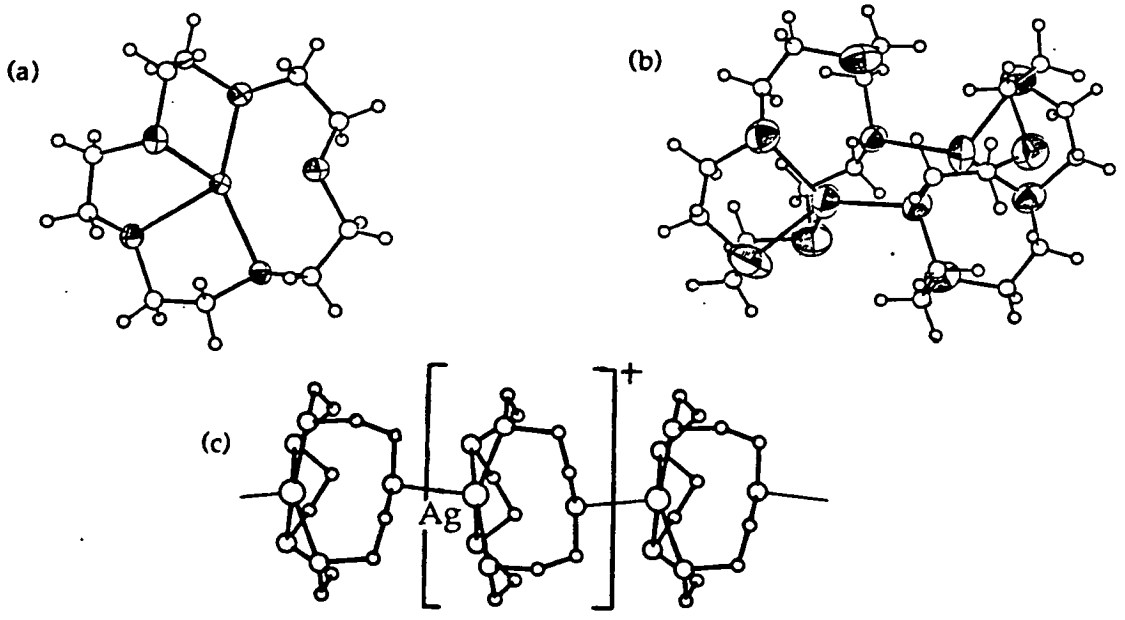

These structures illustrate quite clearly the effect different counter-anions can have on the cation structure. Presumably this is due to the dominance of crystal packing effects over long-range S...Metal interactions. Does this variation of cation structure with counter-anion extend to the [Au([15]aneS$_5$)]$^+$ species? This question lead to the rejuvenation of [Au([15]aneS$_5$)](PF$_6$) crystal growing endeavours. Eventually, hexane layering on to a CH_2Cl_2 solution of the complex gave small crystals suitable for an X-ray structure determination.

4.2.3 Structure determination of $[Au([15]aneS_5)](PF_6)(CH_2Cl_2)$

A single crystal X-ray determination on $[Au([15]aneS_5)](PF_6)(CH_2Cl_2)$ was carried out. Details of the solution and refinement of the structure are given in Section 4.4.2. There is substantial disorder in the structure. The Au ion is disordered over two sites. The two alternative Au positions were allowed to refine with associated occupancies, producing a major component of 76% occupancy (Figure 4.4) and a minor component of 24% occupancy. Selected bonds, angles and torsions of the major component are given in Table 4.3. Both the minor and major components are dimeric in the solid-state.

In the major component the monomeric units are related by a crystallographic inversion centre; the Au centre is bound to both $[15]aneS_5$ ligands, Au - S(1) = 2.345(7), Au - S(10') = 2.223(5)Å, with two additional interactions Au...S(4) = 2.887(6), Au...S(13) = 2.992(6)Å producing a [2+2] distorted tetrahedral geometry at Au(I). The closer approach of S(4) and S(13) to the Au(I) centre in the major component of $[Au([15]aneS_5)](PF_6)$ in comparison to $[Au([15]aneS_5)](B(C_6F_5)_4)$ is reflected in the S(1)-Au-S(10') angle of 158.82(22)° versus 169.90(5)° (see Table 4.2). The Au...Au separation is 4.749(10)Å suggesting that the metal centres are non-interacting. The Au-S(10') bond is quite short at 2.223(5)Å, this is probably a consequence of disorder in the cation.

In the minor component, the co-ordination at the Au(I) centre appears to be [2+1] co-ordinate with Au - S(4) = 1.9522(6), Au - S(10') = 2.460(5), Au...S(1) = 2.995(7)Å. Disorder makes genuine discussion of the minor component structure impossible.

Figure 4.4: Single crystal X-ray structure of [Au([15]aneS$_5$)](PF$_6$)

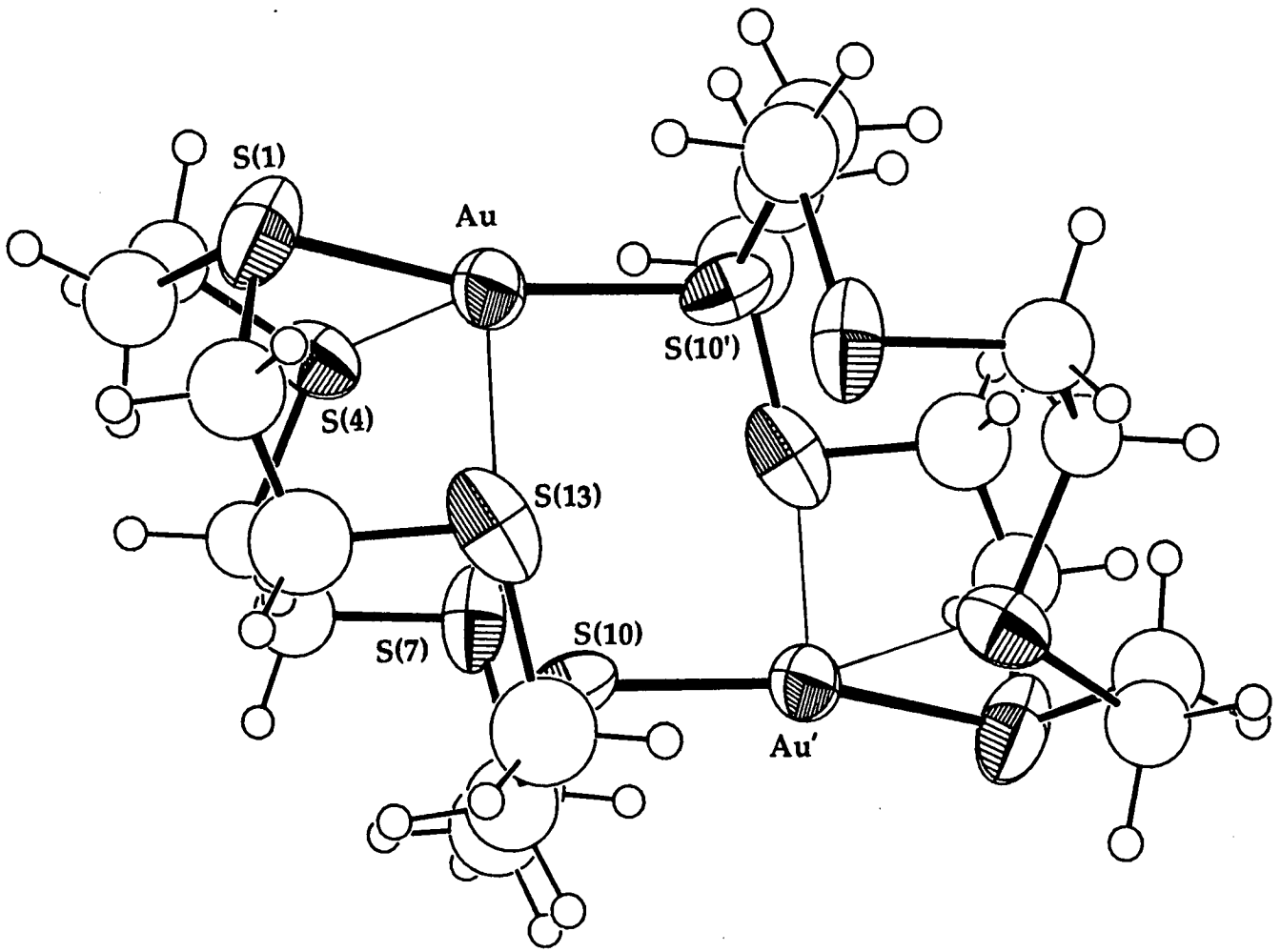

Table 4.3: Selected bonds, angles and torsions for [Au([15]aneS$_5$)](PF$_6$)

Au	- S(1)	2.345(7)	C(6)	- S(7)	1.787(21)
Au	- S(4)	2.887(6)	S(7)	- C(8)	1.811(23)
Au	-S(13)	2.992(6)	C(8)	- C(9)	1.42(3)
Au	-S(10')	2.223(5)	C(9)	-S(10)	1.87(3)
S(1)	- C(2)	1.783(24)	S(10)	-C(11)	1.777(23)
S(1)	-C(15)	1.922(23)	C(11)	-C(12)	1.40(3)
C(2)	- C(3)	1.50(3)	C(12)	-S(13)	1.86(3)
C(3)	- S(4)	1.802(21)	S(13)	-C(14)	1.716(25)
S(4)	- C(5)	1.818(19)	C(14)	-C(15)	1.45(3)Å
C(5)	- C(6)	1.58(3)			

S(1)	- Au	- S(4)	83.64(20)	S(4)	- C(5) - C(6) 107.9(13)
S(1)	- Au	-S(13)	80.49(20)	C(5)	- C(6) - S(7) 114.3(14)
S(1)	- Au	-S(10')	158.82(22)	C(6)	- S(7) - C(8) 102.3(10)
S(4)	- Au	-S(13)	116.03(16)	S(7)	- C(8) - C(9) 119.1(17)
S(4)	- Au	-S(10')	116.21(18)	C(8)	- C(9) -S(10) 111.6(17)
S(13)	- Au	-S(10')	95.90(18)	C(9)	-S(10) -C(11) 86.1(11)
Au	- S(1)	- C(2)	105.4(8)	S(10)	-C(11) -C(12) 108.5(17)
Au	- S(1)	-C(15)	103.4(7)	C(11)	-C(12) -S(13) 123.6(19)
C(2)	- S(1)	-C(15)	100.0(10)	Au	-S(13) -C(12) 124.2(8)
S(1)	- C(2)	- C(3)	114.8(16)	Au	-S(13) -C(14) 90.0(8)
C(2)	- C(3)	- S(4)	114.0(15)	C(12)	-S(13) -C(14) 98.5(12)
Au	- S(4)	- C(3)	90.7(7)	S(13)	-C(14) -C(15) 106.7(17)
Au	- S(4)	- C(5)	112.8(6)	S(1)	-C(15) -C(14) 117.9(17)°
C(3)	- S(4)	- C(5)	98.1(9)		

C(15)	- S(1)	- C(2)	- C(3)	150.5(16)	S(7) - C(8) - C(9) -S(10)	51.3(22)
C(2)	- S(1)	-C(15)	-C(14)	-74.5(19)	C(8) - C(9) -S(10) -C(11)	177.8(19)
S(1)	- C(2)	- C(3)	- S(4)	-69.4(19)	C(9) -S(10) -C(11) -C(12)	177.6(18)
C(2)	- C(3)	- S(4)	- C(5)	-65.2(16)	S(10) -C(11) -C(12) -S(13)	-49.5(25)
C(3)	- S(4)	- C(5)	- C(6)	-142.4(13)	C(11) -C(12) -S(13) -C(14)	-63.2(23)
S(4)	- C(5)	- C(6)	- S(7)	-55.3(16)	C(12) -S(13) -C(14) -C(15)	-175.3(17)
C(5)	- C(6)	- S(7)	- C(8)	-95.9(15)	S(13) -C(14) -C(15) - S(1)	-74.1(19)°
C(6)	- S(7)	- C(8)	- C(9)	61.1(20)		

Although the final refinement of $[Au([15]aneS_5)](PF_6)(CH_2Cl_2)$ structure gave R, R_w = 0.0722, 0.0841 respectively, care must be taken in the precise interpretation of the structure due to the disorder. The disorder in the macrocycles prevented anisotropic refinement of the carbons, this is an indication of the limited quality of the crystal. Despite the disorder it is still possible to ascertain the general co-ordination at the Au(I) centre in the major component as discussed.

In general terms, the co-ordination at Au(I) in the major component of the PF_6^- salt is similar to that observed in the $[Au([15]aneS_5)](B(C_6F_5)_4)$ structure. The [2+2] distorted tetrahedral geometry at Au(I) prevails in both structures; although the interactions of S(4) and S(13) are reduced in the $[B(C_6F_5)_4^-]$ salt.

Unlike the $[Ag([15]aneS_5)]^+$ structures, the different anions have not significantly affected the structures of $[Au([15]aneS_5)]^+$. In $[Ag([15]aneS_5)](B(C_6F_5)_4)$, the Ag(I) centre is encapsulated within the ring; the mean ionic radius of Ag(I) (115 pm) is compatible with the cavity size of $[15]aneS_5$. However in $[Au([15]aneS_5)](B(C_6F_5)_4)$, the ligand is bound to Au(I) in an endodentate manner. The slightly larger mean ionic radius of Au(I) (137 pm) along with its preference for [2+2] distorted tetrahedral co-ordination clearly prevents the inclusion of the metal centre within the macrocycle. If the Au(I) was co-ordinated within $[15]aneS_5$ in the same [2+2] stereochemistry as previously observed for $[Au([9]aneS_3)_2]^+$, $[Au([18]aneS_6)]^+$, considerable strain would be imposed upon the $-SCH_2CH_2SCH_2CH_2S-$ linkage expected to span the largest angle at the metal centre i.e. S(1) - Au - S(10) $\simeq$ 155° (Figure 4.5).

Figure 4.5: Systematic diagram of a strained Au(I) complex of [15]aneS$_5$

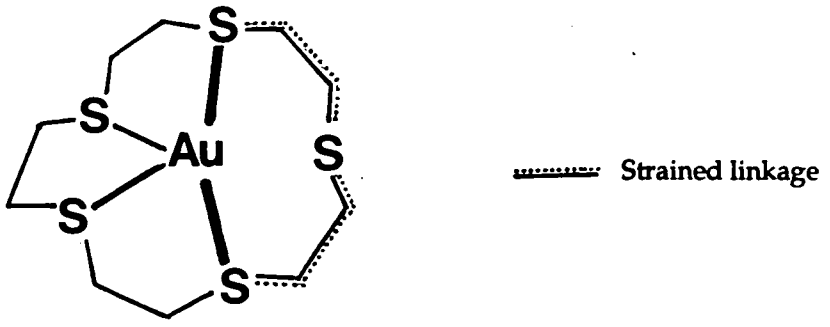

4.2.4 ^{197}Au Mössbauer spectroscopic data for [Au([15]aneS$_5$)](PF$_6$)

The ^{197}Au Mössbauer spectrum for [Au([15]aneS$_5$)](PF$_6$) shows a doublet with I.S. = 2.38(7) mms^{-1} and Q.S. = 6.71(14)mms^{-1} (Figure 4.6). From these results the geometry at the Au(I) centre was interpreted as being effectively three co-ordinate, since the I.S. value was not high enough for two co-ordination in view of Q.S. value obtained.[224]

Figure 4.6: ^{197}Au Mössbauer spectrum for [Au([15]aneS$_5$)](PF$_6$)

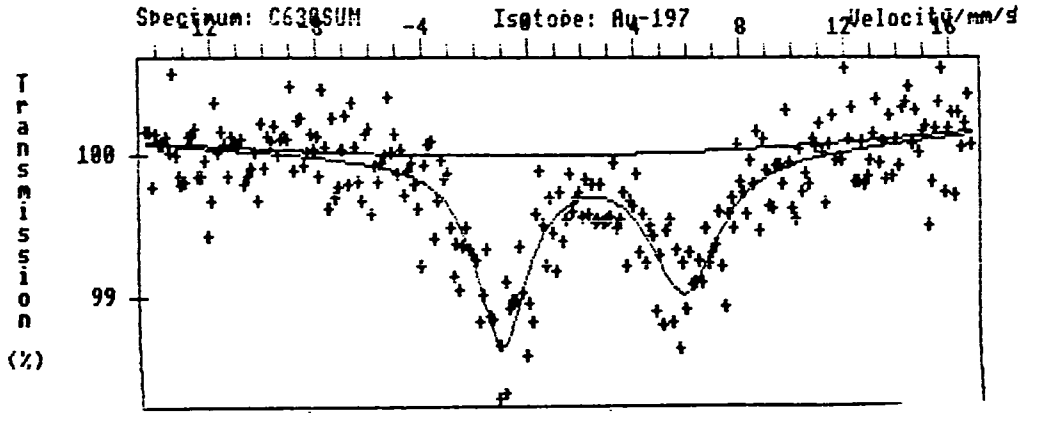

The ^{197}Au Mössbauer spectroscopic data for [Au([9]aneS$_3$)$_2$](PF$_6$), [Au([18]aneS$_6$)](PF$_6$) and [Au([15]aneS$_5$)](PF$_6$) are the first recorded Au(I) systems with all S-donor ligands and effective co-ordination numbers greater than two.[220] The paucity of comparable data makes precise interpretation difficult.

4.2.5 Solution studies

Various attempts to obtain ^1H n.m.r.spectra showed that [Au([15]aneS$_5$)](PF$_6$) decomposes in $(CD_3)_2CO$, CD_3CN, CD_3NO_2 to give metallic/colloidal gold and a green solution in ~20-30 mins therefore, n.m.r. studies of [Au([15]aneS$_5$)](PF$_6$) were not feasible.

To ascertain if the dimeric solid-state structure of [Au([15]aneS$_5$)]$^+$ was retained in solution, a conductivity study of the complex in $MeNO_2$ was carried out. Unfortunately the linear relationship between the equivalent conductance (Λ_e) and the square root of the equivalent concentration (c_e) for [Au([15]aneS$_5$)](PF$_6$) did not correspond correctly, for a 1:1, 2:1, 3:1 or 4:1 electrolyte.[225] [Au([15]aneS$_5$)](PF$_6$) may not be sufficiently stable in $MeNO_2$ for the accurate measurement of molar conductivities. In addition to decomposition, complicated solution behaviour (e.g. dimer/monomer equilibrium) may explain these anomalous results.

4.2.6 Electrochemical studies of [Au([15]aneS$_5$)](PF$_6$)

Cyclic voltammetry of [Au([15]aneS$_5$)](PF$_6$) at platinum electrodes was carried out in a variety of solvents.

Acetonitrile: Cyclic voltammetry of [Au([15]aneS$_5$)](PF$_6$) in MeCN (0.1M $^nBu_4NPF_6$) shows two quasi-reversible oxidations at $E_{1/2}^1$ = +0.36V (ΔE_p = 85mV) and $E_{1/2}^2$ = +0.54V (ΔE_p = 60mV) (Figure 4.7) and an irreversible reduction of E_{pc}^1 = -0.35V vs Fc/Fc^+ at a scan rate of 100mVs^{-1}.

Coulometric measurements confirmed these processes to be one-electron transfer steps

Figure 4.7: Cyclic voltammogram of [Au([15]aneS$_5$)](PF$_6$)

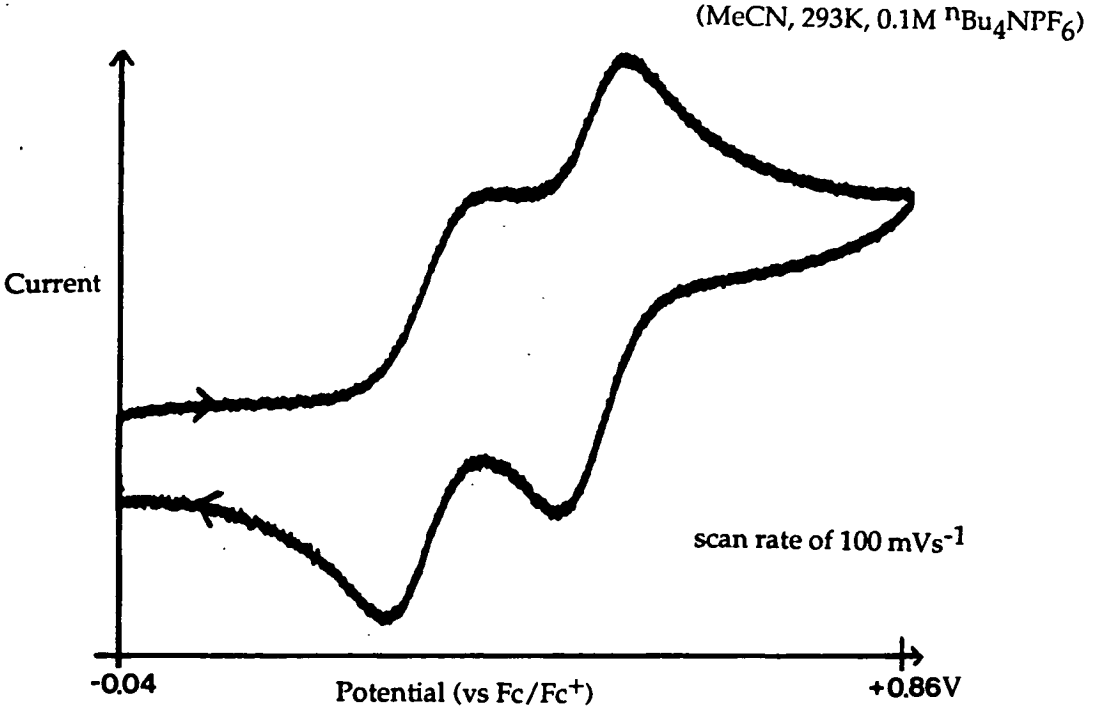

Electrogeneration of the first oxidation product at +0.57V (vs Fc/Fc$^+$) affords a green e.p.r. active species. The frozen glass e.p.r. spectrum of the first oxidation product shows a strong anisotropic signal with g_1 = 2.040 (A_1 = 66.0G), g_2 = 2.022 (A_2 = 60.8G), g_3 = 2.009 (A_3 = 67.0G) (Figure 4.8). This signal is consistent with d^9 centre being in an unsymmetrical environment. (Further spectral analysis is discussed in Section 4.2.12).

The e.p.r. spectrum suggests that the first oxidation is largely metal-based producing a Au(II) species. Further oxidation of the Au(II) species at +1.20V produces a blue e.p.r. silent species, consistent with the second oxidation also being metal-based, producing a Au(III) species. The irreversible reduction at Ep_c^1 = -0.35V is assigned as a Au(I)/(O) couple.

Figure 4.8: X-band frozen glass e.p.r. spectrum of first oxidation product of [Au([15]aneS$_5$)](PF$_6$)

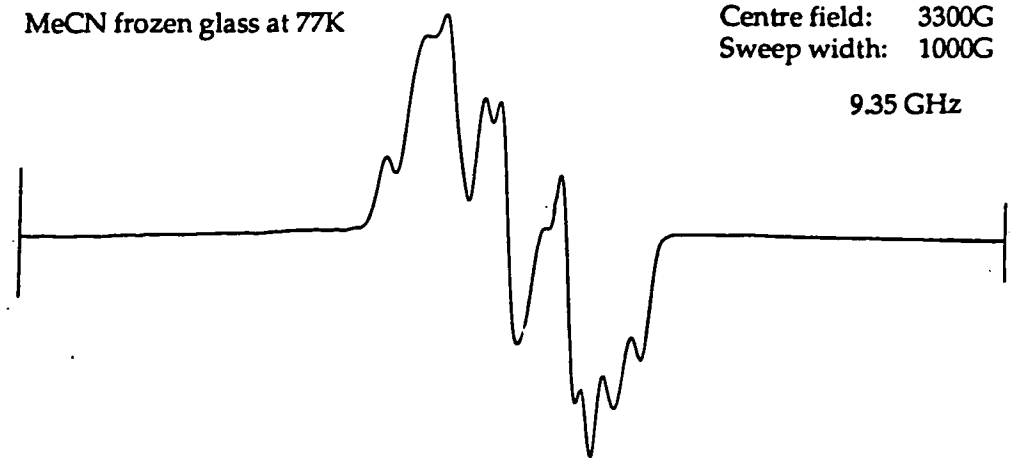

Nitromethane: Cyclic voltammetry of [Au([15]aneS$_5$)](PF$_6$) in $MeNO_2$ (0.1M $^nBu_4NPF_6$) shows two quasi-reversible oxidations $E_{1/2}^1 = +0.39V$ (ΔE_p = 80mV) and $E_{1/2}^2 = +0.66V$ (ΔE_p = 60mV), vs Fc/Fc^+ at a scan rate of 100 mVs^{-1}. Coulometric measurements confirmed these processes to be one-electron steps. Electrogeneration of the first oxidation product at +0.52V (vs Fc/Fc^+) affords a green, e.p.r. active species. E.p.r. spectroscopy confirmed that this Au(II) species is identical to the Au(II) species electrogenerated in MeCN.

Acetone: [Au([15]aneS$_5$)](PF$_6$) exhibits similar electrochemical behaviour in Me_2CO as observed in MeCN and $MeNO_2$. The two quasi-reversible oxidations occur at $E_{1/2}^1 = +0.33V$ (ΔE_p = 120mV) and $E_{1/2}^2 = +0.48V$ (ΔE_p = 80mV) (vs Fc/Fc^+) at a scan rate of 100mVs-1.

Methylene Chloride: Cyclic voltammetry of [Au([15]aneS$_5$)](PF$_6$) in CH_2Cl_2 (0.4M $^nBu_4NPF_6$) shows two quasi-reversible oxidations $E_{1/2}^1$ = +0.40V (ΔE_p = 276mV), and $E_{1/2}^2$ = +0.54V (ΔE_p = 216mV) (Figure 4.9).

Figure 4.9: Cyclic voltammogram of [Au([15]aneS$_5$)](PF$_6$)

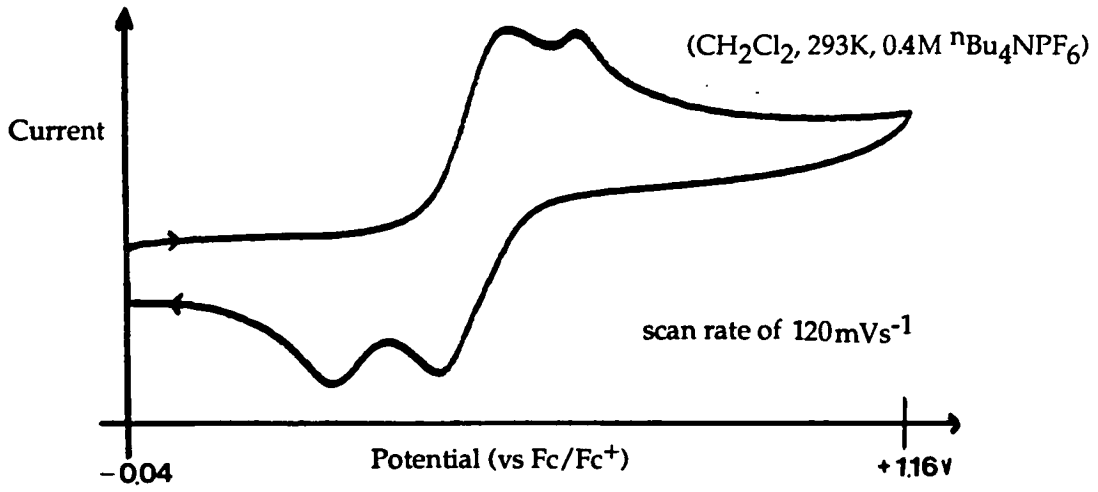

Unlike the electrogeneration in the other solvents, the oxidation at +0.50V (vs Fc/Fc$^+$) in CH_2Cl_2 affords a pale yellow species, further oxidation at +1.00V produces a pale green species (λ_{max} ~ 418 nm). Unfortunately the oxidation products are only sparingly soluble in CH_2Cl_2, making e.p.r. spectroscopic measurement difficult. Although a weak anisotropic signal was recorded for the second oxidation product as a frozen glass at 77K. The interpretation of this data is unclear due to the solubility problem.

The electrochemical behaviour of [Au([15]aneS$_5$)](PF$_6$) is solvent dependent. The potentials of the two largely metal-based oxidations differ in MeCN, $MeNO_2$ and Me_2CO (Table 4.4), although apparently the same Au(II) species can be generated in all three solvents. Therefore, it is likely that the Au(II) species does not contain co-ordinated solvent.

Table 4.4 Summary of cyclic voltammetric data for [Au([15]aneS$_5$)](PF$_6$)

	$E_{1/2}^1$ (ΔE_p/mV)	$E_{1/2}^2$ (ΔE_p/mV)
Me_2CO	+0.33 (120)	+0.48 (80)
MeCN	+0.36 (85)	+0.54 (60)
$MeNO_2$	+0.39 (80)	+0.66 (60)
CH_2Cl_2	+0.40 (280)	+0.54 (220)

All potentials quoted vs Fc/Fc^+ at a scan rate of $100mVs^{-1}$

Coulometric measurements on [Au([15]aneS$_5$)](PF$_6$) are consistent with schemes (1-3)

(1) $$\mathbf{Au(I) \xrightarrow{-e^-} Au(II) \xrightarrow{-e^-} Au(III)}$$

(2) $$\mathbf{Au(I)Au(I) \xrightarrow{-2e^-} Au(II)Au(II) \xrightarrow{-2e^-} Au(III)Au(III)}$$

(3) $$\mathbf{Au(I)Au(I) \rightleftharpoons 2\,Au(I) \xrightarrow{-2e^-} 2\,Au(II) \xrightarrow{2e^-} 2\,Au(III)}$$

The solution structure of [Au([15]aneS$_5$)](PF$_6$) is not known; if the solid-state structure is retained in solution, the dimeric species could undergo oxidations as shown in Scheme 2 and 3. The pre-equilibrium between the dimer and monomer in Scheme 3 could well be solvent dependent, thus explaining the dependence of the electrochemistry with solvent.

4.2.7 Kinetic study on the $[Au([15]aneS_5)]^{+/2+}$ couple

The first oxidation process of $[Au([15]aneS_5)](PF_6)$ is quasi-reversible in MeCN on the cyclic voltammetric time-scale. The peak potential separation is dependent on scan rate. This kinetic behaviour was analysed (using the method described in Section 3.2.6) to determine the heterogeneous electron-transfer rate constant, k_s, for the $[Au([15]aneS_5)]^{+/2+}$ oxidation process.

Cyclic voltammetric measurements on $[Au([15]aneS_5)](PF_6)$ were carried out at platinum electrodes, in MeCN (0.1M $^nBu_4NPF_6$) at 283.0 K. Numerous scans were recorded over the potential range of +0.40V to +1.00V (vs Ag/AgCl), at various scan rates (v= 10 - 200mVs^{-1}).

Using the experimental (i.r. compensated) ΔE_p values, the values for ψ were obtained from the graph of $\log_{10} \psi$ vs ΔE_p (Figure 3.10). A graph of $v^{-1/2}$ vs ψ gave a straight line plot with a slope of 20.23 ± 0.78 (Figure 4.10b) The gradient equals:-

$$\frac{v^{-1/2}}{\psi} = \left\{\frac{\pi n F D_o}{RT}\right\}^{1/2} .k_s^{-1}$$

where $n = 1$

$F = 96487\ Cmol^{-1}$

$R = 8.314\ CV\ K^{-1}mol^{-1}$

$T = 283.OK$

The diffusion coefficient (D_O) for [Au([15]aneS$_5$)](PF$_6$) was calculated from the Levich equation (see Section 3.2.6 Equ^n (3)) using the rotating disc electrode on the same solvent system. Plotting i vs $\omega^{1/2}$ for the first oxidation process gave a straight line with a gradient of $(3.07 \pm 0.04) \times 10^{-5}$ (Figure 4.11a). Hence, the calculation of the diffusion coefficient for [Au([15]aneS$_5$)]$^{+/2+}$. $D_O = (8.6 \pm 0.2) \times 10^{-6}$ cm^{2}s^{-1}. Thus from equation (1) k_S was evaluated:-

$$k_S = (2.7 \pm 0.2) \times 10^{-3} \text{ cms}^{-1}$$

The measurable k_S, the heterogeneous electron-transfer rate constant for the [Au([15]aneS$_5$)]$^{+/2+}$ oxidation is consistent with a structural change accompanying the electron-transfer process.

The rate of electron-transfer is a factor of 10 slower for the oxidation of Au(I) to Au(II) in the [15]aneS$_5$ system ($k_S = 2.7 \times 10^{-3}$ cms^{-1}) than in the [18]aneS$_6$ system ($k_S = 26.7 \times 10^{-3}$ cms^{-1}). This suggests that the stereochemical change occurring on the oxidation of [Au([15]aneS$_5$)]$^+$ to [Au([15]aneS$_5$)]$^{2+}$ is substantially greater than on oxidising [Au([18]aneS$_6$)]$^+$ to [Au([18]aneS$_6$)]$^{2+}$. This observation is consistent with an additional pre-equilibrium between monomer and dimer moieties occurring prior to or during oxidation of [Au([15]aneS$_5$)]$^+$ to [Au([15]aneS$_5$)]$^{2+}$. (see Section 4.2.6)

Figure 4.10a: Graph of i vs $\omega^{1/2}$ for the [Au([15]aneS$_5$)]$^{+/2+}$ couple

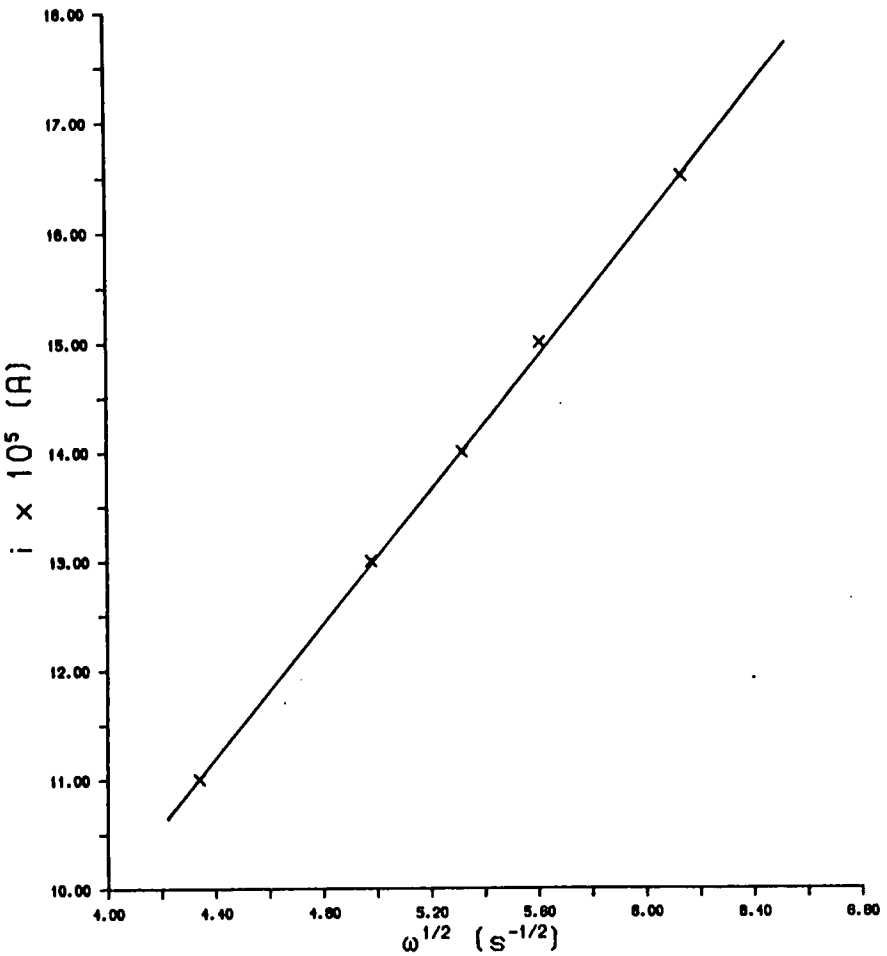

Figure 4.10b: Graph of $\nu^{-1/2}$ vs ψ for the [Au([15]aneS$_5$)]$^{+/2+}$ couple

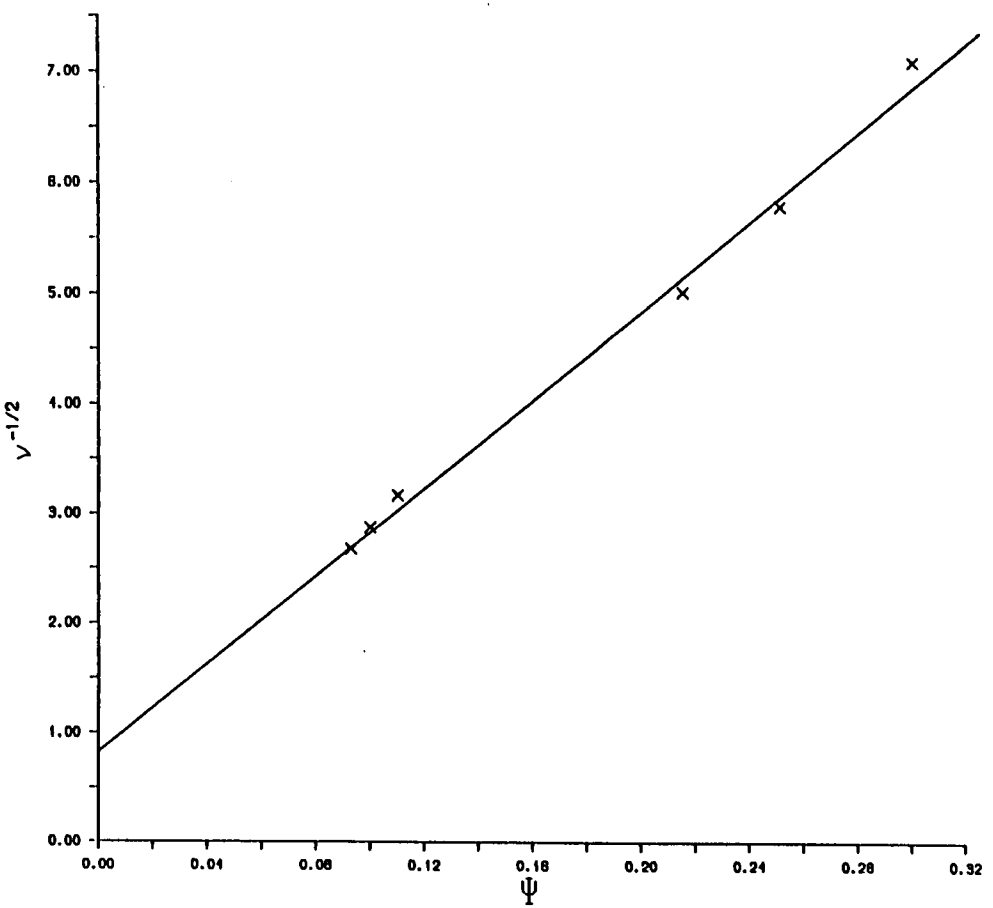

4.2.8 Spectroelectrochemical study of [Au([15]aneS$_5$)](PF$_6$)

The electrochemical behaviour of [Au([15]aneS$_5$)](PF$_6$) can be monitored by UV/Vis spectroscopy. A spectroelectrochemical study in MeCN at 253K shows a clean conversion of Au(I) to the Au(II) species, λ_{max} = 676 nm (ε_{max} = 800 $M^{-1}cm^{-1}$), 413 (5600), 194 (22400), 191 (22700) at +0.48V (vs Fc/Fc^+) (Figure 4.11). This oxidation occurs with isosbestic points at λ_{iso} = 280, 210 nm indicating the absence of any apparent transient intermediates. The Au(II) species can be oxidised at +0.85V (vs Fc/Fc^+) to give the Au(III) species, λ_{max} = 580 (ε_{max} = 715 $M^{-1}cm^{-1}$), 341 (14,850), λ_{iso} = 618, 525, 376, 210 nm) (Figure 4.12). Both these oxidations are chemically reversible.

[Au([15]aneS$_5$)](PF$_6$) decomposes in a variety of solvents, e.g. Me_2CO, MeCN, $MeNO_2$ in 20 mins., to give colloidal/metallic gold and a green solution. The resultant green solution has the same electronic spectrum as recorded for the electrogenerated Au(II) species. The Au(I) species is unstable in solution and disproportionates to Au(O) and Au(II).

[Au([15]aneS$_5$)](PF$_6$) decomposes in DMF to give a maroon species (λ_{max} = 530 nm), which is e.p.r. active. The frozen glass e.p.r. spectrum of [Au([15]aneS$_5$)](PF$_6$) in DMF shows a strong anisotropic signal (Figure 4.13). The spectrum is very different to those observed for the Au(II) species, the signal occurring at a higher g value, g_{av} = 2.090, and has a different structure. [Au([15]aneS$_5$)](PF$_6$) therefore appears to be reduced to colloidal gold in DMF, producing the paramagnetic maroon solution.

Figure 4.11: Spectroelectrochemical study of $[Au([15]aneS_5)](PF_6)$ (oxidation of $[Au([15]aneS_5)]^+$ to $[Au([15]aneS_5)]^{2+}$)

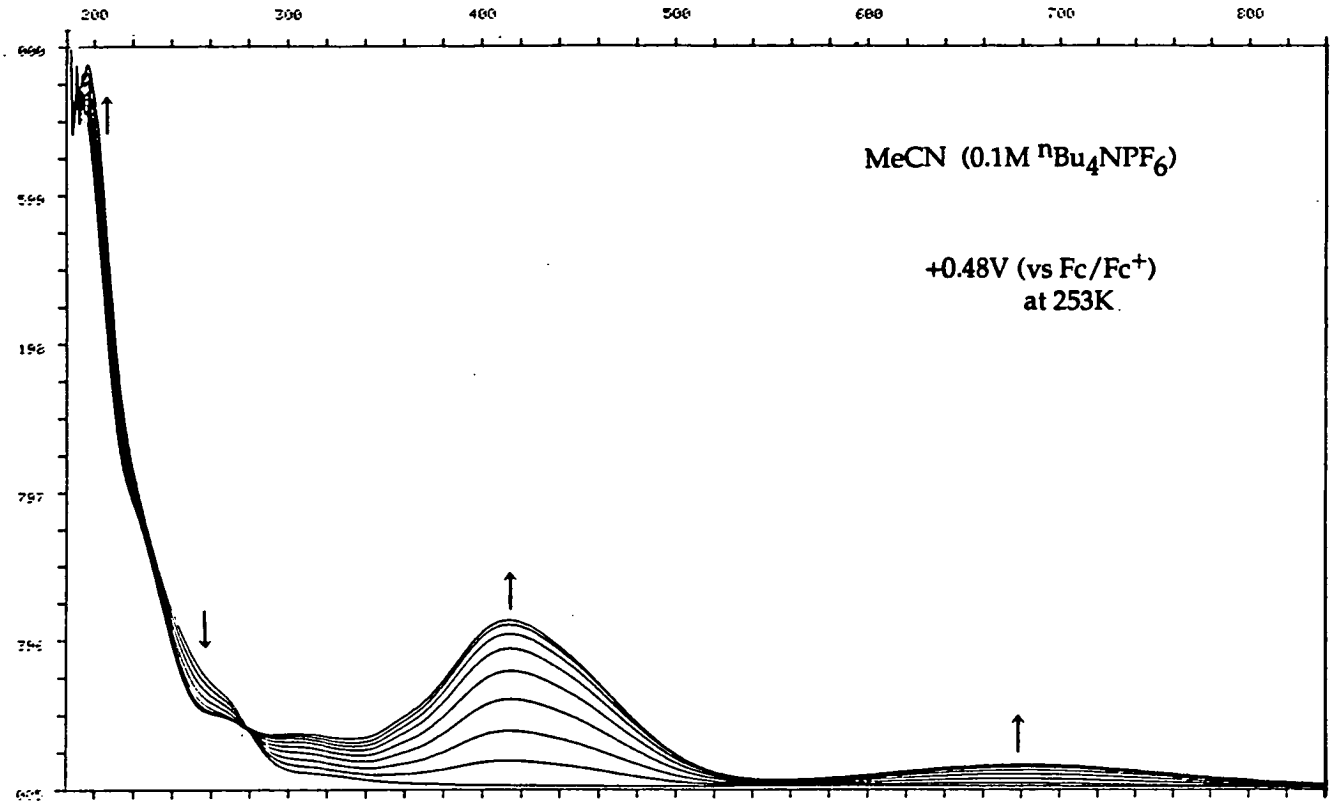

Figure 4.12: Spectroelectrochemical study of $[Au([15]aneS_5)](PF_6)$ (oxidation of $[Au([15]aneS_5)]^{2+}$ to $[Au([15]aneS_5)]^{3+}$)

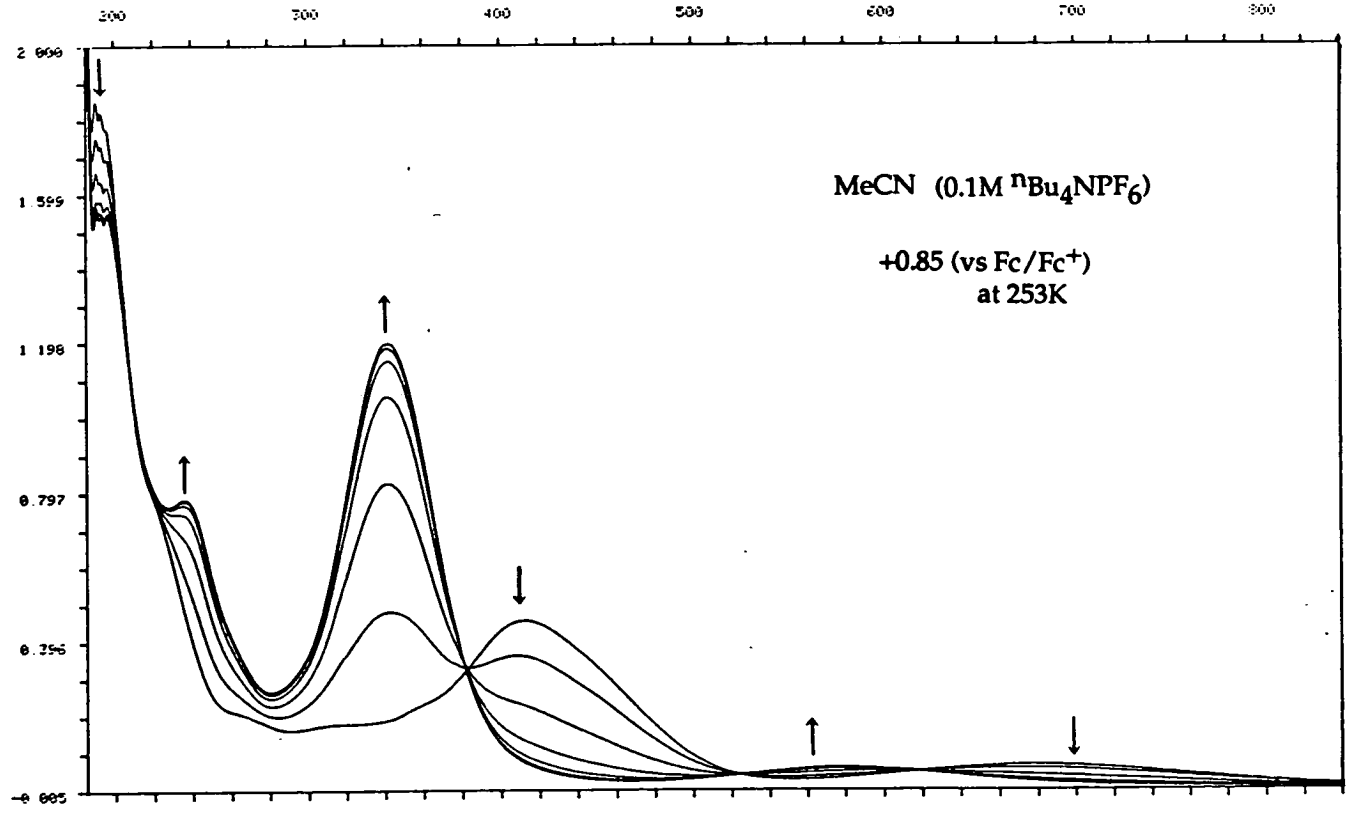

Figure 4.13: X-band frozen glass e.p.r. of [Au([15]aneS$_5$)](PF$_6$) in DMF.

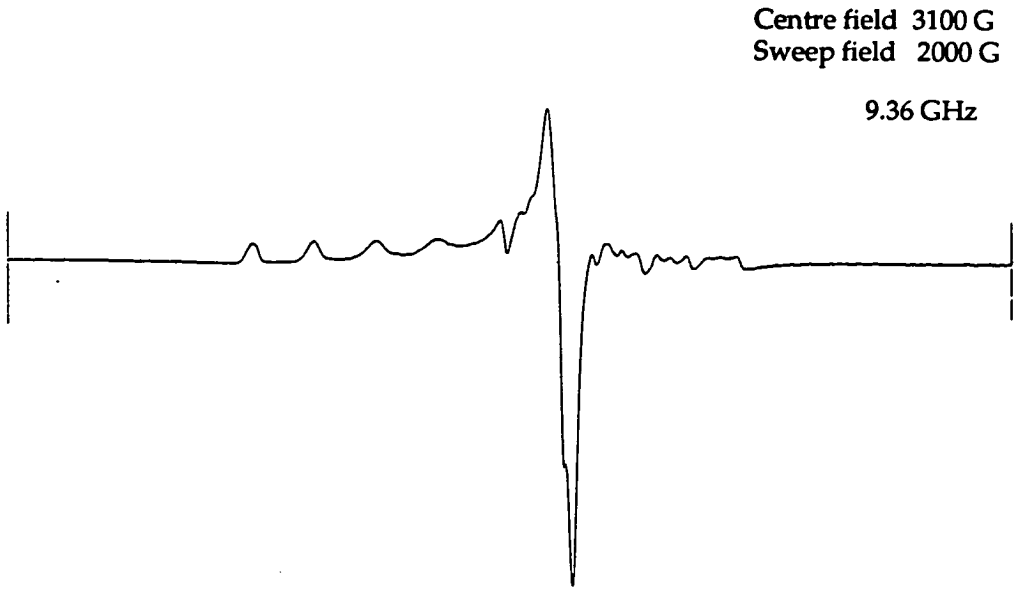

4.2.9 Synthesis and characterisation of [Au([15]aneS$_5$)](PF$_6$)$_2$

The reaction of a 1:1 mixture of KAuCl$_4$ and [Au(tht)$_2$](PF$_6$) with one molar equivalent of [15]aneS$_5$ in MeNO$_2$ afforded a red-orange solution. Addition of NH$_4$PF$_6$ to the reaction mixture resulted in a green solution, which gave a green precipitate on the addition of Et$_2$O. The green solid was recrystallised from MeNO$_2$ and Et$_2$O, under N$_2$. The desired product was stored at -20°C. The complex gave f.a.b. mass spectral peaks at M^+ = 642, 497, corresponding to $[^{197}Au([15]aneS_5+H)PF_6]^+$ and $[^{197}Au([15]aneS_5)]^+$ respectively. Microanalytical data was consistent with the formulation of [Au([15]aneS$_5$)](PF$_6$)$_2$. The i.r. spectrum (KBr disc) was consistent with this assignment, although the green complex turned orange in the presence of KBr, suggesting Br^- uptake of the complex.

$[Au([15]aneS_5)](PF_6)_2$ can be synthesised using a different starting material. Replacing $KAuCl_4$ and $[Au(tht)_2](PF_6)$ with $HAuCl_4$ in the method discussed above, yields the same green product. However, using a combination of Au(I) and Au(III) starting materials affords a cleaner product, which requires minimal recrystallisation. Full experimental details are given in Section 4.4.5. The complex dissolves in MeCN to give a green solution. The electronic absorption spectrum shows bands at λ_{max} = 688 nm (ε_{max} = 700 $M^{-1}cm^{-1}$), 418 (4770), 196(23000), 192(20740), which are similar to the bands observed for the first oxidation product of $[Au([15]aneS_5)]^+$. The absorption at 680nm is assigned as a d-d band, the bands at 196 and 192 nm as ligand to metal charge-transfer bands. Assignment of the band at 416 nm is more difficult, the extinction coefficient is quite large for a pure d-d transition, yet the band is solvent independent and is therefore unlikely to be due to a charge-transfer transition.

Attempts to grow single crystals of $[Au([15]aneS_5)](PF_6)_2$ suitable for an X-ray crystallographic structure determination were unsuccessful. Vapour diffusion of Et_2O into MeCN, $MeNO_2$, Me_2CO solutions of the complex in air and under N_2 resulted in decomposition to Au(I) or metallic/colloidal gold. Hexane layering onto a Me_2CO solution of complex resulted in decomposition. Chemical oxidation of the Au(I) complex using concentrated acids did not produce crystalline material.

4.2.10 ^{197}Au Mössbauer spectroscopic data for [Au([15]aneS$_5$)](PF$_6$)$_2$

The ^{197}Au Mössbauer spectrum for [Au([15]aneS$_5$)](PF$_6$)$_2$ gave a non-standard shape similar to the spectra recorded for [Au([9]aneS$_3$)$_2$](BF$_4$)$_2$ and [Au([18]aneS$_6$)](PF$_6$)$_2$. The model used to fit the data for the [9]aneS$_3$ and [18]aneS$_6$ complexes was applied to the data observed for [Au([15]aneS$_5$)](PF$_6$)$_2$ (Figure 4.14). The peak at 3mm^{-1} was believed to be due to a Au(I) impurity, therefore the doublet observed for [Au([15]aneS$_5$)](PF$_6$) at I.S. = 2.38(7), Q.S. = 6.71(14) mms^{-1} was included in the model programme. The data fitting of [Au([15]aneS$_5$)](PF$_6$)$_2$ gave values of I.S. = 0.6(3) mms^{-1}, Q.S. = +0.5(2) mms^{-1} and B = 18(1)T. The lack of comparable data of Au(II) systems has made the interpretation of the experimental values difficult.

Figure 4.14: ^{197}Au Mössbauer spectrum for [Au([15]aneS$_5$)](PF$_6$)$_2$

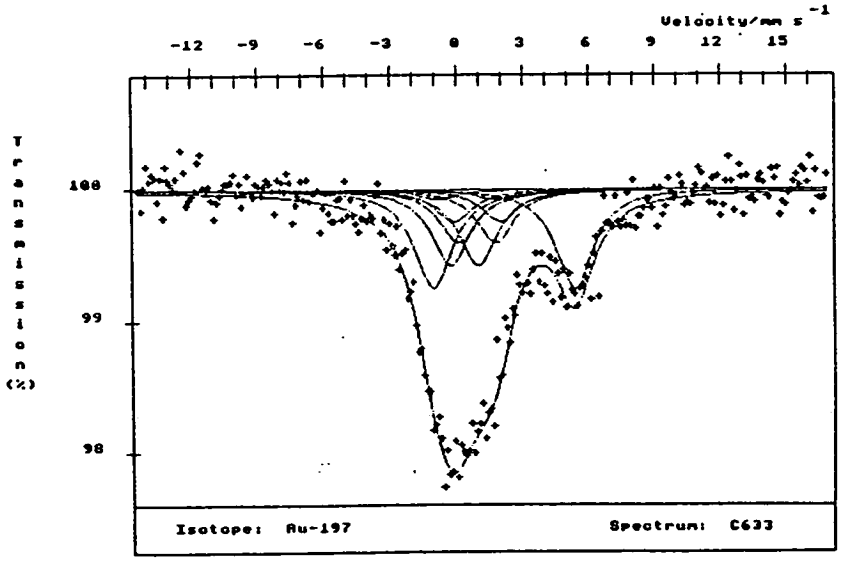

4.2.11 Conductivity study on $[Au([15]aneS_5)](PF_6)_2$

A conductivity study was carried out using the method discussed by Feltham and Hayter.[225] Molar conductivity measurements of $[Au([15]aneS_5)](PF_6)_2$ in $MeNO_2$ were taken for a range of concentrations. A plot of $(\Lambda_e)/ c_e$ gave a linear relationship with a gradient of 490, indicating that $[Au([15]aneS_5)](PF_6)_2$ is a 2:1 electrolyte.[225] $[Au([15]aneS_5)](PF_6)_2$, therefore, is **monomeric** in $MeNO_2$ solution.

4.2.12 E.p.r. studies of $[Au([15]aneS_5)](PF_6)_2$

$[Au([15]aneS_5)]^{2+}$ is e.p.r. active. The solution e.p.r. spectrum of $[Au([15]aneS_5)](PF_6)_2$ in $MeNO_2$ at 293K shows a strong isotropic signal at g_{iso} = 2.014 with hyperfine coupling to ^{197}Au (I = 3/2, 100%) producing a four-line signal with A_{iso} = 43.3G (Figure 4.15).

Figure 4.15: X-band solution e.p.r. spectrum of $[Au([15]aneS_5)](PF_6)_2$

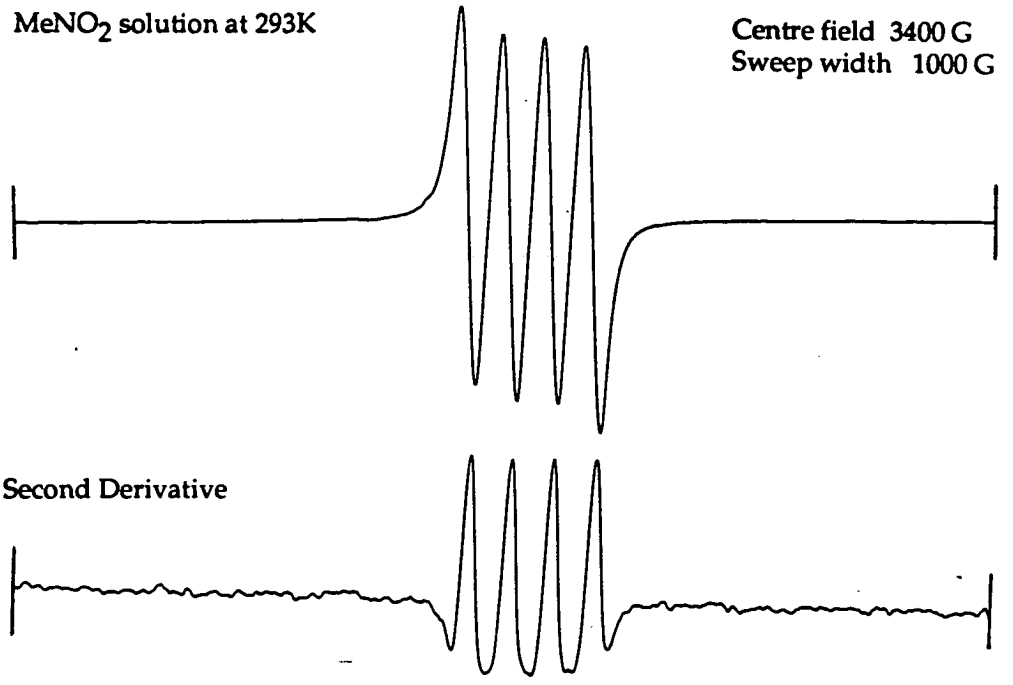

The X-band frozen glass e.p.r. spectrum of $[Au([15]aneS_5)](PF_6)_2$ in MeCN with $^nBu_4NPF_6$ dilutant, at 77K shows an anisotropic signal. The spectrum was assigned using the second derivative as a single rhombic signal with $g_1 = 2.040 (A_1 = 66.0G)$, $g_2 = 2022$ $(A_2 = 608G)$, $g_3 = 2.009$ $(A_3 = 67.0G)$ (Figure 4.16). Simulation of the spectrum on this basis did not reproduce the experimental spectrum (Figure 4.17). The weaker features at g = 2.280, 2.160 (marked by * in Figure 4.16) must be reproduced in a simulation, it is likely that the metal quadrupole effects are important in this system, and must also be considered (see Section 2.2.6).

The frozen glass e.p.r.spectrum of $[Au([15]aneS_5)](PF_6)_2$ is identical to the signal observed for the first oxidation product of $[Au([15]aneS_5)](PF_6)$ in MeCN. These signals are identical in MeCN and $MeNO_2$ suggesting that the green Au(II) species is not a solvated species.

The anisotropic e.p.r. signal observed for $[Au([15]aneS_5)](PF_6)_2$ has a different shape to the spectra recorded for $[Au([9]aneS_3)_2]^{2+}$ and $[Au([18]aneS_6)]^{2+}$ suggesting that the Au(II) centre is situated in a different co-ordination sphere in $[15]aneS_5$. The g tensors indicate covalent character of the Au-S bonding as discussed in Section 2.2.6.

Figure 4.16: X-band frozen glass e.p.r. spectrum of $[Au([15]aneS_5)](PF_6)_2$ with $^nBu_4NPF_6$

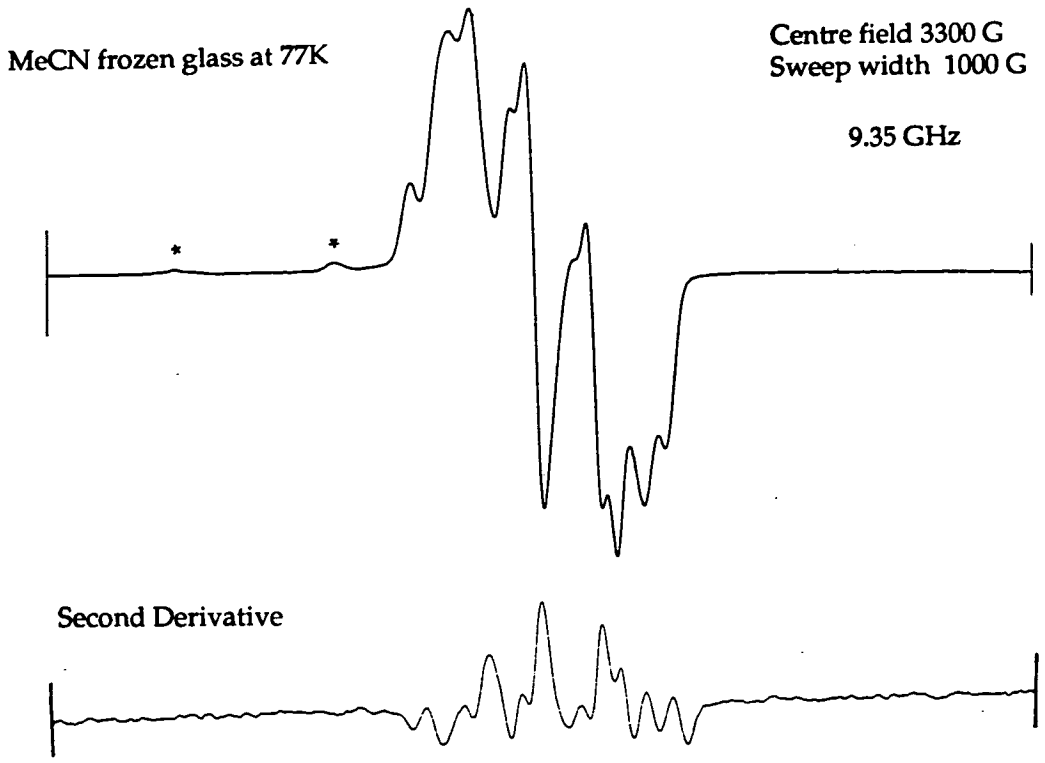

Figure 4.17: Simulated frozen glass e.p.r. spectrum for $[Au([15]aneS_5)](PF_6)_2$

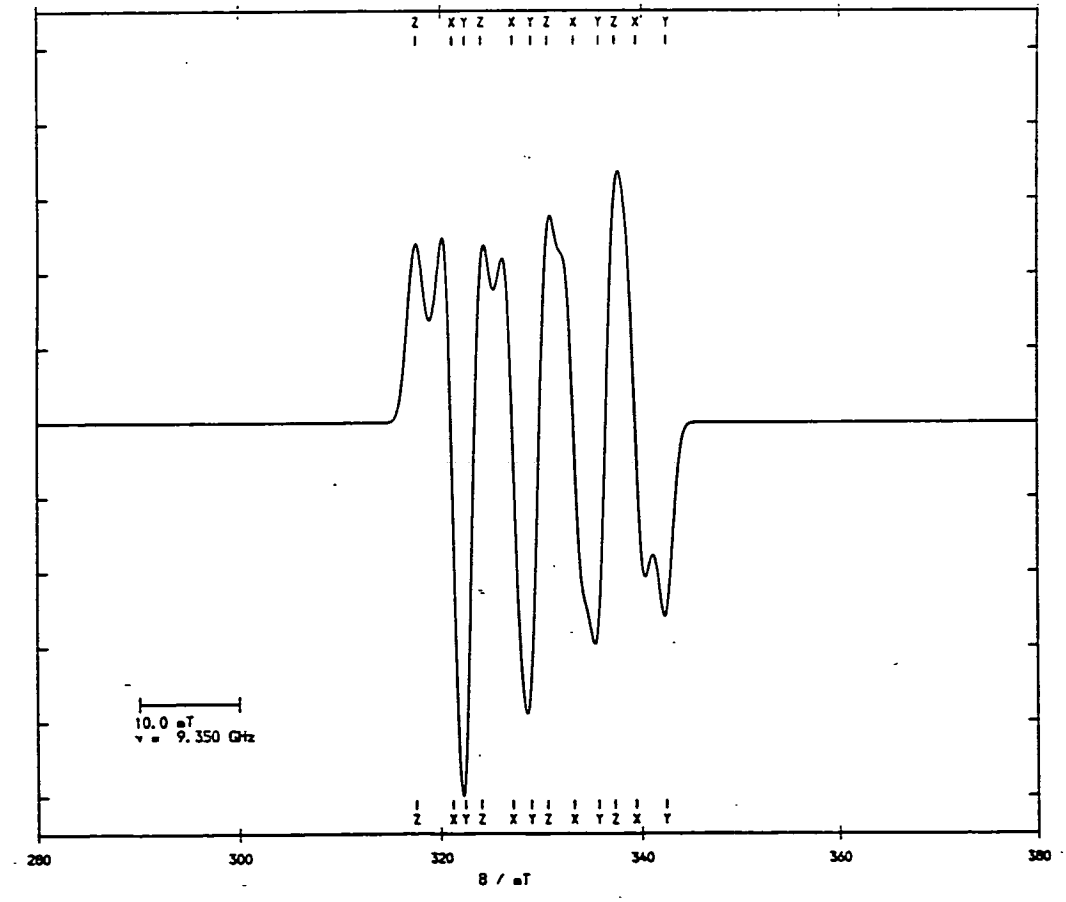

4.3 CONCLUSIONS

[15]aneS$_5$ binds Au(I) in an exocyclic manner to produce a dimeric species with [2+2] distorted tetrahedral co-ordination at the Au(I) centres. The cavity size of [15]aneS$_5$ is incompatible with the desired stereochemistry of the Au(I) centre, resulting in the formation of the exocyclic species. The solution structure of [Au([15]aneS$_5$)]$^+$ was not established, although an equilibrium between monomer and dimer is attractive at this stage. [Au([15]aneS$_5$)](PF$_6$) undergoes quasi-reversible oxidations to Au(II) then onto Au(III). The redox behaviour is solvent dependent. The first oxidation from Au(I) to Au(II) in MeCN has a small electron-transfer rate constant, $k_s = 2.7 \times 10^{-3}$ cms^{-1}, suggesting substantial stereochemical rearrangement is occurring during or prior to the oxidation process.

The Au(II) species can be synthesised directly and exhibits strong e.p.r. behaviour consistent with the d^9 centre being in an unsymmetrical environment and is independent of solvent. [Au([15]aneS$_5$)](PF$_6$)$_2$ was found to be mononuclear by a conductivity study, and shows no evidence from e.p.r. or electronic absorption spectroscopy of being a solvent-adduct species. Therefore it was concluded that the mononuclear Au(II) species contains a four or five co-ordinate Au centre.

If the solid-state structure of [Au([15]aneS$_5$)](PF$_6$) were maintained in solution, the dimeric species must dissociate during or prior to oxidation to the mononuclear Au(II) species (Scheme 1). This process would involve gross stereochemical rearrangement.

$$\text{Au(I)Au(I)} \rightleftharpoons 2\,\text{Au(I)} \xrightarrow{-2e^-} 2\,\text{Au(II)} \xrightarrow{-2e^-} 2\,\text{Au(III)} \qquad (1)$$

Alternatively the dimeric complex may dissociate immediately an solvation (Scheme 2).

$$\text{Au(I)} \xrightarrow{-e^-} \text{Au(II)} \xrightarrow{-e^-} 2\,\text{Au(III)} \qquad (2)$$

The small value of k_s for the $[Au([15]aneS_5)]^{+/2+}$ couple ($k_s = 2.7 \times 10^{-3}$ cms^{-1}) in comparison to k_s for the $[Au([18]aneS_6)]^{+/2+}$ process ($k_s = 26.7 \times 10^{-3}$ cms^{-1}), implies greater stereochemical change occurring than would be involved in purely intrinisic bond breaking/making within a macrocyclic ring. This evidence together with the solvent dependence of the first oxidation favour Scheme (1) and Scheme(2). Unfortunately, the existence of a dimer/monomer pre-equilbrium could not be established unambiguously.

4.4 EXPERIMENTAL SECTION

4.4.1 Synthesis of $[Au([15]aneS_5)](PF_6)$

Reaction of $[15]aneS_5$ (30 mg, 0.1 mmol) with $[Au(tht)_2]PF_6$ (52 mg, 0.1 mmol) in stirring CH_2Cl_2 (5 cm^3) for 1hr.., in the dark gives a colourless solution. Filtration into ice-cold Et_2O (30 cm^3) afforded a white precipitate. The white solid was filtered and washed with Et_2O, then recrystallised from $MeCN/Et_2O$, dried *in vacuo*, stored at -20°C. (Yield 35 mg, 54%). M.Wt. = 642.52. Elemental analyses: found C = 18.6, H = 3.10, S = 25.3%. Calc. for

$C_{10}H_{20}S_5Au_1P_1F_6$: C = 18.7, H = 3.14, S = 25.0%. I.r. spectrum (KBr disc): 2960, 2910, 2850, 1440, 1290, 1265, 1200, 1150w, 1135, 1100, 1020w, 915, 840-820, 740, 690w and 560cm^{-1}. F.a.b. mass spectrum (3-NOBA matrix) : found M^+ = 497. Calc. for [^{197}Au(15]aneS$_5$)]$^+$: M^+ = 497, with correct isotopic distribution. ^{1}H n.m.r. spectrum (CD_3COCD_3, 298K, 200.13 MHz): δ = 3.43-3.40 ppm. ^{13}C n.m.r. spectrum (CD_3COCD_3, 298K, 200. 13 MHz) : δ = 32.92 ppm. (CH_2).

4.4.2 Single crystal structure determination of [Au([15]aneS$_5$)](PF$_6$)(CH$_2$Cl$_2$)

A colourless lath (0.82 x 0.11 x 0.05 mm) suitable for X-ray analysis was obtained by hexane layering onto a solution of the complex in CH_2Cl_2.

Crystal data:

$[C_{20}H_{40}S_{10}Au_2]^{2+}$. 2.($PF_6^-$), M.Wt. = 1454.75, monoclinic, space group $P2_1/c$, a = 12.575(5), b = 17.621(6), c = 10.047(3)Å, α = 90, β = 95.75(4), γ = 90°, U = 2215Å^3 [from 2θ values of 40 reflections measured at $\pm$ ω (20< 2θ< 26°, λ = 0.71073Å)] Z = 1, D_c = 1.090 gcm^{-3}, T = 150 K, μ = 7.382 mm^{-1}, F (000) = 1367.

Data collection and processing:

Stoë STADI-4 four circle diffractometer, graphite-monochromated Mo-K_α X-radiation, T = 150 K, ω - 2θ scans using the learnt-profile method[307], 3012 data measured (2θ_{max} 45°, h -10→10, k 0→18, l 0→13), 2516 unique (R_{int} = 0.0677), giving 1842 with $F \geq 6\ \sigma(F)$ for use in all calculations. Initial absorption corrections were made using ψ scans (maximum transmission factor = 0.2189, minimum = 0.1555). Linear isotropic crystal decay (≈40%).

Structure solution and refinement:

A Patterson synthesis located the Au atom and iterative cycles of least-squares refinement and difference Fourier synthesis located the remaining non-hydrogen atoms. During refinement some disorder in the cation was identified. This was modelled using two alternative sites for the Au atom giving a major component (76%) and a minor component (24%). All isotropic convergence, corrections (min. 0.826, max. 1.238) for absorption were applied using DIFABS.[308] Refinement (by least-squares on ΔF[309]) with anisotropic thermal parameters for the disordered gold fragments and the ordered sulphur atoms and with hydrogen atoms in fixed, calculated positions converged at R_1, R_w = 0.0722, 0.0841 respectively, S = 1.136 for 195 refined parameters, and the final ΔF synthesis showed no feature above 1.282 eÅ^{-3}. The weighting scheme, $w^{-1} = 2.9046(\sigma^2(F) + 0.000600 F^2)$, gave satisfactory agreement analyses and in the final cycle (Δ/σ) max was 0.011.

4.4.3 Synthesis of [Au([15]aneS$_5$)](B(C$_6$F$_5$)$_4$)

To a solution of [Au([15]aneS$_5$)](PF$_6$) (20 mg, 0.03 mmol) in CH_2Cl_2 (3cm^3). Li(B(C$_6$F$_5$)$_4$) (2.5 mg, 0.04 mmol) was added and stirred for 15 mins. Filtration into hexane produced a white suspension. The white product was collected after centrifugation and washed with H_2O. Dried *in vacuo* and stored at -20°C. (Yield 29 mg, 82%). M.Wt. = 1176.58 Elemental analyses: found C = 35.8, H = 2.17, N = 0.31, S = 14.0%. Calc. for $C_{34}H_{10}S_5Au_1B_1F_{20}$: C = 35.0, H = 0.86, S = 13.8%. I.r. spectrum (KBr disc): 2950, 2920, 1640, 1600w, 1515, 1470-1450, 1435, 1415, 1375, 1270, 1180, 1090-1080, 1030, 980, 920, 905, 870, 845, 775, 755, 730, 680, 660, 610, 600, 570, 480w, 450w, 350 and 320w cm^{-1}. F.a.b. mass spectrum (3-NOBA matrix) :

found M^+ = 693, 497; calc. for $[^{197}Au_2([15]aneS_5\text{-}H)]^+$; M^+ = 693; $[^{197}Au([15]aneS_5)]^+$; M^+ = 497, with correct isotropic distributions.

4.4.4 Single crystal structure determination of $[Au([15]aneS_5)](B(C_6F_5)_4)$

A colourless plate (0.16 x 0.37 x 0.49 mm) suitable for X-ray analysis was obtained by hexane layering onto a solution of the complex in CH_2Cl_2.

Crystal data:

$[C_{20}H_{40}S_{10}Au_2]^{2+}.2(BC_{24}F_{20})$, M.Wt = 2332.58, triclinic, space group $P\bar{1}$, a = 8.693(3), b = 14.819(5), c = 16.455(8)Å, α = 66.839(20), β = 89.448(29), γ = 76.720(26)°, U = 1889Å^3 [from 2θ values of 22 reflections measured at ± ω (31< 2θ< 30°, λ = 0.71073Å)] Z = 1, D_c = 2.050 gcm^{-3}, T = 150 K, μ = 4.276 mm^{-1}, F (000) = 1116.

Data collection and processing:

Stoë STADI-4 four circle diffractometer, graphite-monochromated Mo-K_α X-radiation, T = 150 K, # w - 2θ scans using the learnt-profile method[307], 5142 data measured ($2\theta_{max}$ 45°, h -9→9, k -14→15, l 0→17) 4745 unique (R_{int} = 0.0071), giving 4638 with $F \geq 6\,\sigma(F)$ for use in all calculations. Linear isotropic crystal decay (≃ 2%) corrected for during data reduction, no absorption correction.

Structure solution and refinement:

A Patterson synthesis located the Au atom and iterative cycles of least-squares refinement and difference Fourier synthesis located the remaining non-hydrogen atoms. At isotropic convergence, corrections (min 0.912, max. 1.103) for absorption were applied using DIFABS.[308] Refinement (by least-squares on ΔF[309]) with anisotropic thermal parameters for all ordered non-hydrogen atoms and with hydrogen atoms in fixed,

calculated positions, the penta-fluorinated phenyl groups of the $[B(C_6F_5)_4)]^-$ counter-anion were refined as rigid groups, converged at R, R_w = 0.0274, 0.0343, respectively, S = 1.126 for 503 refined parameters, and the final ΔF synthesis showed no feature above 0.885eÅ. The weighting scheme, w^{-1} = $6.3309(\sigma^2(F) - 0.000045\ F^2)$, gave satisfactory agreement analyses and in the final cycle (Δ/σ) max. was 0.065.

4.4.5 Synthesis of $[Au([15]aneS_5)](PF_6)_2$

To a stirring degassed solution of [15]aneS_5 (80 mg, 0.27mmol) in $MeNO_2$ (7 cm^3), solutions of $KAuCl_4$ (49 mg, 0.135 mmol) and$[Au(tht)_2]PF_6$ (70 mg, 0.135 mmol) were added at room temperature.. The resultant red-orange solution turned green on the addition of excess of NH_4PF_6. Schlenk filtration gave a clear green filtrate which afforded a green precipitate on the addition of degassed Et_2O (30 cm^3). Schlenk filtration gave the desired product, which was recrystallised from $MeNO_2/Et_2O$ and stored at -20°C. (Yield 136 mg, 64%). M.Wt. = 787.48 Elemental analyses: found C = 15.3, H = 2.59, N = 0.55%. Calc. for $C_{10}H_{20}S_5Au_1P_2F_{12}$: C = 15.3, H = 2.56%. I.r. spectrum (KBr disc): 3150, 3000, 2990, 2960, 2910, 1570, 1460, 1435, 1370, 1230, 1150, 1050, 840-820, 710, 560 and 485cm^{-1}. F.a.b. mass spectrum (3-NOBA matrix) : found M^+ 642, 497. Calc. for $[^{197}Au([15]aneS_5+H)PF_6]^+$: M^+ = 642; $[^{197}Au([15]aneS_5)]^+$: M^+ = 497, with correct isotopic distributions. UV/Vis spectrum (MeCN) : λ = 688.0 nm (ε_{max} = 700 $M^{-1}cm^{-1}$), 418.4 (4770), 196.4 (23300), 192.0 (20740).

CHAPTER 5

Gold complexes of mixed-donor macrocycles

5.1 INTRODUCTION

Creating an inherent mis-match between the metal ion and the macrocycle can result in complexes that display unusual stereochemical and redox properties.[14,26] (see Section 1.4 (D)). The incompatibility of Au(I) with the ligand cavity of [15]aneS_5 resulted in the formation of an unusual dimeric, exocyclic Au(I) species (Chapter 4).

The aim of the work described in this Chapter was to synthesise Au(I) complexes of the mixed-donor ligands [18]aneN_2S_4 and Me_2[18]aneN_2S_4. These ligands incorporate both 'soft' (S-thioether) and 'hard' (N) donor atoms within a restrictive macrocyclic framework. If the 18-membered rings are compatible with the Au(I) ion, the presence of both 'soft' and 'hard' donors may enhance the stabilisation of particular oxidation states of gold.

Black and McLean first reported the synthesis of [18]aneN_2S_4 in 1968 [230] (Scheme 1). This high-dilution synthesis gave the desired product in a poor yield (4.6%). Lehn and co-workers improved the yield by using an alternative stratagem (Scheme 2). This high-dilution cyclisation gave a 45% yield of [18]aneN_2S_4;[231] Me_2[18]aneN_2S_4 can be synthesised from [18]aneN_2S_4 by using standard methylation procedures.[24]

Scheme 1

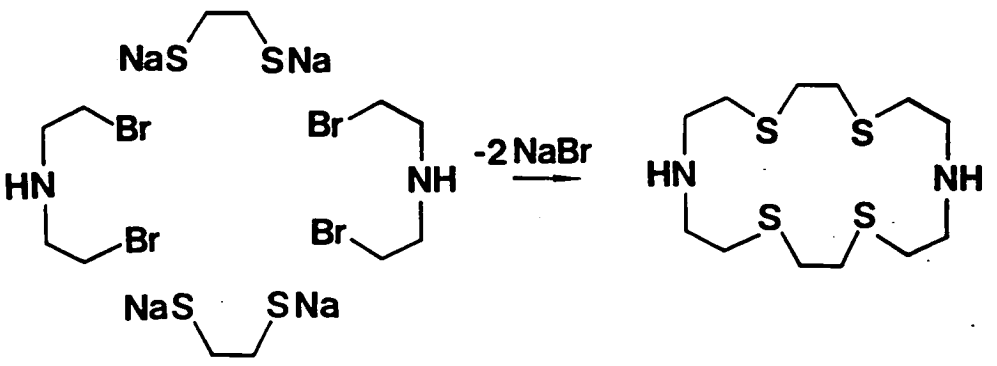

Scheme 2

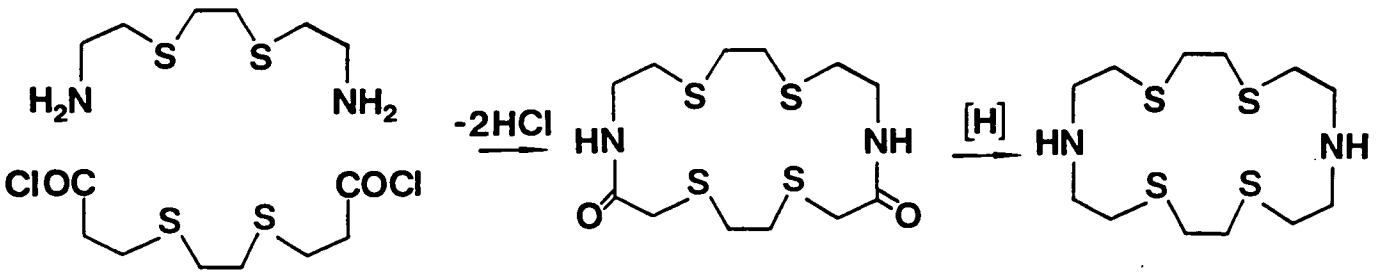

The single crystal X-ray structure of [18]aneN_2S_4 shows the ligand has a crystallographic inversion centre, with the torsion angles at all four C-C-N-C linkages assuming *anti* placements, while all the C-C-S-C units are *gauche*.[232] As discussed in Section 1.4 the majority of unbound homoleptic thioether macrocycles tend to adopt exo-conformations,[15-18] whereas the S-donors in [18]aneN_2S_4 are neither endo- or exo-dentate. The C-S-C unit is almost orthogonal to the macrocyclic plane.[232]

The co-ordination properties of [18]aneN_2S_4 and Me_2[18]aneN_2S_4 have been examined for a number of transition metal centres.[233] Two gross geometric isomers for a hexadentate ligand in an octahedral geometry (1) were defined by Black and co-workers.[230] The two S-N-S linkages can each bind meridionally (racemic isomer (*rac*)) or facially (mesomeric isomer (*meso*)) to the metal centre.

(1)

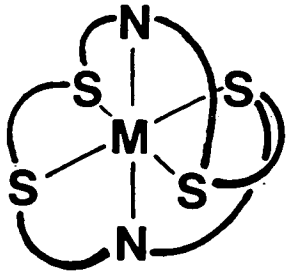

rac

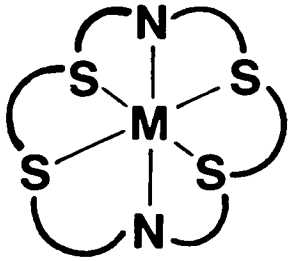

meso

In octahedral complexes of [18]aneS$_6$, [M([18]aneS$_6$)]$^{n+}$, (M = Co(II),[118,119] Ni(II),[112,113] Cu(II),[117] Ru(II),[111] Pd(II),[116] Pt(II),[116] n = 2; M = Pd(III),[114] n = 3; M = Ag(I),[130] n = 1) the ligand exclusively adopts the *meso* configuration, in which unfavourable 1,4-interactions are avoided and the number of *gauche* placements at the C-C-S-C linkages are maximised.[16b,72] In contast, the octahedral Fe(II),[24] Co(III),[24] Rh(III),[24] Ni(II),[24] Hg(II),[233] Ag(I)[235] and Cu(II)[234] (2) complexes of [18]aneN$_2$S$_4$, adopt the *rac* configuration with *anti* C-C-N-C linkages. All the octahedral complexes of Me$_2$[18]aneN$_2$S$_4$ that have been studied were assigned as *meso* isomers[233] (e.g. [Cu(Me$_2$[18]aneN$_2$S$_4$)]$^{2+}$ (3)). The difference in the co-ordinative features of [18]aneN$_2$S$_4$ and Me$_2$[18]aneN$_2$S$_4$ may be a consequence of the steric bulk of the N-Me groups over the N-H functions. Me$_2$[18]aneN$_2$S$_4$ will adopt a *meso* configuration in an octahedral complex in order to relieve the steric interactions between the methyl and methylene protons and minimise to ring strain.

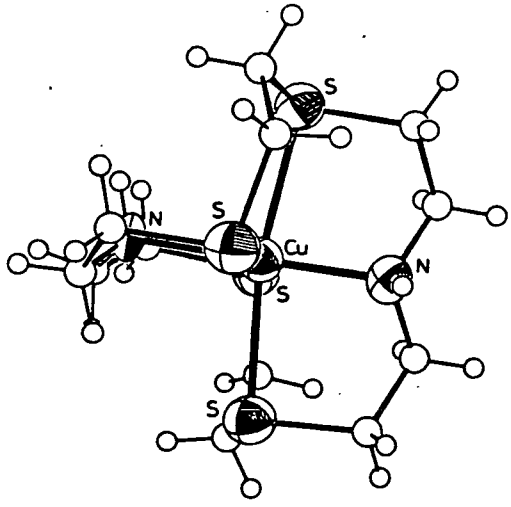

(2) [Cu([18]aneN$_2$S$_4$)]$^{2+}$

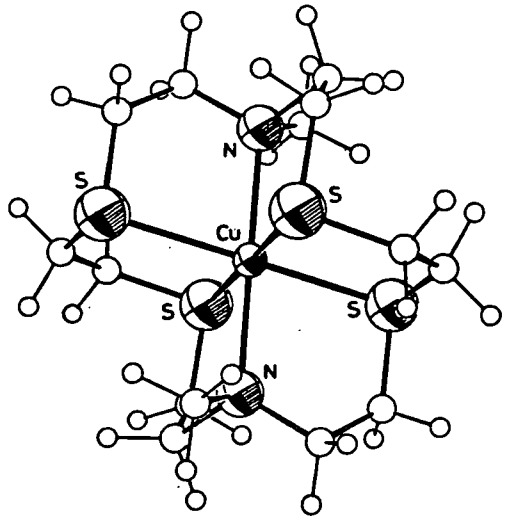

(3) [Cu(Me$_2$(18)aneN$_2$S$_4$)]$^{2+}$

The marked stereochemical differences of complexes [18]aneN$_2$S$_4$ and Me$_2$[18]aneN$_2$S$_4$ are reflected in their redox behaviour.[232] [Cu([18]aneN$_2$S$_4$)]$^{2+}$ and [Cu(Me$_2$[18]aneN$_2$S$_4$)]$^{2+}$ show chemically

reversible Cu(II)/(I) redox couples at $E_{\frac{1}{2}}$ = -0.31V and +0.06V (vs Fc/Fc^+), respectively. The variation in reduction potentials originates from the diminished interaction of the 'hard' N-donors to Cu(II), combined with the greater interaction of the 'soft' S-donors in $[Cu(Me_2[18]aneN_2S_4)]^{2+}$, ensuring the increased stabilisation of Cu(I) by $Me_2[18]aneN_2S_4$ in comparison to $[18]aneN_2S_4$.[24,234] The availability of both 'hard' and 'soft' donors in a cyclic ligand can result in facile redox behaviour (e.g. $[Co([18]aneN_2S_4)]^{2+}$ [24]). The restricted co-ordinative behaviour of these ligands can also impose unusual stereochemistries upon a metal centre: in $[Pd([18]aneN_2S_4)]^{2+}$ the Pd(II) centre is in a highly unusual distorted octahedral stereochemistry.[236]

Various other mixed N- and S- donors macrocycles have been reported, e.g. $[9]aneN_2S$,[237] $[18]aneN_4S_2$,[238] $[24]aneN_2S_4$,[239] and (4).[240] Lindoy and Busch proposed that (4) could only co-ordinate in a *rac* configuration due to the planarity of each S-N-S moiety.[240] Lehn and co-workers have reported a stable binuclear Rh(I) complex (5), along with a binuclear Pd(II) species (6).[241] $[18]aneN_2S_4$ and $Me_2[18]aneN_2S_4$ can also form this type of binuclear complex e.g. $[Pd_2Cl_2([18]aneN_2S_4)]^{2+}$,[24] $[Cu_2(Me_2[18]aneN_2S_4)(NCMe)_2]^{2+}$,[234] $[Pt_2Cl_2(Me_2[18]aneN_2S_4]^{2+}$.[24]

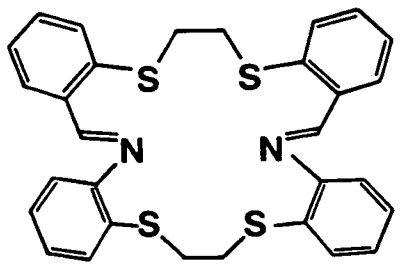

(4)

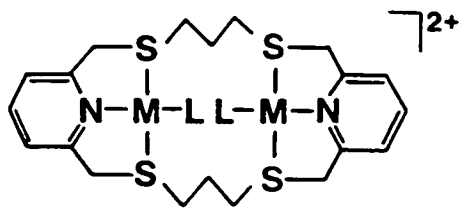

(5) M=Rh(I), L=CO

(6) M=Pd(II), L=Cl⁻

Recently, Beer and co-workers have reported three functionalised [18]aneN_2S_4 ligands, (7) and (8) and a dibenzyl-[18]aneN_2S_4 ligand. Complexation of Cu(II) within the macrocyclic cavity of (7) and (8) perturbs the ferrocene - ferrocenium redox couple.[252] Exploitation of these ligands as potential metallo-sensors is being examined.

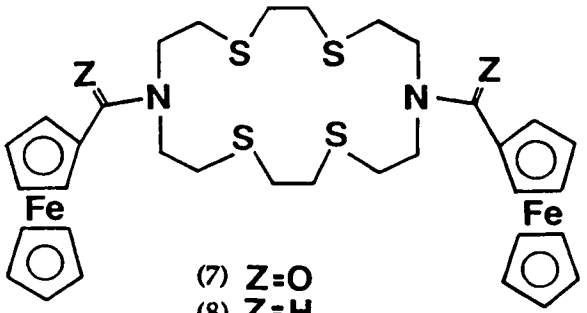

(7) Z=O
(8) Z=H_2

A large range of macrotricyclic (face - to - face) ligands have been reported by Lehn and co-workers.[242-244] These ligands comprise of two chelating subunits held at a specific separation by two bridging links. These three-dimensional, cylindrical ligands can insert either one or two metal centres within the molecular cavity. (9, 10) Sufficient separation between two metal centres may enable the incorporation of substrate molecules within the cavity of a binuclear complex. (11)

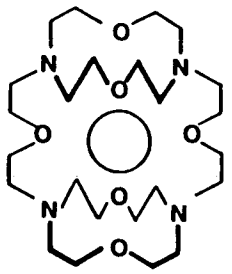

(9) ◯·Cs^+
1:1 inclusion complex

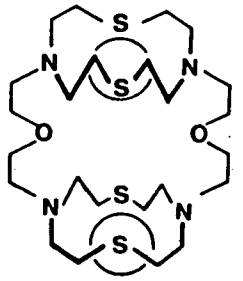

(10) ◯·Cu^{2+}
2:1 inclusion complex

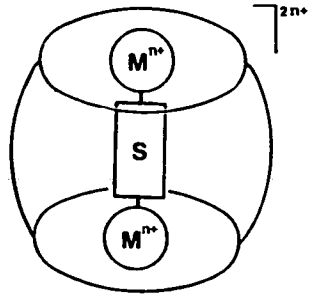

(11) M = Metal
S = Substrate

There are numerous examples of 'face - to - face' ligands incorporating N-, O-, S-donor sets with different bridging links, e.g. ethoxy, amine, aryl units.[242,247-249] The mixed N- and O-donor 'face - to - face' ligands bind alkali metal ions very successfully.[245,249]

Binuclear Cu(II) complexes of (12), (13) and (14) have been reported, together with the Ni(II) and Ag(I) complexes of (12) and (13).[246,250] The 'softer' donor sets of (12-14) have not been employed in the complexation of the 'soft' second- and third-row transition metal ions. Binding of 'soft' metal centres to 'N_2S_4' donor sets has been achieved using the [18]aneN_2S_4 and Me_2[18]aneN_2S_4 ligands.[233]

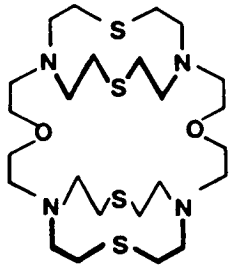

(12)

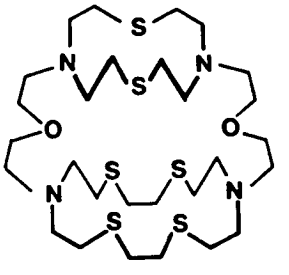

(13)

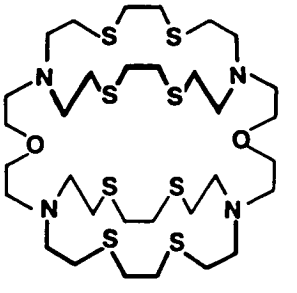

(14)

The second aim of the work discussed in this Chapter was to synthesise a mixed N- and S-donor 'face - to - face' ligand, with the intention of complexing selected 'softer' transition metal centres. A binuclear 'face - to - face' complex containing redox active metal centres is attractive not only in view of its potential to undergo multi-electron processes, but also due to the possiblity of small substrate encapsulation and activation.

5.2 RESULTS AND DISCUSSION

5.2.1 Synthesis and characterisation of [Au([18]aneN$_2$S$_4$)](PF$_6$)

Reaction of [18]aneN$_2$S$_4$ with one equivalent of [Au(tht)$_2$](PF$_6$) in CH_2Cl_2 gave a colourless solution. Filtration into hexane afforded a white precipitate. The isolated solid was recrystallised from Me_2CO and hexane. The f.a.b. mass spectrum of the product shows a peak at M^+ = 523, corresponding to [^{197}Au([18]aneN$_2$S$_4$)]$^+$. The product was assigned as [Au([18]aneN$_2$S$_4$)](PF$_6$) on the basis of this evidence together with i.r. spectroscopic and microanalytical data. The recrystallisation stage of this synthesis is difficult due to decompostion, resulting in a low yield of the pure product. Experimental details are given in Section 5.4.1.

[Au([18]aneN$_2$S$_4$)](PF$_6$) decomposes in MeCN and Me_2CO to give metallic gold; as a result of decomposition and solubility problems n.m.r. studies were unsuccessful. Both ^{1}H and ^{13}C n.m.r. experiments resulted in gold-plated n.m.r. tubes, and gave spectra corresponding to free [18]aneN$_2$S$_4$.

In the structure of the Cu(I) congener, [Cu([18]aneN$_2$S$_4$)]$^+$, the metal centre is bound in a distorted tetrahedral geometry to three S-donors, Cu - S = 2.250(3), 2.245(3), 2.357(4)Å and one N-donor, Cu - N =2.121(9)Å [251] (15). The Cu(I) geometry is similar to that observed in [Cu([18]aneS$_6$)]$^+$.[117] The Ag(I) ion in [Ag([18]aneN$_2$S$_4$)]+ is bound in a highly distorted octahedral geometry,[235] (Ag - S = 2.630(4), 2.664(4), 2.719(4), 2.774(4)Å; Ag - N = 2.553(10), 2.817(5)Å) (16) The ligand adopts a *rac* configuration about the Ag(I) centre.

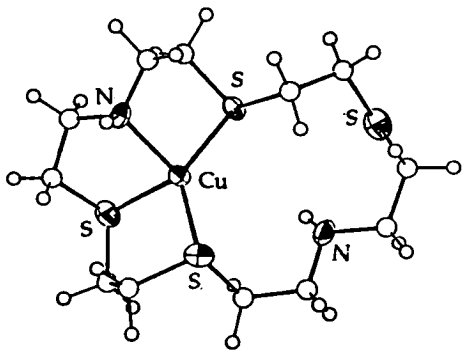

(15) $[Cu([18]aneN_2S_4)]^+$

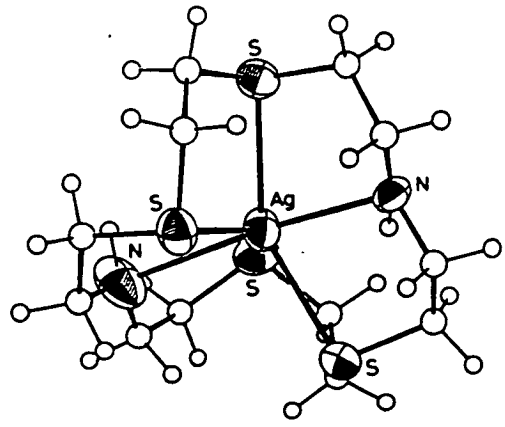

(16) $[Ag([18]aneN_2S_4)]^+$

Proposing a structure for $[Au([18]aneN_2S_4)]^+$ on the basis of the structures of the analogous Cu(I) and Ag(I) complexes is difficult, since Au(I) is known to exhibit different stereochemical preferences. The affinity of Au(I) for 'soft' donors, together with its tendency for linear co-ordination, may affect the resultant stereochemistry of $[Au([18]aneN_2S_4)]^+$.

Complexation of Au(III) with $[18]aneN_2S_4$ was attempted. The reaction of $KAuCl_4$ with $[18]aneN_2S_4$ in $MeNO_2$ under N_2 gave a maroon solution, which turned purple on the addition of excess NH_4PF_6. An orange-red product was isolated from this solution after the addition of Et_2O. The product gave f.a.b. mass spectral peaks at M^+ = 865, 523, 473 corresponding to $[^{197}Au_2Cl_4([18]aneN_2S_4+3H)]^+$, $[^{197}Au([18]aneN_2S_4)]^+$ and $[([18]aneN_2S_4+2H)(PF_6)]^+$ respectively. On the basis of this characterisation together with i.r. spectroscopic data the product was assigned as $[Au_2Cl_4([18]aneN_2S_4)](PF_6)_2$; however, the i.r. spectrum also indicated the presence of a protonated-ligand contaminant. Removal of the impurity was difficult and hindered further characterisation of the gold-containing product.

5.2.2 Cyclic voltammetry of [Au([18]aneN$_2$S$_4$)](PF$_6$)

Cyclic voltammetry of [Au([18]aneN$_2$S$_4$)](PF$_6$) at platinum electrodes in MeCN (0.1M ^{n}Bu$_4$NPF$_6$) shows an irreversible oxidation at E_{pa} = +0.85V (vs Fc/Fc$^+$) at a scan rate of 120mVs^{-1}. The limited quantity and quality of [Au([18]aneN$_2$S$_4$)](PF$_6$) prevented full characterisation of this oxidation process. Preliminary coulometric studies on [Au([18]aneN$_2$S$_4$)](PF$_6$) suggested that the oxidation at +0.85V is a two-electron process. The colourless Au(I) solution turned orange on oxidation at +1.0V.

[Au([18]aneS$_6$)](PF$_6$) shows two quasi-reversible oxidations at $E_{1/2}$= +0.36V, +0.56V (vs Fc/Fc$^+$) under the same solvent and electrode conditions. Clearly the replacement of two S-donors in the macrocyclic donor set with two secondary amine functions has altered the redox behaviour of the Au(I) species dramatically. [18]aneN$_2$S$_4$ appears to stabilise both Au(I) and Au(III), but is unable to stabilise Au(II). This suggests that [18]aneN$_2$S$_4$ cannot encompass a Au(II) centre in a suitable unstrained geometry.

5.2.3 Synthesis and characterisation of [Au(Me$_2$[18]aneN$_2$S$_4$)](PF$_6$)

Reaction of Me$_2$[18]aneN$_2$S$_4$ with one molar equivalent of [Au(tht)$_2$](PF$_6$) in MeCN, under N$_2$ gave a pale yellow solution, which on the addition of Et$_2$O afforded a pale green solid. The product gave f.a.b. mass spectral peaks at M$^+$ = 697, 551 corresponding to [^{197}Au(Me$_2$[18]aneN$_2$S$_4$+H)PF$_6$]$^+$ and [^{197}Au(Me$_2$[18]aneN$_2$S$_4$)]$^+$ respectively. On the basis of this evidence, together with i.r. spectroscopic and microanalytical data, the product was

assigned as [Au(Me_2[18]aneN_2S_4)](PF_6). Full experimental details are given in Section 5.4.2.

[Au(Me_2[18]aneN_2S_4)](PF_6) decomposes in MeCN or Me_2CO in ~60mins., under ambient conditions, to give metallic or colloidal gold and degrades in $MeNO_2$ in 10mins. to produce metallic gold and a blue solution. Due to decomposition and solubility limitations n.m.r. studies were not feasible. To establish the co-ordination at the Au(I) centre and the conformation of the ligand, a single crystal X-ray structure determination was carried out.

5.2.4 Structure determination of [Au(Me_2[18]aneN_2S_4)](PF_6)

A single crystal X-ray structure determination on [Au(Me_2[18]aneN_2S_4)](PF_6) shows the Au(I) centre co-ordinated to two S-donors at Au - S(1) = 2.3043(15), Au - S(10) = 2.3138(14)Å (Figure 5.1). Co-ordination at Au(I) is only marginally distorted from linear, the angle at S(1)-Au-S(10) = 177.30(5)°. An additional long-range interaction to another S-donor, Au - S(4) = 2.8883(15)Å, creates a [2+1] co-ordination at Au(I). The remaining S-donor is non-interacting at 3.6242(15)Å from the Au(I) centre, the N-donors are also non-interacting at 3.795(5) and 3.660(5)Å. Full details of the solution and refinement of the structure are given in Section 5.4.3. Selected bonds, angles and torsions are given in Table 5.1.

Figure 5.1: Single crystal X-ray structure of $[Au(Me_2[18]aneN_2S_4)]^+$

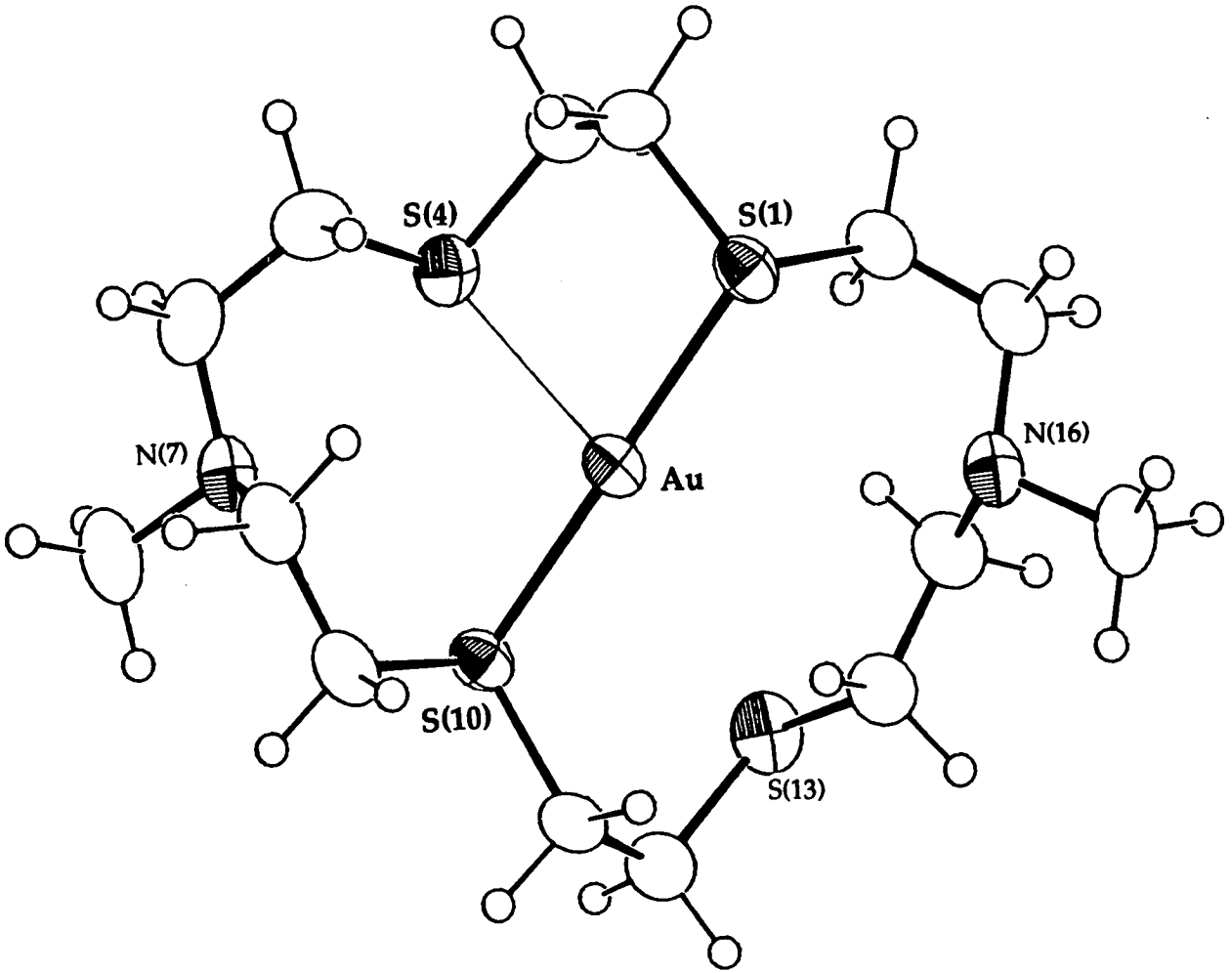

Table 5.1: Selected bonds, angles and torsions for $[Au(Me_2[18]aneN_2S_4)]^+$

Au - S(1)	2.3043(15)	C(8) - C(9)	1.529(8)
Au - S(4)	2.8883(15)	C(9) -S(10)	1.817(6)
Au -S(10)	2.3138(14)	S(10) -C(11)	1.812(6)
S(1) - C(2)	1.816(6)	C(11) -C(12)	1.529(8)
S(1) -C(18)	1.822(6)	C(12) -S(13)	1.804(6)
C(2) - C(3)	1.524(8)	S(13) -C(14)	1.815(6)
C(3) - S(4)	1.797(6)	C(14) -C(15)	1.528(8)
S(4) - C(5)	1.806(6)	C(15) -N(16)	1.467(8)
C(5) - C(6)	1.508(8)	N(16) -C(16N)	1.476(8)
C(6) - N(7)	1.470(8)	N(16) -C(17)	1.472(8)
N(7) -C(7N)	1.464(8)	C(17) -C(18)	1.512(8)
N(7) - C(8)	1.457(7)		

S(1) - Au - S(4)	86.21(5)	N(7) - C(8) - C(9)	113.1(5)
S(1) - Au -S(10)	177.30(5)	C(8) - C(9) -S(10)	110.0(4)
S(4) - Au -S(10)	95.11(5)	Au -S(10) - C(9)	103.90(20)
Au - S(1) - C(2)	103.01(19)	Au -S(10) -C(11)	110.08(19)
Au - S(1) -C(18)	110.13(20)	C(9) -S(10) -C(11)	99.3(3)
C(2) - S(1) -C(18)	100.5(3)	S(10) -C(11) -C(12)	111.8(4)
S(1) - C(2) - C(3)	117.4(4)	C(11) -C(12) -S(13)	114.9(4)
C(2) - C(3) - S(4)	116.0(4)	C(12) -S(13) -C(14)	103.4(3)
Au - S(4) - C(3)	91.99(19)	S(13) -C(14) -C(15)	107.9(4)
Au - S(4) - C(5)	102.11(20)	C(14) -C(15) -N(16)	111.0(5)
C(3) - S(4) - C(5)	100.5(3)	C(15) -N(16) -C(16N)	110.7(5)
S(4) - C(5) - C(6)	110.4(4)	C(15) -N(16) -C(17)	111.9(4)
C(5) - C(6) - N(7)	114.0(5)	C(16N)-N(16) -C(17)	109.8(4)
C(6) - N(7) -C(7N)	109.9(5)	N(16) -C(17) -C(18)	113.5(5)
C(6) - N(7) - C(8)	111.1(4)	S(1) -C(18) -C(17)	109.8(4)
C(7N) - N(7) - C(8)	110.8(5)		

C(18) - S(1) - C(2) - C(3)	66.9(5)	C(8) - C(9) -S(10) -C(11)	166.9(4)
C(2) - S(1) -C(18) -C(17)	158.4(4)	C(9) -S(10) -C(11) -C(12)	162.3(4)
S(1) - C(2) - C(3) - S(4)	63.2(5)	S(10) -C(11) -C(12) -S(13)	49.9(5)
C(2) - C(3) - S(4) - C(5)	65.5(5)	C(11) -C(12) -S(13) -C(14)	61.7(5)
C(3) - S(4) - C(5) - C(6)	173.3(4)	C(12) -S(13) -C(14) -C(15)	-164.1(4)
S(4) - C(5) - C(6) - N(7)	51.3(6)	S(13) -C(14) -C(15) -N(16)	153.1(4)
C(5) - C(6) - N(7) -C(7N)	-170.0(5)	C(14) -C(15) -N(16) -C(16N)	76.9(6)
C(5) - C(6) - N(7) - C(8)	67.0(6)	C(14) -C(15) -N(16) -C(17)	-160.2(5)
C(6) - N(7) - C(8) - C(9)	-165.2(5)	C(15) -N(16) -C(17) -C(18)	64.9(6)
C(7N) - N(7) - C(8) - C(9)	72.4(6)	C(16N)-N(16) -C(17) -C(18)	-171.8(5)
N(7) - C(8) - C(9) -S(10)	52.2(6)	N(16) -C(17) -C(18) - S(1)	53.2(6)

The structure of $[Au(Me_2[18]aneN_2S_4)]^+$ differs from those observed for the Cu(I) and Ag(I) congeners. In $[Cu(Me_2[18]aneN_2S_4)]^+$, the Cu(I) ion is bound to three S-donors (Cu - S = 2.2516(16), 2.2612(16), 2.3342(17)Å) and one N-donor (Cu - N = 2.175(5)Å), creating a distorted tetrahedral geometry (17).[251]

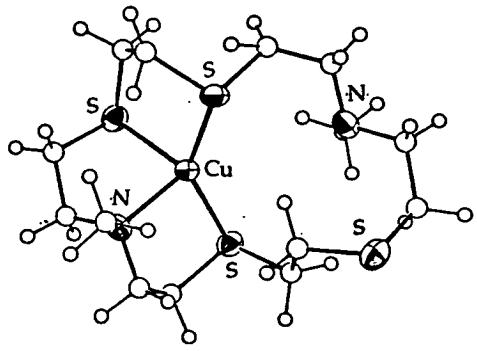

(17) $[Cu(Me_2([18]aneN_2S_4)]^+$

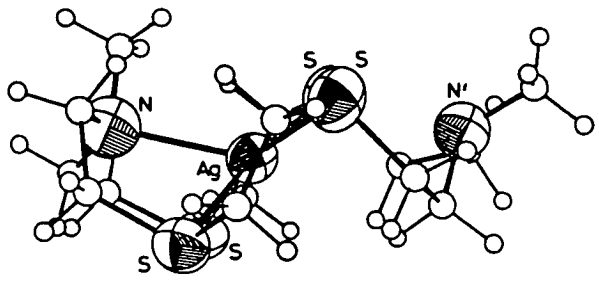

(18) $[Ag(Me_2[18]aneN_2S_4]^+$

The structure of $[Ag(Me_2[18]aneN_2S_4)]^+$ was refined as two components.[235] In the major component (70.2%) the ligand adopts an unusual kite-basd pyramindal geometry at Ag(I) via co-ordination to four S-donors (Ag - S = 2.583(4), 2.819(3), 2.663(4), 2.673(4)Å) and an apically bound N-donor (Ag - N = 2.517(11)Å) (18). This component shows a *meso*-like configuration. In the minor component (29.2%) the second N-donor is also co-ordinated to Ag(I) producing a distorted octahedral stereochemistry; the complex is geniunely in the *meso* configuration.[235]

In homoleptic thioether macrocyclic complexes of Au(I), [2+2] distorted tetrahedral co-ordination predominates, (Chapters 2, 3, 4, 7) whereas in $[Au(Me_2[18]aneN_2S_4)]^+$ the Au(I) is only bound in a [2+1] co-ordination. The 'hard' N-donors do not complete the [2+2] co-ordination at the 'soft' Au(I) centre in $[Au(Me_2[18]aneN_2S_4)]^+$ but remain non-interacting at

3.660(5) and 3.795(5)Å. This mis-match in conjunction with the smaller bite angle of the S-N-S linkage ensure the binding of a near linear Au(I) centre within Me_2[18]aneN_2S_4.

5.2.5 Electrochemical studies on [Au(Me_2[18]aneN_2S_4)](PF_6)

Cyclic voltammetry of [Au(Me_2[18]aneN_2S_4)](PF_6) at platinum electrodes in MeCN (0.1M $^nBu_4NPF_6$) shows two quasi-reversible oxidations at $E_{1/2}^1$ = +0.14V (ΔE_p = 130mV) and $E_{1/2}^2$ = +0.43V (ΔE_p = 60mV) (Figure 5.2) and an irreversible reduction at E_{pc} = -0.80V (vs Fc/Fc^+) at a scan rate of 120mVs^{-1}. Coulometric measurements confirmed the oxidations to be one-electron transfer steps, however on the timescale of the coulometric experiments the second oxidation is not chemically reversible.

Figure 5.2: Cyclic voltammogram of [Au(Me_2[18]aneN_2S_4)](PF_6)

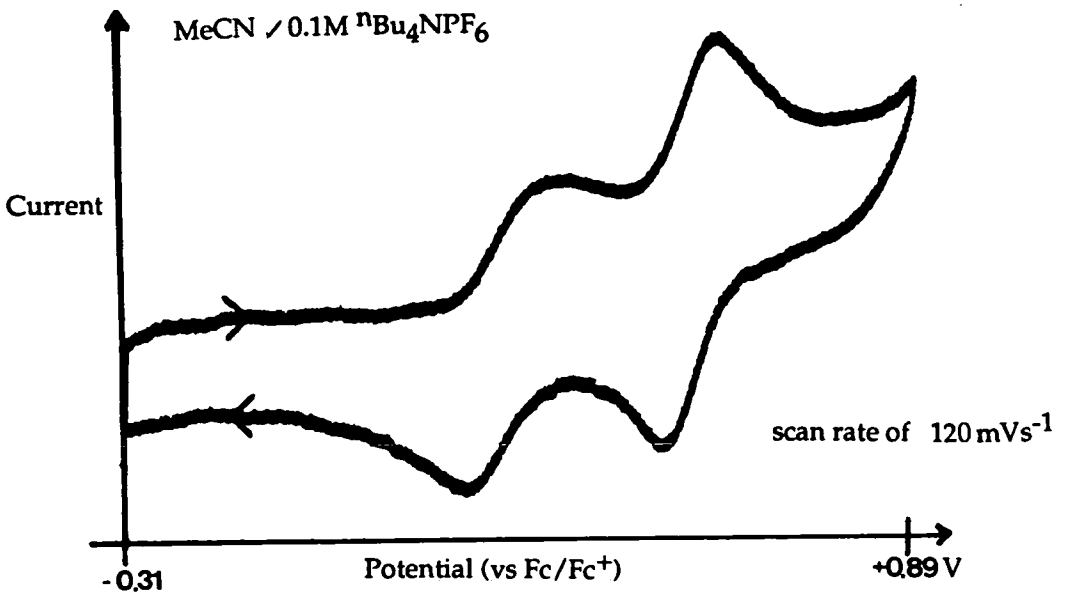

Assuming that the oxidations are metal-based processes, Me_2[18]aneN_2S_4 appears to stabilise Au(I), Au(II) and Au(III). The fact that the second oxidation is not chemically reversible on an extended timescale is consistent

with bound $Me_2[18]aneN_2S_4$ undergoing a ring-opening reaction, similar to the reactions observed for homoleptic thioether macrocycles bound to electro-positive metal centres.[239] (Section 1.4) N.m.r. studies have confirmed that $[Rh(Me_2[18]aneN_2S_4)]^{3+}$ undergoes a ring-opening reaction.[251] Both $[Au(Me_2[18]aneN_2S_4)](PF_6)$ and its $[18]aneS_6$ analogue undergo two quasi-reversible oxidations. Alteration of the ligand donor set affects the relative oxidation potentials of Au(I). (Table 5.2) Substitution of two 'soft' S-donors with 'hard' tertiary amine functions increases the stability of the higher oxidation states of gold, Au(II) and Au(III).

Table 5.2. Comparison of oxidation potentials for two Au(I) macrocyclic complexes

	$E^1_{1/2}$	$E^2_{1/2}$	
$[Au([18]aneS_6)](PF_6)$	+0.36V	+0.56V	
$[Au(Me_2[18]aneN_2S_4)](PF_6)$	+0.14V	+0.43V	(vs Fc/Fc^+)

scan rate of $100mVs^{-1}$

Intriguingly, when Au(I) is bound to a hexadentate ligand that adopts a *meso* configuration about an octahedral centre (e.g. $[18]aneS_6$, $Me_2[18]aneN_2S_4$), the stabilisation of Au(II) appears possible; whereas, Au(II) is not stabilised by $[18]aneN_2S_4$. This suggests that the conformationalconstraints of $[18]aneN_2S_4$ prevent encapsulation of the large Au(II) centre in a suitable stereochemistry.

The first oxidation of $[Au(Me_2[18]aneN_2S_4)]^+$ is quasi-reversible, the peak potential separation varying with scan rate. This kinetic behaviour is consistent with structural rearrangement occurring on oxidation of the Au(I)

centre. Quantifying the electron transfer rate constant using the method discussed in Section 3.2.6 would be useful for comparison with the kinetic data obtained for the $[Au([18]aneS_6)]^{+/2+}$ couple. Unfortunately time did not permit the undertaking of these experiments.

5.2.6 Synthesis of a 'face - to - face' ligand

The macrotricyclic ligand L^1, which incorporates the $[18]aneN_2S_4$ subunit, was reported by Lehn.[242,246] The synthesis follows a sequential strategy involving (i) attachment of two linking appendages to one macrocyclic unit, (ii) activation of the terminal functions of the linking units, (iii) insertion of the second macrocyclic subunit. (Scheme 3)

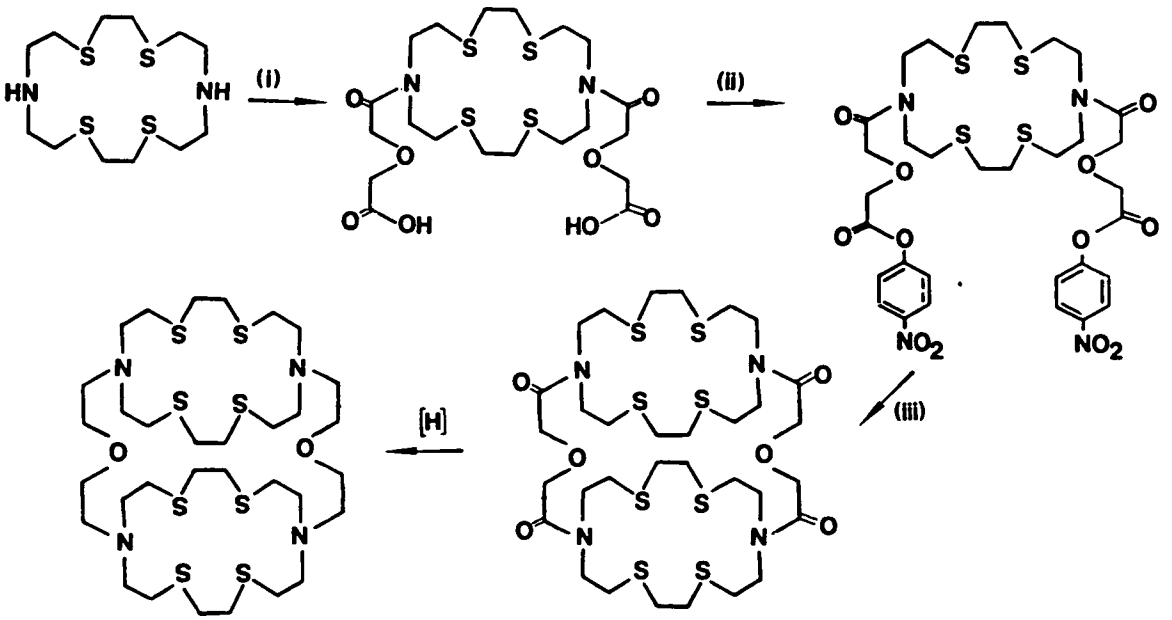

Various attempts at this synthetic route faltered at step (iii), due to very low-yields of steps (i) and (ii). Therefore, another route to a 'N_2S_4'-based 'face - to - face' ligand was sought.

The binuclear Cu(II) complex of the aryl-linked ligand L^2 has been reported,[247] but the actual ligand synthesis has not.

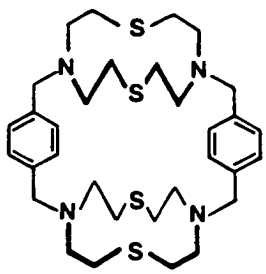

L^2

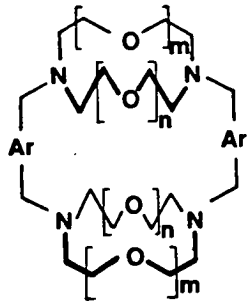

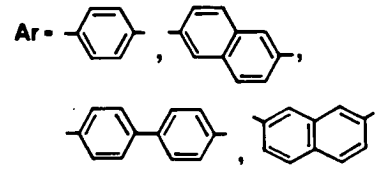

L^3 : m-n-1
L^4 : m-1,n-2
L^5 : m-n-2

Sutherland reported a series of one-step synthesises of ligands L^3-L^5.[254] High dilution [2+2] condensation reactions, in the presence of K_2CO_3 affords these ligands in high-yields. The affinity of the O-donors for K^+ ions improves the efficiency of the reaction. Therefore, we proposed a one-step synthesis of L^6, but using Cs_2CO_3 as a 'templating' agent.

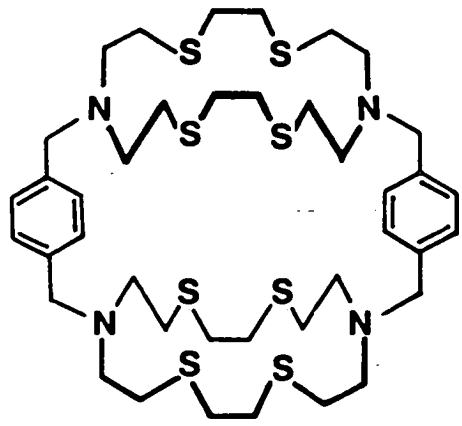

L^6

Synthesis of L^6

Numerous attempts to synthesise L^6 exemplified the fine balance between [2+2] condensation and polymerisation reactions. Clean [2+2] condensation is dependent on the method and rate of addition of the reactants and their concentration, the type of leaving group on the bridging unit and also the solvent used. The final, successful synthetic route to L^6 required a high concentration of Cs_2CO_3.

Direct [2+2] high dilution condensation reaction of [18]aneN_2S_4 with *p*-dibromoxylene in a suspension of Cs_2CO_3 in MeCN at 80°C, lead to a mixture of products after refluxing for 24 hrs. The reaction was monitored by t.l.c. (silica) which showed the presence of two products [R_f = 0.24, 0.40; (7:10 ethylacetate: hexane)] in addition to a small amount of polymeric material. Cs_2CO_3 was separated from the reaction mixture by filtration and the MeCN was removed *in vacuo* from the yellow filtrate. The resultant yellow solid was redissolved in $CHCl_3$ and dried over $CaSO_4$ overnight. $CHCl_3$ was removed *in vacuo* and the residue taken up in CH_2Cl_2. Slow addition of cold hexane to the CH_2Cl_2 solution afforded a creamy precipitate. The product was characterised by i.r. and n.m.r. spectroscopy and f.a.b. mass spectrometry. A second crop of the product can be obtained by organic extraction of the Cs_2CO_3 residue. The contaminant (R_f = 0.24) was removed during recrystallisation. The final product gave f.a.b. mass spectral peaks at M^+ = 857. 429, 327 corresponding to $[L^6+H]^+$, $[C_{20}H_{33}S_4N_2]^+$ and $[([18]aneN_2S_4+H)]^+$ respectively. On this basis the product was assigned as L^6 ($C_{40}H_{64}S_8N_4$).

N.m.r. studies confirmed the assignment of the product. The ^{1}H n.m.r. spectrum showed singlets at δ = 7.39 and 3.61 ppm assigned to 8 aryl and 8 methylene protons of the linking units repectively, a complex multiplet at δ = 2.68 - 2.72 ppm corresponding to the 48 macrocyclic ring protons. (Figure 5.3) These resonances differ from the comparable reference spectra of *p*-dibromoxylene and [18]aneN_2S_4. ^{13}C (DEPT) n.m.r. spectra shows resonances at δ = 128.7 and 59.3 ppm assigned to the aryl carbons and methylene carbons of the linking unit and three other resonances at δ = 55.1, 32.7, 30.5 ppm corresponding to the macrocyclic subunit carbons. The relevant signals have shifted with respect to the free [18]aneN_2S_4 and Me_2[18]aneN_2S_4.

Figure 5.3: ^{1}H n.m.r. spectrum of L^6

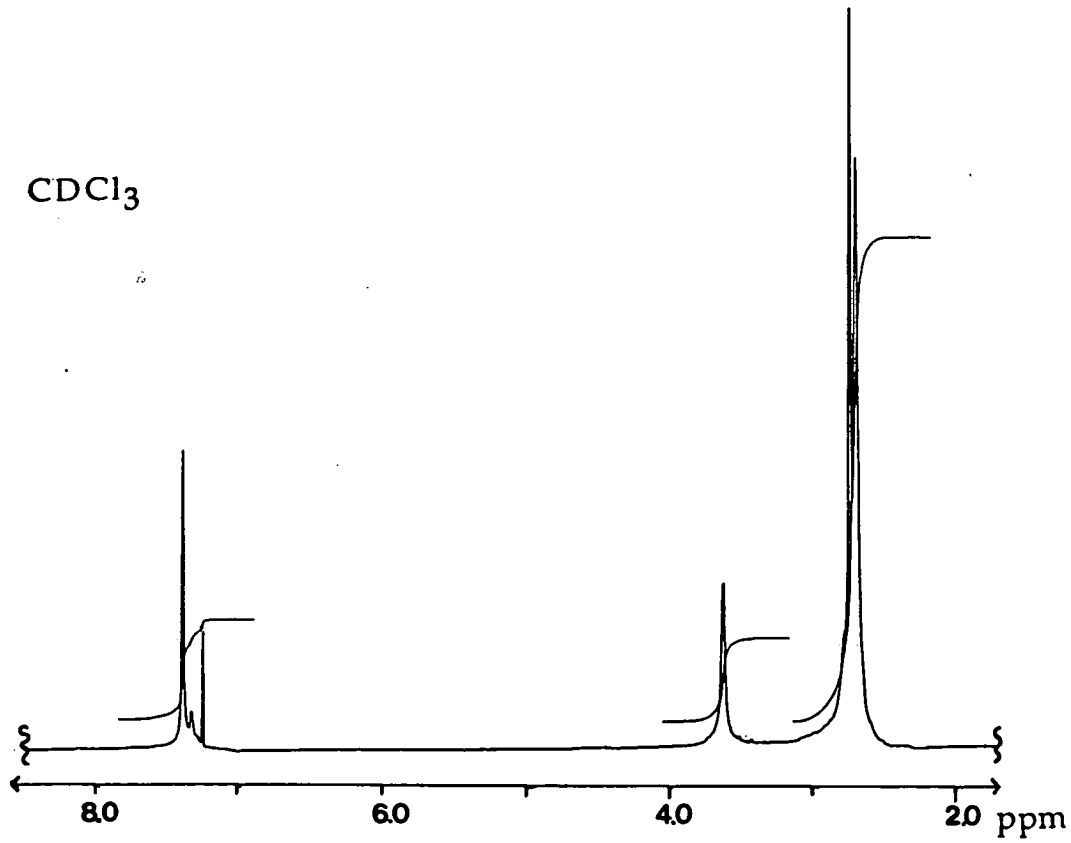

5.2.7 Complexes of L^6

Binuclear Pd(II) complex of L^6

Reaction of L^6 with two equivalents of $PdCl_2$ in a mixture of MeCN and H_2O afforded a yellow solution after reflux in for 2 hrs. A yellow precipitate was formed on the addition of NH_4PF_6 and recrystallised from Me_2CO and Et_2O. The product gave f.a.b. mass spectral peaks at M^+ = 1504, 1357, 1214 corresponding to $[^{106}Pd_2(L^6+H)(PF_6)_3]^+$, $[^{106}Pd_2(L^6-H)(PF_6)_2]^+$ and $[^{106}Pd_2(L^6+H)(PF_6)]^+$ respectively. (Figure 5.4) On the basis of this evidence, together with i.r. spectroscopic data, the product was assigned as $[Pd_2(L^6)](PF_6)_4$.

Figure 5.4: F.a.b. mass spectral peaks for $[Pd_2(L^6)](PF_6)_4$

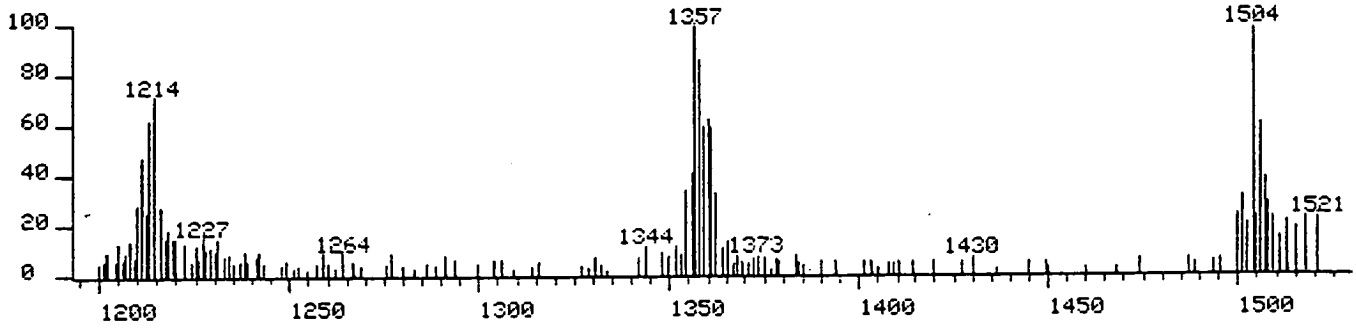

Unfortunately the very-low yield of this synthesis prevented any further characterisation of the binuclear Pd(II) 'face - to - face' complex.

In $[Pd([18]aneN_2S_4)]^{2+}$, the Pd(II) centre has a distorted octahedral stereochemistry, the Pd(II) ion is bound in a square plane to two S-donors, (Pd-S = 2.311(3), 2.367(3)Å) and two N-donors, (Pd-N = 2.068(7), 2.123(7)Å) the two remaining S-donors interact at long-range, (Pd...S = 2.954(4), 3.000(3)Å) [236] (19). Functionalisation of the N-H group to N-Me alters the stereochemistry adopted by the complex. $[Pd(Me_2[18]aneN_2S_4)]^{2+}$ shows a

square-planar stereochemistry with Pd(II) bound to four S-donors, Pd-S = 2.3239(22), 2.3261(22), 2.3331(22), 2.3399(22)Å. [236] (20).

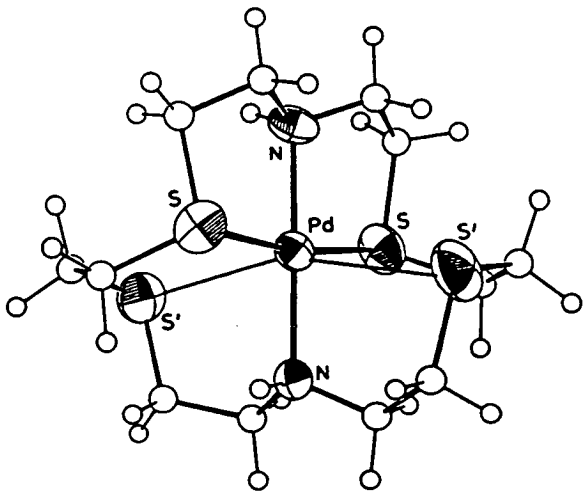

(19) $[Pd([18]aneN_2S_4)]^{2+}$

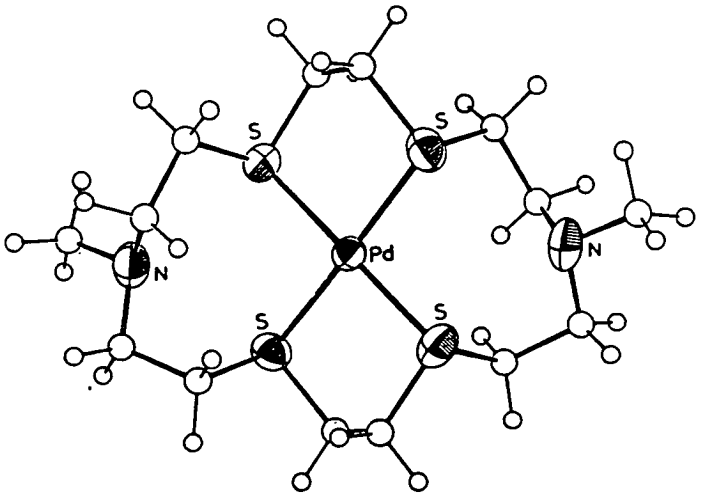

(20) $[Pd(Me_2[18]aneN_2S_4)]^{2+}$

This alteration in stereochemistry is a consequence of the greater steric bulk of N-Me in comparison with N-H.[233] The increase in steric bulk at the N-function in L^6 is considerable. The co-ordination at Pd(II) in L^6 is therefore most likely square-planar to four S-donors. (21)

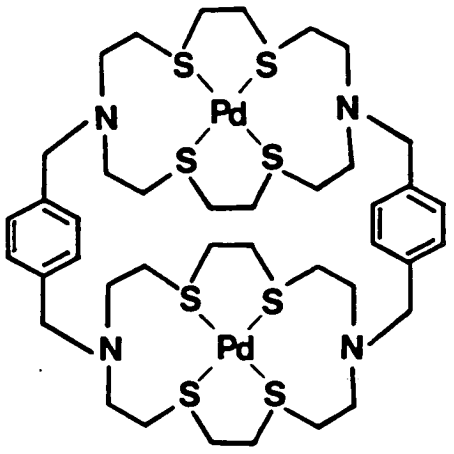

(21)

Gold (I) complex of L^6

Reaction of L^6 with two equivalents of $[Au(tht)_2](PF_6)$ in MeCN for 15 mins. results in a pale green solution. Addition of Et_2O affords a pale green precipitate. The product gave f.a.b. mass spectral peaks at M^+ = 1738, 1591, 1463, 1447, 1395, 1249 corresponding to $[^{197}Au_3(L^6\text{-}H)(PF_6)_2]^+$, $[^{197}Au_3(L^6\text{-}H)(PF_6)]^+$, $[^{197}Au_3(L^6\text{-}2H)(H_20)]^+$, $[^{197}Au_3(L^6)]^+$, $[^{197}Au_2(L^6)(PF_6)]^+$, $[^{197}Au_2(L^6\text{-}H)]^+$ respectively. It is difficult to ascertain if these are genuine peaks due to the complex or are a result of clustering during the f.a.b. mass spectrometry experiment. In conclusion, Au(I) binds to L^6, possibly giving a 2:1 or 3:1 complex.

5.3 CONCLUSIONS

Au(I) complexes of [18]aneN_2S_4 and Me_2[18]aneN_2S_4 have been isolated. In $[Au([Me_2[18]aneN_2S_4]^+$ three S-donors complete the [2+1] co-ordination at Au(I). It is possible that Au(I) is bound to [18]aneN_2S_4 in a similiar manner in view of the related Cu(I) structures. $[Au(Me_2[18]aneN_2S_4)]^+$ exhibits two quasi-reversible oxidations, suggesting the stabilisation of Au(II) and Au(III), whereas $[Au([18]aneN_2S_4)]^+$ undergoes an irreversible oxidation, most likely to Au(III). If the Au(II) centre desires a distorted octahedral geometry, it would appear that Me_2[18]aneN_2S_4, unlike [18]aneN_2S_4, can encapsulate a Au(II) ion in this stereochemistry. Improved syntheses of $[Au(L)](PF_6)$ (L = [18]aneN_2S_4, Me_2[18]aneN_2S_4) are required to allow the full characterisation of their redox processes.

A one-step synthetic route to the binucleating 'face - to - face' ligand L^6 has been established. The 'soft' S-donors of this ligand were exploited in the complexation of Pd(II), yielding a binuclear complex. Further complexation studies of this ligand may produce new binuclear species that undergo facile multi-electron transfer processes.

5.4 EXPERIMENTAL SECTION

5.4.1 Synthesis of [Au([18]aneN$_2$S$_4$)](PF$_6$)

Reaction of [18]aneN$_2$S$_4$ (50 mg, 0.153 mmol) with [Au(tht)$_2$]PF$_6$ (87 mg, 0.168 mmol) in stirring CH_2Cl_2 (10 cm^3) for 2 hrs. at room temperature, in the dark, gives a colourless solution, which was then reduced in volume (3 cm^3) *in vacuo*. Filtration into ice-cold hexane (20 cm^3) afforded a white precipitate on cooling to -20°C. The product was filtered, recrystallised from Me_2CO/hexane and washed with hexane, yielding a white solid which was dried *in vacuo* and stored at -20°C. (Yield 32 mg, 31%). M.Wt. = 668.54. Elemental analyses: found C = 21.4, H = 3.95, N = 3.93, S = 17.7%. Calc. for $C_{12}H_{26}S_4N_2AuPF_6$: C = 21.5, H = 3.92, N = 4.20, S = 19.2%. I.r. spectrum (KBr disc): 3200-3000, 2960, 2910, 2820, 1740, 1480, 1465, 1445, 1420, 1300, 1270, 1210, 1130, 1000, 940, 900, 870, 835, 780, 740, 640 and 555 cm^{-1}. F.a.b. mass spectrum (3-NOBA matrix) : found M^+ = 523. Calc. for [^{197}Au([18]aneN$_2$S$_4$)]$^+$: M^+ = 523, with correct isotopic distribution

5.4.2 Synthesis of $[Au(Me_2[18]aneN_2S_4)](PF_6)$

Reaction of $Me_2[18]aneN_2S_4$ (30 mg, 0.085 mmol) ith $[Au(tht)_2]PF_6$ (44 mg, 0.085 mmol) in stirring MeCN (5 cm^3) for 30 mins at room temperature, in the dark gives a pale yellow solution. Filtration into ice-cold Et_20 (20 cm^3) afforded a precipitate on cooling to -20°C. The product as filtered, ashed ith Et_20, yielding a pale green solid which was and dried *in vacuo* and stored at -20°C. (Yield 25 mg, 42%). M. t. = 696.59. Elemental analyses: found C = 23.0, H = 4.11, N = 4.08, S = 18.8%. Calc. for $C_{18}H_{30}S_4N_2AuPF_6$: C = 24.1, H = 4.34, N = 4.020, S = 18.4%. I.r. spectrum (KBr disc): 2940, 2850, 2800, 2795, 1460, 1450, 1420, 1380, 1310, 1280, 1265, 1250, 1240, 1220, 1200, 1170, 1160, 1100, 1060, 1015, 975, 950, 940, 920, 890, 860-840, 750 and 560 cm^{-1}. F.a.b. mass spectrum (3-NOBA matrix) : found M^+ = 697, 551. Calc. for $[^{197}Au(Me_2[18]aneN_2S_4+H)PF_6]^+$: M^+ = 697, $[^{197}Au(Me_2[18]aneN_2S_4)]^+$; M^+ = 551, with correct isotopic distributions.

5.4.3 Single crystal structure determination of $[Au(Me_2[18]aneN_2S_4)](PF_6)$

A pale yellow columnar crystal (0.12 x 0.14 x 0.54 mm) suitable for X-ray analysis was obtained by vapour diffusion of Et_2O into a solution of the complex in MeCN.

Crystal data:

$[C_{14}H_{30}S_4N_2Au]^+.(PF_6^-)$, M = 696.52, monoclinic, space group $P2_{1/c}$ a .= 12.4809(22), b = 19.6508(24), c = 9.7532(15)Å, β = 102.242(22)°, U = 2338 $Å^3$ [from 2θ values of 45 reflections measured at ± ω (24< 2θ< 26°, λ =

0.71073 Å)] $Z = 4$, $D_c = 1.979$ gcm^{-3}, T = 277 K, $\mu = 67.01$ mm^{-1}, F (000) = 1360.

Data collection and processing:

Stoë STADI-4 four circle diffractometer, graphite-monochromated Mo-K_α X-radiation, T = 277 K, ω - 2θ scans using the learnt-profile method [307], 2195 data measured ($2\theta_{max}$ 45°, h -10→10, k 0→21, l 0→13, giving 2642 ith $F \geq 6\,\sigma(F)$ for use in all calculations. Initial absorption correction was made using ψ scans (maximum transmission factor = 0.3022, minimum = 0.2401).

Structure solution and refinement:

A Patterson synthesis located the Au atom and iterative cycles of least-squares refinement and difference Fourier syntheses located the remaining non-hydrogen atoms. At isotropic convergence, corrections (min 0.852, max. 1.105) for absorption were applied using DIFABS.[308] Disorder in the PF_6^- counter-anion was modelled by allowing partial occupation of alternative sites of selected F atoms. The Au, N, S, C, P and fully occupied F atoms were then refined (by least-squares on F [309]) with anisotropic thermal parameters, and hydrogen atoms were included in fixed, calculated positions. At final convergence at R, R_w = 0.0282, 0.0400, respectively, S = 1.051 for 273 refined parameters, and the final ΔF synthesis show ed no feature above 0.98eÅ^{-3}. The weighting scheme, $w^{-1} = \sigma^2(F) + 0.001027F^2$, gave satisfactory agreement analyses and in the final cycle $(\Delta/\sigma)_{max}$ was 0.049.

5.4.4 Synthesis of L^6

To a vigorously stirring, refluxing suspension of Cs_2CO_3 (25g) in MeCN (160 cm^3), under N_2, solutions of [18]aneN_2S_4 (500 mg, 1.53 mmol) in MeCN : CH_2Cl_2 (4:1 v/v, 100 cm^3) and *p*-dibromoxylene (406 mg, 1.53 mmol) in MeCN (100 cm^3) were added over 2hrs. The resultant mixture was refluxed for 24 hrs. and monitored by t.l.c., which showed the presence of two products (R_f = 0.24, 0.40). Cs_2CO_3 as filtered off to give a yellow filtrate. The solvent as removed from the filtrate in vacuo, the residue was redissolved in MeCN (20 cm^3) and then H_2O (100 cm^3) was added. All the solvent was removed from the white cloudy solution, to give a cream gum. The residue as taken up in $CHCl_3$ (100 cm^3) and dried over $CaSO_4$ for 12 hrs. The product was isolated by precipication with hexane. A second crop of L^6 was obtained by extraction of the Cs_2CO_3 residue. The Cs_2CO_3 in H_2O (100 cm^3) was extracted with portions of CH_2Cl_2 (4 x 30 cm^3). The solvent was removed from the combined extracts *in vacuo*. The resultant yellow oil was dissolved in $CHCl_3$ and dried over $CaSO_4$. The second crop was recrystallised from CH_2Cl_2 and hexane. (Combined yield 150 mg, 23 %) M.Wt = 857.83. Elemental analyses: found C = 54.1, H = 6.77, N = 4.87 %. Calc. for $C_{40}H_{64}S_8N_4$: C = 56.1, H = 7.48, N = 6.54 %. I.r. spectrum (KBr disc) : 3300-3000,2950, 2920, 2800, 1750, 1700, 1620-1600, 1510, 1450, 1420, 1370, 1360, 1270, 1200, 1100, 1040, 1020, 820, 700, 680, 600 and 480 cm^{-1}. F.a.b. mass spectrum (3-NOBA matrix) : found M^+ = 857. Calc. for $[C_{40}H_{65}S_8N_4]^+$: M^+ = 857, with correct isotropic distribution. ^1H n.m.r. spectrum ($CDCl_3$, 298 K, 80.13 MHz) : δ = 7.39 (8H), 3.61 (8H), 2.68-2.72 (48H) ppm ^{13}C (DEPT) n.m.r. spectrum ($CDCl_3$, 298 K, 50.32 MHz) : δ = 128.7 (aryl-CH), 59.3 (CH_2-Ar),

55.1 (CH_2-N), 32.7,30.5 (CH_2-S) ppm. T.l.c. (plastic-backed silica) : (7:10) ethylacetate : hexane R_f = 0.40.

5.4.5 Synthesis of $[Pd_2(L^6)](PF_6)_4$

Reaction of L^6 (~ 30 mg, 0.035 mmol) with $PdCl_2$ (12 mg, 0.068 mmol) in refluxing MeCN : H_2O (60 : 40 cm^3) for 2hrs, under N_2 produced an orange solution. MeCN was removed in vacuo and MeOH (30 cm^3) was added. The solution was then refluxed for a further 6hrs, cooled and filtered. An orange product was formed on the addition of NH_4PF_6. The orange solid was filtered and recrystallised from MeCN and Et_2O. (Yield 17 mg, 29%) M.Wt. = 1649.83. I.r spectrum (KBr disc) : 3200, 2820, 1630, 1510, 1460, 1380, 1300, 1250, 1215, 1185 1130, 1090, 1035, 980, 840, 750, 720, 630 and 560 cm^{-1}. F.a.b. mass spectrum (3-NOBA matrix) : found M^+ = 1504, 1357, 1214; calc. for $[^{106}Pd_2(C_{40}H_{65}S_8N_4)(PF_6)_3]^+$: M^+ = 1504;
$[^{106}Pd_2(C_{40}H_{63}S_8N_4)PF_6)_2]$+ : M^+ = 1357;
$[^{106}Pd_2(C_{40}H_{65}S_8N_4)]^+$: M^+ = 1214 with correct isotopic distributions.

CHAPTER 6

Copper and silver complexes of octathia macrocycles

6.1 INTRODUCTION

A variety of biological processes involve copper containing proteins, these include electron transfer and many oxidase activities.[28,255-257] Numerous spectroscopic studies, both of the original biomolecules and of model systems, have been undertaken in an effort to discover the key features of these enzymes.[258-262,269] Many aspects of their behaviour still remain unclear, hence the continued interest in this area. The study of mononuclear and binuclear Cu(II)/(I) complexes as models for these metalloenzymes is well established.[239,242,263-285]

Binucleating macrocyclic ligands have been used in the synthesis of possible models for haemocyanin, blue oxidases and tyrosinase,[28,255] all known to contain binuclear copper active sites (1).[28,286,287]

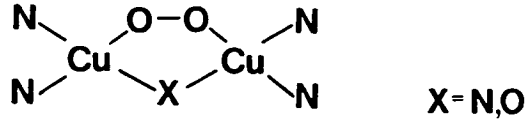

(1) Proposed binuclear copper sites for oxyhaemocyanin

Larger ring systems and compartmental ligands binding two copper centres in close proximity have been synthesised in order to mimic the magnetic and e.p.r. behaviour of these metalloenzymes.[242,278-285] Ligands (2) - (5) are examples of binucleating ligands used to complex two copper ions.

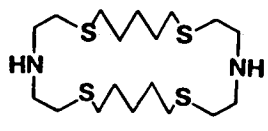

(2)

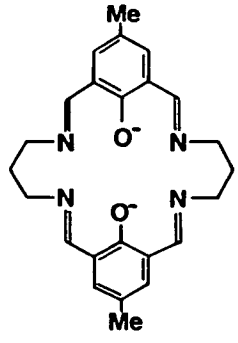

(3)

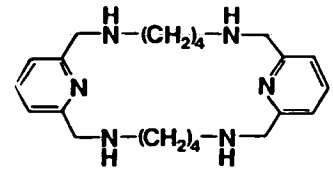

(4)

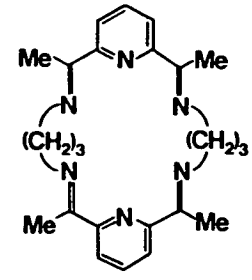

(5)

Several biological systems involve copper co-ordinated to sulphur e.g. plastocyanin[290] and azurin,[291] in which there is believed to be a primary 'S_2N_2' co-ordination about the metal centre. This provided the initial impetus for the investigation of thioether macrocyclic complexes of Cu(II)/(I).[88,108,110,117,292-302]

Rorabacher *et al.* have reported a series of studies on the complexation of Cu(II) and Cu(I) with [15]aneS_5 and various tetrathia macrocycles.[108,110,292-299] The single crystal X-ray structure of $[Cu([15]aneS_5)]^{2+}$ shows a square-based pyramidal stereochemistry, Cu - S_{eq} = 2.289(2), 2.315(2), 2.331(2), 2.338(2), Cu-S_{ap} = 2.398(2)Å, with the copper atom 0.41Å out of the basal plane,[108] (6). Reduction of $[Cu([15]aneS_5)]^{2+}$ affords $[Cu([15]aneS_5)]^{+}$, in which the Cu(I) centre has a distorted tetrahedral geometry in the solid state, Cu - S = 2.243(5), 2.245(5), 2.317(5), 2.338(5)Å, the fifth S- donor is non-bonding and is disordered over the two sites, Cu...S = 3.443(12) and 3.560(11)Å (7).

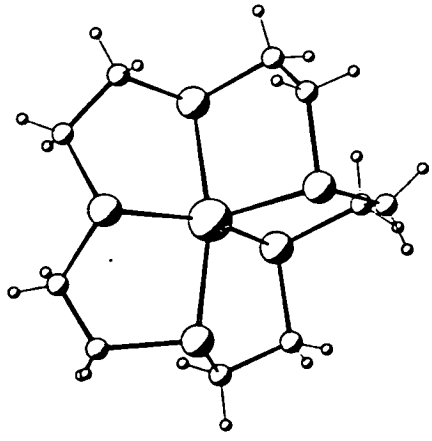

(6) $[Cu([15]aneS_5)]^{2+}$

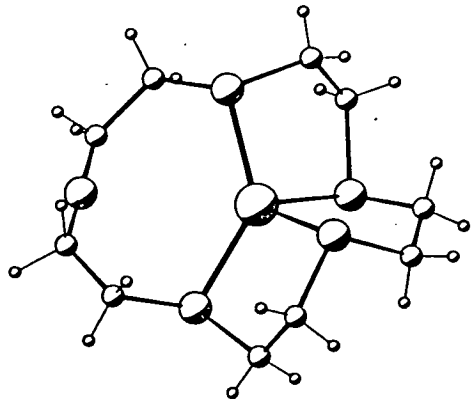

(7) $[Cu([15]aneS_5)]^{+}$

The self-exchange electron-transfer rate constant for the $[Cu([15]aneS_5)]^{2+/+}$ couple is very rapid ($k = 3 \times 10^4\ M^{-1}s^{-1}$).[108] Cooper *et al.* have reported[117] a similar, rapid Cu - S bond cleavage on reduction of $[Cu([18]aneS_6)]^{2+}$. The Cu(II) complex of [18]aneS_6 shows a tetragonally elongated octahedral

stereochemistry, Cu - S = 2.328(1), 2.402(1), 2.635(1)Å (8). Reduction of this complex gives $[Cu([18]aneS_6)]^+$ which, like $[Cu([15]aneS_5)]^+$, shows a tetrahedral stereochemistry at the metal centre, Cu - S = 2.245(2), 2.253(2), 2.358(2), 2.360(2)Å (9).

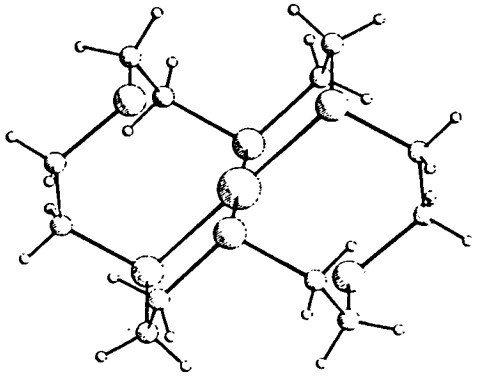

(8) $[Cu([18]aneS_6)]^{2+}$

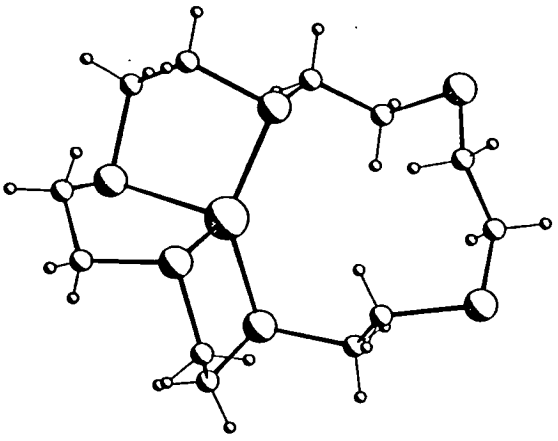

(9) $[Cu([18]aneS_6)]^+$

The interconversion of Cu(II)/(I) centres within the $[15]aneS_5$ and $[18]aneS_6$ ligands therefore involves the formation and breaking of one and two Cu - S bonds, respectively. Lucas *et al.* have reported copper complexes of thioether ligands incorporating a thiophene unit, L^1 *301* and L^2 *302* (10),(11). In the structure of $[Cu(L^1)_2]^+$, the Cu(I) centre has a distorted tetrahedral co-ordination geometry with Cu - S = 2.359(3), 2.307(3), 2.392(3), 2.301(2)Å, with the thiophene unit non-bonding. These results suggested that tetrahedral co-ordination of copper(I) to thioether crowns is preferred, as expected for a d^{10} metal centre.

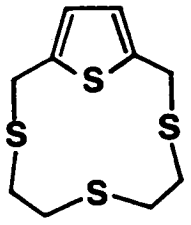

(10)

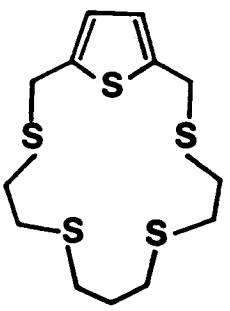

(11)

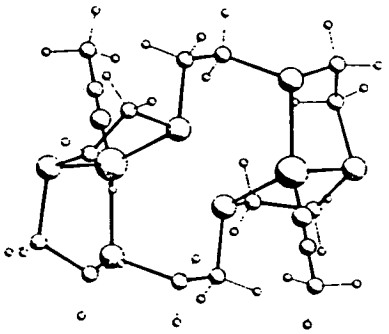

(12) $[Cu_2(NCMe)_2([18]aneS_6)]^{2+}$

The synthesis and structure of binuclear Cu(I) species $[Cu_2(L)(NCMe)_2]^{2+}$, (L = [18]aneS_6[121] (12), Me_2[18]aneN_2S_4[234]) have been reported. In these systems, however, the 18-membered rings lack sufficient sulphur donors and are too small to encapsulate two tetrahedral Cu(I) centres. Therefore a MeCN solvent molecule completes the tetrahedral co-ordination at each Cu(I) centre. The larger ring, octadentate thioether macrocycles, [24]aneS_8 and [28]aneS_8, should be capable of encapsulating two Cu(I) ions tetrahedrally within the macrocyclic framework to give a binuclear, homoleptic thioether complex.

The initial aims of the work described in this Chapter were to synthesise the binuclear Cu(I) complexes of [24]aneS_8 and [28]aneS_8, examine their redox properties, and then hopefully generate active binuclear Cu(II) species with a view to the incorporation of small molecular substrates.

The co-ordination of these two macrocycles has not previously been studied in depth, some complexes of Nb(V),[89] Ni(II),[125] Pd(II),[24,125] Cu(II),[124] Ag(I),[126,127] Hg(II),[126] ions have been reported with these ligands, although the resultant complexes have not been characterised unequivocally.

Due to the paucity of fully characterised complexes of these ligands the pursuit of the binuclear Ag(I) species was also undertaken, providing analogous complexes for comparison with the copper species. As discussed in Chapter 4 complexation of Ag(I) ions to thioether ligands leads to a variety of metal co-ordination geometries depending on the ligand and the counter-ion.[106,107,120,303,304]

6.2 RESULTS AND DISCUSSION

$[Cu_2([24]aneS_8)](X)_2$ $(X = BF_4^-, PF_6^-)$

6.2.1 Synthesis

Reaction of [24]aneS_8 with two molar equivalents of $[Cu(NCMe)_4](BF_4)$ in refluxing MeCN afforded a white precipitate on the addition of Et_2O. Re-crystallisation of this product from hot Me_2CO and Et_2O yielded a white microcrystalline solid, which gave f.a.b. mass spectral peaks at $M^+ = 694$, 606 assigned to $[^{63}Cu_2([24]aneS_8\text{-}H)(BF_4)]^+$, $[^{63}Cu_2([24]aneS_8\text{-}2H)]^+$ respectively. On the basis of this evidence and additional data from microanalyses and i.r. spectroscopy, the product was assigned as $[Cu_2([24]aneS_8)](BF_4)_2$. Full experimental details are given in Section 6.4.1.

The PF_6^- salt was synthesised by the same method except using $[Cu(NCMe)_4](PF_6)$, the product gave f.a.b. mass spectral peaks at $M^+ = 753$, 607 assigned to $[^{63}Cu_2([24]aneS_8)PF_6]^+$, $[^{63}Cu([24]aneS_8\text{-}H)]^+$ respectively. In order to confirm the connectivity and stereochemistry at the Cu(I) centres, and also the conformation of the large-ring macrocycle, a single crystal X-ray structure determination was carried out.

6.2.2 Structure determination of $[Cu_2([24]aneS_8)](BF_4)_2$

A single crystal X-ray structure determination on $[Cu_2([24]aneS_8)](BF_4)_2$ confirmed the compound to be a genuine binuclear Cu(I) complex (Figure 6.1). Full details of solution and refinement of the structure are given in

Section 6.4.2. Selected bonds, angles and torsions for this structure are given in Table 6.1. The two Cu(I) centres are related by a crystallographic inversion centre and are each co-ordinated to four thioether S-donors, Cu - S(1) = 2.263(3), Cu - S(5) = 2.363(3), Cu - S(7) = 2.349(3), Cu - S(10) = 2.261(3)Å. These bond lengths are comparable with Cu - S distances in related complexes:

$[Cu([15]aneS_5)]^+$; Cu - S = 2.243(5) - 2.338(5)Å;[108]

$[Cu([18]aneS_6)]^+$: Cu - S = 2.245(2), 2.360(2);[117]

$[Cu_2([18]aneS_6)(NCMe)_2]^+$: Cu - S = 2.3200(15) - 2.3415(16)Å.[121] The Cu...Cu distance of 5.172(3)Å in the $[Cu_2([24]aneS_8)]^{2+}$ cation indicates that the two metal centres are non-interacting. The angles at the Cu(I) centres are distorted from those expected for strictly tetrahedral co-ordination S(1) - Cu - S(4) = 94.54(10). S(1) - Cu - S(7) = 120.20(11), S(1) - Cu - S(10) = 133.86(11), S(4) - Cu - S(7) = 91.81(10), S(4) Cu - S(10) = 116.39(10), S(7) - Cu - S(10) = 93.57(10)°. The structure shows that the 24-membered macrocyclic ligand is sufficiently flexible and the cavity large enough to encapsulate two isolated tetrahedral metal centres.

6.2.3 N.m.r. studies

The ^1H n.m.r. spectrum of $[Cu_2([24]aneS_8)](BF_4)_2$ shows a broad resonance at δ = 2.13 - 2.93 ppm in CD_3CN. If the solid-state structure of $[Cu_2([24]aneS_8)]^{2+}$ is retained in solution the ^1H n.m.r. spectrum would show a complex second-order multiplet. The expected ^{13}C n.m.r. spectrum should show at least four different methylene resonances for the binuclear distorted tetrahedral co-ordination of the [24]aneS$_8$ ligand. Instead the ^{13}C n.m.r. spectrum ligand $[Cu_2([24]aneS_8)](PF_6)_2$ shows a single resonance at

Figure 6.1: Single crystal X-ray structure of $[Cu_2([24]aneS_8)]^{2+}$

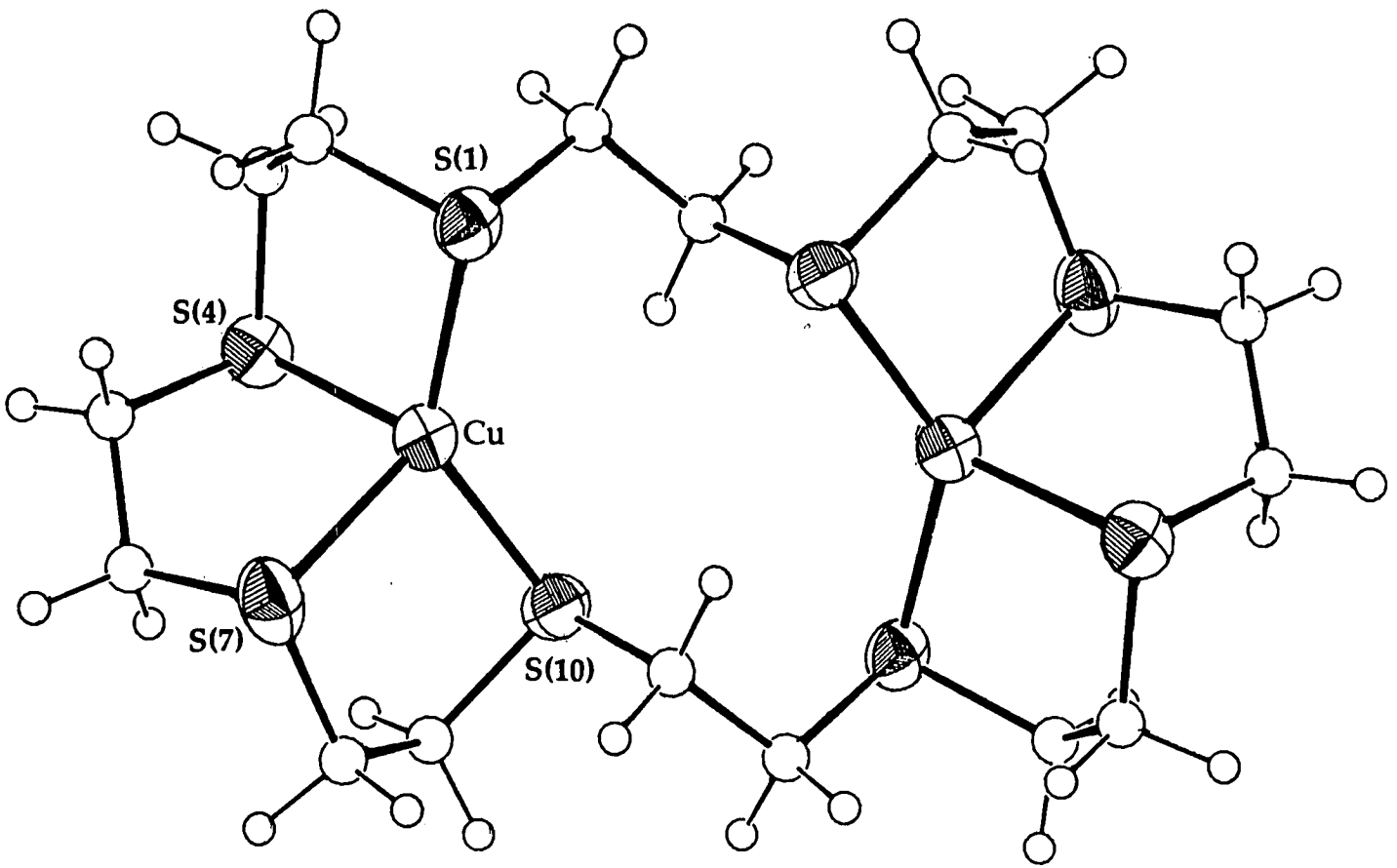

Table 6.1: Selected bonds, angles and torsions for $[Cu_2([24]aneS_8)]^{2+}$

Cu(1) - S(1)	2.263(3)	C(5) - C(6)	1.503(16)
Cu(1) - S(4)	2.363(3)	C(6) - S(7)	1.817(12)
Cu(1) - S(7)	2.349(3)	S(7) - C(8)	1.808(12)
Cu(1) -S(10)	2.261(3)	C(8) - C(9)	1.561(16)
S(1) - C(2)	1.800(10)	C(9) -S(10)	1.814(12)
C(2) - C(3)	1.520(14)	S(10) -C(11)	1.811(10)
C(3) - S(4)	1.816(10)	C(11) -C(12)	1.524(14)
S(4) - C(5)	1.837(12)	C(12) -S(1')	1.807(11)

S(1) -Cu(1) - S(4)	94.54(10)	C(3) - S(4) - C(5)	101.8(5)
S(1) -Cu(1) - S(7)	120.20(11)	S(4) - C(5) - C(6)	110.3(8)
S(1) -Cu(1) -S(10)	133.86(11)	C(5) - C(6) - S(7)	113.1(8)
S(4) -Cu(1) - S(7)	91.81(10)	Cu(1) - S(7) - C(6)	98.0(4)
S(4) -Cu(1) -S(10)	116.39(10)	Cu(1) - S(7) - C(8)	98.8(4)
S(7) -Cu(1) -S(10)	93.57(10)	C(6) - S(7) - C(8)	102.3(5)
Cu(1) - S(1) - C(2)	97.8(3)	S(7) - C(8) - C(9)	116.2(8)
Cu(1) - S(1) -C(12')	110.8(4)	C(8) - C(9) -S(10)	112.7(8)
C(2) - S(1) -C(12')	100.9(5)	Cu(1) -S(10) - C(9)	97.7(4)
S(1) - C(2) - C(3)	115.4(7)	Cu(1) -S(10) -C(11)	107.9(3)
C(2) - C(3) - S(4)	116.3(7)	C(9) -S(10) -C(11)	103.6(5)
Cu(1) - S(4) - C(3)	97.3(3)	S(10) -C(11) -C(12)	113.1(7)
Cu(1) - S(4) - C(5)	96.4(4)	C(11) -C(12) -S(1')	112.7(7)

C(12')- S(1) - C(2) - C(3)	70.7(8)	C(6) - S(7) - C(8) - C(9)	77.6(9)
S(1) - C(2) - C(3) - S(4)	51.1(9)	S(7) - C(8) - C(9) -S(10)	49.9(11)
C(2) - C(3) - S(4) - C(5)	70.6(8)	C(8) - C(9) -S(10) -C(11)	63.7(9)
C(3) - S(4) - C(5) - C(6)	-147.6(8)	C(9) -S(10) -C(11) -C(12)	91.2(8)
S(4) - C(5) - C(6) - S(7)	64.9(9)	S(10) -C(11) -C(12) -S(1')	68.2(8)
C(5) - C(6) - S(7) - C(8)	-141.7(8)		

32.54 ppm in CD_3CN. The appearance of this single carbon resonance implies that the ligand is undergoing a rapid intramolecular averaging process. Lowering the temperature should affect such a process, however this resulted in precipitation of the sample. Repeat studies in different solvents showed similar behaviour. Therefore the elucidation of the solution structure of $[Cu_2([24]aneS_8)](PF_6)_2$ was not possible.

6.2.4 Electrochemical study

Cyclic voltammetry of $[Cu_2([24]aneS_8)](PF_6)_2$ at platinum electrodes in MeCN (0.1M $^nBu_4NPF_6$) shows an irreversible oxidation at Ep_a = +0.88V vs Fc/Fc^+ at a scan rate of 200 mVs^{-1}. Coulometric measurements confirmed this oxidation to be a two-electron process, affording a green e.p.r. active product. The X-band frozen glass e.p.r. spectrum recorded for the oxidation product (Figure 6.2) shows a complicated metal-based multiplet consistent with the electrogeneration of a binuclear Cu(II) species. The extent of the interaction, if any, between the d^9 metal centres is difficult to ascertain. There is a marked similarity between this spectrum and that obtained for ^{63}Cu doped crystals of $[Ni([14]aneS_4)]^{2+}$.[101] However, there is additional structure in the spectrum of the oxidised $[Cu_2([24]aneS_8)]^{2+}$ species. If the vacant axial sites on the Cu(II) centres were occupied by a bound MeCN molecule then an additional coupling to ^{14}N (I = 1) should be present, this may account for the additional features in the spectrum. Interpreting this spectrum requires further analysis and computer simulation to determine whether this signal is due to, (i) two overlapping dissimilar Cu(II) centres, (ii) Cu(II) centres with axially bound solvent molecules, (iii) weakly interacting Cu(II) centres.[333]

Figure 6.2: X-band frozen glass e.p.r. spectrum of the electrochemical oxidation product of $[Cu_2([24]aneS_8)](PF_6)_2$

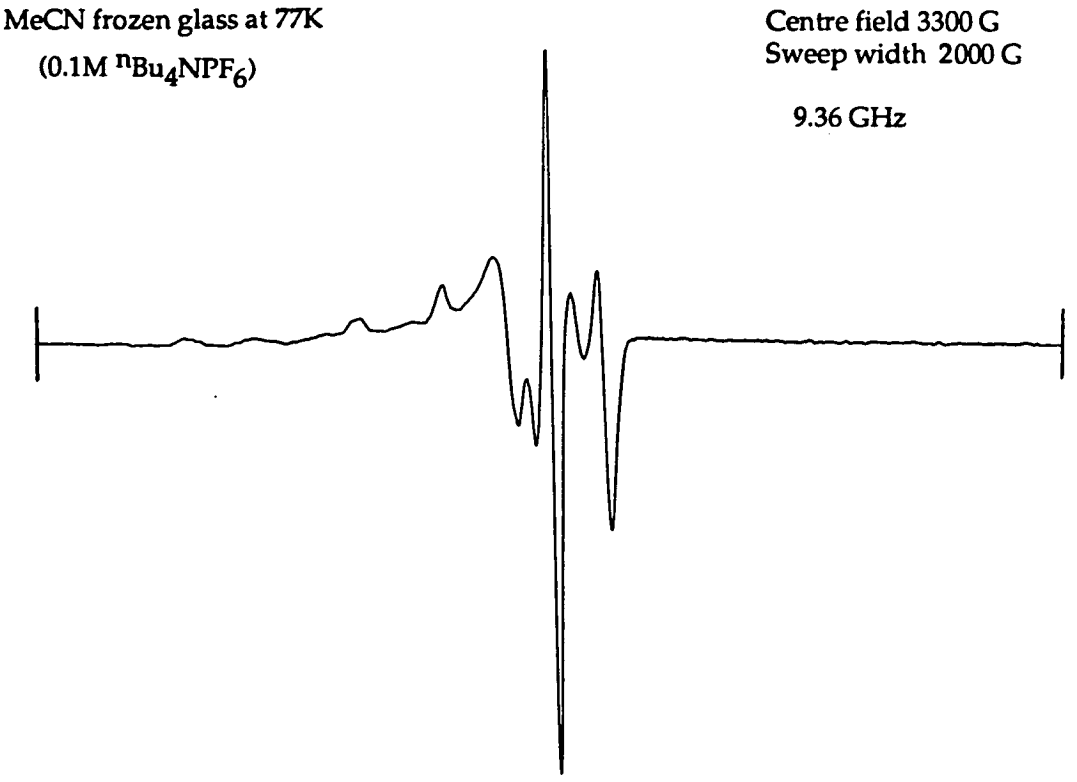

Figure 6.3: Spectroelectrochemical study of $[Cu_2([24]aneS_8)](PF_6)_2$

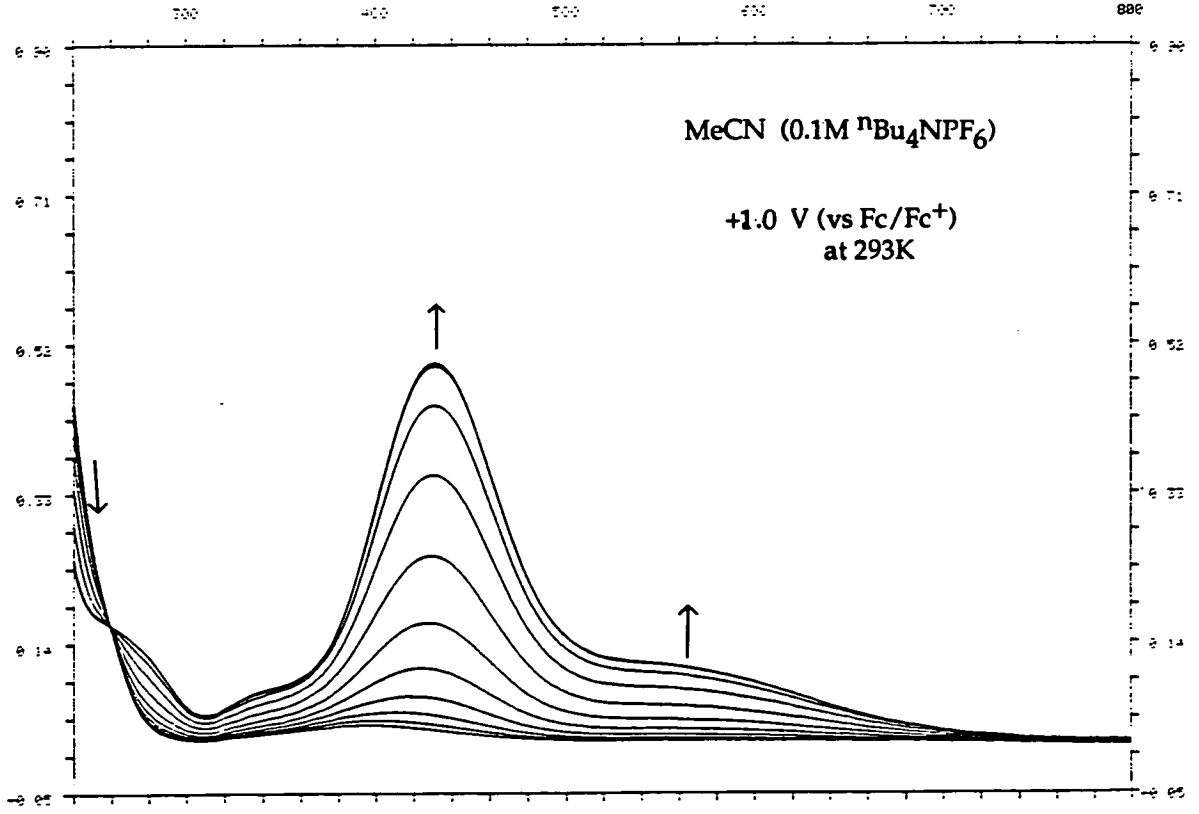

Access to suitable simulation programmes was not available at this time.

The electrogeneration can be monitored by UV/Vis spectroscopy (Figure 6.3). At E = +1.0 V vs Fc/Fc^+ the growth of a broad band of λ_{max} = 430.8 nm (ε_{max} = 8100 $M^{-1}cm^{-1}$) with an isobestic point at λ_{iso} = 258 nm is observed. The collapse of this band is seen on re-reduction at 0 V, however the starting material is not re-generated. The fact that the oxidation is irreversible and prone to decomposition is not surprising since the resultant Cu(II) centres would be expected to tend towards octahedral or at least five co-ordination, and would therefore require extra ligation. Decomposition of the oxidised binuclear Cu(I) species to a mononuclear Cu(II) species via the de-complexation of the second Cu(II) centre cannot be ruled out. There would then be sufficient S-donors available to the lone Cu(II) centre for the satisifaction of a preferred co-ordination.

6.2.5 Chemical oxidation

Oxidation of $[Cu_2([24]aneS_8)](PF_6)_2$ using concentrated HNO_3 and 98% H_2SO_4 affords stable yellow and green paramagnetic species, respectively. The frozen glass e.p.r. spectra alter markedly depending on the mineral acid used and differ from the spectrum of the electrogenerated species, suggesting the incorporation of bound NO_3^- and SO_4^{2-} ions in the chemically oxidised species.

Isolation of these oxidised products proved difficult due to the required presence of such strongly acidic media. The only feasible route to isolation of a product would be via crystallisation at low temperature.

However, the growth of crystals did not occur after storing these oxidised products in acid at -30°C for 18 months.

$[Cu_2([28]aneS_8)](X)_2$ $(X = ClO_4^-, PF_6^-)$

6.2.6 Synthesis

Reaction of [28]aneS_8 with two molar equivalents of $[Cu(NCMe)_4](ClO_4)$ in refluxing MeCN afforded a white precipitate on the addition of Et_2O. Re-crystallisation of this product from hot Me_2CO and Et_2O yielded a white microcrystalline solid which shows f.a.b. mass spectral peaks at $M^+ = 763$, 663 assigned to $[^{63}Cu_2([28]aneS_8)^{35}ClO_4]^+$, $[^{63}Cu_2([28]aneS_8\text{-}H)]^+$ respectively. The product was assigned as $[Cu_2([28]aneS_8)](ClO_4)_2$ on the basis of this evidence, together with microanalyses and i.r. spectroscopic data. Full experimental details are discussed in Section 6.4.3.

The PF_6^- salt was synthesised by the same method except using $[Cu(NCMe)_4](PF_6)$, the product gave f.a.b. mass spectral peaks at $M^+ = 809, 663$ assigned to $[^{63}Cu_2([28]aneS_8)PF_6]^+$, $[^{63}Cu_2([28]aneS_8\text{-}H)]^+$ respectively. To confirm the stereochemistry and a connectivity at the metal centres a single crystal X-ray structure determination was carried out.

6.2.7 Structure determination of $[Cu_2([28]aneS_8)](PF_6)_2$

A single crystal X-ray structure determination of $[Cu_2([28]aneS_8)](PF_6)_2$ confirmed the compound to be a genuine binuclear Cu(I) complex (Figure 6.4). Full details of the solution and refinement of the structure are given in Section 6.4.4. The structure shows similar features to that of the smaller

ring analogue $[Cu_2[24]aneS_8)]^{2+}$ (discussed in Section 6.2.2). The two tetrahedral Cu(I) centres, related by an inversion centre, are co-ordinated to four thioether S-donors, Cu - S(1) = 2.278(5), Cu - S(4) = 2.333(5), Cu - S(8) = 2.328(5), Cu - S(11) = 2.268(5)Å. The angles at the Cu(I) centres are again distorted from those expected for a tetrahedron, S(1) - Cu - S(4) = 93.69(19), S(1) - Cu - S(8) = 108.78(19), S(4) - Cu - S(9) = 105.66(18), S(4) - Cu - S(11) = 119.79(19), S(8) - Cu - S(11) = 93.25(18)°. The Cu...Cu distance of 6.454(3)Å is greater than in the $[Cu_2([24]aneS_8)]^{2+}$ cation, reflecting the greater cavity size of $[28]aneS_8$.

6.2.8 N.m.r. studies

The ^1H n.m.r. spectrum of $[Cu_2([28]aneS_8)](PF_6)_2$ shows a broad resonance at δ = 2.75 - 3.10 ppm assigned to the macrocyclic protons. The ^{13}C n.m.r. spectrum at 298K shows three resonances at 33.60, 31.50 and 25.56 ppm indicating that there is probably a fast intramolecular exchange process occurring either via the continual movement of the macrocylic ligand around the two copper (I) centres or via the rapid alteration of the ligand conformation about the bound metal centre. On cooling to 238K the species ceases to be as flexible giving six resonances at 34.27, 32.69, 32.08, 31.92, 30.35 and 21.90 ppm corresponding to the six unique methylene environments present when each Cu(I) centre is bound identically to an isolated set of four S-donors. This is consistent with each Cu(I) ion having a distorted tetrahedral stereochemistry, as found in the solid-state structure discussed in Section 6.2.7.

Figure 6.4: Single crystal X-ray structure of $[Cu_2([28]aneS_8)]^{2+}$

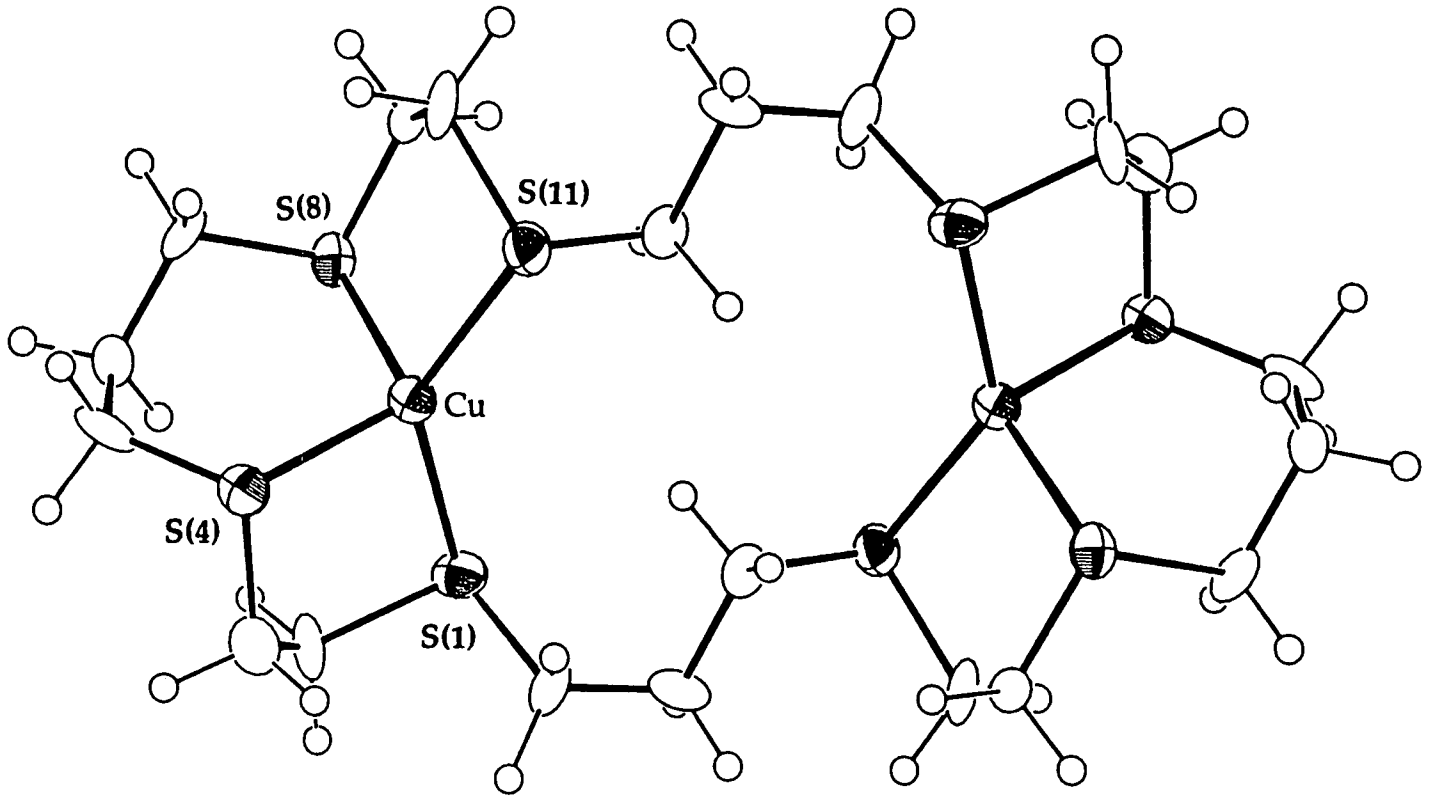

Table 6.2.: Selected bonds, angles and torsions for $[Cu_2([28]aneS_8)]^{2+}$

Cu - S(1)	2.278(5)	C(6) - C(7)	1.56(3)
Cu - S(4)	2.333(5)	C(7) - S(8)	1.794(20)
Cu - S(8)	2.328(5)	S(8) - C(9)	1.804(17)
Cu -S(11)	2.268(5)	C(9) -C(10)	1.493(25)
S(1) - C(2)	1.835(20)	C(10) -S(11)	1.850(19)
C(2) - C(3)	1.55(3)	S(11) -C(12)	1.761(20)
C(3) - S(4)	1.802(19)	C(12) -C(13)	1.56(3)
S(4) - C(5)	1.795(19)	C(13) -C(14)	1.50(3)
C(5) - C(6)	1.50(3)	C(14) -S(1')	1.849(21)

S(1) - Cu - S(4)	93.69(19)	C(6) - C(7) - S(8)	107.5(13)
S(1) - Cu - S(8)	108.78(19)	Cu - S(8) - C(7)	100.5(6)
S(1) - Cu -S(11)	133.39(20)	Cu - S(8) - C(9)	99.6(6)
S(4) - Cu - S(8)	105.66(18)	C(7) - S(8) - C(9)	100.8(8)
S(4) - Cu -S(11)	119.79(19)	S(8) - C(9) -C(10)	117.4(12)
S(8) - Cu -S(11)	93.25(18)	C(9) -C(10) -S(11)	113.3(12)
Cu - S(1) - C(2)	97.2(6)	Cu -S(11) -C(10)	99.3(6)
S(1) - C(2) - C(3)	111.1(13)	Cu -S(11) -C(12)	108.4(7)
C(2) - C(3) - S(4)	115.1(13)	C(10) -S(11) -C(12)	99.8(9)
Cu - S(4) - C(3)	98.6(6)	S(11) -C(12) -C(13)	115.3(14)
Cu - S(4) - C(5)	108.5(6)	C(12) -C(13) -C(14)	113.7(17)
C(3) - S(4) - C(5)	102.4(9)	C(13) -C(14) -S(1')	108.0(14)
S(4) - C(5) - C(6)	121.8(14)	C(14) -S(1') -C(2')	100.1(9)
C(5) - C(6) - C(7)	111.1(16)		

S(1) - C(2) - C(3) - S(4)	-56.2(16)	S(8) - C(9) -C(10) -S(11)	-48.3(16)
C(2) - C(3) - S(4) - C(5)	-80.6(15)	C(9) -C(10) -S(11) -C(12)	-70.6(14)
C(3) - S(4) - C(5) - C(6)	91.5(16)	C(10) -S(11) -C(12) -C(13)	-59.1(15)
S(4) - C(5) - C(6) - C(7)	63.8(20)	S(11) -C(12) -C(13) -C(14)	-167.6(14)
C(5) - C(6) - C(7) - S(8)	-101.4(16)	C(12) -C(13) -C(14) -S(1')	69.7(19)
C(6) - C(7) - S(8) - C(9)	169.3(13)	C(13) -C(14) -S(1') -C(2')	149.6(14)
C(7) - S(8) - C(9) -C(10)	-75.0(14)	C(14) -S(1') -C(2') -C(3')	68.6(14)

6.2.9 Electrochemical study

Cyclic voltammetry of $[Cu_2([28]aneS_8)](PF_6)_2$ at platinum electrodes in MeCN (0.1 M $^nBu_4NPF_6$) shows an irreversible oxidation at E_{pa} = +0.92V vs Fc/Fc^+ at a scan rate of 200 mVs^{-1}. The oxidation was confirmed by coulometry to be two-electron process, generating a green e.p.r. active species. The e.p.r. spectrum recorded (Figure 6.5) is similar to the signal obtained for the electrochemically oxidised $[Cu_2([24]aneS_8)]^{2+}$ species (Figure 6.2). The signal is consistent with a Cu(II) species, however it is difficult to fully analyse the spectrum without the assistance of computer simulation.

The electrogeneration can be monitored by UV/Vis spectroscopy (Figure 6.6). At E = +1.10V vs Fc/Fc^+ the growth of bands at λ_{max} = 560, 405 nm (ε_{max} = 3085, 19900 $M^{-1}cm^{-1}$) is observed, with an isobestic point at λ_{iso} = 228 nm. This band collapses to give a featureless spectrum on reduction at 0 V. This is a chemically and electrochemically irreversible process, consistent with decomposition to a mononuclear product.

6.2.10 Chemical oxidation

As with the analogous [24]aneS$_8$ complex, $[Cu_2([28]aneS_8)]PF_6)_2$ can be chemically oxidised using concentrated mineral acids, producing coloured paramagnetic species. The frozen glass e.p.r. spectrum of the red species (λ_{max} = 513.2, 410.4 nm, ε_{max} = ~20,000, ~3000 M^{-1} cm^{-1}) generated in 98% H_2SO_4 shows a complicated multiplet which differs in structure from the spectra obtained for the yellow HNO_3 generated species and the green

Figure 6.5: X-band frozen glass e.p.r. spectrum of the electrochemical oxidation product of $[Cu_2([28]aneS_8)](PF_6)_2$

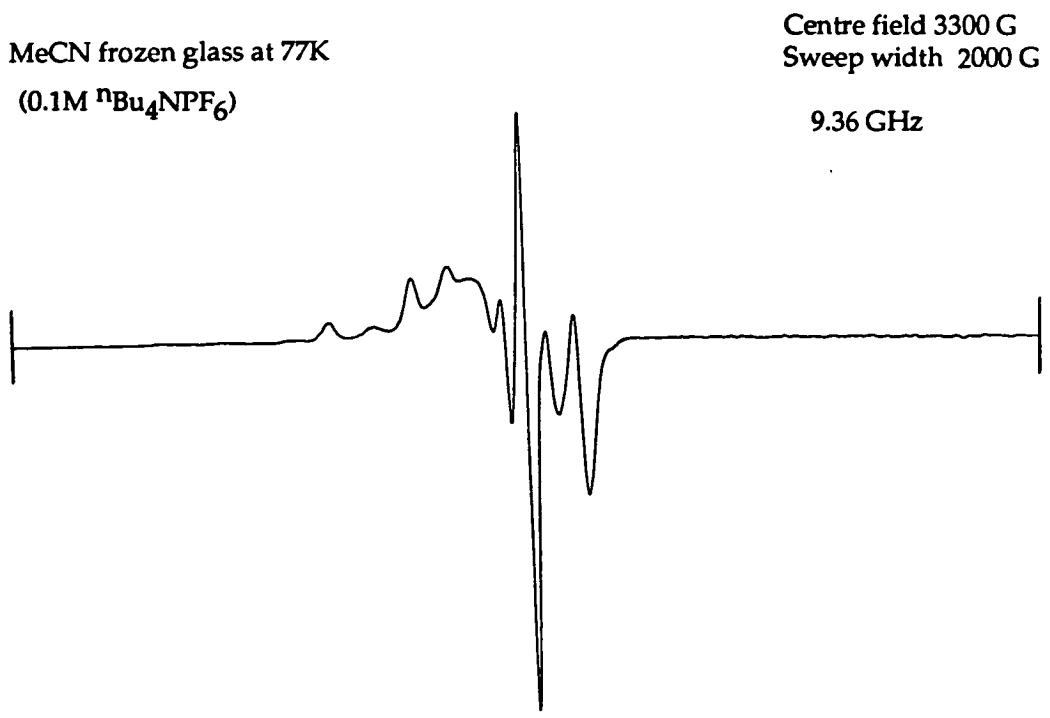

Figure 6.6 Spectroelectrochemical study of $[Cu_2([28]aneS_8)](PF_6)_2$

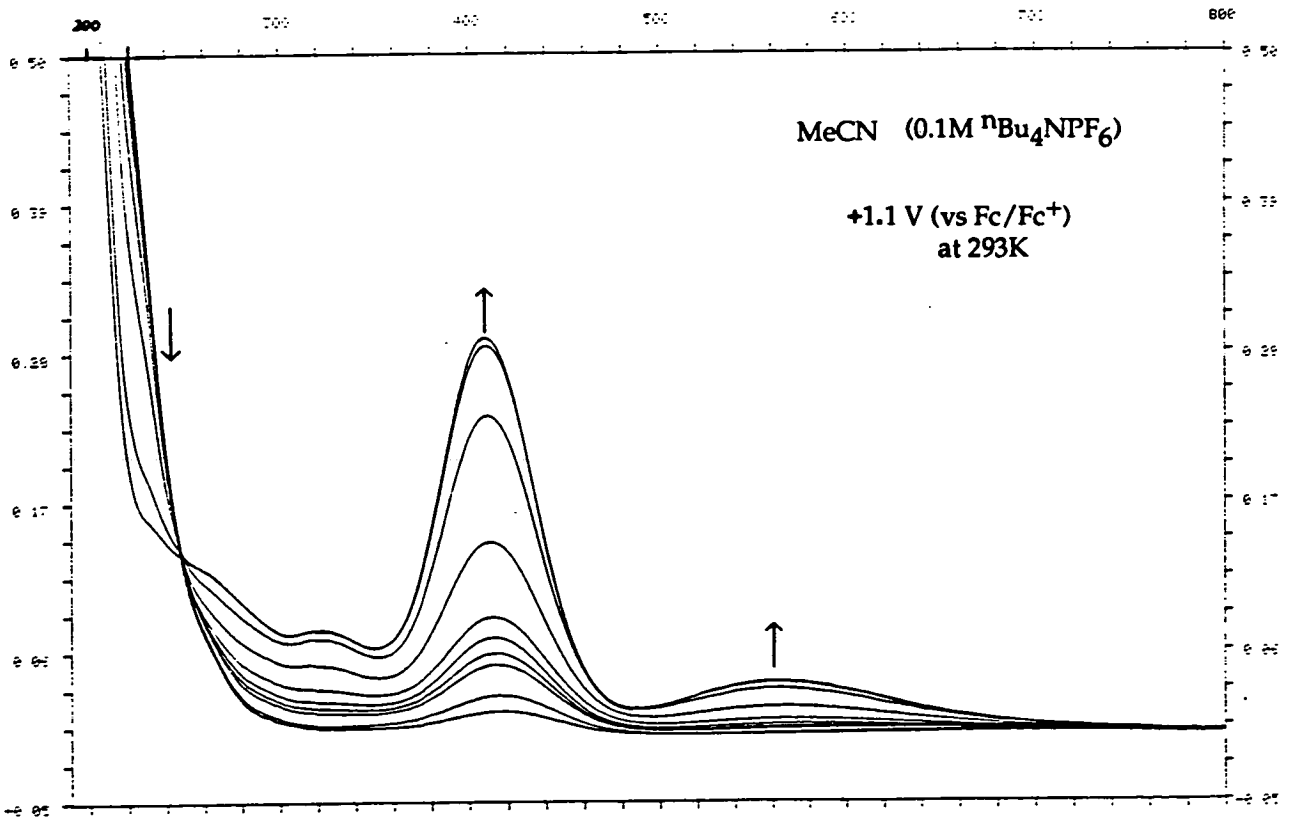

electrogenerated species, suggesting the incorporation of SO_4^{2-} NO_3^- into the chemically oxidised species.

$[Ag_2([24]aneS_8)](PF_6)_2$

6.2.11 Synthesis

Reaction of [24]aneS_8 with two molar equivalents of $AgPF_6$ in $MeNO_2$ afforded a white precipitate on the addition of Et_2O. The white product gave f.a.b. mass spectral peaks at M^+ = 840, 694 assigned to $[^{107}Ag_2([24]aneS_8\text{-}H)PF_6]^+$ and $[^{107}Ag_2([24]aneS_8\text{-}2H)]^+$ respectively. On the basis of this evidence and additional data from microanalyses and i.r. spectroscopy, the product was assigned as $[Ag_2([24]aneS_8)](PF_6)_2$. Full experimental details are discussed in Section 6.4.5.

As discussed in Chapters 2 - 4 various thioether macrocycles are known to complex Ag(I) in a range of stereochemistries. The mononuclear complexes $[Ag([9]aneS_3)2]^+$ [303,304] and $[Ag([18]aneS_6)]^+$ [120] have been characterised structurally and show the Ag(I) bound in octahedral and distorted octahedral co-ordinations respectively. Polymeric species are formed on the complexation of Ag(I) with [12]aneS_4.[106,127,306] The flexibility of the stereochemistry adopted by Ag(I) is illustrated by the various structures of $[Ag([15]aneS_5)]^+$, depending on the anion used, monomeric, dimeric and polymeric structures have been obtained.[106,107] This has already been discussed in detail in Chapter 4.

Repeated attempts to grow crystals of $[Ag_2([24]aneS_8)](PF_6)_2$ suitable for X-ray crystallography have been unsuccessful. Vapour diffusion and solvent layering techniques lead to decomposition or powders.

The co-ordination of the two Ag(I) centres within the $[24]aneS_8$ macrocycle is likely to be tetrahedral, although the cavity may be too small to encapsulate two Ag(I) centres; hence polymeric and bridged species are also possible. The solubility of the isolated product implied that it was unlikely to be polymeric.

6.2.12 Chemical oxidation

$[Ag_2([24]aneS_8)](PF_6)_2$ exhibits no oxidative behaviour up to +1.4V but shows a desorption spike at E_{pc} = -1.5V vs Fc/Fc+ in MeCN (0.1 M $^nBu_4NPF_6$) at a scan rate of 200 mVs^{-1} at platinum electrodes by cyclic voltammetry. However, the complex can be chemically oxidised using 98% H_2SO_4, to form a transient purple species (λ_{max} = 576.4 nm). The X-band solution e.p.r. spectrum shows an isotropic signal, g_{iso} = 2.207, with coupling to a spin 1/2 nuclei, A_{iso} = 27G, consistent with coupling to ^{107}Ag, ^{109}Ag (I = 1/2) (Figure 6.7). The difference between the hyperfine coupling for each isotope of Ag is too small to be observed. On freezing the solution to 77K a rhombic signal is recorded (Figure 6.8), g_1 = 2.060, g_2 = 2.030, g_3 = 2.007, consistent with a Ag(II) species. These e.p.r. spectra show similar characteristics to other Ag(II)-thioether species. $[Ag([9]aneS_3)_2]^{2+}$ has been studied by X-band e.p.r. and UV/Vis spectroscopy;[120] the frozen glass e.p.r. spectrum gave a rhombic signal with g_1 = 2.066, g_2 = 2.034, g_3 = 2.012 , the electronic absorption spectrum showed at band at λ_{max} = 570 nm

($\varepsilon_{max} \simeq 8000\ M^{-1}cm^{-1}$). The analogous Ag(II) complex of [18]aneS_6 gave a similar rhombic signal with $g_1 = 2.063$, $g_2 = 2.028$, $g_3 = 2.007$ and $\lambda_{max} = 564$ nm ($\varepsilon_{max} \simeq 5000\ M^{-1}cm^{-1}$). Ag(I) complexes of [12]aneS_4, [14]aneS_4, [16]aneS_4 and [15]aneS_5 on chemical oxidation all give transient purple/blue Ag(II) species, with comparable e.p.r. spectra.[106]

If $[Ag_2([24]aneS_8)](PF_6)_2$ remains binuclear in its oxidised form, the Ag(II) centres are identical and non-interacting.

Figure 6.7: X-band solution e.p.r. spectrum of $[Ag_2([24]aneS_8)](PF_6)_2$ in 98% H_2SO_4

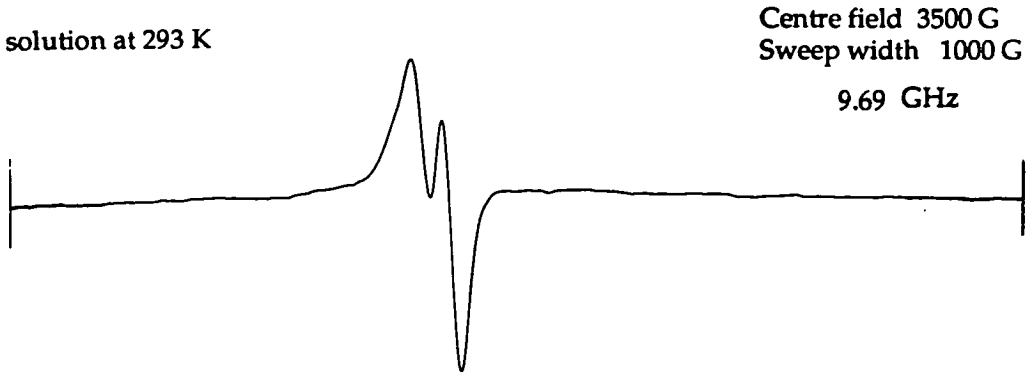

Figure 6.8: X-band frozen-glass e.p.r. spectrum of $[Ag_2([24]aneS_8)](PF_6)_2$ in 98% H_2SO_4

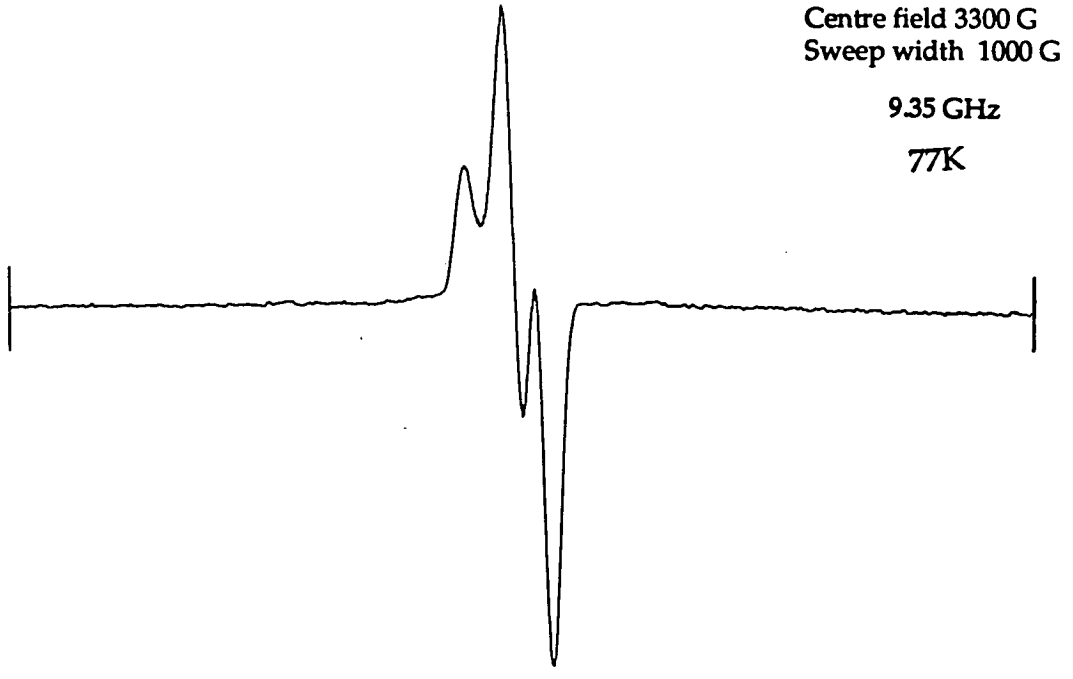

$[Ag_2([28]aneS_8)](PF_6)_2$

6.2.13 Synthesis

Reaction of [28]aneS_8 with two molar equivalents of $AgPF_6$ in $MeNO_2$ afforded a pinky-white precipitate on the addition of Et_2O. The white product gave f.a.b. mass spectral peaks at M^+ = 749, 645 assigned to $[^{107}Ag_2([28]aneS_8\text{-}3H)]^+$ and $[^{107}Ag_2([28]aneS_8)]^+$ respectively. The product was formulated as $[Ag_2([28]aneS_8)](PF_6)_2$ on the basis of this evidence together with microanalytical and i.r. spectroscopic data. Full experimental details are discussed in Section 6.4.6.

The poor solubility together with the low yield of $[Ag_2([28]aneS_8)](PF_6)_2$ prevented successful n.m.r. studies. Numerous attempts to grow single crystals of $[Ag_2([28]aneS_8)](PF_6)_2$ suitable for a X-ray crystallographic study were unsuccessful. Solvent layering and vapour diffusion techniques using a variety of solvents and counter-ions persistently afforded white powders.

The co-ordination of the two Ag(I) centres within the [28]aneS_8 macrocycle is likely to be similar to the analogous $[Cu_2([28]aneS_8)](PF_6)_2$ complex. The larger 28-membered ring macrocycle has a sufficiently large cavity to encapsulate two Ag(I) centres, making the possibility of a polymeric or bridged species less likely than in the smaller 24-membered ring analogue.

6.2.14 Chemical oxidation

Cyclic voltammetry of $[Ag_2([28]aneS_8)](PF_6)_2$ at platinum electrodes in MeCN (O.1M $^nBu_4NPF_6$) shows no oxidation up to +1.4V and a desorption

peak at E_{pc} = -1.6V vs Fc/Fc^+. However, the complex can be oxidised chemically using 98% H_2SO_4, to form a transient purple species (λ_{max} = 536.4 nm). The X-band solution e.p.r. spectrum shows an isotropic signal, g_{iso} = 2.023, with hyperfine coupling to a spin 1/2 nuclei, A_{iso} = 32.4G, consistent with a Ag(II) species (Figure 6.9). The X-band frozen glass spectrum shows a rhombic signal (Figure 6.10) g_1 = 2.059, g_2 = 2.034, g_3 = 2.010, the hyperfine coupling to ^{107}Ag and ^{109}Ag is not observed at X-band. These spectra are consistent with a Ag(II) oxidised product, and the observed g values and hyperfine constants are comparable with those recorded for the oxidised product of $[Ag_2([24]aneS_8)](PF_6)_2$ and the other silver thioether complexes discussed in Section 6.2.12. If the oxidised product of $[Ag_2([28]aneS_8)](PF_6)_2$ is a binuclear species, then the Ag(II) centres are non-interacting and are in identical environments.

Figure 6.9: X-band solution e.p.r. spectrum of $[Ag_2([28]aneS_8)](PF_6)_2$ in 98% H_2SO_4

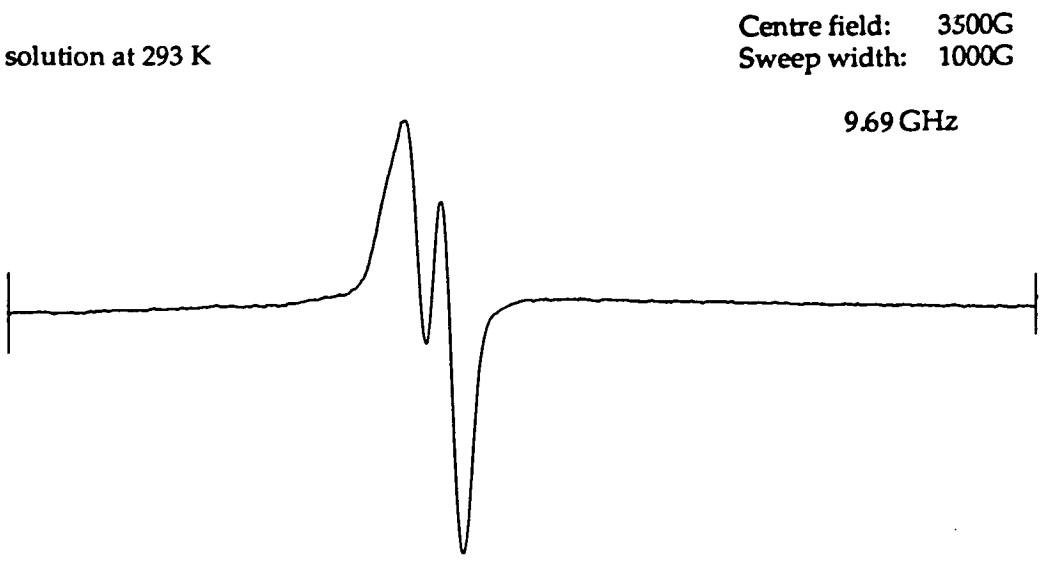

Figure 6.10: X-band frozen-glass e.p.r. spectrum of $[Ag_2([28]aneS_8)](PF_6)_2$ in 98% H_2SO_4

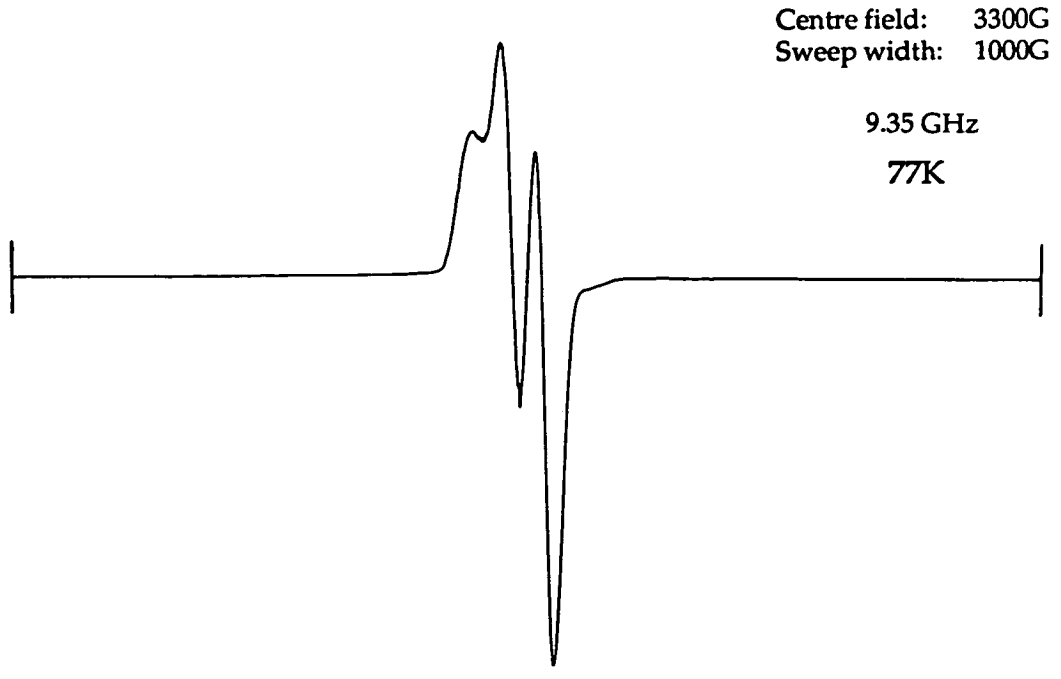

6.3 CONCLUSIONS

The binuclear Cu(I) complexes of [24]aneS_8 and [28]aneS_8 have been synthesised and structurally characterised. It has been shown that these ligands can encapsulate two Cu(I) ions in tetrahedral geometries within the macrocyclic framework. Oxidation of these complexes produces binuclear Cu(II) species, which are proposed to incorporate additional ligands such as SO_4^{2-} and NO_3^-. The very anodic potentials at which these oxidations occur reflect the stabilisation of the Cu(I) state by the π-acidic S-donors and also the de-stabilisation of the Cu(II) state by the restrictive co-ordination geometry available.

The analogous binuclear Ag(I) complexes were synthesised and their oxidation products studied by e.p.r. and UV/Vis spectroscopy. Transient Ag(II) species can be generated in strongly oxidising media. These species cannot be generated electrochemically in organic solvents.

Previous work has shown that binuclear Pd(II) complexes of these ligands can be synthesised.[24] Presumably the Pd(II) centres adopt square planar stereochemistries within the ring. The 24- and 28- membered octathia macrocyclic ligands can therefore co-ordinate two metal ions in isolated tetrahedral or square planar geometries. The possibility of these ligands stabilising the redox processes of metal centres in which these geometries dominate is now open to examination. The metals in which the d^8 and d^{10} configurations are stable forms (e.g. Pt and Au) would be of obvious interest. Substrate activation reactions may be feasible with the control of four-electron oxidations and reductions between two d^{10}/d^{10} and d^8/d^8 centres.

6.4 EXPERIMENTAL SECTION

6.4.1 Synthesis of $[Cu_2([24]aneS_8)(X)_2$ $(X = (BF_4^-, PF_6^-)$

To a solution of [24]aneS_8 (0.192g, 0.4 mmol), dissolved in refluxing MeCN (20 cm^3), was added $[Cu(NCMe)_4](BF_4)$ (0.251 g, 0.8 mmol). The solution was refluxed for 2hrs. filtered and the volume reduced to 5 cm^3. Addition of Et_2O and cooling to -20°C afforded a white precipitate which was recrystallised from Me_2CO-Et_2O to give the desired complex. (Yield 225 mg, 72%) M.Wt. = 781.5. Found C = 24.7; H = 4.1. Calc. for $C_{16}H_{32}Cu_2S_8B_2F_8$: C = 24.6; H = 4.1%. I.r. spectrum (KBr disc): 2980, 2920, 1425, 1410, 1285, 1255, 1200w, 1170w, 1050br, 920w, 910w, 89w, 850w, 820, 770, 680, 620w, 520, 455 and 415 cm^{-1}. F.a.b. mass spectrum (3-NOBA matrix): Found M^+ = 694, 606. Calc. for $[^{63}Cu_2([24]aneS_8\text{-}H)BF_4]^+$: M^+ = 694; $[^{63}Cu_2([24]aneS_8)\text{-}2H]^+$: M^+ = 606, with correct isotopic distributions. ^1H n.m.r. spectrum (CD_3CN, 298 K, 80.13 MHz): δ = 2.93 - 2.13 ppm (32H).

The complex $[Cu_2([24]aneS_8)](PF_6)_2$ was prepared in 72% yield by the same method by using $[Cu(NCMe)_4]PF_6$ as a starting material. (Yield 280 mg, 78%) M.Wt. = 987.5. Found: C = 21.2; H = 3.6. Calc. for $C_{16}H_{32}Cu_2S_8P_2F_{12}$: C = 21.4; H = 3.6%. I.r. spectrum (KBr disc): 2980, 2920, 1420, 1395, 1320, 1290, 1255, 1210, 1170,1150, 1130, 1120, 1080, 1050, 920, 840, 740w, 680, 660w, 630, 610w, 560 and 455 cm^{-1}. F.a.b. mass spectrum (3-NOBA matrix): Found: M^+ = 753, 607, Calc. for $[^{63}Cu_2([24]aneS_8)PF_6]^+$: M^+ = 753; $[^{63}Cu_2([24]aneS_8\text{-}H)]^+$: M^+ = 607, with correct isotopic distributions. ^1H n.m.r spectrum (CD_3CN, 298 K, 200.13 MHz): δ = 2.93 - 2.97 ppm (32H). ^{13}C n.m.r. spectrum (CD_3CN, 298 K, 50.32 MHz): δ = 32.54 ppm (CH_2).

6.4.2 Single crystal structure determination of $[Cu_2([24]aneS_8)](BF_4)_2$

A colourless plate (0.85 x 0.36 x 0.035 mm) suitable for X-ray analysis was obtained by vapour diffusion of Et_2O into a solution of the complex in MeCN.

Crystal data:

$[C_{16}H_{32}S_8Cu_2]^{2+}.2(BF_4^-)$, M = 781.5, monoclinic, space group $P2_1/n$, a = 6.480(6), b = 20.040(11), c = 11.327(6)Å, β = 91.84(5)°, U = 1470Å^3 [from 2θ values of 22 reflections measured at ± ω (24< 2θ <26°, λ = 0.71073Å)] Z = 2, D_c = 1.765 gcm^{-3}, T = 298 K, μ = 2.014 mm^{-1}, F (000) = 792.

Data collection and processing:

Stoë STADI- four circle diffractometer, graphite-monochromated Mo-K_α X-radiation, T = 298 K, ω - 2θ scans using the learnt-profile method [307], 2231 data measured (2θ max 45°, h -6→6, k 0→21, l 0→12, giving 1468 with $F > 4\sigma(F)$ for use in all calculations. No significant crystal decay was observed.

Structure solution and refinement:

A Patterson synthesis located the Cu atom and iterative cycles of least-squares refinement and difference Fourier synthesis located the remaining non-hydrogen atoms. At isotropic convergence, corrections (min 0.750, max. 1.615) for absorption were applied using DIFABS.[308] Disorder in the BF_4^- counter-anion was modelled by two fully-occupied and four half-occupied fluorine atoms. Refinement (by least-squares on F[309]) with anisotropic thermal parameters, for all ordered non-hydrogen atoms and with hydrogen atoms in fixed, calculated positions converged at at R, Rw = 0.0652, 0.0827, respectively, S = 1.141 for 157 refined parameters, and the

final ΔF synthesis showed no feature above 0.79eÅ^{-3}. The weighting scheme, $w^{-1} = \sigma^2(F) + 0.000264\ F^2$, gave satisfactory agreement analyses and in the final cycle $(\Delta/\sigma)_{max}$ was 0.072.

6.4.3 Synthesis of $[Cu_2([28]aneS_8)](X)_2$ $(X = (ClO_4^-, PF_6^-)$

To a solution of [28]aneS_8 (0.215 g, 0.4 mmol) dissolved in refluxing MeCN (25 cm^3) was added $[Cu(NCMe)_4]ClO_4$ (0.261 g, 0.8 mmol). The solution was refluxed for 2hrs, filtered and the volume reduced to 5 cm^3. Addition of Et_2O and cooling to -20°C afforded a white precipitate which was recrystallized from Me_2CO-Et_2O to give the desired complex (Yield 276 mg, 80%). M.Wt. = 863.05. Found: C = 27.5: H = 4.6% Calc. for $C_{20}H_{40}Cu_2S_8Cl_2O_8$: C = 27.4; H = 4.7%. I.r. spectrum (KBr disc): 2960, 2920, 2850, 1440, 1405, 1340w, 1300w, 1255, 1240, 1140, 1090, 940w, 920, 910, 850, 840, 805w, 635 and 625 cm^{-1}. F.a.b. mass spectrum (3-NOBA matrix): Found: M^+ = 763, 663. Calc. for $[^{63}Cu([28]aneS_8)^{35}ClO_4]^+$: M^+ = 763; $[^{63}Cu([28]aneS_8\text{-}H)]^+$: M^+ = 663, with correct isotopic distributions. ^1H n.m.r. spectrum (CD_3CN, 298 K, 200.13 MHz); δ = 2.72 - .97 ppm (28H). ^{13}C n.m.r. spectrum (CD_3CN, 298 K. 50.32 MHz): δ = 33.14, 31.23, 26.10 ppm (CH_2). (CD_3CN, 238 K, 50.32 MHz); δ = 34.27, 32.69, 32.08, 31.92, 30.35, 21.90 ppm (CH_2).

The complex $[Cu_2([28]aneS_8)](PF_6)_2$ can be prepared by the same method using $[Cu(NCMe)_4]PF_6$ as a starting material. (Yield 313 mg, 82%) M.Wt. = 954.05. Found: C = 25.2; H = 4.2% Calc. for $C_{20}H_{40}Cu_2S_8P_2F_{12}$; C = 25.2; H = 4.3%. I.r. spectrum (KBr disc): 2980, 2920, 1440, 1430, 1420, 1410, 1340w, 1300, 1290, 1255, 1245, 1210w, 1140, 1130, 1020, 935, 840, 740, 660 and 555

cm^{-1}. F.a.b. mass spectrum (3-NOBA matrix): Found: M^+ = 809, 663, Calc. for $[^{63}Cu_2([28]aneS_8)PF_6]^+$: M^+ = 809; $[^{63}Cu_2([28]aneS_8\text{-}H)]^+$: M^+ = 663, with correct isotopic distributions. ^1H n.m.r. spectrum (CD_3CN, 298 K, 200.13 MHz): δ = 2.75-3.10 ppm (28H). ^{13}C n.m.r. spectrum (CD_3CN, 298 K. 50.32 MHz): δ = 33.60, 31.50, 25.56 ppm (CH_2).

6.4.4 Single crystal structure determination of $[Cu_2([28]aneS_8)](ClO_4)_2$

A pale yellow needle (0.47 x 0.05 x 0.05 mm) suitable for X-ray analysis was obtained by vapour diffusion of Et_2O into a solution of the complex in MeCN.

Crystal data:

$[C_{20}H_{40}S_8Cu_2]^{2+}.2(ClO_4^-)$, M = 863.0, monoclinic, space group $P2_1/n$, a = 6.999(7), b = 20.000(21), c = 11.780(7)Å, β = 102.37(7)°, U = 1611Å^3 [from setting angles of 10 reflections with 2θ = 20-22°, λ = 0.71073Å] Z = 2, D_c = 1.779 gcm^{-3}, T = 173 K, μ = 2.032 mm^{-1}, F(000) = 888.

Data collection and processing:

Stoë STADI four circle diffractometer, graphite-monochromated Mo-K_α X-radiation, T = 173 K, ω-2θ scans using the learnt-profile method [307], 2727 data measured (2θ max 45°, h -7→7, k 0→21, l 0→12, 1799 unique (R_{int} = 0.071), giving 1039 with $F \geq 4\sigma(F)$ for use in all calculations. Linear isotropic crystal decay (ca. 21%) corrected for during data reduction, no absorption correction.

Structure solution and refinement:

A Patterson synthesis located the Cu atom and iterative cycles of least-squares refinement and difference Fourier synthesis located the

remaining non-hydrogen atoms: these were then refined (by least-squares on F^{309}) with anisotropic thermal parameters for all non-hydrogen atoms and with hydrogen atoms in fixed, calculated positions. At final convergence R, R_w = 0.0656, 0.0784, respectively, S = 0.947 for 182 refined parameters, and the final ΔF synthesis showed no feature above 0.74eÅ^{-3}. An isotropic extinction parameter refined to 6(4) x 10^{-8}. The weighting scheme $w^{-1} = \sigma^2(F) + 0.0007F^2$ gave satisfactory agreement analyses and in the final cycle $(\Delta/\sigma)_{max}$ was 0.11.

6.4.5 Synthesis of $[Ag_2([24]aneS_8)](PF_6)_2$

Reaction of $AgPF_6$ (30 mg, 0.117 mmol) with $[24]aneS_8$ (27 mg, 0.056 mmol) in $MeNO_2$ (5 cm^3) for 24hrs. under N_2, in the dark yields a colourless solution. Filtration into Et_2O (20 cm^3) to and cooling to -20°C afforded a white precipitate which was filtered and washed with CH_2Cl_2 and Et_2O to give the desired complex. (Yield 32 mg, 58%). M.Wt. = 986.61. Elemental analyses: found C = 19.7, H = 3.32% . Calc. for $C_{16}H_{32}S_8Ag_2P_2F_{12}$: C = 19.5, H = 3.27%. I.r. spectrum (KBr disc): 2960, 2900, 1550, 1420, 1300w, 1260, 1200, 1140, 840-820, 740W, 560 and 435 cm^{-1}. F.a.b. mass spectrum (3-NOBA matrix) : found M^+ = 840, 714, 694, 588. Calc. for $[^{107}Ag_2([24]aneS_8\text{-}H)PF_6]^+$: M^+ = 840; $[^{107}Ag_2([24]aneS_8)H_2O]^+$: M^+ = 714; $[^{107}Ag_2([24]aneS_8\text{-}2H)]^+$: M^+ = 694, $[^{107}Ag_2([24]aneS_8\text{-}H)]^+$: M^+ = 588, with correct isotopic distributions.

6.4.6 Synthesis of $[Ag_2([28]aneS_8)](PF_6)_2$

Method as for 6.4.5, using $AgPF_6$ (30 mg, 0.117 mol) with $[28]aneS_8$ (30 mg, 0.056 mmol). The product was isolated as a white solid. (Yield 37 mg, 63%). M.Wt. = 1042.71. Elemental analyses: found C = 23.0, H = 3.92, S = 24.7%. Calc. for $C_{20}H_{40}S_8Ag_2P_2F_{12}$: C = 23.0, H = 3.87, S = 24.6%. I.r. spectrum (KBr disc): 2915, 1560, 1450, 1435, 1410, 1405, 1375w, 1310, 1295w, 1285, 1265, 1250, 1205w, 1190, 1160, 1155, 1120w, 1050w, 1030, 950w, 840-820, 750, 720w, 640, 625w, 615w, 560 and 435 cm^{-1}. F.a.b. mass spectrum (3-NOBA matrix) : found M^+ = 749, 645. Calc. for $[^{107}Ag_2([28]aneS_8\text{-}3H)]^+$: M^+ = 749; $[^{107}Ag_2([28]aneS_8)]^+$; M^+ = 645, with correct isotopic distribution.

CHAPTER 7

Gold complexes of tetrathia and octathia macrocycles

7.1 INTRODUCTION

The affinity of Cu(I) and Ag(I) for 'soft' S-donors has been exploited in the synthesis of copper and silver thioether macrocyclic complexes.[26] The biological relevance of copper thioether macrocyclic systems has been discussed in Chapter 6, The copper complexes of the tetrathia ligands having been studied extensively by Rorabacher and co-workers.[108,110,292-298] The structure of $[Cu([14]aneS_4)]^+$ shows tetrahedral co-ordination at Cu(I) with the metal ion bound to three S-donors of one $[14]aneS_4$. Cu - S = 2.260(4), 2.327(4), 2.338(4)Å and to one S-donor of a second ligand, Cu - S = 2.342(3)Å producing a polymeric chain[295,334] (1). The structure of the Cu(II) complex of $[14]aneS_4$ shows that the octahedral co-ordination at Cu(II) is completed by the co-ordinating ClO_4^- ions. $[14]aneS_4$ is bound equationally through four S-donors, Cu - S = 2.297(1), 2.308(1)Å with the ClO_4^- ions are bound apically through O-donors, Cu - O = 2.652(4)Å.[299] Monomeric Cu(I) and Cu(II) complexes of $[16]aneS_4$ have been prepared.[106,300] The dimeric species $[Cu_2Cl_4([16]aneS_4)]$ was isolated from the reaction of $CuCl_2$ with $[16]aneS_4$.[300]

(1) $[Cu([14]aneS_4)]^+$, part of polymer

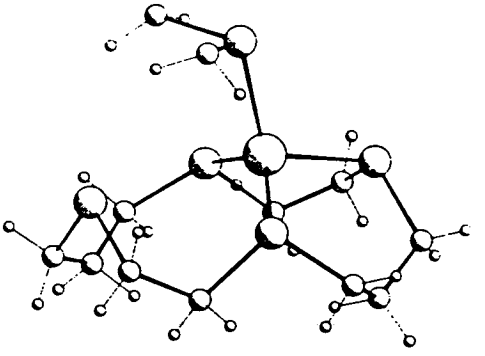

The extraction of Cu(II), Cu(I) and Ag(I) by $[14]aneS_4$ and related tetrathia ligands has been described.[26,126] Both $[Ag([14]aneS_4)]^+$ and $[Ag_2([14]aneS_4)]^{2+}$ have been isolated, along with Ag(I) complexes of

[12]aneS$_4$ and [16]aneS$_4$.[106,127,335] The structures of these species are unknown although their solubility suggests polymeric structure.

The initial aim of the work discussed in this Chapter was to synthesise gold complexes of the tetrathia ligands, [16]aneS$_4$, [14]aneS$_4$ and [12]aneS$_4$. The synthesis of binuclear copper and silver complexes of [24]aneS$_8$ and [28]aneS$_8$ has been described in Chapter 6, and it was therefore decided to extend these aims also to the synthesis and characterisation of binuclear gold complexes of the octathia ligands.

7.2 RESULTS AND DISCUSSION

7.2.1 Synthesis and characterisation of [Au([16]aneS$_4$)](PF$_6$)

Reaction of [16]aneS$_4$ with one molar equivalent of [Au(tht)$_2$](PF$_6$) in MeCN afforded a white suspension on the addition of Et$_2$O. The product was collected by centrifugation. The white solid shows a f.a.b. mass spectral peak at $M^+ = 493$, assigned to [^{197}Au([16]aneS$_4$)]$^+$. On the basis of this evidence together with microanalytical and i.r. spectroscopic data the product was assigned as [Au([16]aneS$_4$)](PF$_6$). Full experimental details are given in Section 7.4.1. This product is sparingly soluble in MeCN and MeNO$_2$, insoluble in Me$_2$CO, MeOH, EtOH and CH$_2$Cl$_2$.

Repeated attempts to obtain single crystals of [Au([16]aneS$_4$)](PF$_6$) suitable for an X-ray structure determination were unsuccessful. Vapour diffusion of Et$_2$O into MeNO$_2$ or MeCN solutions of the complex, yielded white powders and metallic gold respectively.

7.2.2 Electrochemical and e.p.r. studies [Au([16]aneS$_4$)](PF$_6$)

Cyclic voltammetry of [Au([16]aneS$_4$)](PF$_6$) at platinum electrodes in MeCN (0.1M ^{n}Bu$_4$NPF$_6$) shows a broad chemically reversible oxidation at $E_{1/2}$= +0.14 V (ΔE_p = 190mV) vs Fc/Fc$^+$ at a scan rate of 80 mVs^{-1} (Figure 7.1). Coulometric measurements confirmed that the oxidation was a two-electron process.

Figure 7.1: Cyclic voltammogram of [Au([16]aneS$_4$)](PF$_6$)

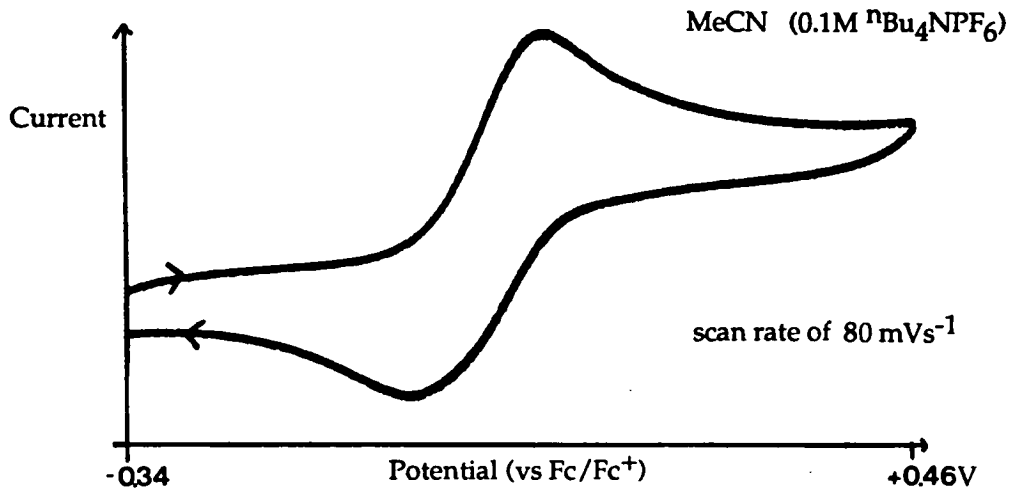

Electrogeneration of the oxidation product at +0.50 V (vs Fc/Fc$^+$) affords a pale yellow, e.p.r. silent species, consistent with the two-electron oxidation being metal-based producing a Au(III) species. During the oxidation to Au(III) a transient paramagnetic, orange species can be detected. The frozen glass e.p.r. spectrum recorded for the orange species shows a complicated multiplet ($g_{av} \simeq$ 2.040) (Figure 7.2). The oxidation of [Au([16]aneS$_4$)]$^+$ to [Au([16]aneS$_4$)]$^{3+}$ therefore appears to proceed via a Au(II) intermediate; Assignment of the e.p.r. spectrum is difficult without signal analysis and computer simulation.

If [Au([16]aneS$_4$)]$^+$ is monomeric in solution, it is likely that the d^{10} Au(I) ion is bound in a distorted tetrahedral manner. Co-ordination of square planar

d^8 ions can be attained by [16]aneS_4 (e.g. [Pd([16]aneS_4)]$^{2+}$). The stabilisation of Au(III) by [16]aneS_4 would suggest the ligand cavity size is sufficiently large to accommodate a square planar Au(III) centre. The transient d^9 Au(II) species may also be square planar, but it is conceivable that the d^9 centre would prefer a distorted octahedral co-ordination sphere. Extra ligation would be required to satisfy the six co-ordinate Au(II) centre. The uptake of solvent molecules in the vacant sites would achieve this, either to give (2) *trans* or (3) *cis* isomers depending on the fit of the Au(II) ion in the ligand cavity.

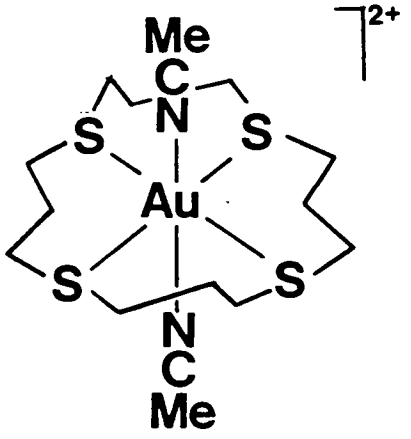

(2)

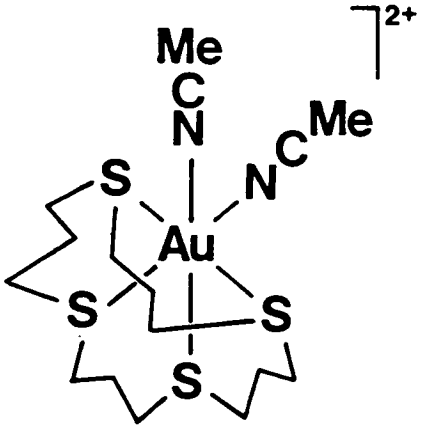

(3)

Binding of NCMe to the Au(II) centre would present the unpaired electron an additional coupling to ^{14}N (I = 1), complicating the e.p.r. spectrum. Electrogeneration of the Au(II) intermediate in different solvents would help establish if these transient species contained bound solvent.

Figure 7.2: X-band frozen glass e.p.r. spectrum of the transient intermediate detected on the oxidation of [Au([16]aneS$_4$)](PF$_6$)

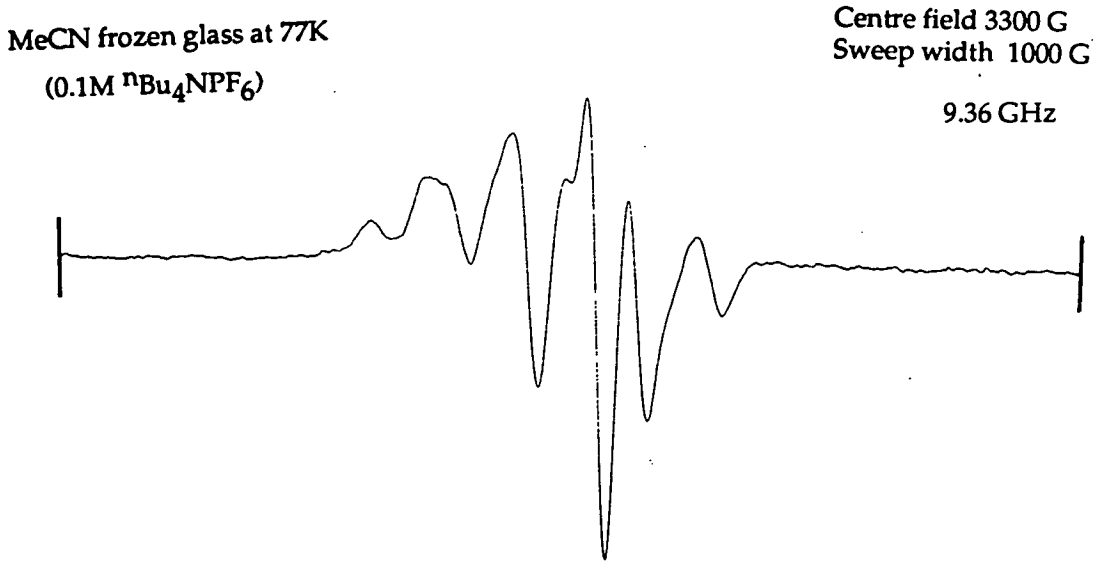

Figure 7.3: Spectroelectrochemical study of [Au([16]aneS$_4$)](PF$_6$)

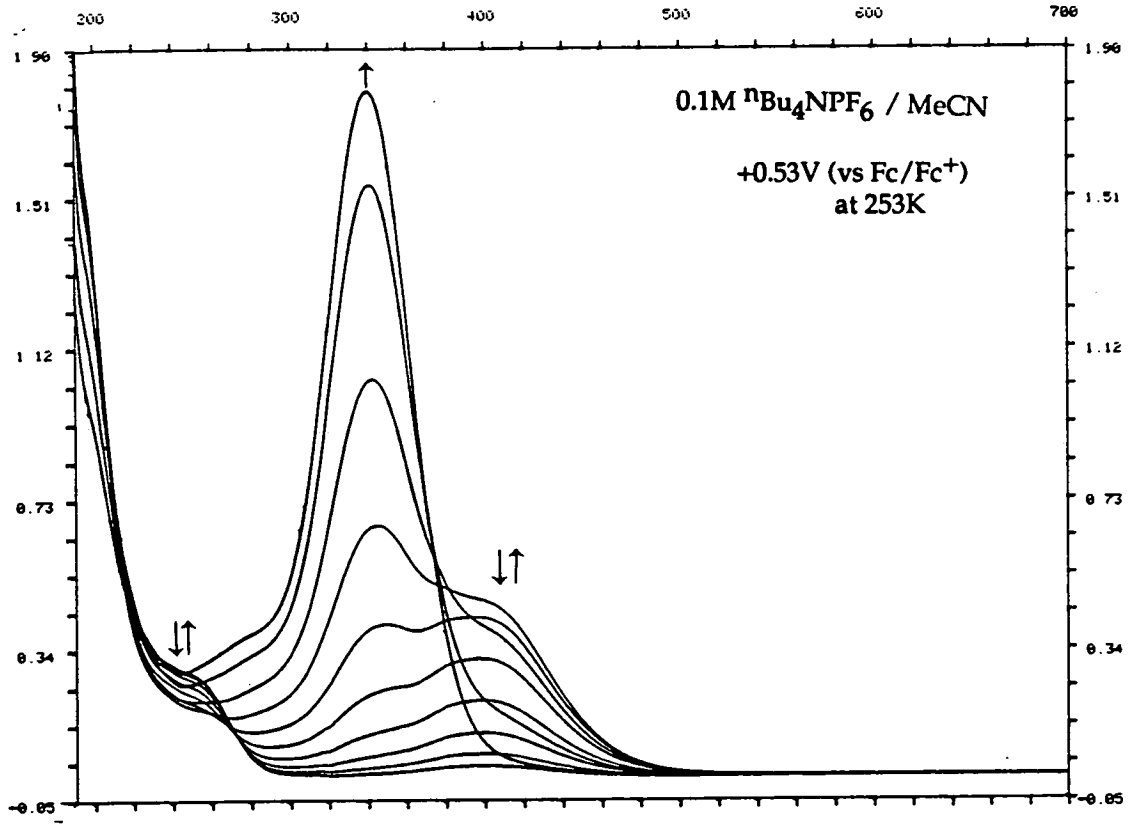

7.2.3 Spectroelectrochemical study of [Au([16]aneS$_4$)](PF$_6$)

The electrogeneration of redox products can be monitored by UV/Vis spectroscopy using the O.T.E. technique. The spectroelectrochemical study of [Au([16]aneS$_4$)](PF$_6$) in MeCN at 253K shows the conversion of the Au(I) species to the Au(III) species, λ_{max} = 340 nm (ε_{max} = 23380 $M^{-1}cm^{-1}$) via a transient intermediate (λ_{max} = 400 nm) at an applied potential of +0.53V (vs Fc/Fc^+). The reduction of Au(III) back to Au(I) involves the same intermediate species, and is chemically reversible (Figure 7.3).

7.2.4 Gold complexes of [12]aneS$_4$ and [14]aneS$_4$

The reaction of [Au(tht)$_2$](PF$_6$) with one molar equivalent of [14]aneS$_4$ in MeCN afforded an insoluble grey solid. The product shows a f.a.b. mass spectral peak at M^+ = 465 assigned to $[^{197}Au([14]aneS_4)]^+$. The insolubility of the complex prevented further re-crystallisation and also suggested a polymeric structure for the complex. The analogous reaction using [12]aneS$_4$ resulted in an insoluble grey solid, which decomposed in the solid-state.

From these results it was concluded that the ligand cavity sizes of [14]aneS$_4$ and [12]aneS$_4$ are probably too small to accommodate the stereochemical preferences of the relatively Au(I) centre.

7.2.5 Synthesis and characterisation of $[Au_2([28]aneS_8)](PF_6)_2$

Reaction of $[28]aneS_8$ with two molar equivalents of $[Au(tht)_2](PF_6)$ in $MeNO_2$ afforded a white precipitate on the addition of ice-cold Et_2O. The product shows f.a.b. mass spectral peaks of M^+ = 1075, 929, 733 assigned to $[^{197}Au_2([28]aneS_8)PF_6]^+$, $[^{197}Au_2([28]aneS_8\text{-}H)]^+$ and $[^{197}Au([28]aneS_8)]^+$ respectively. On the basis of this evidence together with microanalytical and i.r. spectroscopic data, the product was assigned as $[Au_2([28]aneS_8)](PF_6)_2$. Full experimental details are given in Section 7.4.2

To establish the connectivity and stereochemistry at the Au(I) centres, a single crystal X-ray structure determination was carried out.

7.2.6 Structure determination of $[Au_2([28]aneS_8)](PF_6)_2$

A single crystal X-ray structure determination of $[Au_2([28]aneS_8)](PF_6)_2$ confirmed the compound to be a genuine binuclear Au(I) complex (Figure 7.4). The two encapsulated Au(I) centres are related by a crystallographic inversion centre and are each co-ordinated to two S-donors, Au - S(1) = 2.3301(10) Au - S(11) = 2.3378(18)Å, with two additional longer interactions, Au...S(4) = 2.7891(20), Au...S(8) = 2.7629(20)Å conferring a [2+2] distorted tetrahedral geometry on the metal ion. The co-ordination at Au(I) is comparable to that observed for Cu(I) in the analogous $[Cu_2([28]aneS_8)]^{2+}$ cation, the main difference is the angle at S(1) - M - S(11). The preference of Au(I) for linear co-ordination is reflected in the opening up of this angle to 155.58(6)° from 133.39(20)° in the copper cation. The exaggered distorted tetrahedral geometry for the Au(I) complex pushes the

Au(I) centres closer together, 5.6977(6)Å in comparison to 6.454(3)Å between the two Cu(I) centres. Full details of the solution and refinement of the structure are given in Section 7.4.3. Selected bonds, angles and torsions for this structure are given in Table 7.1.

Interestingly, the [2+2] distorted tetrahedral stereochemistry at Au(I) in $[Au_2([28]aneS_8)](PF_6)_2$ is very similar to that observed for Au(I) when bound to other thioether ligands e.g. $[9]aneS_3$, $[18]aneS_6$, $[15]aneS_5$, (see Table 4.1).

7.2.7 N.m.r studies

The ^1H n.m.r. spectrum of $[Au_2([28]aneS_8)](PF_6)_2$ at 298 K in CD_3CN shows a broad resonances at δ = 2.82 - 3.15 ppm assigned to the macrocyclic protons. The ^{13}C (DEPT) n.m.r. spectrum shows two broad resonances at δ = 25.92 - 27.07 ppm and 30.86 - 32.94 ppm. These spectra indicate that the species is undergoing a fluxionality process; lowering the temperature to 215 K this process is minimised. The ^1H n.m.r. spectrum of the complex at 215 K shows four complicated resonances at δ = 2.44, 2.66, 2.88 and 3.30 - 4.28 ppm; the ^{13}C n.m.r. spectrum shows six resonances at δ = 22.61, 25.34, 27.20, 28.14, 32.47 and 32.85 ppm (Figure 7.5) assigned to six unique carbon resonances. This is consistent with each Au(I) centre being bound in a distorted tetrahedral co-ordination, similar to the solid-state structure determined by X-ray crystallography (Section 7.2.6).

Figure 7.4: Single crystal X-ray structure of $[Au_2([28]aneS_8)]^{2+}$

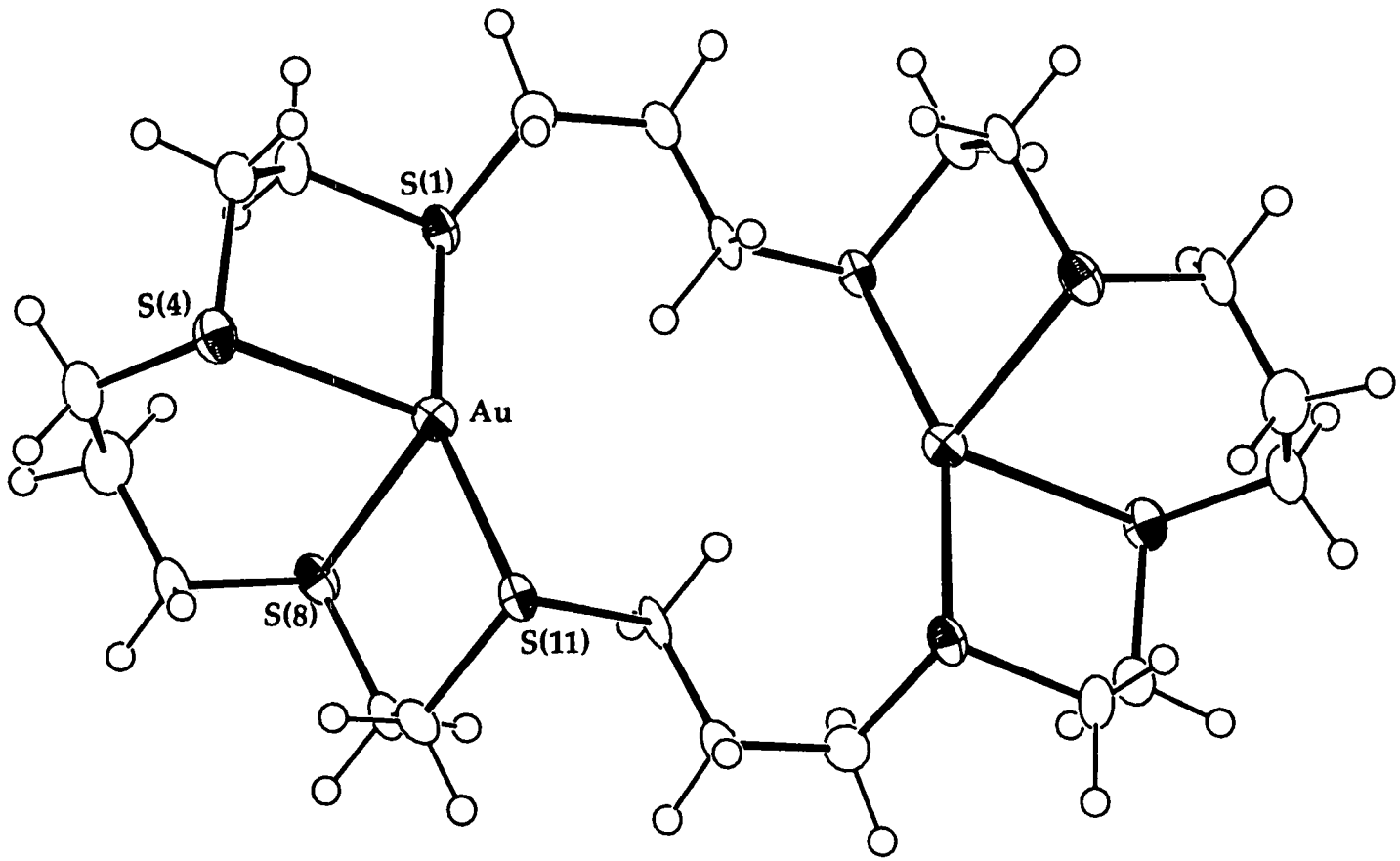

Table 7.1: Selected bonds, angles and torsions for $[Au_2([28]aneS_8)]^{2+}$

Au	- S(1)	2.3301(19)	C(7)	- S(8)	1.809(7)
Au	- S(4)	2.7891(20)	S(8)	- C(9)	1.804(7)
Au	- S(8)	2.7629(20)	C(9)	-C(10)	1.528(10)
Au	-S(11)	2.3378(18)	C(10)	-S(11)	1.818(7)
S(1)	- C(2)	1.807(8)	S(11)	-C(12)	1.821(7)
C(2)	- C(3)	1.517(11)	C(12)	-C(13)	1.521(10)
C(3)	- S(4)	1.813(8)	C(13)	-C(14)	1.537(11)
S(4)	- C(5)	1.814(8)	C(14)	-S(15)	1.826(8)
C(5)	- C(6)	1.505(11)	S(15)	-C(16)	1.806(8)
C(6)	- C(7)	1.537(11)			

S(1)	- Au	- S(4)	86.24(6)	C(5)	- C(6) - C(7)	114.6(7)
S(1)	- Au	- S(8)	108.14(6)	C(6)	- C(7) - S(8)	110.5(5)
S(1)	- Au	-S(11)	155.58(6)	Au	- S(8) - C(7)	99.76(24)
S(4)	- Au	- S(8)	91.88(6)	Au	- S(8) - C(9)	95.88(24)
S(4)	- Au	-S(11)	113.93(6)	C(7)	- S(8) - C(9)	101.6(3)
S(8)	- Au	-S(11)	85.77(6)	S(8)	- C(9) -C(10)	116.7(5)
Au	- S(1)	- C(2)	104.5(3)	C(9)	-C(10) -S(11)	115.4(5)
S(1)	- C(2)	- C(3)	115.0(6)	Au	-S(11) -C(12)	104.10(24)
C(2)	- C(3)	- S(4)	117.5(6)	C(10)	-S(11) -C(12)	103.9(3)
Au	- S(4)	- C(3)	93.3(3)	S(11)	-C(12) -C(13)	112.8(5)
Au	- S(4)	- C(5)	114.0(3)	C(12)	-C(13) -C(14)	112.0(6)
C(3)	- S(4)	- C(5)	103.0(4)	C(13)	-C(14) -S(15)	109.1(5)
S(4)	- C(5)	- C(6)	117.1(6)	C(14)	-S(15) -C(16)	102.8(4)

S(1)	- C(2)	- C(3)	- S(4)	60.1(7)	S(8)	- C(9) -C(10)	-S(11) 57.2(7)
C(2)	- C(3)	- S(4)	- C(5)	77.8(6)	C(9)	-C(10) -S(11)	-C(12) 63.3(6)
C(3)	- S(4)	- C(5)	- C(6)	-95.1(6)	C(10)	-S(11) -C(12)	-C(13) 65.8(6)
S(4)	- C(5)	- C(6)	- C(7)	-63.5(8)	S(11)	-C(12) -C(13)	-C(14) 166.7(5)
C(5)	- C(6)	- C(7)	- S(8)	114.3(6)	C(12)	-C(13) -C(14)	-S(15) -71.2(7)
C(6)	- C(7)	- S(8)	- C(9)	-167.8(5)	C(13)	-C(14) -S(15)	-C(16) -157.3(5)
C(7)	- S(8)	- C(9)	-C(10)	67.9(6)	C(14)	-S(15) -C(16)	-C(17) -73.8(6)

Figure 7.5: ^{13}C n.m.r. spectrum of $[Au_2([28]aneS_8)](PF_6)_2$

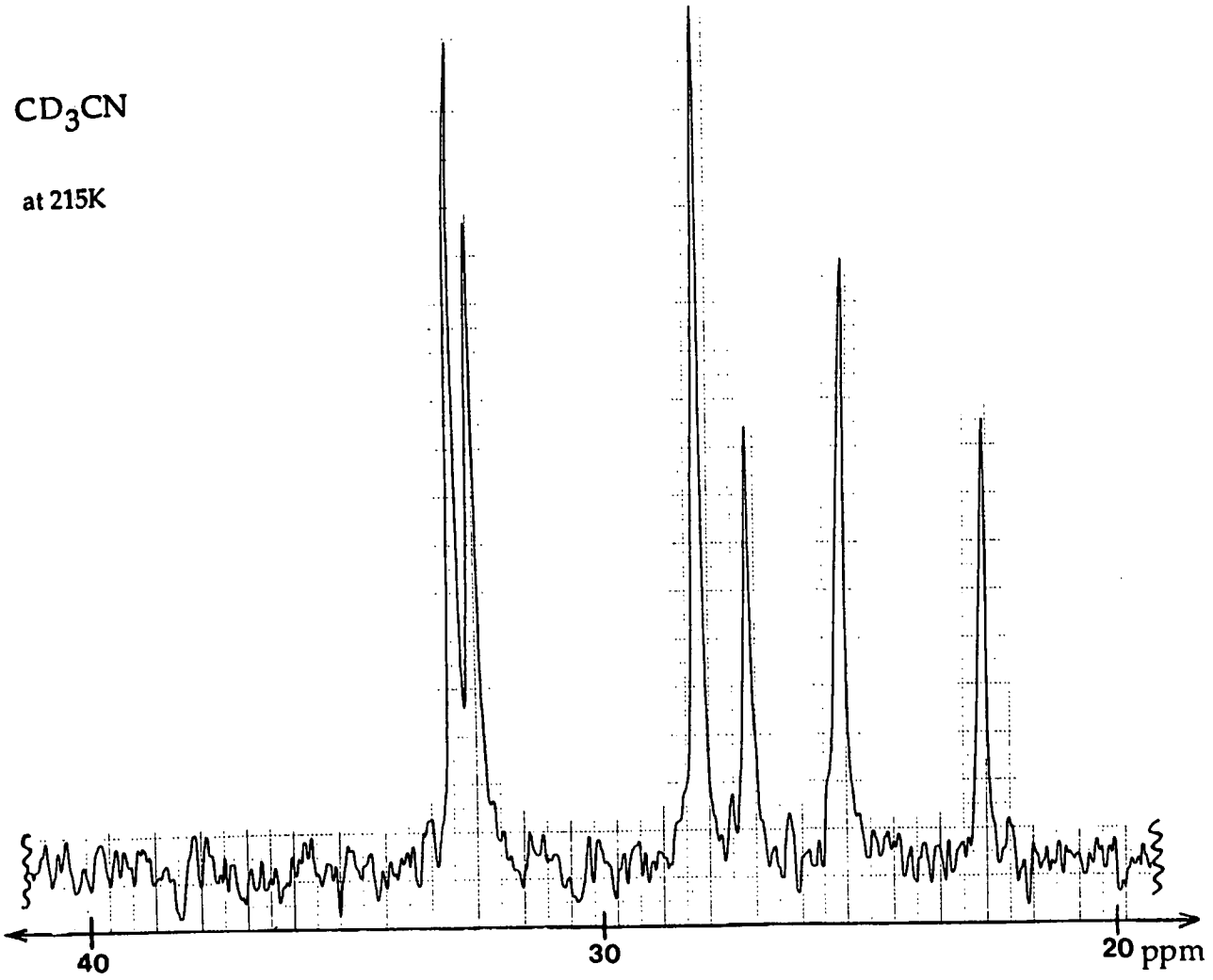

7.2.8 Electrochemical and e.p.r. studies of $[Au_2([28]aneS_8)](PF_6)_2$

Cyclic voltammetry of $[Au_2([28]aneS_8)](PF_6)_2$ at platinum electrodes in MeCN (0.1M $^nBu_4NPF_6$) shows a broad chemically reversible oxidation at $E_{1/2}$ = +0.55V (ΔE_p = 230mV) vs Fc/Fc^+ at a scan rate of 140 mVs^{-1} (Figure 7.6). Coulometric measurements confirmed this process to be a four-electron transfer step.

Figure 7.6: Cyclic voltammogram of $[Au_2([28]aneS_8)](PF_6)_2$

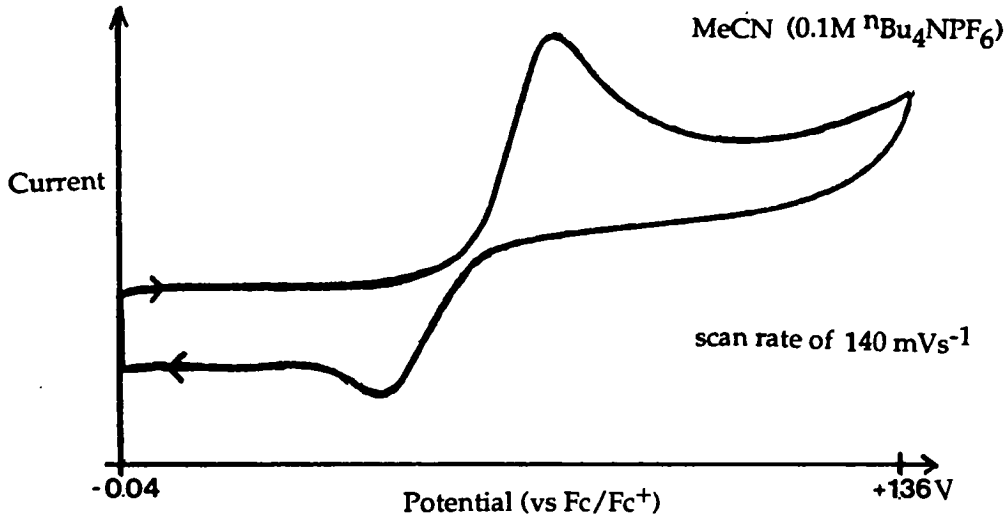

Electrogeneration of $[Au_2([28]aneS_8)](PF_6)_2$ at +1.0V (vs Fc/Fc^+) affords a pale yellow, e.p.r. silent species, consistent with the production of a binuclear Au(III) species. During the oxidation of the colourless Au(I) complex to the pale yellow Au(III) product a transient, paramagnetic canary yellow species is formed. The frozen glass e.p.r. spectrum recorded for the intermediate species shows a complicated multiplet ($g_{av} \simeq 2.019$) (Figure 7.7). The oxidation is chemically reversible, confirming that the oxidised product is binuclear. The return reduction to $[Au_2([28]aneS_8)]^{2+}$ involves the same intermediate. Assuming that the four-electron oxidation is predominantly metal-based, various paramagnetic intermediates may be formed.

In Scheme (1) species (b) and (e) would be e.p.r. active, while species (c) may be e.p.r. active, if the d^9 centres are not completely spin-coupled.

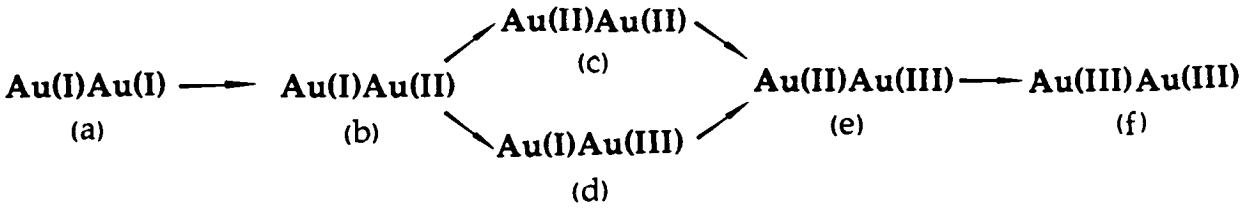

The oxidation of $[Au_2([28]aneS_8)]^{2+}$ to $[Au_2([28]aneS_8)]^{6+}$ probably involves transient Au(II) centres. Unfortunately assignment of the e.p.r. spectrum recorded for the canary yellow intermediate was not possible. The signal may be due to a mixture of intermediates. The signal observed for the paramagnetic $[Au_2([28]aneS_8)]^{n+}$ (n = 3 - 5) species is similar to the e.p.r. spectrum recorded for $[Au([16]aneS_4)]^{2+}$ (Figure 7.2) however, the signal line intensities differ.

7.2.9 Spectroelectrochemical study of $[Au_2([28]aneS_8)](PF_6)_2$

The four-electron oxidation of $[Au_2([28]aneS_8)](PF_6)_2$ was monitored by UV/Vis spectroscopy. The *in situ* electrogeneration of $[Au_2([28]aneS_8)](PF_6)_2$ was carried out in MeCN (0.1 M $^nBu_4NPF_6$) at 253K. The study shows the conversion of $[Au_2([28]aneS_8)]^{2+}$ (λ_{max} = 238 nm (ε_{max} = 17500 $M^{-1}cm^{-1}$) to $[Au_2([28]aneS_8)]^{6+}$ (λ_{max} = 324 nm (ε_{max} = 26750 $M^{-1}cm^{-1}$), 245 (14770)) at +1.0V (vs Fc/Fc^+) (Figure 7.8). The oxidation proceeds through an intermediate species, confirmed by the presence of the overlapping band at λ_{max} = 400 nm. This process is chemically reversible with the starting material being re-generated on re-reduction at +0.1V.

Figure 7.7: X-band frozen glass e.p.r. spectrum of the transient intermediate detected on the oxidation of $[Au_2([28]aneS_8)](PF_6)_2$

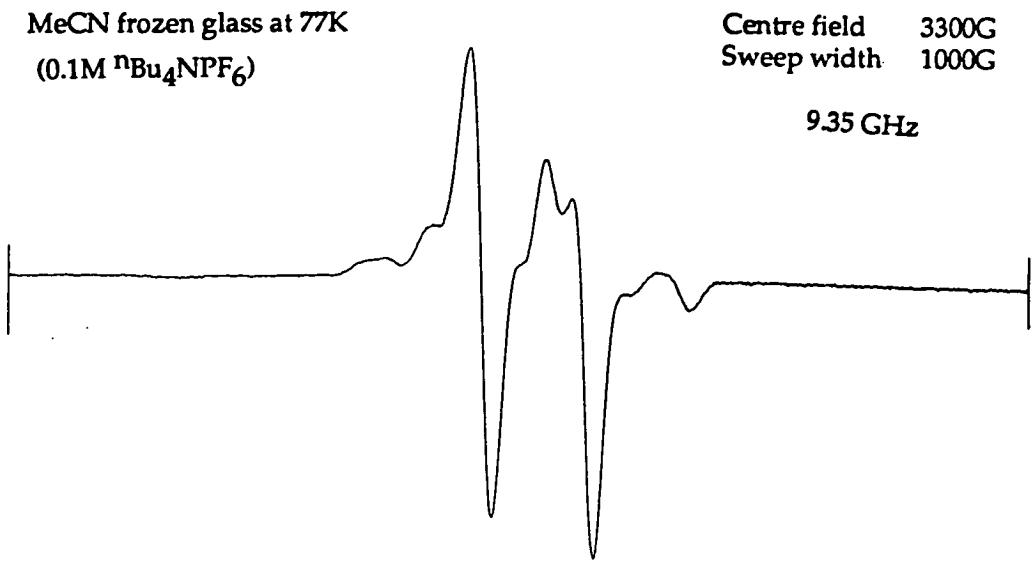

Figure 7.8: Spectroelectrochemical study of $[Au_2([28]aneS_8)](PF_6)_2$

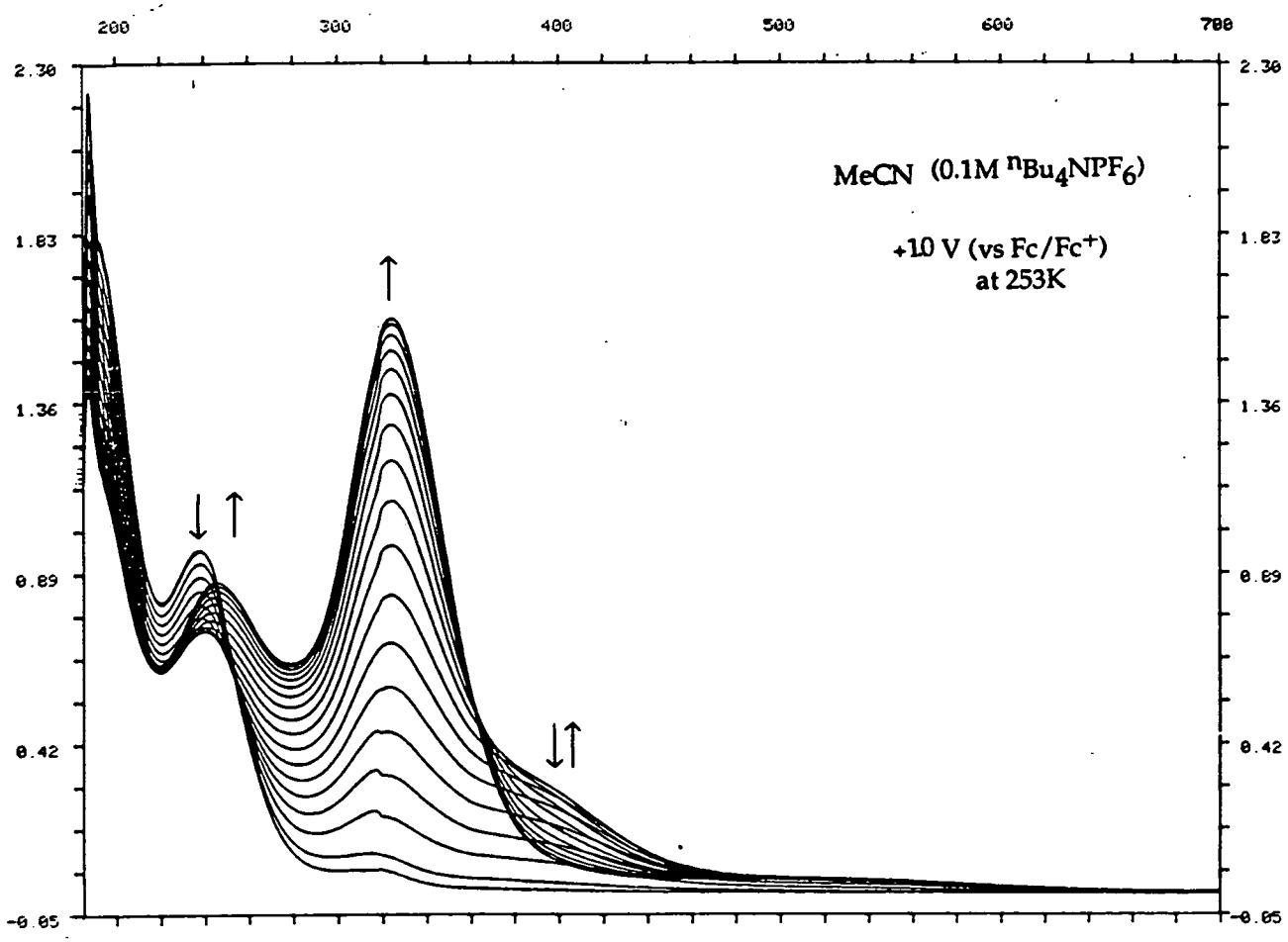

7.2.10 Gold complexes of [24]aneS$_8$

The reaction of [24]aneS$_8$ with two molar equivalents of [Au(tht)$_2$](PF$_6$) in MeNO$_2$ afforded a white precipitate on the addition of Et$_2$O. The product shows f.a.b. mass spectral peaks at M^+ = 1019, 873, 677 assigned to [^{197}Au$_2$([24]aneS$_8$)PF$_6$]$^+$, [^{197}Au$_2$([24]aneS$_8$-H)]$^+$ and [^{197}Au([24]aneS$_8$)]$^+$ respectively. On this basis together microanalytical and i.r. spectroscopic data, the product was assigned as [Au$_2$([24]aneS$_8$)](PF$_6$)$_2$. Full experimental details are given in Section 7.4.4.

The complex is unstable both in solution and in the solid-state, making further characterisation difficult. Attempts to grow suitable single crystals for an X-ray structure determination resulted in decomposition of the complex to colloidal gold. Due to this instability, a pure sample of [Au$_2$([24]aneS$_8$)](PF$_6$)$_2$ for electrochemical studies was not obtained. These results suggest that the Au(I) centres are bound in very strained stereochemistries by [24]aneS$_8$ in comparison to the unstrained co-ordination at Au(I) in the stable [28]aneS$_8$ analogue. This is a function of the smaller ring size of [24]aneS$_8$ in comparison to [28]aneS$_8$. The smaller cavity size of [24]aneS$_8$ may promote demetallation of the binuclear complex to form a mononuclear.

7.3 CONCLUSIONS

Au(I) complexes of [16]aneS$_4$ and [28]aneS$_8$ have been isolated. The stability of [Au([16]aneS$_4$)]$^+$ and [Au$_2$([28]aneS$_8$)]$^{2+}$ in comparison to their smaller ring analogues, [Au([14]aneS$_4$)]$^+$ and [Au$_2$([24]aneS$_8$)]$^{2+}$ respectively, illustrates the importance of metal ion/ligand cavity compatibility. [Au([16]aneS$_4$)]$^+$ can be oxidised to [Au([16]aneS$_4$)]$^{3+}$ via a transient [Au([16]aneS$_4$)]$^{2+}$ species which has been confirmed by e.p.r. and electronic absorption spectroscopy. [Au$_2$([28]aneS$_8$)]$^{2+}$ undergoes a four-electron oxidation to [Au$_2$([28]aneS$_6$)]$^{6+}$. This process also proceeds via a paramagnetic intermediate. The similarity of the e.p.r. and electronic absorption spectroscopic data for the intermediates [Au([16]aneS$_4$)]$^+$ and [Au$_2$([28]aneS$_8$)]$^{n+}$ (n = 3 - 5), suggests that their nature and structure are alike, and therefore probably both contain isolated uncoupled Au(II) centres.

The d^9 centres in the intermediates may require additional stabilising ligation to complete the preferred distorted octahedral stereochemistries. The relative fit of Au(II) with respect to the macrocyclic ligand conformation will determine the isomer form of such species.

[28]aneS$_8$ can encapsulate two Au(I) centres in [2+2] distorted tetrahedral geometries. The complex undergoes a four-electron oxidation, to presumably, a binuclear Au(III) species. Related work in Edinburgh[24] has shown that [28]aneS$_8$ can co-ordinate two d^8 Pd(II) or Pt(II) centres, probably in square planar geometries. Therefore, the encapsulation of two square planar Au(III) centres within the S$_8$- donor macrocyclic framework appears feasible.

7.4 EXPERIMENTAL SECTION

7.4.1 Synthesis of [Au([16]aneS$_4$)](PF$_6$)

Reaction of [16]aneS$_4$ (30 mg, 0.101 mol) with [Au(tht)$_2$]PF$_6$ (52 mg, 0.101 mmol). in stirring MeCN (5 cm^3) for 1hrs., in the dark gives a colourless solution. Filtration into ice-cold Et$_2$O (30 cm^3) afforded a white precipitate on cooling to -20°C. The product was collected by centrifugation, washed with Et$_2$O and CH$_2$Cl$_2$, yielding a white solid. Dried *in vacuo*, stored at -20°C. (Yield 47 mg, 73%). M.Wt. = 638.51. Elemental analyses: found C = 22.3, H = 3.72, S = 19.8%. Calc. for C$_{20}$H$_{40}$S$_4$AuPF$_6$: C = 22.6, H = 3.79, S = 20.1%. I.r. spectrum (KBr disc): 2930, 2920, 2895, 2850, 1440, 1420, 1345, 1295, 1260, 1195, 1140w, 1050, 1025w, 1010, 1000w, 980w, 920w, 875, 850-830, 780w, 770, 730, 710, 685w and 560 cm^{-1}. F.a.b. mass spectrum (3-NOBA matrix) : found M^+ = 493. Calc. for [^{197}Au([16]aneS$_4$)]$^+$: M^+ = 493, with correct isotopic distribution.

7.4.2 Synthesis of [Au$_2$([28]aneS$_8$)](PF$_6$)$_2$

Reaction of [28]aneS$_8$ (40 mg, 0.075 mmol) with [Au(tht)$_2$]PF$_6$ (83 mg, 0.160 mmol) in stirring MeNO$_2$ (10 cm^3) for 3 h., in the dark gives a colourless solution, which was then reduced in volume (3 cm^3) *in vacuo*. Filtration into ice-cold Et$_2$O (30 cm^3) afforded a white precipitate on cooling to -20°C. The product was filtered, washed with Et$_2$O and CH$_2$Cl$_2$, yielding a white microcrystalline solid. Dried *in vacuo*, stored at -20°C. (Yield 82mg, 75%). M.Wt. = 1220.76. Elemental analyses: found C = 19.7, H = 3.26, S = 19.6%. Calc. for C$_{20}$H$_{40}$S$_8$Au$_2$P$_2$F$_{12}$: C = 19.7, H = 3.30, S = 21.0%. I.r. spectrum

(KBr disc): 2910, 2860, 1550, 1440, 1420, 1340w, 1300, 1260, 1250, 1240, 1200, 1140, 1040, 920, 860-840, 740, 650 and 555 cm^{-1}. F.a.b. mass spectrum (3-NOBA matrix) : found $M^+ = 1075$, 929, 733. Calc. for $[^{197}Au_2([28]aneS_8)PF_6]^+$: $M^+ = 1075$; $[^{197}Au_2([28]aneS_8\text{-}H)]^+$: $M^+ = 929$; $[^{197}Au([28]aneS_8)]^+$: $M^+ = 733$, with correct isotopic distribution. ^1H n.m.r. spectrum (CD_3CN, 298 K, 200.13 MHz) : δ = 2.82-3.15 ppm, (CD_3CN, 215 K, 200.13 MHz) : δ = 2.44b, 2.66b, 2.88b, 3.30 - 4.28 ppm. ^{13}C (DEPT) n.m.r. (CD_3CN, 298K, 50.32 MHz): δ = 25.92 - 32.94 ppm, ^{13}C n.m.r. (CD_3CN, 215 K, 50.52 MHz) : δ = 22.61, 25.34, 27.20, 28.14, 32.47, 32.85 ppm.

7.4.3 Single crystal structure determination of $[Au_2([28]aneS_8)](PF_6)_2$

A colourless lath (0.69 x 0.12 x 0.04 mm) suitable for X-ray analysis was obtained by vapour diffusion of Et_2O into a solution of the complex in $MeNO_2$.

Crystal data:

$[C_{20}H_{40}S_8Au_2]^{2+}.2(PF_6^-)$, M.Wt. = 1220.76, monoclinic, space group $P2_1/n$, a = 6.6156(14), b = 19.836(5), c = 13.190(6)Å, β = 97.728(24)°, U = 1715Å^3 [from 2θ of 38 with reflections 2θ = 27-28°, λ = 0.71073Å] Z = 2, D_c = 2.363 gcm^{-3}, T = 173 K, μ = 9.171 mm^{-1}, $F(000)$ = 1168.

Data collection and processing:

Stoë STADI-4 four circle diffractometer, graphite-monochromated Mo-K_α X-radiation, T = 173 K, ω-2θ scans using the learnt-profile method[307], 3166 data measured (2θ_{max} 45°, h -7→7, k 0→21, l 0→14, 2166 unique (R_{int} = 0.0156), giving 1912 with $F \geq 6\sigma(F)$ for use in all calculations. Initial absorption correction was made using ψ scans (maximum transmission

factor = 0.1880, minimum = 0.0743). Linear isotropic crystal decay (ca. 4%) corrected for during data reduction.

Structure solution and refinement:

A Patterson synthesis located the Au atom and iterative cycles of least-squares refinement and difference Fourier synthesis located the remaining non-hydrogen atoms. At isotropic convergence, corrections (min. 0.823, max. 1145) for absorption were applied using DIFABS.[308] Refinement (by least-squares on F[309]) with isotropic thermal parameters for all ordered non-hydrogen atoms and with hydrogen atoms in fixed, calculated positions converged at R, R_w = 0.0288, 0.0336, respectively, S = 0.997 for 200 refined parameters, and the final ΔF synthesis showed no feature above 1.08eÅ^{-3}. The weighting scheme, $w^{-1} = \sigma^2(F) + 0.000059F^2$, gave satisfactory agreement analyses and in the final cycle $(\Delta/\sigma)_{max}$ was 0.083.

7.4.4 Synthesis of $[Au_2([24]aneS_8)](PF_6)_2$

Reaction of [24]aneS_8 (40 mg, 0.083 mmol) with $[Au(tht)_2]PF_6$ (90 mg, 0.174 mmol) in stirring MeCN (10 cm^3) for 3 hrs., in the dark gives a colourless solution, which was then reduced in volume (5 cm^3) *in vacuo*. Filtration into ice-cold Et_2O (30 cm^3) afforded a white precipitate on cooling to -20°C. (Yield 72 mg, 28%). M.Wt. = 1164.81. Elemental analyses: found C = 17.8, H = 3.01, N = 0.31%. Calc. for $C_{16}H_{32}S_8Au_2P_2F_{12}$: C = 16.5, H = 2.75%. I.r. spectrum (KBr disc): 2920w, 2960, 1420, 1260, 1200, 1140, 860-840 and 560 cm^{-1}. F.a.b. mass spectrum (3-NOBA matrix) : found M^+ = 1019, 873, 677. Calc. for $[^{197}Au_2([24]aneS_8)PF_6]^+$: M^+ = 1019; $[^{197}Au_2[24]aneS_8\text{-}H)]^+$: M^+ = 873; $[^{197}Au([24]aneS_8)]^+$: M^+ = 677, with correct isotopic distributions.

CHAPTER 8

Chemistry of metal-free [9]aneS_3

8.1 INTRODUCTION

The co-ordination complexes of [9]aneS_3 have been studied extensively.[26] Stabilisation of unusual metal oxidation states by this unique ligand has been a particular impetus of the work carried out in Edinburgh. However, the chemistry of [9]aneS_3 itself has only received limited attention.

Structural studies of [9]aneS_3 have been carried out in the solid- and gaseous-states. As discussed in Chapter 2, [9]aneS_3 is unique among thioether macrocyclic ligands, since in the solid-state the ligand adopts a [333] *endo* conformation with the S-donors directed towards the centre of the ligand cavity, C - S = 1.820(5), 1.823(5)Å and C - C = 1.510(6)Å [19] (1). The transannular S...S distance of 3.451(2)Å is less than the sum of van der Waals radii for S (3.70Å). If the symmetry of ligand found in the crystal is maintained in solution, the [9]aneS_3 can be considered to be pre-organised for facial co-ordination to a metal centre.

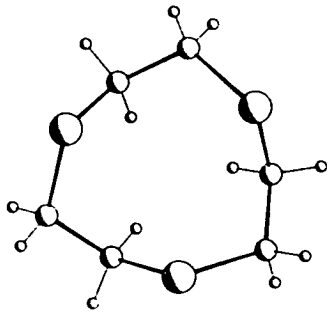

(1)

Photoelectron spectroscopic studies of [9]aneS_3 suggested that the [333] conformation is retained in the gas phase.[258] Electron diffraction and molecular mechanics studies on [9]aneS_3 have recently been carried out in Edinburgh.[259] The assignment of symmetry of [9]aneS_3 in the gaseous-state was ambiguous. C_3, C_2 and C_1 (2) symmetry models all fitted the

experimental data but the quality of the fit varied. The molecular mechanics calculations favoured the C_1 and C_3 models. Conclusions from the combined work suggest that [9]aneS_3 is probably in a mixture of C_1 and C_3 conformations.[259]

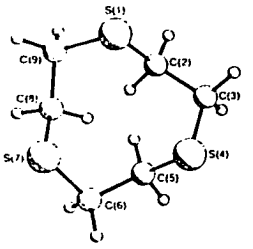

(2) C_3 model

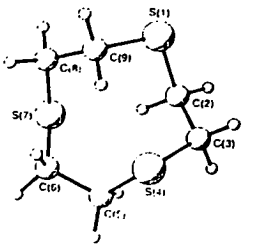

C_2 model

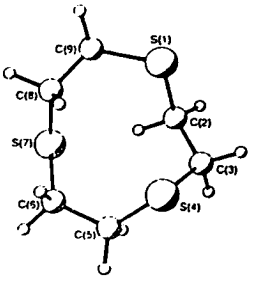

C_1 model

[9]aneS_3 undergoes reactions itself in its bound and unbound forms. [9]aneS_3 can undergo a ring-opening reaction when bound to a high valent metal centre· (Section 1.4).[229] The deprotonation of bound [9]aneS_3 results in a ligand transformation to afford a co-ordinated vinyl thioether moiety with a terminal thiolate donor,[229] (see $[Rh([9]aneS_3)(S(CH_2)_2S(CH_2)_2SCH = CH_2)]^{2+}$ Section 1.4 (22b))

Wieghardt and co-workers have shown that one of the thioether S-donors in $[Fe([9]aneS_3)_2]^{2+}$, can be oxidised to a sulphoxide in the presence of H_2O_2.[255] (3) A metal-based oxidation can also be achieved using PbO_2 in H_2SO_4 to give $[Fe([9]aneS_3)_2]^{3+}$.[255] Full oxidation of [9]aneS_3 using H_2O_2 affords the hexaoxo species.[256]

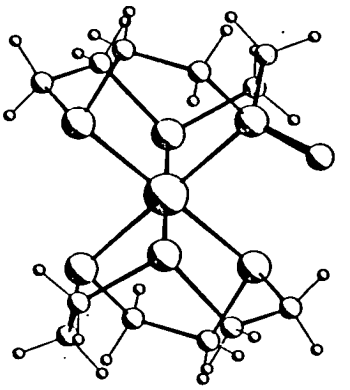

(3)

During the synthesis of $[Au([9]aneS_3)_2]^{2+}$ (Chapter 2) a non-metal containing by-product was isolated. The aim of the work discussed in this chapter was to identify and characterise this new [9]aneS$_3$-derived product and study the oxidation products of [9]aneS$_3$.

8.2 RESULTS AND DISCUSSION

8.2.1 Characterisation of [9]aneS$_3$-derived by-product

In the final stages of the synthesis of $[Au([9]aneS_3)_2]^{2+}$ a non-metal containing by-product was isolated. The product gave an accurate f.a.b. mass spectral peak at $M^+ = 179.00228$, corresponding to $[C_6H_{11}S_3]^+$. I.r. spectroscopy (KBr disc) indicated the presence of BF_4^- in the product. The ^1H n.m.r. spectrum of the by-product showed a doublet of doublets at * $\delta = 3.09 - 4.30$ ppm (10H) (Figure 8.1). ^{13}C (DEPT) n.m.r. spectrum shows one methyne or methyl resonance at $\delta = 59.29$ ppm and four methylene resonances at $\delta = 47.55, 35.22, 34.00, 26.19, 23.37$ ppm (Figure 8.2).

On the basis of the spectroscopic and microanalytical data the product was assigned as $[C_6H_{11}S_3](BF_4)$. $[C_6H_{11}S_3](PF_6)$ can synthesised in good yield by reacting [9]aneS$_3$ with one molar equivalent of the hydride abstractor ($Ph_3C^+PF_6^-$) in $MeNO_2$.

---

* $\delta = 5.28$ ppm (1H) and a complicated multiplet at

Figure 8.1: ^{1}H n.m.r. spectrum of $[C_6H_{11}S_3](PF_6)$

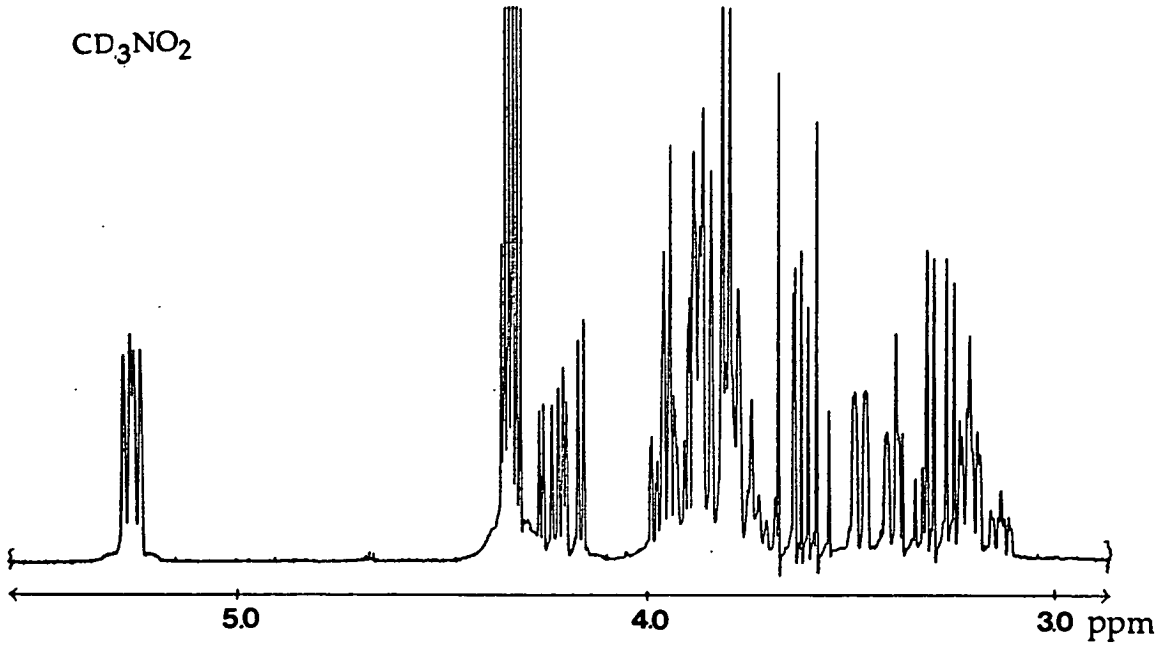

Figure 8.2: ^{13}C (DEPT) n.m.r. spectrum of $[C_6H_{11}S_3](PF_6)$

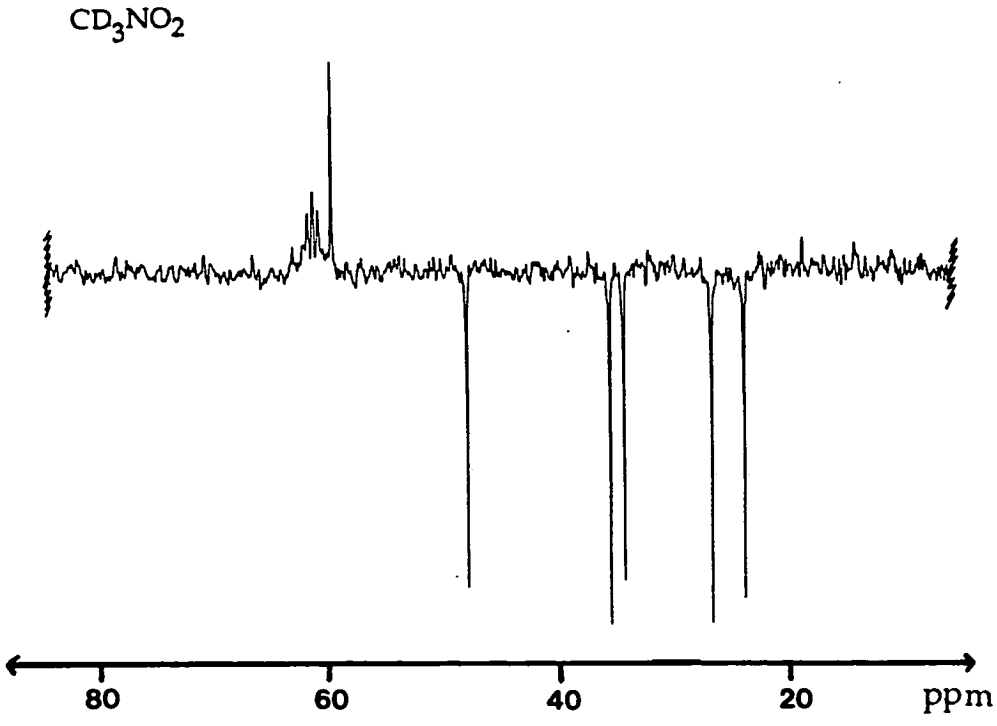

To establish the exact connectivity of $[C_6H_{11}S_3](BF_4)$ an X-ray single crystal determination was carried out.

8.2.2 Structure determination of $[C_6H_{11}S_3](BF_4)$

The single crystal X-ray determination of $[C_6H_{11}S_3](BF_4)$ confirmed the compound to be a bicyclic sulphonium salt, 4,7-dithia-1-thionia-bicyclo[4,3,0]nonane, which incorporates fused six- and five- membered rings (Figure 8.3).

Figure 8.3: Single crystal X-ray structure of $[C_6H_{11}S_3]^+$

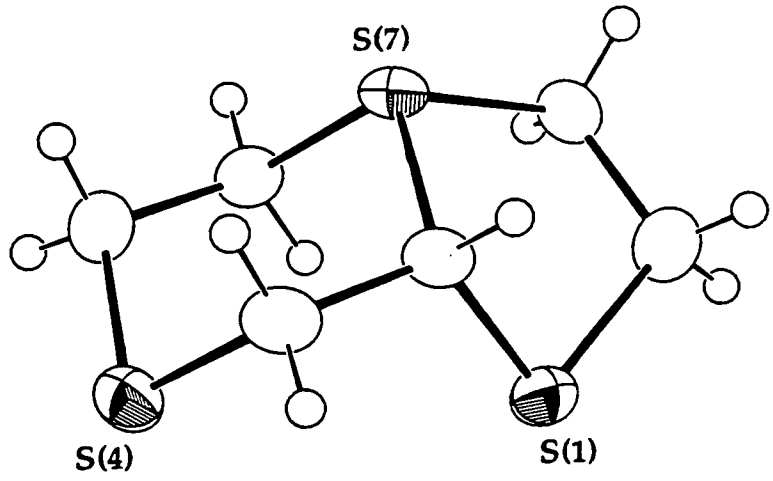

The six-membered ring adopts a chair conformation with the sulphonium salt at the bridgehead, (outer C - S = 1.798(3) - 1.817(3)Å, bridge C - S = 1.8414(24)Å, C - C = 1.511(4) - 1.520(4)Å). Full details of the solution and refinement are given in Section 8.4.2. Selected bonds, angles and torsions are given in Table 8.1.

Table 8.1: Selected bonds, angles and torsions for $[C_6H_{11}S_3]^+$

S(1) - C(2)	1.7976(24)	C(5) - C(6)	1.513(4)
S(1) - C(9)	1.807(3)	C(6) -H(6A)	0.99(3)
C(2) - H(2)	0.95(3)	C(6) -H(6B)	0.94(3)
C(2) - C(3)	1.520(4)	C(6) - S(7)	1.816(3)
C(2) - S(7)	1.8414(24)	S(7) - C(8)	1.817(3)
C(3) -H(3A)	0.91(3)	C(8) -H(8A)	0.91(3)
C(3) -H(3B)	0.94(3)	C(8) -H(8B)	0.99(3)
C(3) - S(4)	1.798(3)	C(8) - C(9)	1.511(4)
S(4) - C(5)	1.815(3)	C(9) -H(9A)	0.88(3)
C(5) -H(5A)	0.99(3)	C(9) -H(9B)	1.00(3)
C(5) -H(5B)	0.89(3)		

C(2) - S(1) - C(9)	91.00(13)	C(5) - C(6) -H(6B)	111.6(17)
S(1) - C(2) - H(2)	107.2(16)	C(5) - C(6) - S(7)	110.80(18)
S(1) - C(2) - C(3)	116.56(17)	H(6A) - C(6) -H(6B)	110.3(23)
S(1) - C(2) - S(7)	106.23(12)	H(6A) - C(6) - S(7)	105.2(16)
H(2) - C(2) - C(3)	109.1(16)	H(6B) - C(6) - S(7)	103.1(17)
H(2) - C(2) - S(7)	105.6(16)	C(2) - S(7) - C(6)	101.28(11)
C(3) - C(2) - S(7)	111.45(17)	C(2) - S(7) - C(8)	96.17(12)
C(2) - C(3) -H(3A)	109.5(18)	C(6) - S(7) - C(8)	102.43(12)
C(2) - C(3) -H(3B)	109.3(17)	S(7) - C(8) -H(8A)	105.2(17)
C(2) - C(3) - S(4)	116.00(18)	S(7) - C(8) -H(8B)	104.1(15)
H(3A) - C(3) -H(3B)	110.3(24)	S(7) - C(8) - C(9)	110.19(19)
H(3A) - C(3) - S(4)	103.4(17)	H(8A) - C(8) -H(8B)	113.5(23)
H(3B) - C(3) - S(4)	108.0(17)	H(8A) - C(8) - C(9)	111.3(17)
C(3) - S(4) - C(5)	99.12(13)	H(8B) - C(8) - C(9)	112.0(15)
S(4) - C(5) -H(5A)	107.9(16)	S(1) - C(9) - C(8)	110.63(21)
S(4) - C(5) -H(5B)	106.8(18)	S(1) - C(9) -H(9A)	107.3(19)
S(4) - C(5) - C(6)	113.31(19)	S(1) - C(9) -H(9B)	111.4(16)
H(5A) - C(5) -H(5B)	107.0(24)	C(8) - C(9) -H(9A)	115.9(19)
H(5A) - C(5) - C(6)	111.1(16)	C(8) - C(9) -H(9B)	108.6(16)
H(5B) - C(5) - C(6)	110.5(19)	H(9A) - C(9) -H(9B)	102.7(24)
C(5) - C(6) -H(6A)	115.0(16)		

C(9) - S(1) - C(2) - H(2)	-66.2(17)	S(4) - C(5) - C(6) - S(7)	-70.26(21)
C(9) - S(1) - C(2) - C(3)	171.29(20)	H(5A) - C(5) - C(6) -H(6A)	170.5(24)
C(9) - S(1) - C(2) - S(7)	46.44(14)	H(5A) - C(5) - C(6) -H(6B)	-62.9(25)
C(2) - S(1) - C(9) - C(8)	-47.46(21)	H(5A) - C(5) - C(6) - S(7)	51.4(17)
C(2) - S(1) - C(9) -H(9A)	-174.8(19)	H(5B) - C(5) - C(6) -H(6A)	-70.9(26)
C(2) - S(1) - C(9) -H(9B)	73.4(17)	H(5B) - C(5) - C(6) -H(6B)	55.6(27)
S(1) - C(2) - C(3) -H(3A)	58.6(19)	H(5B) - C(5) - C(6) - S(7)	169.9(20)
S(1) - C(2) - C(3) -H(3B)	179.6(18)	C(5) - C(6) - S(7) - C(2)	60.80(20)
S(1) - C(2) - C(3) - S(4)	-58.02(23)	C(5) - C(6) - S(7) - C(8)	159.79(19)
H(2) - C(2) - C(3) -H(3A)	-63.0(25)	H(6A) - C(6) - S(7) - C(2)	-64.1(16)
H(2) - C(2) - C(3) -H(3B)	58.0(25)	H(6A) - C(6) - S(7) - C(8)	34.9(16)
H(2) - C(2) - C(3) - S(4)	-179.6(17)	H(6B) - C(6) - S(7) - C(2)	-179.7(17)
S(7) - C(2) - C(3) -H(3A)	-179.3(19)	H(6B) - C(6) - S(7) - C(8)	80.7(17)
S(7) - C(2) - C(3) -H(3B)	-58.3(18)	C(2) - S(7) - C(8) -H(8A)	-117.8(18)
S(7) - C(2) - C(3) - S(4)	64.13(21)	C(2) - S(7) - C(8) -H(8B)	122.5(16)
S(1) - C(2) - S(7) - C(6)	70.84(14)	C(2) - S(7) - C(8) - C(9)	2.27(21)
S(1) - C(2) - S(7) - C(8)	-33.18(14)	C(6) - S(7) - C(8) -H(8A)	139.2(18)
H(2) - C(2) - S(7) - C(6)	-175.5(17)	C(6) - S(7) - C(8) -H(8B)	19.5(16)
H(2) - C(2) - S(7) - C(8)	80.5(17)	C(6) - S(7) - C(8) - C(9)	-100.76(20)
C(3) - C(2) - S(7) - C(6)	-57.09(19)	S(7) - C(8) - C(9) - S(1)	30.0(3)
C(3) - C(2) - S(7) - C(8)	-161.11(18)	S(7) - C(8) - C(9) -H(9A)	152.5(21)
C(2) - C(3) - S(4) - C(5)	-59.04(21)	S(7) - C(8) - C(9) -H(9B)	-92.6(17)
H(3A) - C(3) - S(4) - C(5)	-179.0(18)	H(8A) - C(8) - C(9) - S(1)	146.3(18)
H(3B) - C(3) - S(4) - C(5)	64.1(18)	H(8A) - C(8) - C(9) -H(9A)	-91.3(28)
C(3) - S(4) - C(5) -H(5A)	-61.9(17)	H(8A) - C(8) - C(9) -H(9B)	23.7(25)
C(3) - S(4) - C(5) -H(5B)	-176.6(19)	H(8B) - C(8) - C(9) - S(1)	-85.4(17)
C(3) - S(4) - C(5) - C(6)	61.50(21)	H(8B) - C(8) - C(9) -H(9A)	37.1(27)
S(4) - C(5) - C(6) -H(6A)	48.9(17)	H(8B) - C(8) - C(9) -H(9B)	152.0(23)
S(4) - C(5) - C(6) -H(6B)	175.4(18)		

The product is formally the deprotonated, two- electron oxidation product of [9]aneS_3 . Transannular S - C bond formation and C - H bond cleavage result in a bicyclic species; the formation of the fused five- and six- membered rings is presumably the driving force for the production of this species.

8.2.3 Reactions of $[C_6H_{11}S_3]^+$

Theoretically, reduction of the bicyclic sulphonium salt $[C_6H_{11}S_3]^+$ could result in the formation of [9]aneS_3 , via attack at position (A) (4). Equally attacked may occur at positions B and C.

(4)

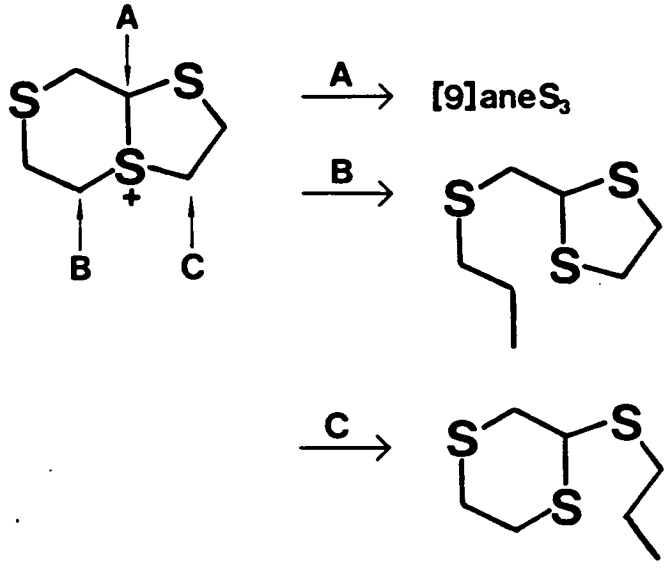

Preferential nucleophilic attack at position (A) could represent a route to C-functionalisation of [9]aneS_3. Attempted reduction of the bicyclic sulphonium salt using $NaBH_4$ gave no reaction after 3 days. n-Selectride reacts with the bicyclic sulphonium salt to give a mixture of products while the reaction of MeLi consistently gave a product that showed 9 methylene carbon resonances in the ^{13}C (DEPT) spectrum, and one methyl or methyne

resonance. Assignment of this product was not possible, although comparison with the ^{13}C n.m.r. spectroscopic data for the recently synthesised methylated [9]aneS_3[261] established that Me^- had not preferentially attacked at the bridge position (A) in the sulphonium salt.

Endeavours to use less vigorous nucleophiles (e.g. BuLi) gave no apparent reaction. Templeton and co-workers have reported the synthesis of a ten-membered ring from a sulphonium salt,[260] using the reaction shown below (5).

(5)

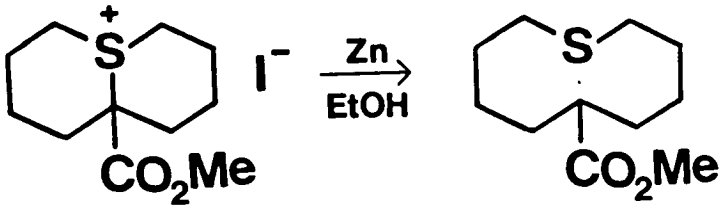

Exploitation of this route may yield [9]aneS_3 from the bicyclic sulphonium salt; insufficient time was available to attempt this reaction.

8.2.4 Electrochemical oxidation of [9]aneS_3

Cyclic voltammetry of [9]aneS_3 in MeCN (0.1M $^nBu_4NPF_6$) at platinum electrodes shows an irreversible oxidation at Ep_a = +0.98V (vs Fc/Fc+), with a return wave of Ep_c = -0.57V at a scan rate of 250 mVs^{-1}. The reduction at -0.57V is not present on initially scanning from 0 to -1.0V indicating that the return wave corresponds to the reduction of an oxidation product of [9]aneS_3.

Cyclic voltammetry of $[C_6H_{11}S_3](PF_6)$ in MeCN (0.1M $^nBu_4NPF_6$) at platinum electrodes shows an irreversible reduction at Ep_c = -2.14V

(vs Fc/Fc^{+}) at a scan rate of 250 mVs^{-1}. Therefore, it can be deduced that $[C_6H_{11}S_3]^+$ is not the major electrochemical oxidation product of [9]aneS_3.

Electrogeneration of [9]aneS_3 in MeCN at +1.2V (vs Fc/Fc^{+}) affords a pale yellow, e.p.r. active species. The frozen glass e.p.r. spectrum of the electrochemical oxidation product of [9]aneS_3 shows a complex multiplet (Figure 8.4).

Figure 8.4: X-band frozen glass spectrum of the electrochemical oxidation product of [9]aneS_3

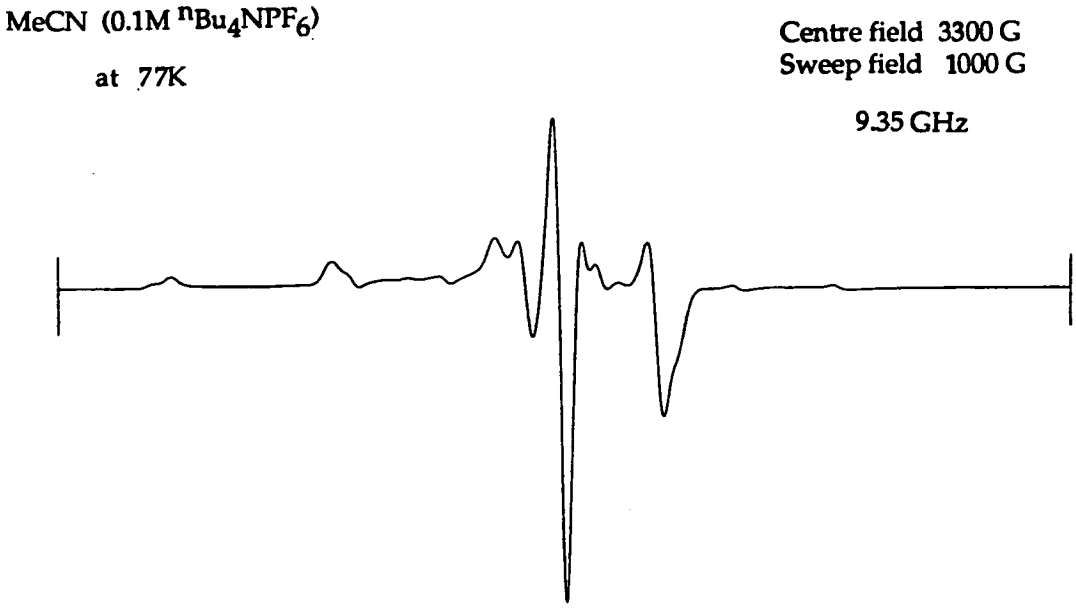

Numerous sulphur-based radical species have been reported in the literature.[262-272] Thioether cation radicals and dications have been reported by Musker and co-workers[273-276]; these highly reactive dithioether species were proposed to incorporate S...S interactions[274-275] (6 - 8). The experimental and simulated e.p.r. spectrum reported for (8)[276] is similar to the e.p.r. spectrum observed for the electrochemically oxidised [9]aneS_3.

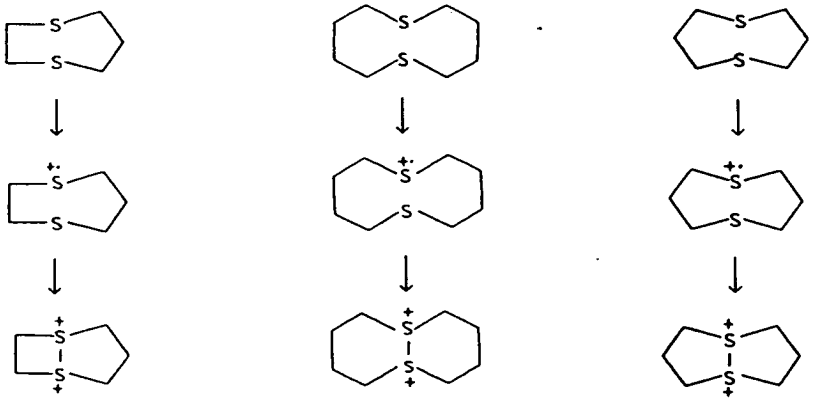

(6) (7) (8)

Coulometric measurements carried out at E = +1.2V vs Fc/Fc^+ on the oxidation of [9]aneS_3 were irreproducible and gave values for n ranging from two to six electrons. It seems likely that the electrochemical oxidation product of [9]aneS_3 is a sulphur-based radical cation, probably incorporating a stabilising transannular S....S interaction. (9) It is difficult to determine the number of sulphur-radical centres present in one ring species due to the ambiguity of the coulometric measurements. Possible quenching of the thioether radicals by trace amounts of H_2O (affording sulphoxide species) may affect the coulometric measurements.

(9)

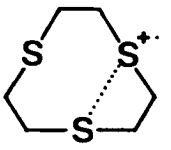

Cyclic voltammetry of the electrochemically oxidised product shows three irreversible reductions at Ep_c = -0.69, -1.48, -2.15V (vs (Fc/Fc^+) at a scan rate of 320 mVs^{-1}.

8.2.5 Chemical oxidation of [9]aneS_3

The chemical oxidation of [9]aneS_3 in MeCN by **one** molar equivalent of $NOBF_4$ affords a yellow solution. The yellow product is e.p.r. active, the frozen glass e.p.r. spectrum (Figure 8.5) is very similar to that observed for the electrochemically oxidised species, (Figure 8.4) suggesting that this oxidation product of [9]aneS_3, is also probably the radical cation species.

Figure 8.5: X-band frozen glass spectrum of the chemical oxidation product of [9]aneS_3

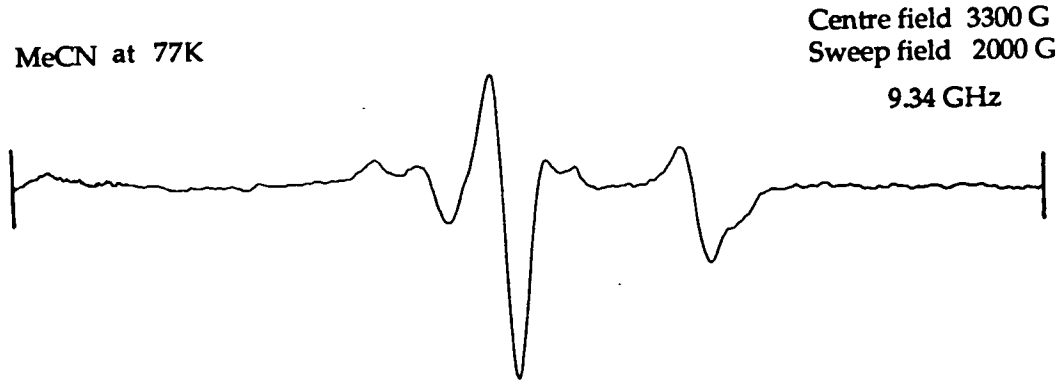

Chemical oxidation of [9]aneS_3 in CD_3NO_2 with **two** molar equivalents of $NOBF_4$ also produces a yellow product. The ^{13}C (DEPT) n.m.r. spectrum of this species shows six resonances at 23.06, 25.77, 42.07, 43.87, 47.78 and 49.95 ppm. Further characterisation was not possible due to decompostion during the isolation of the product.

The product generated by the chemical oxidation of [9]aneS_3 using two equivalents of $NOBF_4$, shows three irreversible reductions (by cyclic voltammetry) Ep_c = 0.96, -1.63, -2.18V (vs Fc/Fc^+) at a scan rate of 210 mVs^{-1}. Interestingly, therefore, the chemical and electrochemical radical oxidation products of [9]aneS_3 differ.

8.3 CONCLUSIONS

[9]aneS$_3$ undergoes oxidation chemically and electrochemically to give radical cation or dication species. These species are probably stabilised by transannular S....S interactions.

[C$_6$H$_{11}$S$_3$](BF$_4$), a stable non-radical oxidation product of [9]aneS$_3$, was isolated and characterised. This bicyclic sulphonium salt is formally the deprotonated, two-electron oxidation product of [9]aneS$_3$. The formation of this salt may occur via radical cation and/or dication intermediates (Scheme 1); alternatively a concerted mechanism can be postulated (Scheme 2).

Scheme 1

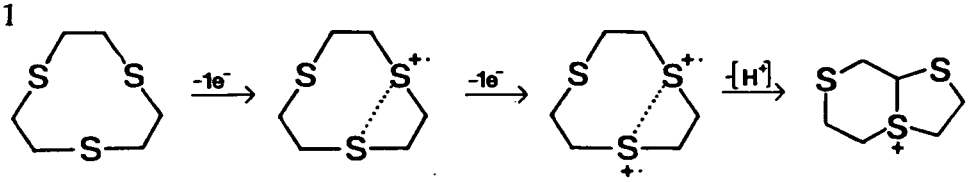

Scheme 2

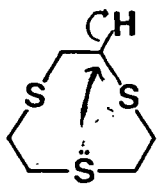

The reaction of HAuCl$_4$ with [9]aneS$_3$ in 40%aq. HBF$_4$ produces the Au(II) complex [Au([9]aneS$_3$)$_2$](BF$_4$)$_2$ together with the bicyclic sulphonium salt of [9]aneS$_3$. Thus, oxidation of [9]aneS$_3$ to [C$_6$H$_{11}$S$_3$]$^+$ in this system occurs via the reduction of Au(III) to Au(II).

$$2\ \text{Au(III)} + 5\ [9]\text{aneS}_3 \longrightarrow 2\ [\text{Au}([9]\text{aneS}_3)_2]^{3+} + [\text{C}_6\text{H}_{11}\text{S}_3]^+ + \text{H}^+$$

8.4.1 Synthesis of $[C_6H_{11}S_3](PF_6)$

Reduction of [9]aneS_3 (50 mg, 0.28 mmol) with ($Ph_3C^+PF_6^-$) (105 mg, 0.28 mmol) in degassed $MeNO_2$ (5 cm^3) under N_2, initially afforded a dark brown solution that progressively turned orange whilst stirring for 72 hours at room temperature. Filtration into Et_2O (30 cm^3) produced a white precipitate. The product was washed with H_2O (5 cm^3), CH_2Cl_2 (10 cm^3) and Et_2O (10 cm^3). Recrystallisation of the cream product from MeCN-Et_2O yielded a white powder. (Yield 77 mg, 85%) M.Wt = 324.32. Elemental analyses: found C = 22.1, H = 3.5%. Calc. for $C_6H_{11}S_3P_1F_6$: C = 22.2, H = 3.39%. I.r. spectrum (KBr disc): 3000, 1430, 1420, 1400, 1300, 1220, 1140, 940, 900, 840, 660 and 560 cm^{-1}. Accurate f.a.b. mass spectrum: found M^+ = 179.00228, Calc. for $[C_6H_{11}S_3]^+$: M^+ = 179.00229. ^1H n.m.r. spectrum (CD_3NO_2, 298K, 200.13 MHz): δ = 5.28 (dd,1H), δ = 3.09 - 4.30 ppm (10H). ^{13}C (DEPT) n.m.r. spectrum (CD_3NO_2, 298K, 50.32 MHz): δ = 59.29 (CH), 47.55, 35.22, 34.00, 26.19, 23.37 ppm (CH_2).

8.4.2 Structure determination of $[C_6H_{11}S_3](BF_4)$

A colourless lath (0.22 x 0.38 x 0.85 mm) suitable for X-ray analysis was obtained by vapour diffusion of Et_2O into a solution of the complex in MeCN.

Crystal data:

$[C_6H_{11}S_3]^+.(BF_4)^-$, M.Wt = 266.10, monoclinic, space group $P2_1/c$, a = 5.140(3), b = 9.1036(20), c = 21.947(4)Å, β = 90.73(3)°, U = 1027Å^3 [from setting

angles for 15 centred reflections with 2θ = 30-32°, λ = 0.71073Å], Z = 4, D_c =1.721 gcm^{-3}, μ = 0.706 mm^{-1}, $F(000)$ = 554.

Data collection and processing:

CAD4 four-circle diffractometer, Mo-K_α X-radiation, T = 295 K, ω-2θ with ω scan width (1.0 + 0.34 tanθ)° gave 1433 reflections ($2\theta_{max}$ 45°), 1314 unique reflections (R_{int} = 0.006), of which 1168 with $F > 6\sigma(F)$ were used in all calculations.

Structure solution and refinement:

Automatic direct methods[336] located all non-H atoms, which were then refined anisotropically[307] : H atoms were refined postionally with a common U_{iso} of 0.0478(24)Å^2. At final convergence, R, R_w = 0.0251, 0.0359, respectively, S = 1.119 for 161 parameters and the final ΔF synthesis showed no feature above 0.31 eÅ^{-3}. The weighting scheme $w^{-1} = \sigma^2 + 0.000185F^2$ gave satisfactory agreement analysis and in the final cycle $(\Delta/\sigma)_{max}$ was 0.036.

CHAPTER 9

Overall conclusions

OVERALL CONCLUSIONS

Thioether macrocycles have proved to be excellent stabilising ligands for gold in its +1, +2 and 3+ oxidation states. By the control of solvent and temperature the isolation of Au(I) and Au(II) compounds has been possible. In the Au(I) thioether macrocyclic complexes studied in the solid-state, the d^{10} centre has repeatedly displayed a tendency for [2+2] distorted tetrahedral co-ordination (Table 9.1). Not only can these ligands accommodate the two co-ordinate metal centre, but additional S-donors are also available encouraging the Au(I) centre to increase its co-ordination number. It is interesting to note that in $[Au(Me_2[18]aneN_2S_4)]^+$ the metal centre prefers to take [2+1] co-ordination to three S-donors even in the presence of additional S- and N-donors; presumably a combination of chelate ring size and mis-matched donor type effects is responsible for the resultant stereochemistry. The introduction of 'hard' N-donors into the macrocyclic ring, as anticipated, affected the stabilisation of Au(II) and Au(III) (Table 9.2).

Table 9.2: Oxidations potentials for selected Au(I) macrocyclic complexes

	$E^1_{1/2}$ /V (ΔE_p/mV)	$E^2_{1/2}$ /V (ΔE_p/mV)
$[Au([18]aneS_6)](PF_6)$	+0.36 (150)	+0.56 (60)
$[Au([15]aneS_5)](PF_6)$	+0.36 (150)	+0.54 (60)
$[Au([18]aneN_2S_4)](PF_6)$	+0.87 (irrev.)	
$[Au(Me_2[18]aneN_2S_4)](PF_6)$	+0.14 (130)	+0.43 (60)
$[Au([16]aneS_4)](PF_6)$	+0.14 (200)	
$[Au_2([28]aneS_8)](PF_6)_2$	+0.55 (210)	

All potentials quoted vs Fc/Fc^+ (0.1 M $^nBu_4NPF_6$ in MeCN)

Table 9.1 Comparison of [2+2] co-ordination at Au(I) for selected macrocyclic structures

	S(1) -Au-S(10)	Au-S bonds		Au...S interactions	
$[Au([9]aneS_3)_2]^+$	153.98(23)	2.302(6)	2.350(9)	2.733(8)	2.825(8)Å
$[Au([18]aneS_6)]^+$	155.93(12)	2.320(4)	2.321(3)	2.870(3)	2.856(4)Å
$[Au([15]aneS_5)](B(C_6F_5)_4)$	169.90 (5)	2.2927(13)	2,300(13)	3.1055(13)	3.2088(14)Å
$[Au([15]aneS_5)](PF_6)$ (Major)	158.82(22)	2.223(5)	2.345(7)	2.887(6)	2.992(6)Å
$[Au_2([28]aneS_8)](PF_6)_2$	155.58(6)	2.3301(10)	2.3378(18)	2.7891(20)	2.7629(20)Å
$[Au(Me_2[18]aneN_2S_4)](PF_6)$	177.30(5)*	2.3043(15)	2.3138(14)	2.8883(15)Å	

The ligand cavity size has been shown to be critical in the co-ordination of Au(I) in its desired stereochemistry; [9]aneS_3 and [15]aneS_5 have to bind Au(I) in an exocyclic fashion. Notably these exocyclic complexes {$[Au([9]aneS_3)_2]^+$ and $[Au([15]aneS_5)]^+$} are relatively unstable in solution, tending to disproportionate to Au(0) and Au(II) more so than the endocyclic species {[Au([18]aneS_6)]+ and $[Au_2([28]aneS_8)]^{2+}$}.

The synthesis of a variety of Au(II) compounds presented us with the opportunity to study this unusual oxidation state of gold. E.p.r. and Mössbauer spectroscopic studies suggested that the quadrupole and nuclear Zeeman interactions are significant in these species. A degree of covalency in the Au-S bonding is indicated in the g values obtained in the solution e.p.r. data (Table 9.3).

Table 9.3: Solution e.p.r. spectroscopic data for selected Au(II) species

	g_{iso} (G)	A_{iso} (cm^{-1})
$[Au([9]aneS_3)_2](BF_4)_2$	2.016	42.0×10^{-4}
$[Au([18]aneS_6)](PF_6)_2$	2.026	43.2×10^{-4}
$[Au([15]aneS_5)](PF_6)_2$	2.014	40.7×10^{-4}

All measurements for $MeNO_2$ solutions were taken at 293 K

Hopefully this work will be continued in order to establish the exact role of the S-atoms in the stabilisation of Au(II) and to expand the range of gold macrocyclic complexes.

REFERENCES

1. "Co-ordination Chemistry of Macrocyclic Compounds", Ed. G.A. Melson, Plenum, New York 1979.
2. "The Chemistry of Macrocyclic Ligand Compounds", L.F. Lindoy, Cambridge University Press, Cambridge 1989.
3. D.K. Cabbiness and D.W. Margerum; J. Amer. Chem. Soc., 1969, 91, 6540.
4. F.P. Hinz and D.W. Margenum; Inorg. Chem., 1974, 13, 2941.
5. A. Dei and R. Gori; Inorg. Chim. Acta., 1975, 14, 157.
6. L. Fabrizzi, P. Paoletti and A.B.P. Lever; ibid, 1976, 15, 1502.
7. M. Kodama and E. Kimura; J. Chem. Soc., Dalton Trans., 1976, 116.
8. L. Fabbrizzi, P. Paoletti, A. Anichini and R.M. Clay; J. Chem. Soc., Dalton Trans., 1978, 577.
9. L. Fabbrizzi, P. Paoletti, and R.M. Clay; Inorg. Chem., 1978, 17, 1042.
10. G.F. Smith and D.W. Margerum; J. Chem. Soc., Chem. Comm.,1975, 807.
11. D.K. Cabbiness and D.W. Margerum; J. Amer. Chem. Soc., 1970, 92, 2151.
12. T.E.Jones, L.L. Zimmer, L.L.Diaddario, D.B. Rorabacher and L.A. Ochrymowycz; Inorg. Chem., 1985, 97, 7163.
13. D.H. Busch, K. Farmery, V. Goedken, V. Katovic, A.C. Melnyk, C.R. Sperati and N. Tokel; Adv. Chem. Ser., 1971, 100, 44.
14 a) K. Henrick, P.A. Tasker and L.F. Lindroy; Prog. Inorg. Chem., 1985, 33, 1.

b) R.D. Hancock and A.E. Martell; Comments Inorg. Chem., 1988, 6, 237.

c) R.D. Hancock, A. Evers, P.M. Ngwenya and P.W. Wade; J. Chem. Soc., Chem. Comm., 1987, 14, 1129.

d) R.D. Hancock, P.N. Wade, P.M. Ngewenya, A.S. DeSousa, and K.V. Darnu; Inorg. Chem., 1990 29, 1968.15. S.C. Rawle, G.A.Admans and S.R. Cooper; J. Chem. Soc., Dalton Trans., 1988, 93.

16. a) G.H. Robinson and S.A. Sangokoya; J. Amer. Chem. Soc., 1988, 110, 1494.

17. R.E. DeSimone and M.D. Glick; J. Amer. Chem. Soc., 1976, 98, 762.

18. J.R. Hartman, R.E. Wolf, B.M. Foxman and S.R. Cooper; J. Amer. Chem. Soc., 1983, 105, 131.

19. R.S. Glass, G.S. Wilson and W.N. Setzer; J. Amer. Chem. Soc., 1980, 102, 5068.

20. V.L. Goedken, in "Co-ordination Chemistry of Macrocyclic Compounds", Chpt. 10. "Natural Product Model Systems", p. 603-654, and references within.

21. a) D.H. Busch, Y. Hung, L.Y. Martin, S.C. Jackels and A.M. Tait; J. Amer. Chem. Soc., 1979, 99, 4029.
b) D.H. Busch, E.S. Gove and F.V. Lovecchio; J. Amer. Chem. Soc., 1974, 96, 3109.

22. M. Kodama and E. Kimura; J. Chem. Soc., Chem. Comm., 1975, 326.

23. G. Reid, A.J. Blake, T.I. Hyde and M. Schröder; J. Chem. Soc., Chem. Comm., 1988, 1397.

24. G. Reid, Ph.D. Thesis, Edinburgh, 1989.

26. A.J. Blake and M. Schröder; Adv. Inorg. Chem., 1990, 35, 1.

27. A.J. Blake, R.O. Gould, J.A. Greig, A.J. Holder, T.I. Hyde and M. Schröder; J. Chem. Soc., Chem. Comm., 1989, 876.

28. S. Otsuka and T. Yamanaka " Metalloproteins", Elsevier, 1988, Amsterdam.

29. H.A.O. Hill in "Inorganic Biochemistry" Chpt. 30, "Corrinoids", p 1067-1136.

30. R.W. Hay "Bio-Inorganic Chemistry", Ellis Horwood, Chichester, 1984.

31. D.R. Williams "An Introduction to Bio-Inorganic Chemistry", Thomas 1976.

32. J.M. Rifkind in "Inorganic Biochemistry", Ed. G.L. Eichhorn, Elsevier, Amsterdam, Chpt. 5, "Haemoglobin and Myoglobin", p 832-902.

33. J.J. Katz in "Inorganic Biochemistry ", Chpt 29, "Chlorophyll", p. 1022-1066.

34. D.G. Brown; Prog. Inorg. Chem., 1973, 18, 177 and references therein.

35. H.A. Harburg and R.H.L. Marks in "Inorganic Biochemistry", Chpt. 26 "Cytochromes b and c" p.902-955.

36. H.A.O. Hill; Chem. Brit., 1976, 12, 119.

37. J.P.Collman, R.G. Gagné, T.R. Halbert, J.C. Marchen and C.A. Reed; J. Amer. Chem. Soc., 1973, 95, 7868.

38. P.L.Burk, J.A. Osborn, M-T. Youinou, Y. Agnus, R. Louis and R. Weiss; J. Amer. Chem. Soc., 1981, 103, 1273.

39. K. Wieghardt, I. Tolksdorf and W. Herrman; Inorg. Chem., 1985, 24, 1230.

40. L. Que and A.E. True; Prog. Inorg. Chem., 1990, 38, 97.

41. A. Nakamura and N. Ueyama; Adv. Inorg. Chem., 1989, 33, 39.

42. P.N. Turowski, W.H., Armstrong, M.E. Roth and S.J. Lippard; J. Amer. Chem. Soc., 1990, 112, 681.

43. B. Fisher and R. Eisenberg; J. Amer. Chem. Soc., 1980, 102, 7361.

44. S. Meshitsuka, M. Ichikawa and K. Tamura; J. Chem. Soc., Chem. Comm., 1974, 158.

45. D.A. Gangi and R.R. Durand; J. Chem. Soc., Chem. Comm., 1986, 697.

46. J.P. Collman, P.Denisevich, M. Marrocco, K. Koval and F.C. Anson; J. Amer. Chem. Soc., 1980, 102, 6027.

47. M. Beley, J.P. Collin, R. Ruppert and J.P. Sauvage J. Chem. Soc., Chem. Comm., 1984, 1315.

48. M. Beley, J.P. Collin, R.Ruppert and J.P. Sauvage; J. Chem. Soc., Chem. Comm., 1986, 7461.

49. J.P. Collin and K. Kim; J. Amer. Chem. Soc., 1986, 108, 7847.

50. D. Pletcher and D.J. Pearce; J. Electroanal. Chem., 1987, 197, 317.

51. Y. LeMest, M. L'Her, J. Courtot-Coupez, J.P. Collman, E.R. Eritt and C.S. Benscosme; J. Chem. Soc., Chem. Comm., 1983, 1286.

52. M.J. Camenzind, D. Dolphin and B.R. James; J. Chem. Soc., Chem. Comm., 1986, 1137.

53. I. Taniguchi, N. Nakaskima and K. Yasutouchi; J. Chem. Soc., Chem. Comm., 1986, 1814.

54. B.B. Wayland and A.R. Newman, Inorg. Chem., 1981, 20, 3093.

55. R.R. Durrand, C.S. Bencosme, J.P. Collman and F.C. Anson; J. Amer. Chem. Soc., 1983, 105, 2710.

56. F.P. Guengerich and T.L. Macdonald; Acc. Chem. Res., 1984, 17, 9.

57. R. Breslaw, A.B. Brown, R.D. McCullough and P.W. White; J. Amer. Chem. Soc., 1989, 111, 4517.

58. T.C. Bruice; Acc. Chem. Res., 1991, 24, 243.

59. T.G. Traylor and J.P. Ciccone; J. Amer. Chem. Soc., 1989, 111, 8413.

60. K.R. Rodgers, I.M. Arafa and H.M. Goff; J. Chem. Soc., Chem. Comm., 1990, 1323.

61. Y. Watanabe, K. Takehira, M. Shimizu, T. Hayakama, and H. Orita; J. Chem. Soc., Chem. Comm., 1990, 927.

62. Y. Naruta, F. Taki and K. Maruyama; J. Chem. Soc., Chem. Comm., 1990, 1378.

63. K. Shin and H.M. Goff; J. Chem. Soc., Chem. Comm., 1990, 461.

64. E. Baciocchi, M. Crescenzi and O. Lansalinga; J. Chem. Soc., Chem. Comm., 1990, 687.

65. J.P. Collman and P.J. Brothers; Acc. Chem. Res., 1986, 19, 209 and references therein.

66. J.Y. Becker, B. Vainas, R. Eger and L. Kaufman; J. Chem. Soc., Chem. Comm., 1985, 1471.

67. D.H. Busch, W.D. Lenke, K.E. Travis and N.E. Tokvoryan; Adv. Chem. Serv., 1977, 150, 358.

68. J.P. Collman, J.I. Brauman and A.M. Madonik; Organometallics, 1986, 5, 311.

69. D. Pletcher, R.Roas, J.Y. Becker and J.B. Kerr; J. Electroanal. Chem., 1981, 117, 87.

70. S.G. Murray and F.R. Hartley; Chem. Rev., 1981, 81, 365.

71. C.G. Kuehn and S.S. Isied; Prog. Inorg. Chem., 1980. 27, 163.

72. S.R. Cooper; Acc. Chem. Res., 1988, 21, 141.

73. M. Schröder; Pure Appl. Chem., 1988, 60, 517.

74. A. Muller and E. Dieman; in "Comprehensive Co-ordination Chemistry", Eds. G. Wilkinson, R.D. Gillard and J.A. McCleverty. Vol. 2, p551-558. Pergamon Press, Oxford, 1987.

75. J. Buter and R.M. Kellogg; J. Chem. Soc., Chem. Comm., 1980 , 466.

76. J. Buter and R.M. Kellogg; J. Org. Chem., 1981, 46, 4481.

77. D.P. Riley and J.D. Oliver; Inorg. Chem., 1983, 22, 3361.

78. R.E. Wolf, J.R. Hartman, J.M.E. Storey, B.M. Foxman and S.R. Cooper; J. Amer. Chem. Soc., 1987, 109, 4328 and references therein.

79. D. Gerber, P.Chongsawangvirod, A.K. Leung and L.A. Ochrymowycz; J. Org. Chem., 1977, 42, 2644.

80. D. Sellmann, L. Zapf, J. Keller and M. Moll; J Organomet. Chem., 1985, 289, 57.

81. P.J. Blower and S.R. Cooper; Inorg. Chem., 1987, 26, 2099.

82. M. Halcrow; Ph.D. Thesis, Edinburgh, 1991.

83. M.N. Bell, A.J. Blake, H-J. KÜppers, M. Schröder and K. Wieghardt; Angew. Chem., 1987, 99, 253, Angew Chem. Int. Ed. Engl., 1987, 26, 250.

84. S.C. Rawle and S.R. Cooper, J. Chem. Soc., Chem. Comm., 1987, 308.

85. S.C. Rawle, J.R. Hartman, D.J. Watkins and S.R. Cooper; J. Chem. Soc., Chem. Comm., 1986, 1083.

86. A.J. Blake, R.O. Gould, A.J. Holder, T.I. Hyde and M. Schröder; J. Chem. Soc., Dalton Transc., 1988, 1861.

87. S.C. Rawle, R. Yagabasan, K. Prout and S.R. Cooper; J. Amer. Chem. Soc., 1987, 109, 6181.

88. W.N. Setzer, C.A. Ogle, G.S. Wilson and R.S. Glass; Inorg. Chem., 1983, 22, 266.

89. R.E. DeSimone and T.M. Tighe; J. Inorg. Nucl. Chem., 1976, 38, 1623.

90. A.J. Blake, R.O. Gould, A.J. Holder, T.I. Hyde, M.O. Odulate, A.J. Lavery and M. Schröder; J. Chem. Soc., Chem. Comm., 1987, 118.

91. H-J. KÜppers, K. Wieghardt, Y-H. Tsay, C. KrÜger, B. Nuber and J.Weiss; Angew. Chem., 1987, 99, 583; Angew Chem. Int. Ed. Engl., 1987, 26, 575.

92. A.J. Blake, A.J. Holder, T.I. Hyde, G. Reid and M. Schröder; J. Chem. Soc., Dalton Trans., submitted.

93. A.J. Blake, A.J. Holder, T.I. Hyde, Y.V. Roberts, A.J. Lavery and M. Schröder; J. Organomet. Chem., 1987, 323, 261.

94. K. Wieghardt, H-J. K üppers, E. Raade and C. KrÜger; Angew. Chem; 1986, 98, 1136; Angew Chem. Int. Ed. Engl. 1986, 25, 1101.

95. A.J. Blake, A.J. Holder, T.I. Hyde and M. SchrÖder; J. Chem. Soc., Chem. Comm., 1987, 987.

96. Y.V. Roberts; Ph.D. Thesis, Edinburgh, 1991.

97. J.A. Greig; Ph.D. Thesis, Edinburgh, 1991.

98. T.I. Hyde; unpublished results.

99. G.H. Robinson and S.A. Sangokoya; J. Amer. Chem. Soc., 1988, 110, 1494.

100. T-F. Lai and C-K. Poon; J. Chem. Soc., Dalton Trans. 1982, 1465.

101. P.H. Davis, P.L. White and R.L. Bedford; Inorg, Chem., 1975, 14, 1753.

102. R.E.DeSimone and M.D. Glick; J. Amer. Chem. Soc., 1976, 98, 762.

103. A.J. Blake, G. Reid and M. Schröder; J. Chem. Soc., Dalton Trans., 1989, 1675.

104. A.J. Blake, A.J. Holder, T.I. Hyde and M. Schröder; unpublished results.

105. A.J. Blake, A.J. Holder, T.I. Hyde and M. Schröder; unpublished results.

106. G. Reid, unpublished results.

107. A.J. Blake, R.O. Gould, G. Reid and M. Schröder; J. Chem. Soc., Chem. Comm., 1990, 974.

108. P.W.R. Corfield, C.Ceccarelli, M.D. Glick, I. N-Y Moy, L.A. Ochrymowycz and D.B.Rorabacher; J. Amer. Chem. Soc., 1985, 107, 2399.

109. E.R. Dockal, T.E. Jones, W.F. Sokol, R.J. Engerer and D.B. Rorabacher; J. Amer. Chem. Soc., 1976, 98, 4322.

110. D.B. Rorabacher, M.M. Bernado, A.M.Q., Vande Linde, G.H. Leggett, C.B. Westerby, M.J. Martin and L.A. Ochrymowycz; Pure Appl. Chem., 1988, 60, 501.

111. M. Bell, A.J. Blake, A.J. Holder, T.I. Hyde and M. Schröder; J. Chem. Soc., Dalton Trans., 1990, 3841.

112. S.R. Cooper, S.C. Rawle, J.R. Hartman, E.J. Hintsa and G.A. Admans; Inorg. Chem., 1988, 27, 1209.

113. E.J. Hintsa, J.R. Hartman and S.R. Cooper; J. Amer. Chem. Soc., 1983, 105, 3738.

114. A.J. Blake, A.J. Holder, T.I. Hyde and M. Schröder; J. Chem.Soc., Chem. Comm., 1987, 987.

115. A.J. Blake, R.O. Gould, A.J. Holder and M. Schröder; unpublished results.

116. A.J. Blake, R.O. Gould, A.J. Lavery and M. Schröder; Angew. Chem., 1986, 98, 282; Angew. Chem. Int. Ed. Engl., 1986, 25, 274.

117. J.R. Hartman and S.R. Cooper; J. Amer. Chem. Soc., 1986, 108, 1202.

118. J.R. Hartman, E.J. Hintsa and S.R. Cooper; J. Amer. Chem. Soc., 1984, 386.

119. J.R. Hartman, E.J. Hintsa and S.R. Cooper; J. Amer. Chem. Soc., 1986, 108, 1208.

120. A.J. Blake, R.O. Gould, A.J. Holder, T.I. Hyde and M. Schröder; Polyhedron, 1989, 8, 513.

121. R.O. Gould, A.J. Lavery and M. Schröder; J. Chem. Soc., Chem. Comm., 1985, 1492.

122. M.N. Bell, A.J. Blake, M. Schröder and T.A.Stephenson; J. Chem. Soc., Chem. Comm., 1986, 471.

123. J.S. Bradshaw, J.Y. Hui, B.L. Haymore, R.M. Izatt, and J.J. Christensen; J. Heterocycl. Chem., 1974, 11, 45.

124. A.C. Braithwiate, C.E.F. Rickard and T.N. Waters; Aust. J. Chem., 1981, 34, 2665.

125. K. Travis and D.H. Busch; J. Chem. Soc., Chem. Comm., 1970, 1041.

126. K. Saito, Y. Masudo and E. Sekido; Anal. Chim. Acta, 1983, 151, 447.

127. D. Sevidic and H. Meider; J. Inorg. Nucl. Chem., 1977, 39, 1403.

128. F.A. Cotton and G. Wilkinson (Eds) "Advanced Inorganic Chemistry", Chpt. 19, p948-954.

129. R.J. Puddephatt, "The Chemistry of Gold", Elsevier, Amsterdam, 1978.

130. H. Schmidbaur and K.C. Dash; Adv. Inorg. Chem. Radiochem., 1982, 25, 239.

131. R.J. Puddephatt in "Comprehensive Co-ordination Chemistry", ed. G. Wilkinson, R.D. Gilland and J.A, McCleverty Pergamon, Oxford, 1987, Vol 5, Chpt 55

132. P.G. Jones, Gold. Bull., 1981, 14, 102; 1981 14, 159; 1983, 16, 114.

133. "Bio-organic Chemistry of Gold Co-ordination Compounds " ed. B.M.Sutton and R.G. Franz, Smith Kline and French, Philadelphia, 1983.

134. D.H. Brown and W.E. Smith; Chem. Soc. Rev., 1980, 9, 217.

135. P.J. Sadler; Adv. Inorg. Chem., 1991, 36, 1.

136. B. Armev and H.Schmidbaur; Angew. Chem. Int. Ed. Engl., 1970, 9, 101.

137. R.J. Puddephatt in "Comprehensive Organometallic Chemistry" ed., G. Wilkinson, F.G. A. Stone and E.N. Abel, Pergamon, 1982, Chpt 15.

138 a) P. Pyykkö and J.P.Desdaux; Acc. Chem. Res., 1979, 12, 276.

b) P. Pyykkö, Chem. Rev., 1988, 88, 563.

c) K.S. Pitzer, Acc. Chem. Res., 1979, 12, 271.

139. L.E. Orgel; J. Chem. Soc., 1958, 4186.

140. H. Basch and H.B. Gray; Inorg. Chem., 1967, 6, 365.

141. W.R. Mason and H.B. Gray; J. Amer. Chem Soc., 1968, 90, 5721.

142. D.H. Brown and W.E. Smith; J. Chem. Soc., Dalton Trans., 1976, 848.

143. R. Roulet, N.Q. Lan, W.R. Mason and G.P. Fenske; Helv. Chim. Acta., 1973, 56, 2405.

144. D.I. Nicholas and S.A.Charleson; J. Chem. Soc. A., 1969, 2581.

145. J.G. Wijnhoven, W.P.J.H. Bosman and P.T. Beurskens; J. Cryst. Mol. Struct., 1972, 2, 7.

146. N.W. Alcock, P. Moore, P.A. Lampe and K.F. Mok; J. Chem. Soc., Dalton Trans., 1982, 207.

147. J.M. Meyer and A.L. Allred; J. Inorg. Nucl. Chem., 1968, 30, 1328.

148. A.D. Westland; Can. J. Chem., 1969, 47, 4135.

149. J.W. Collier, A.R.Fox, I.G. Hinton and F.G. Mann; J. Chem. Soc., 1964, 1819.

150. G.P. Fenske and W.R. Mason; Inorg. Chem., 1974, 13, 1783.

151. M. Khan, C. Oldham and D.G. Tuck; Can. J. Chem., 1981, 59, 2714.

152. P.G. Jones, G.M. Sheldrick, J.A. Muir, M.M. Muir and L.B. Pulgar; J. Chem. Soc., Dalton Trans., 1982, 2123.

153. L.J. Guggenberger, J. Organmet. Chem., 1974. 81, 271.

154. F. Klanberg, E.L. Muetterties and L.G. Guggenberger, Inorg. Chem., 1968, 7, 2272.

155. P.G. Jones, Acta. Cryst., Sect. B, 1980, 36, 3105.

156 a) R. Usón, A. Laguna, and J. Vicente; J. Organomet. Chem., 1977, 131, 491.

b) R. Usón, A. Laguna, M. Laguna and E. Fernandez; J. Chem. Soc., Dalton Trans., 1982, 1971.

c) R. Usón, A. Laguna, M. Laguna and A. Usón; Inorg. Chim. Acta., 1983, 73, 63.

d) R. Usón, A. Laguna, J. Vicente, J. Garcia, P.G. Jones and G.M. Sheldrick; J. Chem. Soc., Dalton Trans., 1981, 655.

157. R. Usón, A. Laguna, M. Laguna and A. Usón; Inorg. Chim. Acta., 1983, 73, 63.

158. R. Usón, A. Laguna and B. Bergareche; J. Organomet. Chem., 1979, 184, 411.

159. R. Usón, A. Laguna, A. Navarro, R.V. Parish and L.S. Moore; Inorg. Chim. Acta., 1986, 112, 205.

160. W. Ludwig and W. Meyer; Helv. Chim. Acta, 1982, 65, 934.

161. R. Usón, A. Laguna And J. Vicente; J. Organomet. Chem., 1976, 104, 401.

162. H. Schmidbaur and F.E. Wagner; Chem. Ber., 1979, 112, 496.

163. H. Schmidbaur and A.A.M. Aly; Angew Chem., 1980, 92, 66.

164. H. Schmidbaur and J.R. Mandl; Angew. Chem., Int. Engl., 1977, 16, 640.

165. C.E. Briant, K.P. Hall and D.M.P. Mingos; J. Organomet. Chem., 1982, 229, C5.

166. W.S. Crane and H. Beall; Inorg. Chim. Acta., 1978, 31, L469.

167. E.S. Clark, D.H. Templeton and C.H. MacGillavry; Acta. Cryst., 1958 11, 284.

168. S. Yamada and K. Yamanouchi; Bull. Chem. Soc. Jpn., 1970, 43, 1744.

169. W.T. Robinson and E. Sinn; J. Chem. Soc., Dalton Trans., 1975, 726.

170. R.J. Charlton, C.M. Harris, H. Patil and N.C. Stephenson; Inorg. Nucl. Chem. Lett., 1966, 2, 409.

171. R.Usón, J. Vicente, M.T. Chicote, P.G. Jones and G.M. Sheldrick; J. Chem. Soc., Dalton Trans., 1983, 1131.

172. N.F. Borkett and M.I. Bruce; Inorg. Chim. Acta., 1975, 12, L33.

173. A.J. Canty, N.J. Minchin, J.M. Patrick and A.H. White; Aust. J. Chem., 1983, 36, 1107.

174. B.T. Heaton and R.J. Kelsey; Inorg. Nucl. Chem. Lett., 1975, 11, 363.

175. A.L. Hormann, C.F. Shaw, D.W. Bennett and W.M. Reiff; Inorg. Chem., 1986, 25, 3953.

176. C.A. McAuliffe, R.V. Parish and P.D. Randall; J. Chem. Soc., Dalton Trans., 1979, 1730.

177 K.C. Dash and H. Schmidbaur; Chem. Ber., 1973. 106, 221.

178. A.R. Latham, V.C. Mascall and H.B. Gray; Inorg. Chem., 1965, 4, 788.

179. J.H. Enermark and J.A. Ibers; Inorg. Chem., 1975, 14, 2556.

180. P.T. Beurskens, H.J.A. Blaauw, J.A. Cras and J.J. Steggerda; Inorg. Chem., 1968, 7, 805.

181. H.J.A. Blaauw, R.J.F. Nivard and G.J. M. van der Ker; J. Organomet. Chem., 1964, 2 236.

182. M. Weishaupt and J. Straehle; Z. Naturforsch., Teil, B, 1976, 31, 554.

183. C.S. Gibson and W.M. Colles; J. Chem. Soc., 1931, 2407.

184. G. Nardin, L.Randaccio, G. Annibale, G. Natile and B. Pitten; J. Chem. Soc., Dalton Trans., 1980, 220.

185. R. Timkovich and A. Tulinsky; Inorg. Chem., 1977, 16, 962.

186. P. Bamfield and P.A. Mack; J. Chem. Soc. (C), 1968, 1961.

187 a) J.H. Kim and G.W. Everett, Jr.; Inorg. Chem., 1979, 18, 3145.

b) E. Kimura and Y. Kurogi; International Macrocyclic Symposium, Sheffield, 1991.

188. J.H. Kim and G.W. Everett, Jr.; Inorg. Chem., 1981, 20, 853.

189. D.B. Dell'Amico, F. Calderazzo, F. Marchetti and S. Mertino; J. Chem. Soc., Dalton Trans., 1982, 2257.

190. J.P. Fackler, Jr., B. Trzcinska-Bancroft; Organomet., 1985, 4, 1891.

191. J.D. Basil, M.H. Murray, J.P. Fackler, Jr., J. Tocher, A.M. Mazany, B. Trzcinska-Bancroft, H. Knachel, D.Dudis, T.J. Delford and D.O. Marler; J. Amer. Chem Soc., 1985, 107, 6908.

192. H. Schmidbaur, C. Hartmann, J. Riede, B. Huber and G. MÜller; Organomet., 1986, 5,, 1652.

193 a) H. Schmidbaur; Acc. Chem. Res., 1975, 8, 62.

b) H. Schmidbaur and P. Jandik; Inorg.,Chim. Acta., 1983, 74, 97.

c) H. Schmidbaur and R. Franke; Inorg. Chim. Acta., 1975, 13, 79.

d) H.M. Murray, J.P. Fackler, L.C. Porter and A.M. Mazany; J. Chem. Soc., Chem. Comm., 1986, 321.

194. J.P. Fackler and L.C. Porter; J. Amer. Chem. Soc., 1986, 108, 2750.

195. M.A. Bennett, S.K. Bhargava, K.D. Griffiths and G.B. Robertson; Angew. Chem., Int., Ed. Engl., 1987, 26, 260.

196. C. King, D.D. Heinrich, G. Garzon, J-C. Wang and J.P. Fackler, Jr.; J. Amer. Chem Soc., 1989, 111, 2300.

197. H. Schmidbaur, A. Wohlleben, F.E. Wagner, D.F. van de Vandel and G.P. van der Kelen; Chem. Ber., 1977, 110, 2758.

198. T. Vanngard and S. Akerström; Nature (London), 1959, 184, 183.

199. T.J. Bergendahl and E.M. Bergendahl; Inorg. Chem., 1972, 11, 638.

200. J.H. Waters and H.B. Gray; J. Amer. Chem Soc., 1965, 87, 3334.

201. J.H. Waters, T.J. Bergendahl and S.R. Lewis; J. Chem. Soc., Chem. Comm., 1971, 834.

202. R.L. Schlupp and A.H. Maki; Inorg. Chem., 1974, 13, 44.

203. J.G.M. van Rens and E. de Boer; Mol. Phys., 1970, 19, 745.

204. J.G.M. van Rens, M.P.A. Viegels and E. de Boer; Chem. Phys. Lett., 1974, 28, 104.

205. A. MacCragh,and W.S. Koski; J. Amer. Chem. Soc., 1965, 87, 2496.

206. L.F. Warren and M.F. Hawthorne; J. Amer. Chem Soc., 1968, 90, 4823.

207. A.P. Koley, S. Purohit, S. Ghosh, L.S. Praad and P.T. Manoharan, J. Chem. Soc., Dalton Trans., 1988, 2607.

208. L. Malatesta; Gold. Bull., 1975, 8, 48.

209. G. Schmid, R. Pfeil, R. Boese, F. Bandermann, S. Meyer, G.M.M. Calis and J.W.A. van der Velden, Chem., Ber., 1981, 114, 3634.

210. G.K. Anderson, Adv. Organomet. Chem., 1982, 20, 39.

211. A.A. Islab and P.J. Sadler, J. Chem. Soc., Dalton Trans., 1981, 1657.

212. C.K. Mirabelli, C-M. Sung., J.P. Zimmermen, D.T. Hill, S. Mong and S.T. Crooke; Biochem. Pharm. 1986, 35, 1427.

213. C.K. Mirabelli, J.P. Zimmerman, H.R. Bartus, C-M. Sung and S.T. Cooke; Biochem. Pharm., 1986, 35, 1435.

214. C.E. Blank and J.C. Dabrowiak; J. Inorg. Biochem., 1985, 21, 21.

215. H.S. Allavdeen, R.M. Snyder, M.H. Whitman and S.T. Cooke, Biochem. Pharm., 1985, 34, 3243.

216. T.M. Simon, D.H. Kumshima, D.H. Vibert and A. Lorder, Cancer Res., 1981, 41, 94.

217. A.J. Blake, R.O. Gould, J.A. Greig, A.J. Holder, T.I. Hyde and M. Schröder; J. Chem. Soc., Chem. Comm., 1989, 876.

218. A.J. Blake, J.A. Greig, A.J. Holder, T.I. Hyde, A. Taylor and M. Schröder; Angew. Chem., Int. Ed.Engl., 1990, 29, 197.

219. J. Clarkson, R. Yagabasan, P.J. Blower, S.C. Rawle and S.R. Cooper, J. Chem. Soc., Chem. Comm., 1987, 950.

220. M. Melnik and R.C. Parish;; Coord. Chem. Rev., 1986, 70, 157.

221. R.J. Lancashire, in "Comprehensive Co-ordination Chemistry" eds G. Wilkinson, R.O. Gillard and J.A. McCleverty,

222. R.S. Nicholson, Anal. Chem., 1965, 37 (11), 1351.

223. W.E. Geiger, Prog. Inorg. Chem., 1985, 33, 275.

224. R.V. Parish, Personal communication.

225. R.D. Feltham & R.G. Hayter, J. Chem. Soc., 1964, 4587.

226. D. Collison, Personal communication.

227. D. Parker, P.S. Roy, G. Ferguson and M.M. Hunt; Inorg. Chim. Acta., 1989, 155, 277.

228. A.J. Holder, Personal communication.

229. A.J. Blake, A.J. Holder, T.I. Hyde, H-J. KÜppers, M. Schröder, S. Stötzel and K. Wieghardt, J. Chem. Soc., Chem. Comm., 1989, 1600.

230. D. St. C. Black and I.A. McLean; J. Chem. Soc., Chem. Comm., 1968, 1024, Tetra. Lett., 1969, 3961; Aust. J. Chem., 1971, 24, 1401.

231. B. Dietrich, J-M. Lehn and J.P. Sauvage; J. Chem. Soc., Chem. Comm., 1970, 1055.

232. M.L. Ammon, K. Chandrasekhar, S.K. Bhattacharjee, S. Shirkai, and Y. Honda; Acta. Cryst. Sect. C, 1984, 40, 2061.

233. G. Reid and M. Schröder; Chem. Soc. Rev., 1990, 19, 239.

234. N. Atkinson, A.J. Blake, M.G.B. Drew, G. Forsyth, A.J. Lavery, G. Reid and M. Schröder: J. Chem. Soc., Chem. Comm., 1989, 984.

235. A.J. Blake, G. Reid and M. Schröder; J. Chem. Soc., Dalton Trans., 1991, 615.

236. A.J. Blake, G. Reid and M. Schröder; J. Chem. Soc., Dalton Trans., 1991, 3363; J. Chem. Soc., Chem. Comm., 1988, 1397.

237. L. Fabbrizzi and D.M. Prosperio; J. Chem. Soc., Dalton Trans., 1989, 229.

238. A.S. Craig, R. Kataky, D. Parker, H. Adams, N. Bailey and H. Schneider; J. Chem. Soc., Chem. Comm., 1989, 1870.

239. Y. Agnus, R. Louis and R. Weiss, J. Amer. Chem. Soc., 1979, 101, 3381.

240. L.F. Lindoy and D.H. Busch, J. Chem. Soc., Chem. Comm., 1968, 1598.

241. D. Parker J-M. Lehn and J. Rimmer, J. Chem. Soc., Dalton Trans., 1985, 1517; G. Ferguson, K.E. Matthews and D. Parker, J. Chem. Soc., Chem. Comm., 1987, 1350

242. J-M. Lehn; Pure Appl. Chem., 1980, 32, 2441.

243. J-M. Lehn, J. Simon and J. Wagner; Angew Chem., Int. Ed. Engl., 1973, 12, 578, 579.

244. J-M. Lehn; Acc. Chem. Res., 1978, 11, 49.

245 a) J. Cheney, J-M. Lehn, J.P. Sauvage and M.E. Stubbs; J. Chem. Soc., Chem. Comm., 1972, 1100.

b) J-M. Lehn and J. Simon; Helv. Chim. Acta., 1977, 60, 141.

246. A.H. Albert, R. Annunziata and J-M. Lehn; J. Amer. Chem. Soc., 1977, 99, 8502.

247. O. Kahn, I. Morgenstein-Badarau, J.P. Andiere, J-M. Lehn and S.A. Sullivan; J. Amer. Chem. Soc., 1980, 102, 5936.

248. R. Louis, Y. Agnus and R. Weiss; J. Amer. Chem. Soc., 1978, 100, 3604.

249. J-M Lehn and M.E. Stubbs; J. Amer. Chem. Soc., 1974, 96 4011.

250. A.H.Alberts, J-M. Lehn and D. Parker; J. Chem. Soc., Dalton Trans., 1985, 2311.

251. G. Reid, unpublished results

252. P.D. Beer, J.E. Nation, S.L.W. McWhinnie, M.E. Harman, M.B. Hursthouse, M.I. Ogden and A.H. White; J. Chem. Soc., Dalton Trans., 1991, 2485.

253. J-M. Lehn, personal communication,

254. J. Sutherland, personal communication. 10th International Macrocyclic Symposium, Hamburg, 1988.

255. H. Sigel, (Ed), 'Metal ions in Biological Systems', Marcel Dekker, 1981, New York, Vol. 13, "Copper Proteins".

256. K.D. Karlin and J. Zubieta, (Eds.), 'Copper Co-ordination Chemistry', Vols 1 and 2, Adenine Press, Guilderland New York, 1982, 1984.

257. E.I. Solomon, K.W. Penfield and D. Wilcox, Structure and Bonding (Berlin), 1983, 53, 1.

258. K.M. Kadish, (Ed.), "Electrochemical and Spectrochemical Studies of Biological Redox Components"; Advances in Chemistry Series, 201 Washington, 1982.

259. A.G. Skyes, Chem. Soc. Rev., 1985, 14, 283.

260. J.McGinnis, W.J. Ingledew and A.G. Skyes, Inorg. Chem., 1986, 25, 3730.

261. D.F. Blair, G.W.Campbell, J.R. Schoonover, S.I. Chan, H.B. Gray, B.G. Malmstrom, I. Pecht, B.I. Swanson, W.H. Woodruff, W.K. Cho, A.M. English, H.A. Fry, V. Hum, K.A. Norton, J. Amer. Chem. Soc., 1985, 107, 5755.

262. K.W. Penfield, A.A. Gewirth and E.I. Solomon, J. Amer. Chem. Soc., 1985, 107, 4519.

263. T.N. Sorrell and M.L. Garrity, Inorg. Chem., 1991, 30, 210.

264. A.C. Vansteenberger, E. Bounman, R. deGraaff, W.L. Driessen and J. Reedijk and P. Zarello, J. Chem. Soc., Dalton Trans., 1990, 3175.

265. S. Knapp, T.P. Keenan, X. Zhang, R. Fihar, J.A. Potenza and H.J. Schugar. J. Amer. Chem. Soc., 1990, 112, 3452.

266. W.B. Tolman, R.L. Rardin and S.J. Lippard, J. Amer. Chem. Soc., 1989, 111, 4532.

267. P.R. Coughlin and S.J. Lippard, J. Amer. Chem. Soc., 1981,103, 3228.

268. K.D. Karlin and J. Zubieta, (Eds.), 'Copper Co-ordination Chemistry: Biochemical and Inorganic Perspectives'. Adenine Press, Guilderland, New York, 1983.

269. D E Fenton, Advances in Inorganic and Bioinorganic Mechanisms (Edited by A.G. Skyes) Academic Press, London, 1983, p187.

270. D.E. Fenton, Pure Appl. Chem., 1989, 61, 903.

271. R.R. Gagné, R.P. Kreh and J.A. Dodge, J. Amer. Chem. Soc., 1979, 101, 6917,

272. D.E. Fenton and R.L. Lintvedt, J. Amer. Chem. Soc., 1978, 100, 6367.

273. J.E. Bulkowski, P.L. Burk, M.F. Lundman and J.A. Osborn, J. Chem. Soc., Chem. Comm., 1977, 498.

274. M.G. Simmons and L.J. Wilson, J. Chem. Soc., Chem. Comm., 1978, 634.

275. M.G.B. Drew, S.M. Nelson and J. Readijk, Inorg. Chim. Acta., 1981, 54, L161.

276. R.R. Gagné, C.L. Spiro, T.J. Smith, C.A. Hamann, W.R. Thies and A.K. Shienke, J. Amer. Chem. Soc., 1981, 103, 4073.

277. M. Fernanda Cabral, J. Cabral, J. Trocha-Grimshaw, K.P, McKillop,, S.M. Nelson and J. Nelson, J. Chem. Soc., Dalton Trans., 1989, 1351.

278. K.D. Karlin, R.W. Cruse, Y. Gultneh, J.C. Hayes and J. Zubieta, J. Amer. Chem. Soc., 1984, 106, 3372.

279. S.M. Nelson, F. Esho, A. Lavevy and M.G.B. Drew, J. Amer. Chem. Soc., 1977, 99, 6730.

280. U. Sakaguchie and A.W. Addison, J. Amer. Chem. Soc., 1977 99, 5189.

281. H. Yokoi and A.W. Addison, Inorg. Chem., 1977, 16, 1341.

282. J. Peeling, B.G. Haslett, I.M. Evans, D.T. Clark and D. Boulter, J. Amer. Chem. Soc., 1977, 99, 1025.

283. J.V. Dagdigian, V. McKee and C.A. Reed, Inorg. Chem., 1982, 21, 1332.

284. M.A. Augustin, J.K. Yandell, A.W. Addison and K.D. Karlin, Inorg. Chim. Acta., 1981, 55, L35.

285. G. Kolks and S.J. Lippard, J. Amer. Chem. Soc., 1977, 99, 5804.

286. W.P.J. Gaykema, W.G.J. Mol, J.M. Vereijken, N.M. Soeter, H.J. Bak and J.J. Beintema, Nature, 1984, 309, 23.

287. N.C. Eickman, R.S. Himmelwright and E.I. Solomon, Proc. Natl. Acad. Sci. USA, 1979, 76, 2094.

288. J.E. Fee, Structure and Bonding, 1975, 23, 1.

289. S.H. Laurie and E.S. Mohammed, Co-ord. Chem. Rev., 1980, 38, 279.

290. P.M. Colman, H.C. Freeman, J.M. Guss, M. Murata, V.A. Morris, J.A.M. Ramshaw and M.P. Venkatappa, Nature, 1978, 272, 319.

291. E.L.Sabbam, L.A. Greene and M. Goldstein, J. Biol. Chem., 1983, 258, 7812.

292. T.E. Jones, D.B. Rorabacher and L.A. Ochrymowycz, J. Amer. Chem. Soc., 1975, 97, 7485.

293. T.E. Jones, L.L. Zimmer, L.L. Diadario, D.B. Rorabacher and L.A. Ochrymowycz, Inorg. Chem. 1975, 14, 7163.

294. N.S. Ferris, W.H. Woodruff, D.B. Rorabacher, T.E.Jones and L.A. Ochrymowycz, J. Amer. Chem. Soc., 1978, 100, 5939.

295. L.L. Diaddario, L.L. Zimmer, T.E. Jones, K. L.S.W.L. Sokol, R.B. Cruz, E.L.Yee, L.A. Ochrymowycz and D.B. Rorabacher. J. Amer. Chem. Soc., 1979, 101, 3511.

296. L.L. Diaddario, E.R. Pockal. M.D. Glick, L.A. Ochrymowycz and D.B. Rorabacher, Inorg. Chem. 1985, 24, 356.

297. I.R. Young, L.A. Ochrymowycz and D.B. Rorabacher, Inorg. Chem., 1986, 25, 2576.

298. V.B. Pett, G.H. Leggett, T.H. Cooper, P.R. Reed, D. Situmeang, L.A.Ochrymowycz and D.B. Rorabacher, Inorg. Chem. 1988, 27, 2164.

299. M.D. Glick, D.P. Gavel, L.L. Diadario and D.B. Rorabacher, Inorg. Chem., 1976, 15, 1190.

300. B.V. Gorewit and W.K. Murker, J. Co-ord. Chem., 1976, 5, 67.

301. C.M. Lucas, L. Shuang, M.J. Newlands, J-P. Charland and E.J. Gabe, Can. J. Chem. 1988, 66, 1506.

302. C.M. Lucas, L. Shuang, M.J. Newlands, J-P. Charland and E.J. Gabe, Can. J. Chem. 1989, 67, 639.

303. K. Wieghardt, H-J Küppersand J. Weiss, Inorg. Chem. 1985, 24, 3967.

304. J. Clarkson, R. Yaghason, P.J. Blower, S.C. Rawle and S.R. Cooper, J. Chem. Soc., Chem. Comm. 1987, 950.

305. S.M. Nelson, Pure Appl. Chem. 1980, 52, 2461.

306. D. Devdic, L. K. Fekete and H. Meider, J. Inorg. Nucl. Chem. 1980, 42, 885.

307. W. Clegg, Acta Cryst., 1981, A37, 22.

308. N. Walker and D. Stuart, DIFABS, Program for Empirical Absorption Correction, Acta Cryst., 1983, A39, 158.

309. G.M. Sheldrick, SHELX 76, Program for Crystal Structure Refinement. University of Cambridge, UK., 1976.

310. J. Cosier and A.M. Glazer; J. Appl. Cryst., 1986, 19, 105.

311. D.T. Cromer and J.L. Mann; Acta. Cryst., 1968, A24, 321.

312. R.O. Gould and P. Taylor, CALC, Program for Molecular Geometry Calculations. University of Edinburgh, UK., 1985.

313. P.D. Mallinson and K.W. Muir, ORTEP II, Interactive Science Version, J. Appl. Cryst., 1985, 18, 51.

314. H-J. Küppers, K. Wieghardt, B. Nuber, J.Weiss, E. Bill and A.X. Tranthwein; Inorg. Chem., 1987, 26, 3762.

315. A.J.Blake and M. Sullivan and M. Schröder, unpublished results.

316. L. Pauling, "The Nature of the Chemical Bond", 3rd. Ed. p260, Cornell University Press, Ithaca, New York, 1960.

317. W.N. Setzer, B.R. Coleman, G.S. Wilson and R.S. Glass; Tetrahedron, 1981, 37, 2743.

318. R. Blom, D.W.H. Rankin, H.E. Robertson, M. Schröder and A. Taylor; J. Chem. Soc., Perkin Trans.2., 1991, 773.

319. D.M. Roush, E,.M. Price, L.K. Templeton, D.H. Templeton and C.H. Heathcock; J. Amer. Chem. Soc., 1979, 101, 2971.

320. R.J. Smith, G.D. Adams, A.P. Richardson, H-J. KÜppers and P.J. Blower, J. Chem. Soc., Chem. Comm., 1991, 475.

321. N. Furukawa, A. Kawada and T. Kawai: J. Chem. Soc., Chem. Comm., 1984, 1151.

322. B.C. Gilbert, D.K.C. Hodgeman and R.O.C. Norman, J. Chem. Soc., Perkin Trans. 2., 1973, 1748.

323. M. Boniface, H. Möckel, D. Bahnemann and K-D. Asmus: J. Chem. Soc., Perkin Trans. 2., 1975, 675.

324. R.S. Glass, M. Hojjatie, A. Petsom, G.S. Wilson, M. Göbl, S. Mahling and K-D. Asmus; Phosphorus and Sulphur, 1985, 23, 143.

325. T. Kataska, K. Tsutsumi, T. Iwama, H. Shimizu and M. Hori; Tetra Letts., 1990, 31, 3027.

326. R.J. Batchelor, F.W.B. Einstein, I.D. Gray. J-H. Gu, B.M. Pinto and X-M.Zhou; J. Amer. Chem. Soc., 1990, 112, 3706.

327. H. Fiyihara, R. Akaishi and N. Furukawa; J. Chem. Soc., Chem. Comm., 1987, 930.

328. K-D. Asmus; Acc. Chem. Res., 1979, 12, 436.

329. W.K. Musker; Acc. Chem. Res., 1980, 13, 200.

330. W.K. Musker, T.L. Wolford and P.B. Rousch; J. Amer. Chem. Soc., 1978, 100, 6416.

331. W.K. Musker and P.B. Rousch; J. Amer. Chem. Soc., 1976, 98, 6745.

332. W.K. Musker and T.L. Wolford; J. Amer. Chem. Soc., 1976, 98, 3055.

333. T.D. Smith and J.R. Pilbrow; Coord. Chem. Rev., 1974, 13,173.

334. E.R. Dockal, L.L. Diaddario, M.D.Glick and D.B. Rorabacher; J. Amer. Chem. Soc., 1976, 98, 4322.

335. D. Serdic, L. Fekerte and H. Meider; J. Inorg. Nucl. Chem., 1980, 42, 885.

336. G.M. Sheldrick; SHELX86, Program for crystal solution, University of Göttingen, F.R.G., 1986.

337. M.D. Bell, Ph.D. thesis, University of Edinburgh, 1987

338. N. Taylor, Condecon 510: convolution techniques and studies of reaction mechanisms, University of Leeds.

APPENDIX

MATERIALS AND METHODS

All solvents were purified according to standard procedures. HPLC grade MeCN (Aldrich), spectroscopic grade Me_2CO (Fisons) and HPLC grade CH_2Cl_2 (Fisons) were used in the electrochemical experiments. Tetrahydrothiophene (tht) (Aldrich) was used without further purification. $HAuCl_4$, $KAuCl_4$ and $PdCl_2$ (Johnson Matthey plc) were all used as supplied. All thioether ligands: [9]aneS_3, [12]aneS_4, [14]aneS_4, [16]aneS_4, [15]aneS_5, [18]aneS_6, [24]aneS_8 and [28]aneS_8 (Aldrich) were all used without further purification. [18]aneN_2S_4 (Lancaster Synthesis) was used as supplied. The methylated analogue was prepared by the method described by Reid.[24] Tetrabutylammonium hexafluorophosphate ($^nBu_4NPF_6$) was prepared by neutralisation of 40% $^nBu_4NOH$ (Aldrich) with 60% HPF_6 (Strem) and recrystallisation from hot MeOH. Nucleophilic reagents MeLi, BuLi, and n-Selectide (Aldrich) were used as supplied, as was trityl hexafluorophosphate ($PhC^+PF_6^-$).

Infra-red spectra (4000-200 cm^{-1}) were recorded on a Perkin-Elmer 548 spectrometer as KBr discs or Nujol mulls. Fast atom bombardment (f.a.b.) mass spectra were executed by a Kratos MS 50TC spectrometer using 3-NOBA matrix. Electronic absorption spectra were run on a Perkin-Elmer Lamda-9 UV/Vis/NIR spectrophotometer using quartz cells. ^1H n.m.r. spectra were measured on Bruker WP80 and Brucker WP200 instruments operating at 80.13 MHz and 200.13 MHz respectively. ^{13}C and ^{13}C (DEPT) n.m.r. spectra were run on a Brucker WP200 machine at 50.32 MHz. X-band e.p.r. measurements were recorded using a Brucker ER-200D spectrometer using 100KHz field modulation. A quartz flat cell was employed for the

solution samples, frozen glass samples were taken using quartz tubes (4mm O.D., 3mm I.D.) and powder samples held in Q- band tubes.

Electrochemical measurements were carried out on a Brucker 310 Universal Modular Polarograph using a three electrode system in stated solvent with (0.1 M or 0.4 M) $^{n}Bu_4NPF_6$ as supporting electrolyte. Platinum button microelectrodes were utilised as working and auxiliary electrodes, Ag/AgCl was used as the reference electrode. All quoted potentials are versus ferrocene which is oxidised at +0.43 - +0.45 V versus Ag/AgCl. A three compartment cell together with a three electrode system (Pt basket and Pt gauze as working and auxiliary electrodes) were used for coulometry and electrolysis experiments. Slow scan cyclic voltammetric measurements made for the kinetic studies were recorded on a EG & G Princeton Applied Research Potentiostat Model 273 interfaced with an IBM computer using the Condecon 510 programme;[338] the temperature was controlled using a Haake F3 temperature controller and a Haake Q bath. Diffusion coefficients were determined by use of the ring-rotating disc electrode.

Spectroelectrochemical studies were carried out using an in situ UV/Vis spectroscopic technique. The optically Transparent Electrode (O.T.E.) technique was designed and built in Edinburgh. The set up consists of a specially designed UV/Vis/NIR quartz cell of 0.5mm cell pathlength (Figure A.1) fitted with a fine Pt grid gauze working electrode (transparency ~40%), together with an auxiliary (Pt wire) and reference electrode (Ag/Ag^{+}) both separated from the bulk solution by porous glass frits. This unit was inserted into a PTFE cell block screwed into Perkin-Elmer Lamda-9 spectrophotometer. Control of the temperature was maintained by the

passage of both dry N_2 and pre-cooled N_2 ,in combination through the cell block and was monitored by digital thermometer. Solutions of the complexes were thoroughly degassed with argon, then electrolysed at the working electrode in the cell situated in the beam of the spectrophotometer. The electrolysis was maintained until the current decay had reached a small residual value, the potential was then reversed to record the re-generation of the original starting solution to ensue the chemical reversibilty of the redox process.

Key to Figure A.1 :

A - auxiliary electrode protected from bulk solution by porous frit

B - reference electrode protected from bulk solution by porous frit

C - working electrode connection protected from bulk solution by PTFE sleeve

D - PTFE cell top

E - Degassed sample solution

F - 0.5mm quartz cell containing Pt grid working electrode

G - Pt grid working electrode

H - PTFE cell block

I - variable temperature N_2 inlet ports

J - dry N_2 inlet ports

K - quartz cell block windows

Figure A1. Design of the Optically Transparent Electrode

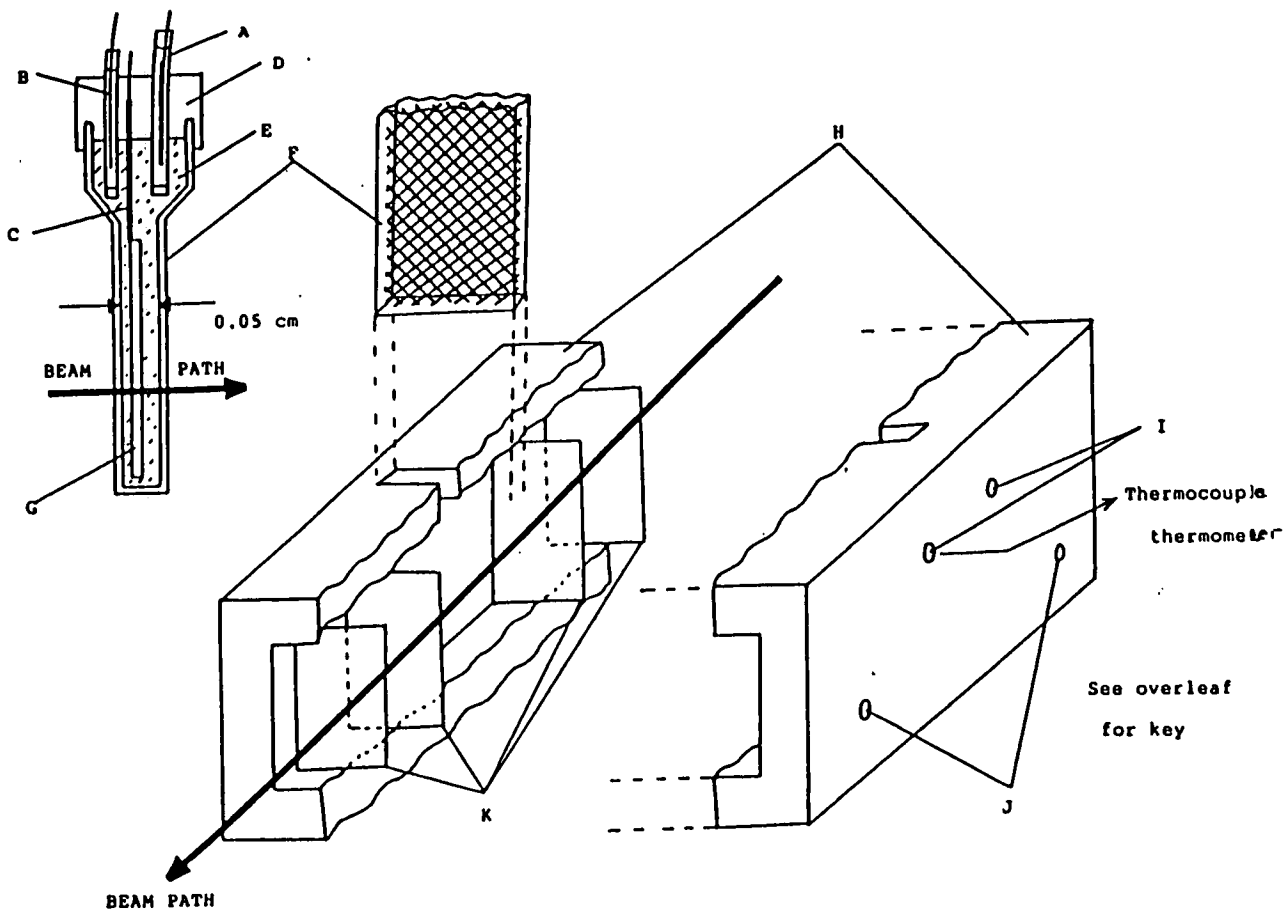

List of abbreviations

[9]aneS_3	1,4,7-trithiacyclononane
[12]aneS_4	1,4,7,10-tetrathiacyclodecane
[14]aneS_4	1,4,8,11-tetrathiacyclotetradecane
[16]aneS_4	1,5,9,13-tetrathiacyclohexadecane
[15]aneS_5	1,4,7,10,13-pentathiacyclopentadecane
[18]aneS_6	1,4,7,10,13,16-hexathiacyclooctadecane
[24]aneS_8	1,4,7,10,13,16,19,22-octathiacyclotetracosane
[28]aneS_8	1,4,8,11,15,18,22,25-octathiacyclooctacosane
[18]aneN_2S_4	1,4,7,10-tetrathia-7,16-diazacyclooctadecane
ap	apical
bipy	2,2'-bipyridyl
$^nBu_4NPF_6$	tetra-^{n}butylammonium hexaflurophosphate
CH_2Cl_2	methylene chloride
DEPT	distortionless enhancement by polarisation transfer
DMF	dimethylformamide
e.p.r.	electron paramagnetic resonance
eq	equatorial
e.s.d.	estimated standard derivation
Et	ethyl
Et_2O	diethylether
EtOH	ethanol
f.a.b.	fast atom bombardment
Fc/Fc^+	ferrocene/ferrocenium
hr	hour

i.r.	infra-red
M^+	molecular ion peak
Me	methyl
Me_2CO	acetone
MeCN	acetonitrile
$MeNO_2$	nitromethane
MeOH	methanol
MHz	megahertz
mins	minutes
M.Wt.	molecular weight
NIR	near infra-red
3-NOBA	3-nitrobenzylalcohol
n.m.r.	nuclear magnetic resonance
OEP	octaethylporphyrin
Ph	phenyl
phen	1,10-phenathroline
ppm	parts per million
tht	tetrahydrothiophene
UV/Vis	ultra-violet/visible

MEETINGS AND LECTURE COURSES ATTENDED

1. Butler Postgraduate Electrochemistry Meeting, Edinburgh 1990,1991.
2. Departmental Inorganic Colloquia and Friday Discussion Group (3 years).
3. Royal Society of Chemistry Annual Chemical Congress, Belfast, 1990.
4. IV International Platinum Group Metals Conference, Cambridge 1990.
5. American Chemical Society 200th National Meeting, Washington DC, 1990.
6. University of Strathclyde Inorganic Club Conferences, 1989, 1990, 1991.
7. UK One-day Macrocycles Symposium, Durham, 1988; Warwick 1990; Manchester 1991.
8. Electro-analytical Methods
   Dr H.H. Girault, Edinburgh
9. Heavy Metals
   Dr M. Schröder, Edinburgh
10. X-ray Crystallograhy - Structure Solution and Refinement
    Drs A.J. Blake and R.O. Gould, Edinburgh
11. Current Advances in Inorganic Chemistry
    Drs S. Chapman, M. Schröder, A.J. Welch and L.J. Yellowlees, Edinburgh
12. Medicinal Inorganic Chemistry
    Dr S. Chapman, Edinburgh
13. E.p.r. Spectroscopy
    Dr R.E.P. Winpenny, Edinburgh

PUBLICATIONS

ANGEWANDTE
CHEMIE
Volume 29 · Number 2
February 1990
Pages 197–198
International Edition in English
Reprint

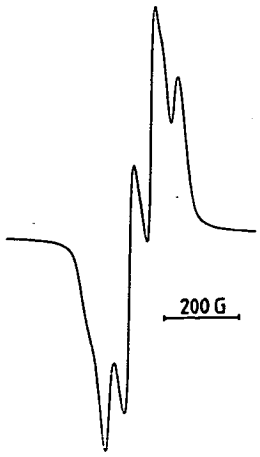

Fig. 1. ESR spectrum of $[Au([9]aneS_3)_2]^{2\oplus}$ in CH_3CN at 77 K.

Bis(1,4,7-trithiacyclononane)gold Dication: A Paramagnetic, Mononuclear Au^{II} Complex**

By *Alexander J. Blake, John A. Greig, Alan J. Holder, Timothy I. Hyde, Anne Taylor,* and *Martin Schröder**

We have shown previously that the potentially six-electron donor macrocycle $[9]aneS_3$ (1,4,7-trithiacyclononane), which prefers to bind metal ions facially,[1,2] is capable of modifying its coordination to accommodate a range of transition-metal stereochemistries.[3] As part of a study of third-row transition-metal complexes of $[9]aneS_3$,[3b] we report herein the preparation of $[Au([9]aneS_3)_2]^{2\oplus}$, the first structurally characterized mononuclear Au^{II} complex.

Reaction of $KAuCl_4$ with two molar equivalents of $[9]aneS_3$ in refluxing aqueous HBF_4(40%)/MeOH affords a reddish brown solution, which was extracted with CH_3NO_2 after addition of water. The CH_3NO_2 solution was filtered, the solvent removed in vacuo, and the residue taken up in CH_3CN. Vapor diffusion with diethyl ether afforded the complex $[Au([9]aneS_3)_2](BF_4)_2$ in 50% yield. $[Au([9]aneS_3)_2]^{2\oplus}$ shows characteristic UV/VIS absorption bands at $\lambda_{max} = 398$ ($\varepsilon = 7990$), 234 nm ($\varepsilon = 15000\ M^{-1}\,cm^{-1}$) and a strong signal in the ESR spectrum at $g_{av} = 2.010$ (77 K). Hyperfine coupling to ^{197}Au ($I = 3/2$, 100%) is observed clearly with $A_{av} = 57.3$ G (Fig. 1).

Crystals of $[Au([9]aneS_3)_2](BF_4)_2 \cdot 2CH_3CN$ suitable for X-ray diffraction were grown from CH_3CN/Et_2O. The single-crystal X-ray structure[4] of the complex (Fig. 2) confirms unequivocally its assignment as a genuine, mononuclear d^9 Au^{II} species: in the centrosymmetric cation, Au^{II} is bound to six thioether donors in a tetragonally elongated stereochemistry (Au-S1 2.839(5), Au-S4 2.462(5), Au-S7 2.452(5) Å). The two $[9]aneS_3$ macrocycles therefore encapsulate the d^9 Au^{II} center to give a Jahn–Teller-distorted octahedral stereochemistry. Interestingly, the related d^9 complex cation $[Cu([9]aneS_3)_2]^{2\oplus}$ also shows an octahedral stereochemistry, although in this case the tetragonal elongation is less than in the Au^{II} analogue (Cu-S1 2.419(3), Cu-S4 2.426(3), Cu-S7 2.459(3) Å[1]).

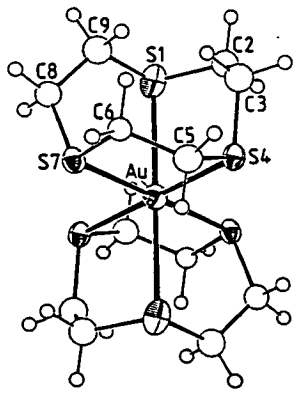

Fig. 2. Structure of the cation $[Au([9]aneS_3)_2]^{2\oplus}$.

$[Au([9]aneS_3)_2]^{2\oplus}$ is air-stable in the solid state. It can be reduced in MeOH or more slowly in CH_3CN to a colorless d^{10} Au^{I} species, $[Au([9]aneS_3)_2]^{\oplus}$ ($E_{pc} = +0.10$ V vs $Fc^{\oplus}$/Fc, Fc = ferrocene), and can be oxidized to the corresponding d^8 Au^{III} complex $[Au([9]aneS_3)_2]^{3\oplus}$ ($E_{\frac{1}{2}} = +0.46$ V vs $Fc^{\oplus}$/Fc).[3b] When the oxidation of Au^{II} to Au^{III} ($\lambda_{max} = 334$ ($\varepsilon = 19765$), 246 nm ($\varepsilon = 20265\ M^{-1}\,cm^{-1}$)) is monitored by UV/VIS spectroscopy, isosbestic points ($\lambda_{iso} = 372$, 208 nm) are observed. The chemical synthesis of $[Au([9]aneS_3)_2]^{2\oplus}$ depends on control of these redox reactions. Isolation of the Au^{II} species from electrosynthesis experiments is hampered by problems associated with removing the base electrolyte and purifying the complex.

Very few examples of mononuclear Au^{II} species have been reported in the literature. Most of these examples are transient or intermediate species or involve significant charge delocalization onto the ligands (e.g., $[Au(mnt)_2]^{2\ominus}$, mnt = 2,3-dimercapto-2-butanedinitrile[5]). The ligand $[9]aneS_3$ is redox-inactive up to + 0.99 V (vs $Fc^{\oplus}$/Fc),[2] suggesting that delocalization of the positive charge in $[Au([9]aneS_3)_2]^{2\oplus}$ onto the thioether donors will be limited. The coordination about the Au center in $[Au([9]aneS_3)_2]^{2\oplus}$ is fully consistent with that of a d^9 transition-metal center and reflects the ability of $[9]aneS_3$ to encapsulate and stabilize an otherwise highly reactive metal radical center. Interestingly, we have found that the hexathia ligand $[18]aneS_6$ is also capable

[*] Dr. A. J. Blake, J. A. Greig, Dr. A. J. Holder, Dr. T. I. Hyde, A. Taylor, Dr. M. Schröder
Department of Chemistry, University of Edinburgh
West Mains Road, GB-Edinburgh EH9 3JJ (Scotland)

[**] We thank the British Science and Engineering Research Council (SERC) for support and Amersham International Plc and SERC for a CASE Award to JAG.

of stabilizing Au^{I}, Au^{II} and Au^{III} centers in the complexes $[Au([18]aneS_6)]^{\oplus/2\oplus/3\oplus}$, respectively.

Received: September 4, 1989 [Z 3536 IE]
German version: *Angew. Chem. 102* (1990) 203

[1] R. S. Glass, W. N. Setzer, C. A. Ogle, G. S. Wilson, *Inorg. Chem. 22* (1983) 266.

[2] K. Wieghardt, H.-J. Küppers, J. Weiss, *Inorg. Chem. 24* (1985) 3067; H.-J. Küppers, A. Neves, C. Pomp, D. Ventur, K. Wieghardt, B. Nuber, J. Weiss, *ibid. 25* (1986) 2400.

[3] a) M. Schröder, *Pure Appl. Chem. 60* (1988) 517, and references therein; M. N. Bell, A. J. Blake, R. O. Gould, A. J. Holder, T. I. Hyde, A. J. Lavery, G. Reid, M. Schröder, *J. Inclusion Phenom. 5* (1987) 169; b) A. J. Blake, R. O. Gould, J. A. Greig, A. J. Holder, T. I. Hyde, M. Schröder, *J. Chem. Soc. Chem. Commun. 1989*, 876.

[4] Structure determination of $[Au([9]aneS_3)_2]^{2\oplus} \cdot 2BF_4^{\ominus} \cdot 2CH_3CN$: An orange-red column-shaped crystal ($0.55 \times 0.3 \times 0.2$ mm), bathed in mother liquor, was sealed in a Lindemann capillary tube and cooled to 173 ± 0.1 K on a Stoe STADI-4 four-circle diffractometer equipped with an Oxford Cryosystems low-temperature device [6]. $M_r = 813.28$, orthorhombic, space group *Pcab*, $a = 8.6921(13)$, $b = 14.823(3)$, $c = 21.5687(23)$ Å, $V = 2779.0$ Å^3 [from 2Θ values of 42 reflections measured at $\pm\omega(2\Theta = 24 \rightarrow 26°$, $\lambda = 0.71073$ Å)], $T = 173$ K, $\varrho_{calcd} = 1.944$ g cm^{-3}, $Z = 4$, $\mu(Mo_{K\alpha}) = 5.781$ mm^{-1}, $T = 173$ K, $\omega-2\Theta$ scans, 2715 reflections measured ($2\Theta_{max} = 45°$), 1586 unique ($R_{int} = 0.022$), initial correction for absorption by means of ψ scans, giving 1146 data with $F \geq 4\sigma(F)$. Intensity statistics indicated the position of the Au atom on an inversion center and, using this information, DIRDIF [7] located the S atoms. Iterative rounds of least-squares refinement and difference Fourier synthesis [8] then located all other non-H atoms. At isotropic convergence, final corrections for absorption were made using DIFABS [9]. Some disorder in the $BF_4^{\ominus}$ anion required modeling. H atoms were included in fixed, calculated positions [8]. At final convergence, $R, R_w = 0.0663$ and 0.0859, respectively, for 123 parameters, $S = 1.209$. The maximum and minimum residues in the final ΔF syntheses were $+1.50$ and -1.21 eÅ^{-3} respectively. Further details of the crystal structure investigation are available on request from the Director of the Cambridge Crystallographic Data Centre, University Chemical Laboratory, Lensfield Road, Cambridge CB2 1EW (UK), on quoting the full journal citation.

[5] R. J. Puddephatt in G. Wilkinson, R. D. Gillard, J. A. McCleverty (Eds): *Comprehensive Coordination Chemistry, Vol. 5*, Pergamon Press, Oxford 1987, chapter 54, p. 861; A. MacCragh, W. S. Koski, *J. Am. Chem. Soc. 87* (1965) 2496; J. H. Waters, H. B. Gray, *ibid. 87* (1965) 3534; I. F. Warren, M. F. Hawthorne, *ibid. 90* (1968) 4823; J. H. Waters, T. J. Bergendahl, S. R. Lewis, *J. Chem. Soc. Chem. Commun. 1971*, 834; R. Kirmse, B. Lorenz, W. Windsch, E. Hoyer, *Z. Anorg. Allg. Chem. 384* (1971) 160; T. J. Bergendahl, E. M. Bergendahl, *Inorg. Chem. 11* (1972) 638; R. L. Schlupp, A. H. Maki, *ibid. 13* (1974) 44; J. G. M. Rens, M. P. A. Viegers, E. de Boer, *Chem. Phys. Lett. 28* (1974) 104; T. J. Bergendahl, J. H. Waters, *Inorg. Chem. 14* (1975) 2556; W. S. Crane, H. Beall, *Inorg. Chim. Acta 31* (1978) L469, and references therein.

[6] J. Cosier, A. M. Glazer, *J. Appl. Crystallogr. 19* (1986) 105.

[7] DIRDIF: P. T. Beurskens, W. P. Bosman, H. M. Doesbury, T. E. M. van den Hark, P. A. J. Prick, J. H. Noordik, G. Beurskens, R. O. Gould, V. Parthasarathia, *Applications of Direct Methods to Difference Structure Factors*, University of Nijmegen, Netherlands, 1983.

[8] SHELX76: G. M. Sheldrick, *Program for Crystal Structure Determinations*, University of Cambridge 1976.

[9] DIFABS: N. Walker, D. Stuart, *Program for Empirical Absorption Corrections, Acta Crystallogr. Sect. A 39* (1983) 158.

  0570-0833/90/0202-0198 $ 02.50/0

Polyhedron Vol. 9, No. 24, pp. 2911–2918, 1990
Printed in Great Britain

0277-5387/90 $3.00+.00

COPPER THIOETHER CHEMISTRY: SYNTHESIS AND X-RAY CRYSTAL STRUCTURES OF BINUCLEAR COPPER(I) COMPLEXES $[Cu_2(L)]^{2+}$ {L = [24]aneS$_8$, [28]aneS$_8$}* INCORPORATING OCTATHIA MACROCYCLES

ALEXANDER J. BLAKE, ANNE TAYLOR and MARTIN SCHRÖDER†

Department of Chemistry, University of Edinburgh, West Mains Road, Edinburgh EH9 3JJ, Scotland, U.K.

(*Received* 10 *May* 1990; *accepted* 6 *August* 1990)

Abstract—Reaction of L {L = [24]aneS$_8$, [28]aneS$_8$} with two molar equivalents of $[Cu(NCMe)_4]X$ (X^- = ClO_4^-, BF_4^-, PF_6^-) in MeCN affords the white binuclear copper(I) complexes $[Cu_2(L)]^{2+}$. A single crystal X-ray structure determination of $[Cu_2([24]aneS_8)](BF_4)_2$ shows two tetrahedral copper(I) centres, each of which is coordinated to four thioether sulphur-donors, Cu—S(1) = 2.263(3), Cu—S(4) = 2.363(3), Cu—S(7) = 2.349(3), Cu—S(10) = 2.261(3) Å. The Cu···Cu distance is 5.172(3) Å. A single crystal X-ray structure determination of $[Cu_2([28]aneS_8)](ClO_4)_2$ shows that this complex also contains two tetrahedral copper(I) centres, each coordinated to four thioether sulphur-donors, Cu—S(1) = 2.278(5), Cu—S(4) = 2.333(5), Cu—S(8) = 2.328(5), Cu—S(11) = 2.268(5) Å. The Cu···Cu distance of 6.454(3) Å is greater than in $[Cu_2([24]aneS_8)]^{2+}$, reflecting the greater cavity size in $[Cu_2([28]aneS_8)]^{2+}$. Cyclic voltammetry of $[Cu_2([24]aneS_8)]^{2+}$ and $[Cu_2([28]aneS_8)]^{2+}$ at platinum electrodes in MeCN (0.1 M $^nBu_4NPF_6$) shows irreversible oxidations at E_{pa} = +0.88 V, +0.92 V vs Fc/Fc^+, respectively, at a scan rate of 200 mV s^{-1}. Coulometric measurements in MeCN confirm these oxidations to be two-electron (one electron per copper) processes to give binuclear copper(II) species. Oxidation of the binuclear copper(I) precursors with H_2SO_4 or HNO_3 affords ESR-active copper(II) species which presumably incorporate SO_4^{2-} and NO_3^- bridges.

The study of mono- and binuclear $Cu^{II/I}$ complexes as models for copper-containing metallo-enzymes is well established.[1] Several biological systems involve copper coordinated to sulphur,[2] and this has led several groups to investigate the incorporation of $Cu^{II/I}$ centres into thioether crowns.[3–8] Rorabacher and co-workers have reported a series of studies on the complexation of copper(II) and copper(I) by polythia macrocyclic ligands.[3,5,6] The single crystal X-ray structure of $[Cu([15]aneS_5)]^{2+}$ shows a square-based pyramidal stereochemistry, Cu—S_{eq} = 2.289(2), 2.315(2), 2.331(2), 2.338(2), Cu—S_{ap} = 2.398(2) Å with the copper atom 0.41 Å out of the basal plane.[5] Reduction of $[Cu([15]aneS_5)]^{2+}$ affords $[Cu([15]aneS_5)]^+$, in which the copper(I) centre has a distorted tetrahedral geometry in the solid state, Cu—S = 2.243(5), 2.245(5), 2.317(5), 2.338(5) Å; the fifth sulphur-donor is non-bonding and is disordered over two sites, Cu···S = 3.442(12) and 3.560(11) Å. The self-exchange electron-transfer rate constant for $[Cu([15]aneS_5)]^{2+/+}$ is very rapid ($k = 3 \times 10^4$ M^{-1} s^{-1}).[5] Cooper and co-workers have reported[7] a similar, rapid Cu—S bond cleavage on reduction of $[Cu([18]aneS_6)]^{2+}$. $[Cu([18]aneS_6)]^{2+}$ shows a tetragonally elongated octahedral stereochemistry, Cu—S = 2.323(1), 2.402(1), 2.635(1) Å. Reduction of this complex affords $[Cu([18]aneS_6)]^+$ which, like $[Cu([15]aneS_5)]^+$, shows a tetrahedral stereochemistry at the metal centre, Cu—S = 2.245(2), 2.253(2), 2.358(2), 2.360(2) Å.[7] The interconversion of $Cu^{II/I}$ centres with [15]aneS$_5$ and [18]aneS$_6$ com-

*[24]aneS$_8$: 1,4,7,10,13,16,19,22-octathiacyclotetracosane; [28]aneS$_8$: 1,4,8,11,15,18,22,25-octathiacyclooctacosane.

† Author to whom correspondence should be addressed.

plexes therefore leads to the formation and breaking of one and two Cu—S bonds, respectively.

These results suggested that tetrahedral coordination of copper(I) to thioether crowns was preferred, as would be expected for a d^{10} metal centre. We have been interested in the synthesis of binuclear copper complexes of thioether macrocycles and have reported previously the synthesis of the binuclear copper(I) species $[Cu_2(L)(NCMe)_2]^{2+}$ {L = [18]aneS$_6$,[4] Me$_2$[18]aneN$_2$S$_4$[9]}. In these systems, however, the 18-membered rings are too small and lack sufficient sulphur-donors to encapsulate two copper(I) centres tetrahedrally. As a result, a solvent MeCN molecule completes the tetrahedral coordination sphere at each copper(I) centre. We argued that larger ring S_8-donor crowns would be capable of encapsulating two copper(I) ions tetrahedrally to give a binuclear, homoleptic thioether product. We report herein the synthesis and single crystal X-ray structure determination of two such complexes, $[Cu_2(L)]^{2+}\cdot 2X^-$ {L = [24]aneS$_8$, $X^- = BF_4^-$; L = [28]aneS$_8$, $X^- = ClO_4^-$}.

RESULTS AND DISCUSSION

Reaction of L {L = [24]aneS$_8$, [28]aneS$_8$} with two molar equivalents of $[Cu(NCMe)_4]X$ ($X^- = ClO_4^-$, BF_4^-, PF_6^-), in MeCN under reflux, affords the white, binuclear copper(I) complexes $[Cu_2(L)]^{2+}\cdot 2X^-$. This assignment of the products is based on IR, NMR and FAB mass spectroscopy and elemental analysis. In order to confirm the connectivity and stereochemistry at the copper(I) centres, and also the conformation of these coordinated large-ring thia macrocycles, single crystal X-ray structure determinations were carried out. Although examples of coordination compounds with these octathia ligands have been described previously,[10,11] none has been characterized crystallographically.

A single crystal X-ray structure determination on $[Cu_2([24]aneS_8)](BF_4)_2$ confirms [Fig. 1(a) and (b)] the complex to be a genuine binuclear copper(I) complex. The two copper(I) centres are related by a crystallographic inversion centre and are each coordinated to four thioether sulphur-donors, Cu—S(1) = 2.263(3), Cu—S(4) = 2.363(3), Cu—S(7) = 2.349(3), Cu—S(10) = 2.261(3) Å. These bond lengths are comparable with Cu—S distances in related copper(I)–thioether complexes.[4-8] The Cu···Cu distance of 5.172(3) Å indicates that the two copper(I) centres are non-interacting. The angles at the copper(I) centres are distorted from those values expected for a tetrahedron, ∠S(1)CuS(4) = 94.54(10), ∠S(1)CuS(7) = 120.20(11),

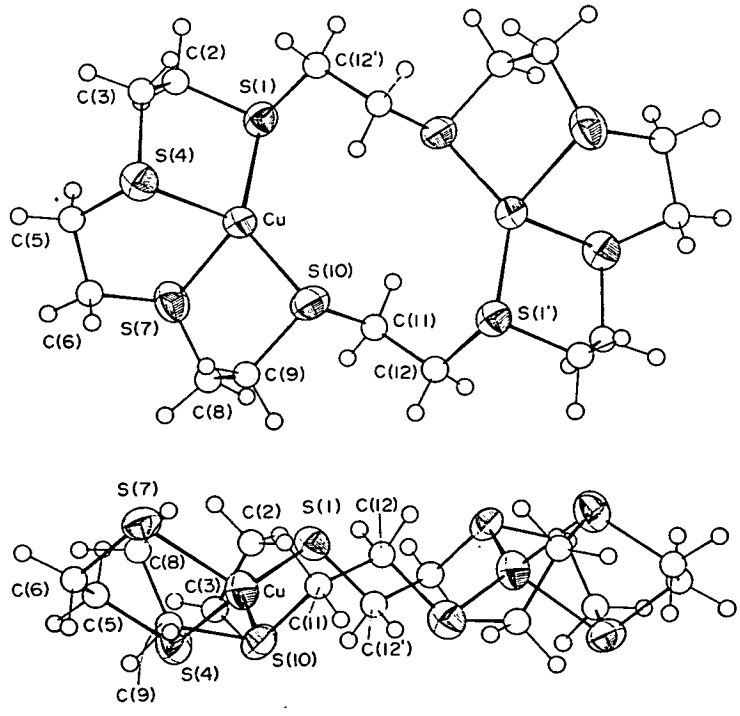

Fig. 1. (a) View of the $[Cu_2([24]aneS_8)]^{2+}$ cation with atom numbering scheme adopted; (b) Orthogonal view showing the conformation of the macrocycle.

∠S(1)CuS(10) = 133.86(11), ∠S(4)CuS(7) = 91.81(10), ∠S(4)CuS(10) = 116.39(10), ∠S(7)CuS(10) = 93.57(10)°. The structure of $[Cu_2([28]aneS_8)](ClO_4)_2$, the analogous complex with the larger, 28-membered ring macrocycle, shows similar features: a single crystal X-ray structure determination of this species [Fig. 2(a) and (b)] also shows two tetrahedral copper(I) centres each coordinated to four thioether sulphur-donors, Cu—S(1) = 2.278(5), Cu—S(4) = 2.333(5), Cu—S(8) = 2.328(5), Cu—S(11) = 2.268(5) Å, ∠S(1)CuS(4) = 93.69(19), ∠S(1)CuS(8) = 108.78(19), ∠S(1)CuS(11) = 133.39(20), ∠S(4)CuS(8) = 105.66(18), ∠S(4)CuS(11) = 119.79(19), ∠S(8)CuS(11) = 93.25(18)°. The Cu···Cu distance of 6.454(3) Å is greater than in $[Cu_2([24]aneS_8)]^{2+}$, reflecting the greater cavity size of [28]aneS$_8$.

These results confirm that the 24- and 28-membered ring ligands are large enough to encapsulate two isolated tetrahedral metal centres. Interestingly, we have found that [24]aneS$_8$ and [28]aneS$_8$ can also complex two palladium(II) ions to give the $[Pd_2(L)]^{4+}$ species.[12,13] The coordination geometry at palladium(II) in these complexes is likely to be square-planar. Thus, the binucleating octathia ligands, [24]aneS$_8$ and [28]aneS$_8$, are capable of complexing both tetrahedral *and* square-planar metal centres. This opens up the possibility of unusual redox capabilities; for example, reduction of the square-planar, binuclear platinum(II) complexes $[Pt_2(L)]^{4+}$ should afford the platinum(0) species $[Pt_2(L)]$ in which the metal centres are tetrahedral. Control of this four-electron reduction couple should lead to interesting substrate activation reactions such as O_2 reduction, although ligand oxidation reactions may be a problem in this case.

Cyclic voltammetry of $[Cu_2(L)]^{2+}$ at platinum electrodes in MeCN (0.1 M $^nBu_4NPF_6$) shows irreversible oxidations at $E_{pa} = +0.88$ V {L = [24]aneS$_8$} and $E_{pa} = +0.92$ V vs Fc/Fc^+ {L = [28]aneS$_8$}, at a scan rate of 200 mV s^{-1}. Coulometric measurements confirm these oxidations to be two-electron processes (one electron per copper) to afford green $Cu^{II/I}$ products, $\lambda_{max} = 428$ {L = [24]aneS$_8$}; 560, 406 nm {L = [28]aneS$_8$}. The fact that these oxidations are electrochemically irreversible is not surprising since the resultant copper(II) centres would be expected to tend towards octahedral or at least five coordination, and would therefore require extra ligation. We have, therefore, undertaken a preliminary study of the chemical oxidation of $[Cu_2(L)]^{2+}$ with, for example, $NOBF_4$, HNO_3 and H_2SO_4. Oxidation of the complexes affords stable, coloured paramagnetic species, the ESR spectra of which suggest that the two copper(II) centres are non-interacting.

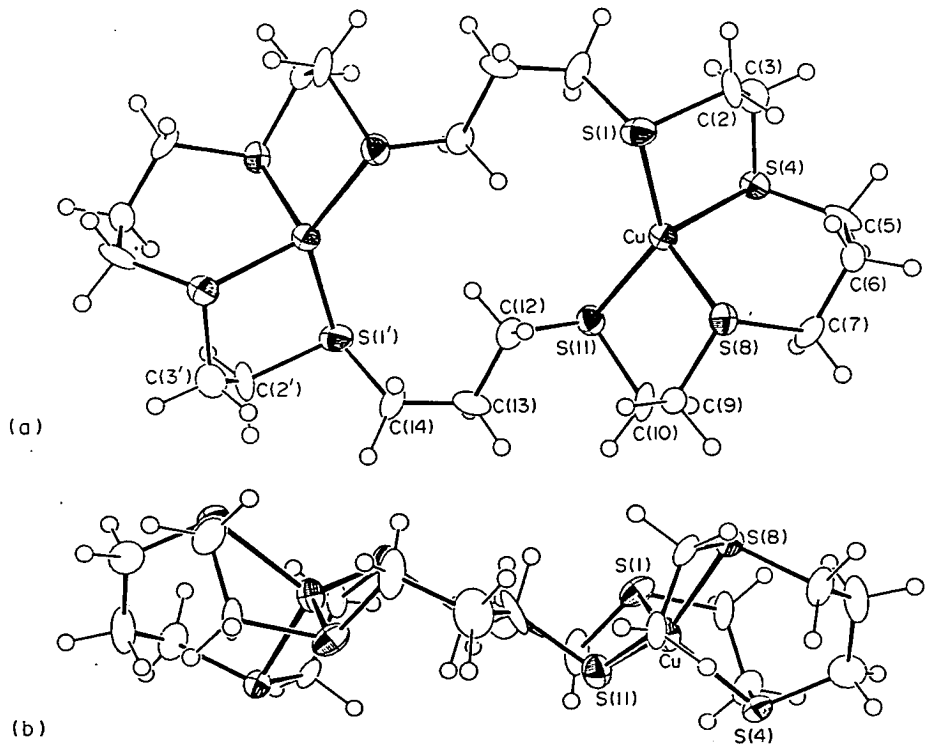

Fig. 2. (a) View of the $[Cu_2([28]aneS_8)]^{2+}$ cation with atom numbering scheme adopted; (b) Orthogonal view showing the conformation of the macrocycle.

Current work is aimed at elucidating the structures and chemistry of these binuclear copper(II) complexes, and to study the redox chemistry of the binuclear copper(I) precursors with small molecule substrates.

EXPERIMENTAL

IR spectra were measured as Nujol mulls, KBr and CsI discs using a Perkin–Elmer 598 spectrometer over the range 200–4000 cm^{-1}. UV–vis spectra were measured in quartz cells using Perkin–Elmer Lambda 9 and Pye Unicam SP8-400 spectrophotometers. Microanalyses were performed by the Edinburgh University Chemistry Department microanalytical service. ESR spectra were recorded as solids or as frozen glasses down to 77 K using a Bruker ER200D X-band spectrometer. ^1H and ^{13}C NMR spectra were recorded at 200.13 and 50.32 MHz, respectively, on a Bruker WP200 spectrometer. Electrochemical measurements were performed on a Bruker E310 Universal Modular Polarograph. All readings were taken using a three-electrode potentiostatic system in acetonitrile containing 0.1 M $^nBu_4NPF_6$ or $^nBu_4NBF_4$ as supporting electrolyte. Cyclic voltammetric measurements were carried out using a double platinum electrode and a Ag/AgCl reference electrode. All potentials are quoted versus ferrocene/ferrocinium, Fc/Fc^+. Mass spectra were run by electron impact on a Kratos MS 902 and by fast atom bombardment on a Kratos MS 50TC spectrometer.

Synthesis of $[Cu_2([24]aneS_8)](PF_6)_2$

To a solution of [24]aneS$_8$ (0.192 g, 0.4 mmol), dissolved in refluxing MeCN (20 cm^3), was added $[Cu(NCMe)_4]PF_6$ (0.298 g, 0.8 mmol). The solution was refluxed for 2 h, filtered and the volume reduced to 5 cm^3. Addition of Et_2O and cooling to −20°C afforded a white precipitate which was recrystallized from acetone–Et_2O to give the desired complex in 78% yield. Found: C, 21.2; H, 3.6. Calc. for $C_{16}H_{32}Cu_2S_8P_2F_{12}$: C, 21.4; H, 3.6%. IR spectrum (KBr disc): 2980, 2920, 1420, 1395, 1320, 1290, 1255, 1210, 1170, 1150, 1130, 1120, 1080, 1050, 920, 840, 740w, 680, 660w, 630w, 610w, 560 and 455 cm^{-1}. FAB mass spectrum (3-NOBA matrix): Found: $M^+ = 753$, 607. Calc. for $[^{63}Cu_2([24]aneS_8)PF_6]^+$: $M^+ = 753$; $[^{63}Cu_2([24]aneS_8)-H]^+$: $M^+ = 607$, with correct isotopic distributions. ^1H NMR spectrum (CD_3CN, 298 K, 200.13 MHz): $\delta = 2.93$–2.97 ppm (32H). ^{13}C NMR spectrum (CD_3CN, 298 K, 50.32 MHz): $\delta = 32.54$ ppm (CH_2).

The complex $[Cu_2([24]aneS_8)](BF_4)_2$ can be prepared in 72% yield by the same method by using $[Cu(NCMe)_4]BF_4$ as a starting material. Found: C, 24.7; H, 4.1. Calc. for $C_{16}H_{32}Cu_2S_8B_2F_8$: C, 24.6; H, 4.1%. IR spectrum (KBr disc): 2980, 2920, 1425, 1410, 1285, 1255, 1200w, 1170w, 1050br, 920w, 910w, 890w, 850, 820, 770, 680, 620w, 520, 455 and 415 cm^{-1}. FAB mass spectrum (3-NOBA matrix): Found $M^+ = 694$, 606. Calc. for $[^{63}Cu_2([24]aneS_8-H)BF_4]^+$: $M^+ = 694$; $[^{63}Cu_2([24]aneS_8)-2H]^+$: $M^+ = 606$, with correct isotopic distributions. ^1H NMR spectrum (CD_3CN, 298 K, 80.13 MHz): $\delta = 2.93$–2.13 ppm (32H).

Crystal structure determination of $[Cu_2([24]aneS_8)](BF_4)_2$

[1,4,7,10,13,16,19,22 - octathiacyclotetracosane - (S^1, S^4, S^7, S^{10})(S^{13}, S^{16}, S^{19}, S^{22})dicopper(I)]$^{2+}$ · $2BF_4^-$. A colourless plate, 0.85 × 0.36 × 0.035 mm, grown by diffusion of Et_2O vapour into a solution of the complex in MeCN, was mounted on a Stoë STADI-4 four-circle diffractometer.

Crystal data. $C_{16}H_{32}Cu_2S_8^{2+} \cdot 2BF_4^-$, $M = 781.5$, monoclinic, space group $P2_1/n$ (alt. $P2_1/c$, No. 14), $a = 6.480(6)$, $b = 20.040(11)$, $c = 11.327(6)$ Å, $\beta = 91.84(5)°$, $U = 1470$ Å^3 [from 2θ values of 22 reflections measured at $\pm\omega(2\theta =$ 24–26°, $\lambda = 0.71073$ Å), $T = 298$ K], $Z = 2$, $D_{calc} = 1.765$ g cm^{-3}, $\mu = 2.014$ mm^{-1}, $F(000) = 792$.

Data collection and processing. STADI-4 diffractometer, graphite-monochromated Mo-K_α X-radiation, $T = 298$ K, ω–2θ scans using the learnt-profile method,[14] 2231 unique data collected ($2\theta_{max}$ 45°, h $-6 \rightarrow 6$, k $0 \rightarrow 21$, l $0 \rightarrow 12$), giving 1468 with $F \geqslant 4\sigma(F)$ for use in all calculations. No significant crystal decay was observed.

Structure solution and refinement. A Patterson synthesis located the copper atom and iterative cycles of least-squares refinement and difference

Table 1. Bond lengths for $[Cu_2([24]aneS_8)]^{2+}$ (with standard deviations)

Cu—S(1)	2.263(3)	C(5)—C(6)	1.503(16)
Cu—S(4)	2.363(3)	C(6)—S(7)	1.817(12)
Cu—S(7)	2.349(3)	S(7)—C(8)	1.808(12)
Cu—S(10)	2.261(3)	C(8)—C(9)	1.561(16)
S(1)—C(2)	1.800(10)	C(9)—S(10)	1.814(12)
C(2)—C(3)	1.520(14)	S(10)—C(11)	1.811(10)
C(3)—S(4)	1.816(10)	C(11)—C(12)	1.524(14)
S(4)—C(5)	1.837(12)	C(12)—S(1′)[a]	1.807(11)

[a] Primed atoms are related to their unprimed equivalents by inversion through ($\frac{1}{2}$, 0, 0).

Table 2. Bond angles for $[Cu_2([24]aneS_8)]^{2+}$ (with standard deviations)

S(1)—Cu—S(4)	94.54(10)	C(3)—S(4)—C(5)	101.8(5)
S(1)—Cu—S(7)	120.20(11)	S(4)—C(5)—C(6)	110.3(8)
S(1)—Cu—S(10)	133.86(11)	C(5)—C(6)—S(7)	113.1(8)
S(4)—Cu—S(7)	91.81(10)	Cu—S(7)—C(6)	98.0(4)
S(4)—Cu—S(10)	116.39(10)	Cu—S(7)—C(8)	98.8(4)
S(7)—Cu—S(10)	93.57(10)	C(6)—S(7)—C(8)	102.3(5)
Cu—S(1)—C(2)	97.8(3)	S(7)—C(8)—C(9)	116.2(8)
Cu—S(1)—C(12′)	110.8(4)	C(8)—C(9)—S(10)	112.7(8)
C(2)—S(1)—C(12′)	100.9(5)	Cu—S(10)—C(9)	97.7(4)
S(1)—C(2)—C(3)	115.4(7)	Cu—S(10)—C(11)	107.9(3)
C(2)—C(3)—S(4)	116.3(7)	C(9)—S(10)—C(11)	103.6(5)
Cu—S(4)—C(3)	97.3(3)	S(10)—C(11)—C(12)	113.1(7)
Cu—S(4)—C(5)	96.4(4)	C(11)—C(12)—S(1′)	112.7(7)

Fourier synthesis located the remaining non-hydrogen atoms. At isotropic convergence, corrections (min. 0.750, max. 1.615) for absorption were applied using DIFABS.[15] Disorder in the BF_4^- counter-anion was modelled by two fully-occupied and four half-occupied fluorine atoms. Refinement (by least-squares on F[16]) with anisotropic thermal for all ordered non-hydrogen atoms and with hydrogen atoms in fixed, calculated positions converged at R, $R_w = 0.0652$, 0.0827, respectively, $S = 1.141$ for 157 refined parameters, and the final ΔF synthesis showed no feature above 0.79 e $Å^{-3}$. The weighting scheme, $w^{-1} = \sigma^2(F) + 0.000264F^2$, gave satisfactory agreement analyses and in the final cycle $(\Delta/\sigma)_{max}$ was 0.072. Bond lengths, angles and torsion angles are listed in Tables 1–3.

Synthesis of $[Cu_2([28]aneS_8)](PF_6)_2$

To a solution of $[28]aneS_8$ (0.215 g, 0.4 mmol) dissolved in refluxing MeCN (25 cm^3) was added $[Cu(NCMe)_4]PF_6$ (0.298 g, 0.8 mmol). The solution was refluxed for 2 h, filtered and the volume reduced to 5 cm^3. Addition of Et_2O and cooling to −20°C afforded a white precipitate which was recrystallized from acetone–Et_2O to give the desired complex in 82% yield. Found: C, 25.2; H, 4.2. Calc. for $C_{20}H_{40}Cu_2S_8P_2F_{12}$: C, 25.2; H, 4.3%. IR spectrum (KBr disc): 2980, 2920, 1440, 1430, 1420, 1410, 1340w, 1300, 1290, 1255, 1245, 1210w, 1140, 1130, 1020, 935, 840, 740, 660 and 555 cm^{-1}. FAB mass spectrum (3-NOBA matrix): Found: $M^+ = 809$, 663. Calc. for $[^{63}Cu_2([28]aneS_8)PF_6]^+$: $M^+ = 809$; $[^{63}Cu_2([28]aneS_8) - H]^+$: $M^+ = 663$, with correct isotopic distributions. ^1H NMR spectrum (CD_3CN, 298 K, 200.13 MHz): $\delta = 2.75$–3.10 ppm (28H). ^{13}C NMR spectrum (CD_3CN, 298 K, 50.32 MHz): $\delta = 33.60$, 31.50, 25.56 ppm (CH_2).

The complex $[Cu_2([28]aneS_8)](ClO_4)_2$ can be prepared in 80% yield by the same method by using $[Cu(NCMe)_4]ClO_4$ as a starting material. Found: C, 27.5; H, 4.6. Calc. for $C_{20}H_{40}Cu_2S_8Cl_2O_8$: C, 27.4; H, 4.7%. IR spectrum (KBr disc): 2960, 2920, 2850, 1440, 1405, 1340w, 1300w, 1255, 1240, 1140, 1090, 940w, 920, 910, 850, 840, 805w, 635 and 625 cm^{-1}. FAB mass spectrum (3-NOBA matrix): Found: $M^+ = 763$, 663. Calc. for $[^{63}Cu_2([28]aneS_8)^{35}ClO_4]^+$: $M^+ = 763$; $[^{63}Cu_2([28]aneS_8) - H]^+$: $M^+ = 663$, with correct isotopic distributions. ^1H NMR spectrum (CD_3CN, 298 K, 200.13 MHz): $\delta = 2.72$–2.97 ppm (28H). ^{13}C NMR spectrum (CD_3CN, 298 K, 50.32 MHz): $\delta = 33.14$, 31.23, 26.10 ppm (CH_2).

Table 3. Torsion angles for $[Cu_2([24]aneS_8)]^{2+}$ (with standard deviations)

C(12′)—S(1)—C(2)—C(3)	70.7(8)	C(6)—S(7)—C(8)—C(9)	77.6(9)
S(1)—C(2)—C(3)—C(4)	51.1(9)	S(7)—C(8)—C(9)—S(10)	49.9(11)
C(2)—C(3)—S(4)—C(5)	70.6(8)	C(8)—C(9)—S(10)—C(11)	63.7(9)
C(3)—S(4)—C(5)—C(6)	−147.6(8)	C(9)—S(10)—C(11)—C(12)	91.2(8)
S(4)—C(5)—C(6)—S(7)	64.9(9)	S(10)—C(11)—C(12)—S(1′)	68.2(8)
C(5)—C(6)—S(7)—C(8)	−141.7(8)		

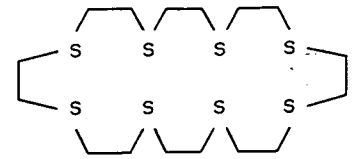

[24]aneS$_8$

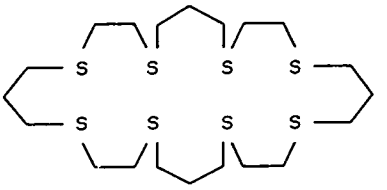

[28]aneS$_8$

Scheme 1.

Crystal structure determination of $[Cu_2([28]aneS_8)](ClO_4)_2$

[1,4,8,11,15,18,22,25 - octathiacyclooctacosane - (S^1,S^4,S^8,S^{11})(S^{15},S^{18},S^{22},S^{25}) dicopper(I)]$^{2+}\cdot 2ClO_4^-$. A pale yellow needle, $0.47\times0.05\times0.05$ mm, grown by diffusion of Et_2O vapour into a solution of the complex in MeCN, was cooled to 173 ± 0.1 K on a Stoë STADI-4 four-circle diffractometer equipped with an Oxford Cryosystems low-temperature device.[18]

Crystal data. $C_{20}H_{40}Cu_2S_8^{2+}\cdot 2ClO_4^-$, M = 863.0, monoclinic, space group $P2_1/n$ (alt. $P2_1/c$, No. 14), a = 6.999(7), b = 20.000(21), c = 11.780(7) Å, β = 102.37(7)°, U = 1611 Å^3 [from setting angles of 10 reflections with 2θ = 20–22°, $\bar{\lambda}$ = 0.71073 Å, T = 173 K], Z = 2, D_{calc} = 1.779 g cm^{-3}, μ = 2.032 mm^{-1}, $F(000)$ = 888.

Table 4. Bond lengths for $[Cu_2([28]aneS_8)]^{2+}$ (with standard deviations)

Cu—S(1)	2.278(5)	C(6)—C(7)	1.56(3)
Cu—S(4)	2.333(5)	C(7)—S(8)	1.794(20)
Cu—S(8)	2.328(5)	S(8)—C(9)	1.804(17)
Cu—S(11)	2.268(5)	C(9)—C(10)	1.493(25)
S(1)—C(2)	1.835(20)	C(10)—S(11)	1.850(19)
C(2)—C(3)	1.55(3)	S(11)—C(12)	1.761(20)
C(3)—S(4)	1.802(19)	C(12)—C(13)	1.56(3)
S(4)—C(5)	1.795(19)	C(13)—C(14)	1.50(3)
C(5)—C(6)	1.50(3)	C(14)—S(1′)[a]	1.849(21)

[a] Primed atoms are related to their unprimed equivalents by inversion through $(2-x, 1-y, 1-z)$.

Data collection and processing. STADI-4 diffractometer, graphite-monochromated Mo-K_α X-radiation, T = 173 K, ω–2θ scans using the learnt-profile method,[14] 2727 data collected ($2\theta_{max}$ 45°, h $-7\rightarrow7$, k $0\rightarrow21$, l $0\rightarrow12$), 1799 unique (R_{int} 0.071), giving 1039 reflections with $F\geqslant4\sigma(F)$ for use in all calculations. Linear isotropic crystal decay (*ca* 21%) corrected for during data reduction, no absorption correction.

Structure solution and refinement. A Patterson synthesis located the metal atom and iterative cycles of least-squares refinement and different Fourier synthesis located the remaining non-hydrogen atoms: these were then refined (by least-squares on F[16]) with anisotropic thermal parameters for all non-hydrogen atoms and with hydrogen atoms in fixed, calculated positions. At final convergence R, R_w = 0.0656, 0.0784, respectively, S = 0.947 for 182 refined parameters, and the final ΔF synthesis showed no feature above 0.74 e Å^{-3}. An isotropic extinction parameter refined to $6(4)\times10^{-8}$. The

Table 5. Bond angles for $[Cu_2([28]aneS_8)]^{2+}$ (with standard deviations)

S(1)—Cu—S(4)	93.69(19)	C(6)—C(7)—S(8)	107.5(13)
S(1)—Cu—S(8)	108.78(19)	Cu—S(8)—C(7)	100.5(6)
S(1)—Cu—S(11)	133.39(20)	Cu—S(8)—C(9)	99.6(6)
S(4)—Cu—S(8)	105.66(18)	C(7)—S(8)—C(9)	100.8(8)
S(4)—Cu—S(11)	119.79(19)	S(8)—C(9)—C(10)	117.4(12)
S(8)—Cu—S(11)	93.25(18)	C(9)—C(10)—S(11)	113.3(12)
Cu—S(1)—C(2)	97.2(6)	Cu—S(11)—C(10)	99.3(6)
S(1)—C(2)—C(3)	111.1(13)	Cu—S(11)—C(12)	108.4(7)
C(2)—C(3)—S(4)	115.1(13)	C(10)—S(11)—C(12)	99.8(9)
Cu—S(4)—C(3)	98.6(6)	S(11)—C(12)—C(13)	115.3(14)
Cu—S(4)—C(5)	108.5(6)	C(12)—C(13)—C(14)	113.7(17)
C(3)—S(4)—C(5)	102.4(9)	C(13)—C(14)—S(1′)	108.0(14)
S(4)—C(5)—C(6)	121.8(14)	C(14)—S(1′)—C(2′)	100.1(9)
C(5)—C(6)—C(7)	111.1(16)		

Table 6. Torsion angles for $[Cu_2([28]aneS_8)]^{2+}$ (with standard deviations)

S(1)—C(2)—C(3)—S(4)	−56.2(16)	S(8)—C(9)—C(10)—S(11)	−48.3(16)
C(2)—C(3)—S(4)—C(5)	−80.6(15)	C(9)—C(10)—S(11)—C(12)	−70.6(14)
C(3)—S(4)—C(5)—C(6)	91.5(16)	C(10)—S(11)—C(12)—C(13)	−59.1(15)
S(4)—C(5)—C(6)—C(7)	63.8(20)	S(11)—C(12)—C(13)—C(14)	−167.6(14)
C(5)—C(6)—C(7)—S(8)	−101.4(16)	C(12)—C(13)—C(14)—S(1′)	69.7(19)
C(6)—C(7)—S(8)—C(9)	169.3(13)	C(13)—C(14)—S(1′)—C(2′)	149.6(14)
C(7)—S(8)—C(9)—C(10)	−75.0(14)	C(14)—S(1′)—C(2′)—C(3′)	68.6(14)

weighting scheme $w^{-1} = \sigma^2(F) + 0.0007F^2$ gave satisfactory agreement analyses and in the final cycle $(\Delta/\sigma)_{max}$ was 0.11. Bond lengths, angles and torsion angles are listed in Tables 4–6.

Atomic scattering factors were inlaid[17] except for copper,[18] molecular geometry calculations utilized CALC[19] and figures were produced by ORTEPII.[20] Atomic coordinates, displacement factor coefficients and F_o/F_c tables have been deposited.

Acknowledgement—We thank the SERC for support.

REFERENCES

1. S. G. Murray and F. R. Hartley, *Chem. Rev.* 1981, **81**, 365; K. D. Karlin and J. Zubieta (Eds), *Copper Coordination Chemistry: Biochemical and Inorganic Perspectives*. Adenine Press, New York (1983); D. E. Fenton, *Advances in Inorganic and Bioinorganic Mechanisms* (Edited by A. G. Sykes), p. 187. Academic Press, London (1983); D. E. Fenton, *Pure Appl. Chem.* 1989, **61**, 903 and refs therein.
2. L. Rydel and J. O. Lundgren, *Nature* (*Lond.*) 1976, **261**, 344; P. M. Collman, H. C. Freeman, J. M. Guss, M. Murata, V. A. Norris, J. A. M. Ramshaw and M. P. Venkatappa, *Nature* (*Lond.*) 1978, **272**, 319; H. C. Freeman, *Coordination Chemistry* (Edited by J. P. Laurent), Vol. 21, p. 29. Pergamon Press, Oxford (1981); E. T. Adman and L. H. Jensen, *Isr. J. Chem.* 1981, **21**, 8.
3. D. B. Rorabacher, M. J. Martin, M. J. Koenigbauer, M. Malik, R. R. Schroeder, J. F. Endicott and L. A. Ochrymowycz, in *Copper Coordination Chemistry: Biochemical and Inorganic Perspectives* (Edited by K. D. Karlin and J. Zubieta), p. 167. Adenine Press, New York (1983); D. B. Rorabacher, M. M. Bernado, A. M. Q. Vande Linde, G. H. Leggett, B. C. Westerby, M. J. Martin and L. A. Ochrymowycz, *Pure Appl. Chem.* 1988, **60**, 501 and refs therein.
4. R. O. Gould, A. J. Lavery and M. Schröder, *J. Chem. Soc., Chem. Commun.* 1985, 1492.
5. P. W. R. Corfield, C. Ceccarelli, M. D. Glick, I. W.-Y. Moy, L. A. Ochrymowycz and D. B. Rorabacher, *J. Am. Chem. Soc.* 1985, **107**, 2399.
6. T. E. Jones. D. B. Rorabacher and L. A. Ochrymowycz, *J. Am. Chem. Soc.* 1975, **97**, 7485; T. E. Jones, L. L. Zimmer, L. L. Diaddario, D. B. Rorabacher and L. A. Ochrymowycz, *Inorg. Chem.* 1975, **14**, 7163; N. S. Ferris, W. H. Woodruff, D. B. Rorabacher, T. E. Jones and L. A. Ochrymowycz, *J. Am. Chem. Soc.* 1978, **100**, 5939; L. L. Diaddario, L. L. Zimmer, T. E. Jones, L. S. W. L. Sokol, R. B. Cruz, E. L. Yee, L. A. Ochrymowycz and D. B. Rorabacher, *J. Am. Chem. Soc.* 1979, **101**, 3511; L. L. Diaddario Jr, E. R. Dockal, M. D. Glick, L. A. Ochrymowycz and D. B. Rorabacher, *Inorg. Chem.* 1985, **24**, 356; I. R. Young, L. A. Ochrymowycz and D. B. Rorabacher, *Inorg. Chem.* 1986, **25**, 2576; V. B. Pett, G. H. Leggett, T. H. Cooper, P. R. Reed, D. Situmeang, L. A. Ochrymowycz and D. B. Rorabacher, *Inorg. Chem.* 1988, **27**, 2164.
7. J. R. Hartman and S. R. Cooper, *J. Am. Chem. Soc.* 1986, **108**, 1202.
8. M. D. Glick, D. P. Gavel, L. L. Diaddario and D. B. Rorabacher, *Inorg. Chem.* 1976, **15**, 1190; B. V. Gorewit and W. K. Murker, *J. Coord. Chem.* 1976, **5**, 67; W. N. Setzer, C. A. Ogle, G. S. Wilson and R. S. Glass, *Inorg. Chem.* 1983, **22**, 266; H-J. Küppers, K. Wieghardt, Y.-H. Tsay, C. Krüger, B. Nuber and J. Weiss, *Angew Chem.* 1987, **99**, 583; *Angew. Chem. Int. Edn. Engl.* 1987, **26**, 575; S. C. Rawle, G. A. Admans and S. R. Cooper, *J. Chem. Soc., Dalton Trans.* 1988, 93; C. M. Lucas, L. Shuang, M. J. Newlands, J.-P. Charland and E. J. Gabe, *Can. J. Chem.* 1988, **66**, 1506; C. M. Lucas, L. Shuang, M. J. Newlands, J.-P. Charland and E. J. Gabe, *Can. J. Chem.* 1989, **67**, 639.
9. N. Atkinson, A. J. Blake, M. G. B. Drew, G. Forsyth, A. J. Lavery, G. Reid and M. Schröder, *J. Chem. Soc., Chem. Commun.* 1989, 984.
10. A. J. Blake and M. Schröder, *Adv. Inorg. Chem.* 1990, **35**, 1.
11. R. E. DeSimone and T. M. Tighe, *J. Inorg. Nucl. Chem.* 1976, **38**, 1623; D. Sevdić and H. Meider, *J. Inorg. Nucl. Chem.* 1977, **39**, 1403; A. C. Braithwaite, C. E. F. Rickard and T. N. Waters, *Aust. J. Chem.* 1981, **34**, 2665; K. Saito, Y. Masudo and E. Sekido, *Anal. Chim. Acta* 1983, **151**, 447.
12. K. Travis and D. H. Busch, *J. Chem. Soc., Chem. Commun.* 1970, 1041.
13. G. Reid, PhD thesis. University of Edinburgh, U.K. (1989).
14. W. Clegg, *Acta Cryst.* 1981, **A37**, 22.
15. N. Walker and D. Stuart, DIFABS, Program for

Empirical Absorption Correction, *Acta Cryst.* 1983, **A39**, 158.
16. G. M. Sheldrick, SHELX76, Program for Crystal Structure Refinement. University of Cambridge, U.K. (1976).
17. J. Cosier and A. M. Glazer, *J. Appl. Cryst.* 1986, **19**, 105.
18. D. T. Cromer and J. L. Mann, *Acta Cryst.* 1968, **A24**, 321.
19. R. O. Gould and P. Taylor, CALC, Program for Molecular Geometry Calculations. University of Edinburgh, U.K. (1985).
20. P. D. Mallinson and K. W. Muir, ORTEPII, Interactive Version, *J. Appl. Cryst.* 1985, **18**, 51.

Is the Molecular Structure of 1,4,7-Trithiacyclononane([9]aneS$_3$) as Symmetrical in the Gas Phase as it is in the Crystal? An Electron Diffraction Study

Richard Blom,† David W. H. Rankin*, Heather E. Robertson, Martin Schröder and Anne Taylor
Department of Chemistry, University of Edinburgh, West Mains Road, Edinburgh, EH9 3JJ, Scotland, UK

The molecular structure of [9]aneS$_3$ has been studied by gas electron diffraction (GED) and by molecular-mechanics calculations (MM2). Four molecular models have been fitted to the experimental data, one having D_3 symmetry, one C_3 symmetry, one C_2 symmetry and one C_1 symmetry. The D_3 model was incompatible with the GED data and was discarded. The C_1 model gave the lowest R-factor in the GED analysis, and the C_2 model gave only a slightly poorer fit to the data. The C_3 model, which corresponds to the conformation observed in the crystalline state, could not be completely excluded, but the model gave a significantly worse fit to the GED data than the C_2 and C_1 models. MM2 calculations also favoured the C_1 model, but with the C_3 model only 0.13 kJ mol^{-1} higher in strain energy. The C_2 and D_3 models were higher in energy by 8.3 and 9.9 kJ mol^{-1} respectively.

The co-ordination chemistry of macrocyclic sulphide ligands has been the subject of much recent interest.[1,2] Whereas sulphides, R_2S, are often poor donors to transition metal ions,[3] their cyclic analogues have been found to co-ordinate to a wide range of metal ions to form stable complexes.[1] The trithia macrocycle [9]aneS$_3$ (1,4,7-trithiacyclononane), in particular, usually binds facially to metal ions and therefore parallels the co-ordination of cyclopentadienyl, aryl, tripyrazolylborate and triphos ligands.[1] The single-crystal X-ray structure of metal-free

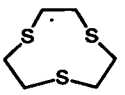

[9]aneS$_3$
1,4,7-trithiacyclononane

1,4,7-trithiacyclononane ([9]aneS$_3$) shows it to adopt a [333][4] *endo* conformation with C_3 symmetry.[5] Approximate C_3 symmetry of the ligand is retained in most metal complexes, although C_2 symmetry has been observed in some cases, particularly with d^8 metal ions.[6] If the ligand symmetry found in the crystal is maintained in solution, the *S*-donors in the metal-free ligand are pre-organised[7] for facial co-ordination to metal ions. In contrast, the solid-state structures of other polysulphides S_4-, S_5- and S_6-donor crowns show that they tend to adopt *exo* conformations in which the donor atoms point out of the macrocyclic cavities.[8,9] Rearrangement from an *exo* to an *endo* conformation is therefore a common feature of the co-ordination chemistry of these latter ligands,[8,10] but not for [9]aneS$_3$.

Conformational analysis of [9]aneS$_3$ using photoelectron spectroscopy has suggested that the [333] conformation is retained in the gas phase.[11] We wished to probe the conformation of metal-free [9]aneS$_3$ further, particularly with respect to pre-organisation effects. We report here a gas-phase electron-diffraction study and the results of molecular-mechanics (MM2) calculations on uncoordinated [9]aneS$_3$.

Experimental

Synthesis.—[9]aneS$_3$ was synthesised according to the template method of Sellmann and Zapf[12] or purchased directly from the Aldrich Chemical Co.

Electron Diffraction.—Electron diffraction scattering intensities were recorded photographically on Kodak Electron Image plates using the Edinburgh gas diffraction apparatus,[13] operating at *ca.* 44.5 kV. During the measurements the sample was maintained at 473 K and the nozzle at 493 K. Three plates were exposed with the distance between nozzle and plate set at 258 mm and three at 95 mm. Data for benzene were recorded to provide calibration of the camera distances and electron wavelength (Table 1). The ranges of the data sets and weighting points used in setting up the off-diagonal weight matrix, scale factors and correlation parameters are also listed in Table 1. Absorbance data were obtained using a Joyce–Loebl MDM6 microdensitometer at the SERC Laboratory, Daresbury. The scanning program[14] and programs used subsequently for data reduction[15] and least-squares refinements are those described previously. The scattering factors used were those reported by Fink *et al.*[16] The experimental molecular scattering intensity curves are shown in Fig. 2.

NMR Spectra.—In an attempt to ascertain which conformation was preferentially adopted, or whether there was an equilibrium mixture of co-existing conformers, ^{13}C NMR spectra were recorded at low temperatures. Using a Bruker WH360 spectrometer, only a single peak was observed in the ^{13}C spectrum of a solution in toluene, from room temperature down to 190 K. This was the lowest temperature that could be attained using solvents in which an appreciable amount of [9]aneS$_3$ could be dissolved.

Structure Refinements.—Four different molecular models were considered in the structural analysis of [9]aneS$_3$ based on electron-diffraction data. The four models had D_3, C_3, C_2 and C_1 symmetry and are shown in Fig. 1. For all four models all C–H bond lengths were assumed to be equal, the HCH angles were fixed at 110° and the CH_2 groups were placed so that the plane defined by the atoms of each group bisected the SCC angle at the corresponding carbon atom. Each model is described in detail below.

The D_3 *Model.*—This represents one of two possible conformers described as [333] when using Dale's nomenclature[4] and is shown in Fig. 1(*a*). The ring geometry can be described by four independent parameters: the distance between the sulphur atoms, r(S···S), the sulphur–carbon bond length, r(S–C), the carbon–carbon bond length, r(C–C), and one valence angle, chosen as CSC. Together with r(C–H) and the

† On leave from Department of Chemistry, University of Oslo.

Table 1 Camera heights, electron wavelengths, weighting functions, correlation parameters and scale factors for the ED data[a]

Camera height/ mm	λ/pm	Δs	s_{min}	sw_1	sw_2	s_{max}	Correlation parameter	Scale factor
		nm^{-1}						
256.46	5.670	2	20	40	140	164	0.4511	0.807(8)
94.17	5.671	4	100	140	300	352	0.3725	0.801(26)

[a] The correlation parameters and scale factors are in principle different for the models presented in this paper. The differences are, however, very small, and only the data for the C_2 model are listed here.

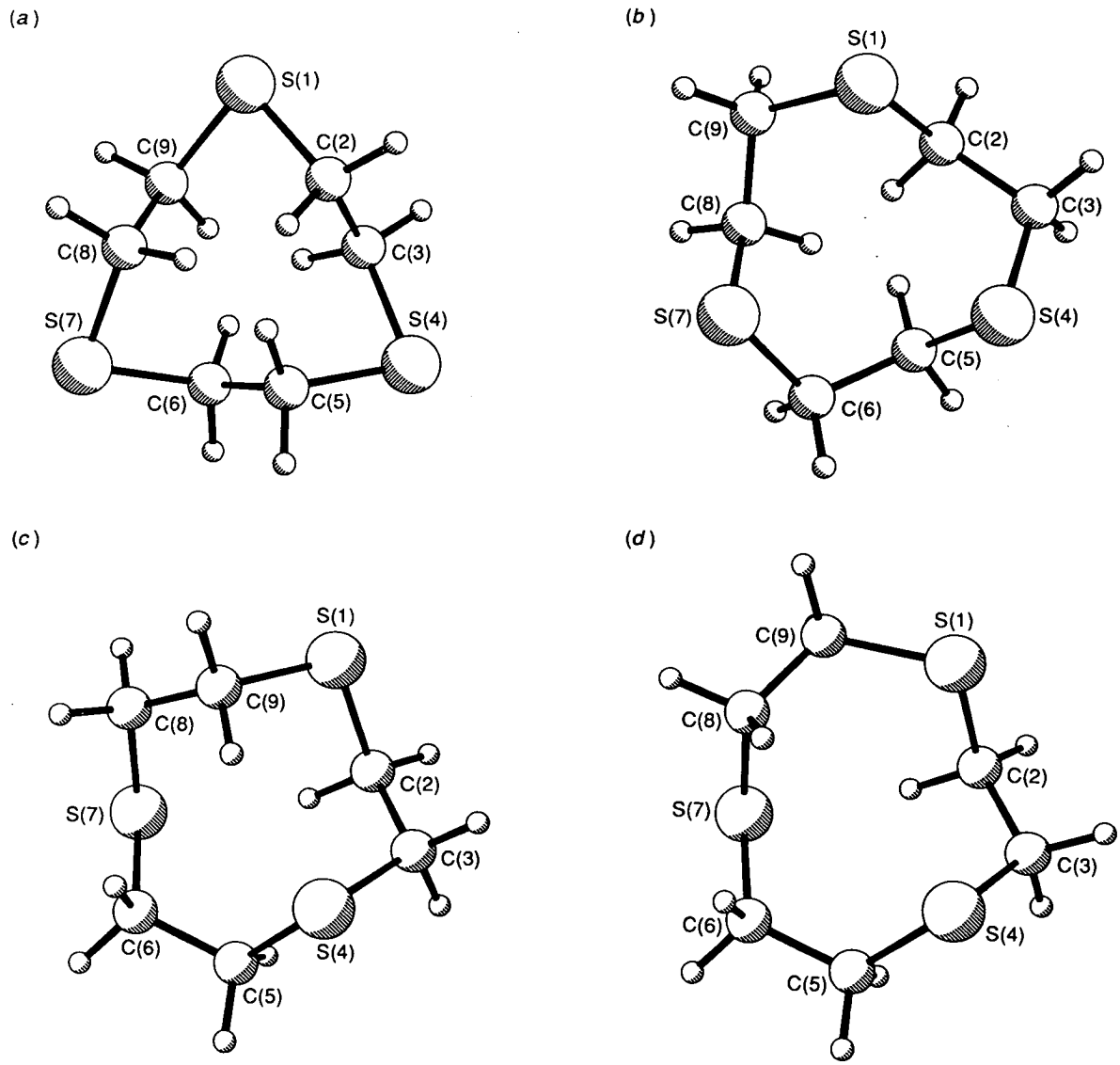

Fig. 1 The molecular models considered in the gas electron-diffraction study of [9]aneS$_3$ (*a*) D_3 model, (*b*) C_3 model, (*c*) C_2 model and (*d*) C_1 model. Numbering of the atoms is shown.

angle HCH this makes six independent parameters which together describe the whole molecular structure. The D_3 model was found to be incompatible with the electron-diffraction data. The curves labelled (*b*) in Figs. 2 and 3 are the differences between experimental and theoretical curves for a reasonable molecular model of D_3 symmetry. The reason for the great discrepancy between the theoretical and observed molecular scattering intensity curves obtained is mainly a consequence of the very long S · · · S distance, which is inevitable for this model if the valence angles are sensible. It is reasonable to assign the peak at approximately 360 pm in the radial distribution curve [Fig. 3(*a*)] to the S · · · S distances. This is much shorter than the S · · · S distance of 440 pm expected for the D_3 model (see Table 4).

The C_3 *Model.*—This conformer is the second [333] conformer, and is shown in Fig. 1(*b*). The ring geometry can be described by seven independent parameters. By fixing the S_3 triangle in the *xy* plane the six carbon atoms will form two triangles which must be parallel to the S_3 plane. One such plane is defined by the atoms 2, 5 and 8 and the other by the atoms 3, 6 and 9. One of the parameters was chosen as the distance between the sulphur atoms, *r*(S · · · S), and three parameters were then needed to define each C_3 plane. They were chosen to be the C · · · C distances of the two C_3 triangles, *d*(2,5,8) and *d*(3,6,9), the perpendicular distances between the S_3 plane and the two C_3 planes, *z*(2,5,8) and *z*(3,6,9), and the rotations about the *z*-axis of the two C_3 triangles relative to the fixed S_3 triangle, τ(2,5,8) and τ(3,6,9), defined as positive for clockwise

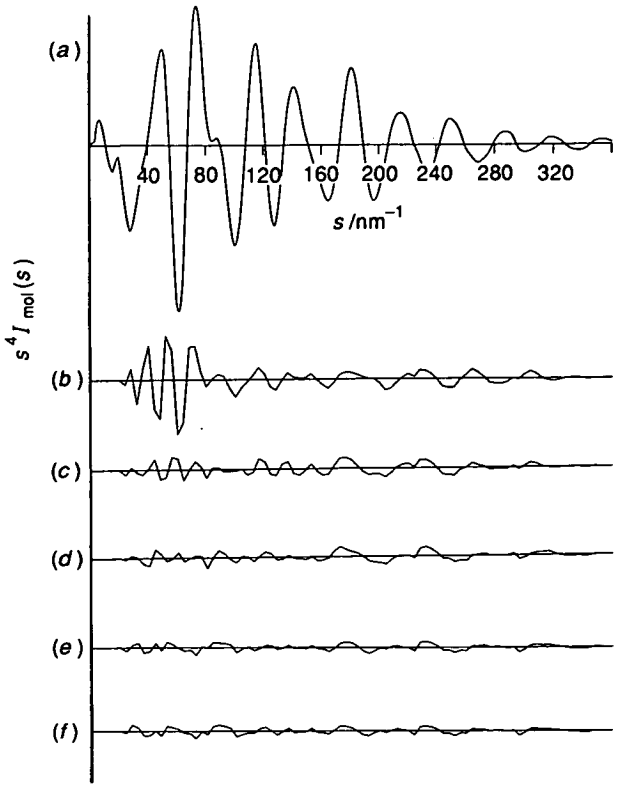

Fig. 2 (*a*) The combined experimental molecular scattering intensity curve for [9]aneS$_3$. The lower part of the figure shows the difference curves (experimental–theoretical) for (*b*) D_3 model, (*c*) constrained C_3 model (see the text), (*d*) non-constrained C_3 model, (*e*) C_2 model and (*f*) C_1 model.

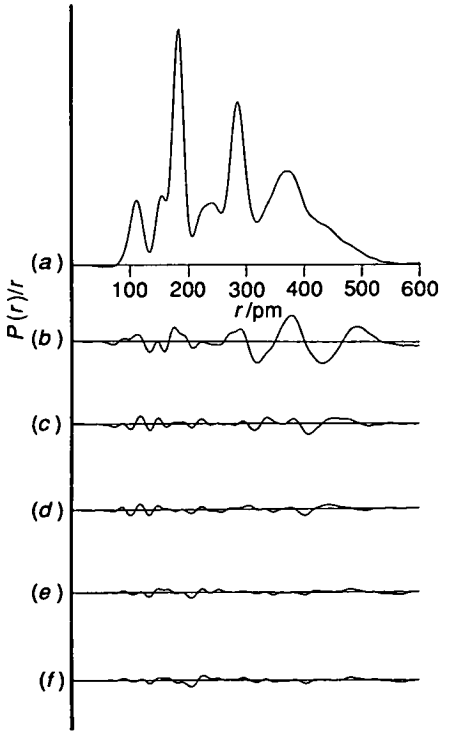

Fig. 3 (*a*) The experimental radial distribution curve, $P(r)/r$, for [9]aneS$_3$. The lower part of the figure shows the difference between experimental and theoretical curves for (*b*) the D_3 model, (*c*) the constrained C_3 model, (*d*) the non-constrained C_3 model, (*e*) the C_2 model and (*f*) the C_1 model. Before Fourier inversion the data were multiplied by $s \exp(-0.000\,02s^2)/(Z_C - f_C)(Z_S - f_S)$.

rotations. Together with r(C–H) and the angle HCH there are thus nine independent parameters. Eight of these could be refined, together with six RMS amplitudes of vibration (u-values). The values of the parameters obtained are presented in Table 2, and the corresponding bond lengths and angles and amplitudes of vibration are listed in Table 3. Refinements in which CSC was loosely constrained to 103(1)°, SC(2) to 112.5(5)° and CC(3)S to 116.3(5)°, values close to those measured in the crystalline phase, gave a poorer fit to the experimental intensity curves than the unconstrained C_3 model. The R-factors obtained for the constrained C_3 model for the two sets of data were 0.16 and 0.18, respectively. In Figs. 2 and 3 differences between experimental and theoretical intensity and radial distribution curves for the constrained C_3 model (*c*) and the unconstrained C_3 model (*d*) are shown.

The C_2 *Model.*—In Dale's nomenclature this is a [12222] conformer: it is illustrated in Fig. 1(*c*). By assuming that the two S–C bonds which are, in principle, different, are actually of equal length and that the two different types of C–C bond are also of equal length, the ring geometry can be described by eight independent parameters. The S(1) atom was fixed at the origin and the three atoms S(1), C(5) and C(6) were fixed in the xy plane. Two dummy atoms, A at (0,1,0) and B at (1,1,0), were used when calculating the atomic co-ordinates from the bond distances r(S–C), r(C–C) and r(C–H), the four valence angles CS(1)C, SC(2)C, CC(3)S and HCH, and the three torsional angles τ[ABS(1)C(2)], τ[AS(1)C(2)C(3)] and τ[S(1)C(2)C(3)C(4)]. Nine of the independent parameters could be refined together with six RMS amplitudes of vibration.

There are two possible C_2 conformers. One can be made from the D_3 conformer by twisting one of the C–C torsions from $+g$ to $-g$. However, MM2 calculations indicate that the S···S distances of this C_2 conformer are of the same magnitude as the S···S distance in the D_3 conformer (approximately 420 pm), which is not compatible with the peak in the experimental radial distribution curve at about 360 pm assigned to the S···S distances [Fig. 3(*a*)]. The calculations also give 13.8 kJ mol^{-1} higher strain energy for this C_2 conformer compared with that shown in Fig. 1(*c*). For these reasons only the low-energy C_2 conformer shown in Fig. 1(*c*) was considered in the structural analysis based on electron diffraction data. The final values of the refined parameters obtained for this conformer are given in Table 2, and the corresponding geometrical and vibrational parameters are listed in Table 3. The curves labelled (*e*) in Figs. 2 and 3 are the differences between experimental and theoretical curves obtained for the best C_2 model.

The C_1 *Model.*—The molecular model is shown in Fig. 1(*d*). By assuming that the lengths of all the S–C bonds are equal, that the three C–C bond lengths are equal, that the three CSC angles are equal, and that the six SCC angles are equal to within 1.0(8)° (loosely constrained), 13 independent parameters are needed to describe the molecular structure. These parameters were chosen as the three bond distances r(S–C), r(C–C) and r(C–H), the four angles CS(1)C, SC(2)C, CC(3)S and <HCH, and six torsional angles τ[SC(2)C(3)S], τ[CC(3)S(4)C], τ[CS(4)C(5)C], τ[SC(5)C(6)S], τ[CC(6)S(7)C] and τ[CS(7)C(8)C].

There are several reasonable C_1 conformers, and in a structural analysis based on electron diffraction alone we cannot distinguish properly between them. In this case we have chosen to rely on the results from the MM2 calculations and only do structural refinements on the best C_1 model from these calculations, using the calculated parameters as starting values in the electron diffraction analysis. Three different C_1 conformers were obtained, starting from the C_3 and two C_2 conformers, by twisting one C–C torsion in each case. The conformers obtained correspond roughly to [234], [12222] and [234] in Dale's nomenclature.[4] The two different [234]

Table 2 The independent geometrical parameters used to describe the C_3, C_2 and C_1 models for [9]aneS$_3$

	C_3 model		C_2 model		C_1 model	
p_1	r(S ··· S)	353.0(10)	r(S–C)	181.9(1)	r(S–C)	182.0(1)
p_2	d(2,5,8)[b]	287.5(16)	r(C–C)	153.6(4)	r(C–C)	153.3(4)
p_3	z(2,5,8)[c]	−132.7(7)	r(C–H)	110.6(4)	r(C–H)	110.9(4)
p_4	τ(2,5,8)[d]	37.6(2)	<CS(1)C	104.5(12)	<CSC	103.8(7)
p_5	d(3,6,9)[b]	395.7(14)	<SC(2)C	118.2(42)	<SC(2)C	115.0(5)
p_6	z(3,6,9)[c]	−95.2(14)	<CC(3)S	115.8(21)	<CC(3)S	115.7(5)[e]
p_7	τ(3,6,9)[d]	78.4(1)	τ[BAS(1)C(2)][f]	145.4(29)	<HCH	110.0[g]
p_8	r(C–H)	108.6(5)	τ[AS(1)C(2)C][f]	−71.6(11)	τ[SC(2)C(3)S]	59.5(18)
p_9	<HCH	110.0[e]	τ[SC(2)C(3)S]	−113.5(37)	τ[CC(3)S(4)C]	74.6(14)
p_{10}	—		<HCH	110.0[g]	τ[CS(4)C(5)C]	−102.9(14)
p_{11}	—		—		τ[SC(5)C(6)S]	74.3(10)
p_{12}	—		—		τ[CC(6)S(7)C]	−104.2(13)
p_{13}	—		—		[CS(7)C(8)C]	129.6(14)
R_1[h]		0.095		0.080		0.088
R_2[h]		0.149		0.115		0.103

[a] Distances in pm, angles in degrees. [b] $d(a,b,c)$ is the length of the sides of the equilateral triangle a,b,c, where a, b and c are the atom reference numbers. [c] $z(a,b,c)$ is the distance between the plane defined by the three sulphur atoms and the parallel plane defined by the three atoms a, b and c. [d] $\tau(a,b,c)$ is the clockwise rotation of the triangle (a,b,c) relative to the triangle defined by the three sulphur atoms. [e] Constrained to be 1.0(8)° larger than SC(2)C. [f] In order to describe the molecular model two dummy atoms A and B at (0,1,0) and (1,1,0) were used. [g] Fixed value. [h] R_n for data set number n of Table 1. R = **D**′**WD**/**I**′**WI**, where **I** is the vector of observed intensities, **D** the vector of residuals and **W** the weight matrix.

Table 3 Structural parameters obtained for the C_3, C_2 and C_1 models of [9]aneS$_3$ by analysis of gas electron-diffraction data[a]

	C_3 model		C_2 model		C_1 model	
	r_a	u	r_a	u	r_a	u
r(S–C)	182.0(1)	5.9(2)	181.9(1)	5.8(2)	182.0(1)	5.7(2)
r(C–C)	154.2(4)	5.6(5)	153.6(4)	5.5(4)	153.3(4)	5.7(4)
r(C–H)	108.6(5)	7.6(6)	110.6(4)	7.3(4)	110.9(4)	7.2(4)
r(S ··· S)	352(1)	23.0(8)	365(1)	21(1)	350(2)	19(1)
	—	—	368(3)	21[b]	367(1)	19[b]
	—	—	—	—	369(2)	19[b]
r(S ··· C)	290(1)	6.4(7)	288(6)	8.1(17)	283(1)	9.1(2)
	280(1)	6.4[c]	285(3)	8.1[c]	284(1)	9.1[c]
	—	—	278(2)	8.1[c]	284(1)	9.1[c]
	—	—	—	—	283(1)	9.1[c]
	—	—	—	—	284(1)	9.1[c]
	—	—	—	—	283(1)	9.1[c]
<CS(1)C	90.6(7)	—	104.5(12)	—	103.8(7)	—
<SC(2)C	119.1(4)	—	118.2(2)	—	115.0(5)	—
<CC(3)S	111.8(3)	—	115.8(21)	—	115.7[d]	—
<CS(4)C	—	—	103.8(14)	—	103.8[e]	—
<SC(5)C	—	—	111.5(11)	—	115.0[f]	—
<CC(6)S	—	—	—	—	115.7[g]	—
<CS(7)C	—	—	—	—	103.8[e]	—
<SC(8)C	—	—	—	—	115.0[f]	—
<CC(9)S	—	—	—	—	116.1[h]	—
τ[CS(1)C(2)C]	−141.5(5)	—	−71.6(11)	—	−127.1(15)	—
τ[SC(2)C(3)S]	61.7(9)	—	66.5(37)	—	59.5(18)	—
τ[CC(3)S(4)C]	56.1(8)	—	66.1(46)	—	74.6(14)	—
τ[CS(4)C(5)C]	—	—	−110.5(29)	—	−102.9(14)	—
τ[SC(5)C(6)S]	—	—	85.9(17)	—	74.3(10)	—
τ[CC(6)S(7)C]	—	—	—	—	−104.2(13)	—
τ[CS(7)C(8)C]	—	—	—	—	129.6(14)	—
τ[SC(8)C(9)S]	—	—	—	—	−74.9(18)	—
τ[CC(9)S(1)C]	—	—	—	—	63.9(16)	—

[a] Distances and u-values in pm, angles in degrees. [b] The S ··· S u-values were constrained to be equal. [c] The u-values of these similar S ··· C distances were constrained to be equal. [d] Loosely constrained to be 1.0(8)° larger than <SC(2)C. [e] Assumed equal to <CS(1)C. [f] Assumed equal to <SC(2)C. [g] Assumed equal to <CC(3)S. [h] Constrained to be 0.1(8)° smaller than <CC(3)S.

conformers were both about 9.6 kJ mol^{-1} higher in strain energy than the [12222] conformer so only the latter was considered in the electron diffraction analysis. The C_1 [12222] conformer shown in Fig. 1(*d*) is made by twisting the S(2)C(3)S torsion of the C_2 model shown in Fig. 1(*c*) from $+g$ to $-g$. The final refined parameters obtained for this C_1 conformer are given in Table 2 and the corresponding set of bond lengths and angles and vibrational parameters is given in Table 3. The differences between experimental and theoretical intensity data and radial distribution curves obtained for the C_1 [12222] model are shown labelled (*f*) in Figs. 2 and 3, respectively.

Table 4 Structural parameters obtained from MM2 calculations for the D_3, C_3, C_2 and C_1 models of [9]aneS$_3$ [a]

	D_3 model	C_3 model	C_2 model	C_1 model
r[S(1)–C(2)]	182.6	182.1	181.8	182.2
r[C(2)–C(3)]	154.1	154.2	153.7	153.9
r[C(3)–S(4)]	—	182.5	181.7	182.3
r[S(4)–C(5)]	—	—	181.9	182.1
r[C(5)–C(6)]	—	—	154.9	154.0
r[C(6)–S(7)]	—	—	—	182.0
r[S(7)–C(8)]	—	—	—	182.1
r[C(8)–C(9)]	—	—	—	154.1
r[C(9)–S(1)]	—	—	—	182.2
r(C–H)	111.0, 111.5	111.1–111.5	110.8–111.5	111.1–111.5
r[S(1)···S(4)]	432.9	330.9	361.6	336.0
r[S(4)···S(7)]	—	—	377.9	362.4
r[S(7)···S(1)]	—	—	—	383.4
<CS(1)C	102.8	101.4	106.3	101.8
<SC(2)C	112.5	111.5	114.9	110.6
<CC(3)S	—	114.4	115.4	112.4
<CS(4)C	—	—	102.8	100.8
<SC(5)C	—	—	111.5	111.2
<CC(6)S	—	—	—	111.1
<CS(7)C	—	—	—	101.2
<SC(8)C	—	—	—	110.8
<CC(9)S	—	—	—	112.3
τ[CS(1)C(2)C]	61.1	−133.9	−73.7	−124.8
τ[SC(2)C(3)S]	−140.9	52.1	70.2	61.8
τ[CC(3)S(4)C]	—	62.4	58.6	74.2
τ[CS(4)C(5)C]	—	—	−111.3	−122.1
τ[SC(5)C(6)S]	—	—	92.8	82.2
τ[CC(6)S(7)C]	—	—	—	−93.0
τ[CS(7)C(8)C]	—	—	—	134.1
τ[SC(8)C(9)S]	—	—	—	−96.7
τ[CC(9)S(1)C]	—	—	—	75.0
Strain energy (E_s/kJ mol^{-1})	87.74	77.95	86.11	77.82
Dipole moment-(μ/Debye)	0.0	4.3	1.3	1.5

[a] Distances and angles in degrees.

MM2 *Calculations.*—In order to estimate the energy differences between the conformers, molecular-mechanics calculations on [9]aneS$_3$ were carried out using the MM2 program.[17] A number of energy minimisations were performed from different starting parameters and using different symmetry constraints. The structural parameters and final strain energies obtained for the four lowest-energy conformers are shown in Table 4. Study of a model of the molecule indicates that the energy minima are separated by significant barriers, and there can be no doubt that they do represent genuine minima on the calculated energy surface.

Results and Discussion

The aim of this study was to investigate the conformation of [9]aneS$_3$ as a free molecule in the gas phase. We have used molecular-mechanics calculations (MM2) as a tool and electron diffraction (ED) as the experimental method. Because it is necessary to derive the three-dimensional molecular structure from one-dimensional ED data, it is possible to fit more than one molecular model to the experimental data. This means that any conclusion concerning the conformation of such a complex molecule as [9]aneS$_3$ has to be drawn with care. As is seen in Table 4, the strain energies of the conformers studied do not differ enormously, so the MM2 calculations do not allow us to reach absolutely unequivocal conclusions about the conformation(s) present. Nevertheless, these calculations do give information about the likely values of the various structural parameters of the different conformers, as well as giving an indication of the relative stability (and hence abundance) of the various forms. In this way the structures from the MM2 calculations can be used to decide whether or not a structure deduced from the experimental data is reasonable.

Previous conformational studies of medium to large non-co-ordinated cyclic sulphides ($\geq$12 ring atoms) in the crystalline state indicate that most of these compounds adopt the *exo* conformation with the sulphur atoms pointing out of the macrocyclic cavity. This has been explained as a consequence of the tendency of the CCSC linkages to adopt *gauche* conformations.[8,9] A maximum number of such *gauche* arrangements is attained when the sulphur atoms have positions in the 'corners' of the macrocycle. This is in contrast with what is observed for the analogous crown oxyethers, in which the oxygen atoms are not positioned in the corners and the *anti* conformation is preferred for the CCOC linkages. As the ring size becomes smaller ($\leq$11 ring atoms) the flexibility of the ring becomes less and one would expect other effects such as 1,4 and 1,5 interactions across the ring to be significant in determining the conformation of the ring.

For [9]aneS$_3$, the D_3 conformer is the only one in which all the CCSC groups have the *gauche* conformation. This conformer is, however, not present, either in the gas or in the crystalline phase. [9]aneS$_3$ has been found to adopt the C_3 conformation in the crystal, and a C_3 conformer can also be

New J. Chem., 1991, **15**, 511-514

communications

C-H ACTIVATION IN THIOETHER CROWNS: THE SYNTHESIS AND CRYSTAL STRUCTURE OF 4,7-DITHIA-1-THIONIABICYCLO[4,3,0]NONANE TETRAFLUOROBORATE

Anne Taylor, Alexander J. Blake, Alan J. Holder, Timothy I. Hyde and Martin Schröder*

Department of Chemistry, University of Edinburgh, West Mains Road, Edinburgh EH9 3JJ, Scotland.

Received July 16, accepted October 30, 1990.

ABSTRACT. — Oxidation of 1,4,7-trithiacyclononane ([9]aneS$_3$) affords, via C−H cleavage and transannular C−S bond formation, a bicyclic sulphonium salt incorporating fused 5- and 6-membered rings.

The redox chemistry of metal complexes of [9]aneS$_3$ has been the subject of considerable interest recently[1]. Much of this work has concentrated on the stabilisation of unusual metal oxidation states using homoleptic thioether coordination[2]. Although the product from the oxidation of metal-free [9]aneS$_3$ has not been isolated or characterised, the oxidation of organic thioethers to give sulphonium salts and, in certain cases, to lead to transannular S···S interactions has been reported previously[3,4]. On this basis, the assignment[5] of the oxidation product of [9]aneS$_3$ as a sulphonium salt appears reasonable. Furthermore, the oxidation of methionine residues to S-cation radicals have been proposed as possible intermediates in the oxidation of cytochrome C peroxidase[6]. Wieghardt and co-workers have shown that in the presence of O-donor oxidants, one of the thioether S-donors in $[Fe([9]aneS_3)_2]^{2+}$ can be oxidised to the corresponding sulphoxide, while full oxidation of metal-free [9]aneS$_3$ with H_2O_2 affords the corresponding hexaoxo species[7]. The formation of oxo products of [9]aneS$_3$ is not likely to occur in cyclic voltammetric experiments from which O_2 and H_2O have been excluded. We report herein the synthesis and characterisation of an unexpected oxidation product of [9]aneS$_3$.

During studies on the coordination chemistry of [9]aneS$_3$ with Au(III)[8], we isolated a non-metal-containing product in up to 30% yield. The ^{1}H NMR spectrum (200.13 MHz, 298 K, CD_3NO_2) of this species shows a resonance at δ = 5.28 ppm (dd, 1H) with complex multiplets in the region δ = 3.09-4.30 ppm (10H). The ^{13}C DEPT NMR spectrum (50.32 MHz, 298 K, CD_3NO_2) of the product shows (Fig. 1) resonances at δ = 59.29 (*C*H) and 47.55, 35.22, 34.00, 26.19, 23.37 ppm (*C*H$_2$). Elemental analysis and accurate fab mass spectroscopy (found M^+ = 179.00228, calculated M^+ = 179.00229 for $C_6H_{11}S_3^+$ using CsI internal standard) confirm the product to be $[C_6H_{11}S_3]BF_4$, an oxidation product of [9]aneS$_3$ ($C_6H_{12}S_3$). Single crystals of $[C_6H_{11}S_3]BF_4$ were grown by vapour diffusion of Et_2O into a solution of the compound in MeCN. The single crystal X-ray structure† of the compound shows (Fig. 2) it to be

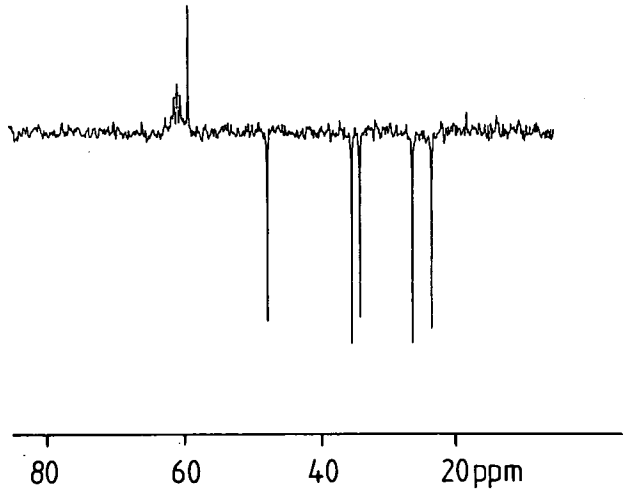

Figure 1. — ^{13}C NMR Spectrum of $[C_6H_{11}S_3]^+$ (50.32 MHz, 298 K, CD_3NO_2).

β = 90.73(3)°, V = 1 027Å^3 [from setting angles for 15 centred reflections with 2θ = 30-32°, $\bar{\lambda}$ = 0.71073 Å, T = 295 K], Z = 4, D_c = 1.721 g.cm^{-3}, μ(Mo−K$_\alpha$) = 0.706 mm^{-1}. A colourless lath (0.22 × 0.38 × 0.85 mm) was mounted on a CAD4 four-circle diffractometer. Data collection using Mo−K$_\alpha$ X-radiation and $\omega-2\theta$ scans gave 1433 reflections ($2\theta_{max}$ 45°), 1314 unique (R_{int} 0.006), of which 1168 with $F \geqslant 6\sigma(F)$ were used in all calculations. Automatic direct methods[10] located all non-H atoms, which were then refined anisotropically[11]: H atoms were refined positionally with a common U_{iso} of 0.0478(24)Å^2. At final convergence, R = 0.0251, wR = 0.0349, S = 1.119 for 161 parameters and the final ΔF synthesis showed no feature above 0.31 eÅ^{-3}. Atomic coordinates, bond lengths and angles have been deposited with the Cambridge Crystallographic Data Centre and can be obtained on request from Dr. Olga Kennard, University Chemical Laboratory, Lensfield Road, Cambridge CB2 1EW, U.K.

— Structure factors and thermal parameters have been deposited with the British Library, Document Supply Center, at Boston Spa, Wetherby, West Yorshire, U.K. as supplementary publication No. SUP 90234 and is available on request from the Document Supply Center. Requesters must quote the relevant SUP number (eg. SUP 12345).

† *Crystal data for* $C_6H_{11}S_3^+ \cdot BF_4^-$: M = 266.10, monoclinic, space group $P2_1/c$, with a = 5.140(3), b = 9.1036(20), c = 21.947(4)Å,

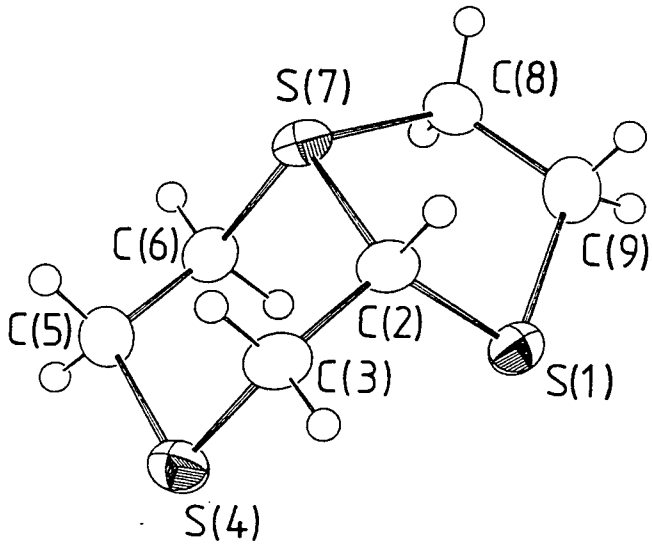

Figure 2. — Single crystal X-ray structure of $[C_6H_{11}S_3]^+$(I) with numbering scheme adopted.

a *bicyclic* sulphonium salt (I) incorporating fused 5- and 6-membered rings. The 6-membered ring adopts a chair conformation with the sulphonium S-atom at the bridgehead. The product is formally, therefore, the deprotonated, two-electron oxidation product of [9]aneS_3. Thus, oxidation of [9]aneS_3 with Au(III) leads to C−H bond cleavage and transannular S−C bond formation. An alternative and better method of synthesising $[C_6H_{11}S_3]^+$ (in 85% yield) is by treatment of [9]aneS_3 with one molar equivalent of the hydride-abstractor $Ph_3C^+PF_6^-$ in $MeNO_2$.

$[C_6H_{11}S_3]^+$ shows an irreversible reduction in MeCN at platinium electrodes at $E_{pc} = -2.14$ V vs Fc/Fc^+. Free [9]aneS_3 shows an irreversible oxidation by cyclic voltammetry at $E_{pa} = +0.98$ V vs Fc/Fc^+ in MeCN (0.1 M $^nBu_4NPF_6$) with a return wave being observed at $E_{pc} = -0.57$V: this return wave is not present when scanning initially from 0 to −1.0 V, but appears only after scanning beyond +1.0 V. This wave, therefore, corresponds to the reduction of an oxidation product of [9]aneS_3. Since $[C_6H_{11}S_3]^+$ does not show a reduction at −0.57 V under the same conditions, it appears that $[C_6H_{11}S_3]^+$ is not a major product in the electrochemical oxidation. Musker and co-workers have reported the synthesis of a range of highly reactive dithioether cation radicals and dications which were proposed to incorporate S···S interactions[3]. A similar dicationic species involving transannular S···S interaction as in (II) is likely to be the electrochemical oxidation product of [9]aneS_3.

The [9]aneS_3 ligand is unique among homoleptic thioether crowns in that it is pre-organised for facial coordination, having its S-donors in *endo* positions. Transannular interactions as in I and II are therefore to be kinetically favoured. In addition, the driving force for the formation of the bicyclic sulphonium salt (I) is presumably the formation of stable fused 5- and 6-membered rings from a relatively unstable 9-membered ring. The synthesis of $C_6H_{11}S_3^+$ from [9]aneS_3 represents a possible route to the *C*-functionalisation of this thioether macrocycle[9].

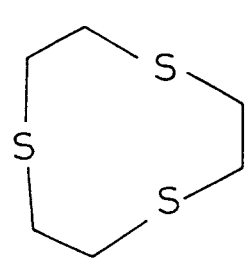

[9] are S_3

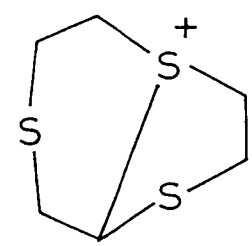

I

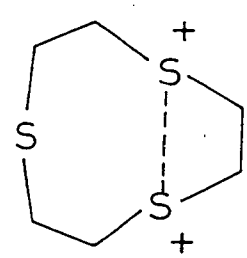

II

Table I. — Bond Lengths (A) with standard deviations.

S(1)	−C(2)	1.7976(24)	C(6)	−H(6B)	0.94(3)
S(1)	−C(9)	1.807(3)	C(6)	−S(7)	1.816(3)
C(2)	−H(2)	0.95(3)	S(7)	−C(8)	1.817(3)
C(2)	−C(3)	1.520(4)	C(8)	−H(8A)	0.91(3)
C(2)	−S(7)	1.8414(24)	C(8)	−H(8B)	0.99(3)
C(3)	−H(3A)	0.91(3)	C(8)	−C(9)	1.511(4)
C(3)	−H(3B)	0.94(3)	C(9)	−H(9A)	0.88(3)
C(3)	−S(4)	1.798(3)	C(9)	−H(9B)	1.00(3)
S(4)	−C(5)	1.815(3)	B(1)	−F(1)	1.379(3)
C(5)	−H(5A)	0.99(3)	B(1)	−F(2)	1.380(3)
C(5)	−H(5B)	0.89(3)	B(1)	−F(3)	1.380(3)
C(5)	−C(6)	1.513(4)	B(1)	−F(4)	1.372(3)
C(6)	−H(6A)	0.99(3)			

Table II. – Angles (degrees) with standard deviations.

C(2)	– S(1)	– C(9)	91.00(13)	H(6A)	– C(6)	– S(7)	105.2(16)
S(1)	– C(2)	– H(2)	107.2(16)	H(6B)	– C(6)	– S(7)	103.1(17)
S(1)	– C(2)	– C(3)	116.56(17)	C(2)	– S(7)	– C(6)	101.28(11)
S(1)	– C(2)	– S(7)	106.23(12)	C(2)	– S(7)	– C(8)	96.17(12)
H(2)	– C(2)	– C(3)	109.1(16)	C(6)	– S(7)	– C(8)	102.43(12)
H(2)	– C(2)	– S(7)	105.6(16)	S(7)	– C(8)	– H(8A)	105.2(17)
C(3)	– C(2)	– S(7)	111.45(17)	S(7)	– C(8)	– H(8B)	104.1(15)
C(2)	– C(3)	– H(3A)	109.5(18)	S(7)	– C(8)	– C(9)	110.19(19)
C(2)	– C(3)	– H(3B)	109.3(17)	H(8A)	– C(8)	– H(8B)	113.5(23)
C(2)	– C(3)	– S(4)	116.00(18)	H(8A)	– C(8)	– C(9)	111.3(17)
H(3A)	– C(3)	– H(3B)	110.3 (24)	H(8B)	– C(8)	– C(9)	112.0(15)
H(3A)	– C(3)	– S(4)	103.4(17)	S(1)	– C(9)	– C(8)	110.63(21)
H(3B)	– C(3)	– S(4)	108.0(17)	S(1)	– C(9)	– H(9A)	107.3(19)
C(3)	– S(4)	– C(5)	99.12(13)	S(1)	– C(9)	– H(9B)	111.4(16)
S(4)	– C(5)	– H(5A)	107.9(16)	C(8)	– C(9)	– H(9A)	115.9(19)
S(4)	– C(5)	– H(5B)	106.8(18)	C(8)	– C(9)	– H(9B)	108.6(16)
S(4)	– C(5)	– C(6)	113.31(19)	H(9A)	– C(9)	– H(9B)	102.7(24)
H(5A)	– C(5)	– H(5B)	107.0(24)	F(1)	– B(1)	– F(2)	108.61(21)
H(5A)	– C(5)	– C(6)	111.1(16)	F(1)	– B(1)	– F(3)	109.04(21)
H(5B)	– C(5)	– C(6)	110.5(19)	F(1)	– B(1)	– F(4)	110.40(21)
C(5)	– C(6)	– H(6A)	115.0(16)	F(2)	– B(1)	– F(3)	108.50(21)
C(5)	– C(6)	– H(6B)	111.6(17)	F(2)	– B(1)	– F(4)	110.61(21)
C(5)	– C(6)	– S(7)	110.80(18)	F(3)	– B(1)	– F(4)	109.63(21)
H(6A)	– C(6)	– H(6B)	110.3(23)				

Table III. – Torsion angles (degrees) with standard deviations.

C(9)	– S(1)	– C(2)	– H(2)	– 66.2(17)		S(4)	– C(5)	– C(6)	– S(7)	– 70.26(21)
C(9)	– S(1)	– C(2)	– C(3)	171.29(20)		H(5A)	– C(5)	– C(6)	– H(6A)	170.5(24)
C(9)	– S(1)	– C(2)	– S(7)	46.44(14)		H(5A)	– C(5)	– C(6)	– H(6B)	– 62.9(25)
C(2)	– S(1)	– C(9)	– C(8)	– 47.46(21)		H(5A)	– C(5)	– C(6)	– S(7)	51.4(17)
C(2)	– S(1)	– C(9)	– H(9A)	– 174.8(19)		H(5B)	– C(5)	– C(6)	– H(6A)	– 70.9(26)
C(2)	– S(1)	– C(9)	– H(9B)	73.4(17)		H(5B)	– C(5)	– C(6)	– H(6B)	55.6(27)
S(1)	– C(2)	– C(3)	– H(3A)	58.6(19)		H(5B)	– C(5)	– C(6)	– S(7)	169.9(20)
S(1)	– C(2)	– C(3)	– H(3B)	179.6(18)		C(5)	– C(6)	– S(7)	– C(2)	60.80(20)
S(1)	– C(2)	– C(3)	– S(4)	– 58.02(23)		C(5)	– C(6)	– S(7)	– C(8)	159.79(19)
H(2)	– C(2)	– C(3)	– H(3A)	– 63.0(25)		H(6A)	– C(6)	– S(7)	– C(2)	– 64.1(16)
H(2)	– C(2)	– C(3)	– H(3B)	58.0(25)		H(6A)	– C(6)	– S(7)	– C(8)	34.9(16)
H(2)	– C(2)	– C(3)	– S(4)	– 179.6(17)		H(6B)	– C(6)	– S(7)	– C(2)	– 179.7(17)
S(7)	– C(2)	– C(3)	– H(3A)	– 179.3(19)		H(6B)	– C(6)	– S(7)	– C(8)	– 80.7(17)
S(7)	– C(2)	– C(3)	– H(3B)	– 58.3(18)		C(2)	– S(7)	– C(8)	– H(8A)	– 117.8(18)
S(7)	– C(2)	– C(3)	– S(4)	64.13(21)		C(2)	– S(7)	– C(8)	– H(8B)	122.5(16)
S(1)	– C(2)	– S(7)	– C(6)	70.84(14)		C(2)	– S(7)	– C(8)	– C(9)	2.27(21)
S(1)	– C(2)	– S(7)	– C(8)	– 33.18(14)		C(6)	– S(7)	– C(8)	– H(8A)	139.2(18)
H(2)	– C(2)	– S(7)	– C(6)	– 175.5(17)		C(6)	– S(7)	– C(8)	– H(8B)	19.5(16)
H(2)	– C(2)	– S(7)	– C(8)	80.5(17)		C(6)	– S(7)	– C(8)	– C(9)	– 100.76(20)
C(3)	– C(2)	– S(7)	– C(6)	– 57.09(19)		S(7)	– C(8)	– C(9)	– S(1)	30.0(3)
C(3)	– C(2)	– S(7)	– C(8)	– 161.11(18)		S(7)	– C(8)	– C(9)	– H(9A)	152.5(21)
C(2)	– C(3)	– S(4)	– C(5)	– 59.04(21)		S(7)	– C(8)	– C(9)	– H(9B)	– 92.6(17)
H(3A)	– C(3)	– S(4)	– C(5)	– 179.0(18)		H(8A)	– C(8)	– C(9)	– S(1)	146.3(18)
H(3B)	– C(3)	– S(4)	– C(5)	64.1(18)		H(8A)	– C(8)	– C(9)	– H(9A)	– 91.3(28)
C(3)	– S(4)	– C(5)	– H(5A)	– 61.9(17)		H(8A)	– C(8)	– C(9)	– H(9B)	23.7(25)
C(3)	– S(4)	– C(5)	– H(5B)	– 176.6(19)		H(8B)	– C(8)	– C(9)	– S(1)	– 85.4(17)
C(3)	– S(4)	– C(5)	– C(6)	61.50(21)		H(8B)	– C(8)	– C(9)	– H(9A)	37.1(27)
S(4)	– C(5)	– C(6)	– H(6A)	48.9(17)		H(8B)	– C(8)	– C(9)	– H(9B)	152.0(23)
S(4)	– C(5)	– C(6)	– H(6B)	175.4(18)						

Acknowledgements

We are very grateful to SERC for suppport and Dr. Hamish McNab for discussions.

REFERENCES

[1] Blake A. J., Schröder M., *Adv. Inorg. Chem.*, 1990, **35**, 1; Schröder M., *Pure Appl. Chem.*, 1988, **60**, 517.

[2] Blake A. J., Gould R. O., Holder A. J., Hyde T. I., Odulate M. O., Lavery A. J., Schröder M., *J. Chem. Soc., Chem. Commun.*, 1987, 118; Blake A. J., Holder A. J., Hyde T. I., Schröder M., *J. Chem. Soc., Chem. Commun.*, 1987, 987; Rawle S. C., Yagbasan R., Prout K., Cooper S. R., *J. Am. Chem. Soc.*, 1987, **109**, 6181; Blake A. J., Gould R. O., Holder A. J., Hyde T. I., Schröder M., *J. Chem. Soc., Dalton Trans.*, 1988, 1861; Blake A. J., Reid G., Schröder M., *J. Chem. Soc. Dalton Trans.*, 1990, 3363.

[3] Musker W. K., Wolford T. L., Roush P. B., *J. Am. Chem. Soc.*, 1978, **100**, 6416 and references therein.

[4] Asmus K.-D., Gillis H. A., Teather G. G., *J. Phys. Chem.*, 1978, **82**, 2677 and references therein. See also: Glass R. S., Hojjatie M., Wilson G. S., Mahling S., Göbl M., Asmus K.-D., *J. Am. Chem. Soc.*, 1984, **106**, 5382; Glass R. S., Coleman B. R., Prabhu U. D.G., Setzer W. N., Wilson G. S., *J. Org. Chem.*, 1982, **47**, 2761; Glass R. S., Petsom A., Wilson G. S., Martinez R., Juanist E., *J. Org. Chem.*, 1986, **51**, 4337; Glass R. S., Hojjatie M., Petsom A., Wilson G. S., Göbl M., Mahling S., Asmus K.-D., *Phosphorus and Sulfur*, 1985, **23**, 143. See also: Fujihara H., Mima H., Chiu J.-J., Furukawa N., *Tetrahedron Lett.*, 1990, **31**, 2307; Kataoka T., Tsutsumi K., Iwama T., Shimizu H., Hori M., *Tetrahedron Lett.*, 1990, **31**, 3027 and references therein.

[5] Wieghardt K., Küppers H. J., Weiss J., *Inorg. Chem.*, 1985, **24**, 3067.

[6] Hoffman B. M., Roberts J. E., Brown T. G., Kang C. H., Margoliash E., *Proc. Natl. Acad. Sci. (USA)*, 1979, **76**, 6132; Ho P. S., Hoffman B. M., Kang C. H., Margoliash E., *J. Biol. Chem.*, 1983, **258**, 4356.

[7] Küppers H. J., Wieghardt K., Nuber B., Weiss J., Bill E., Trautwein A. X., *Inorg. Chem.*, 1987, **26**, 3762.

[8] Blake A. J., Gould R. O., Greig J. A., Holder A. J., Hyde T. I., Schröder M., *J. Chem. Soc., Chem. Commun.*, 1989, 876; Blake A. J., Greig J. A., Holder A. J., Hyde T. I., Taylor A., Schröder M., *Angew. Chem.*, 1990, **102**, 203; *Angew. Chem. Int. Ed. Engl.*, 1990, **29**, 197.

[9] Roush D. M., Price E. M., Templeton L. K., Templeton D. H., Heathcock C. H., *J. Am. Chem. Soc.*, 1979, **101**, 2971.

[10] SHELX86, program for crystal structure solution, Sheldrick G. M., Univ. of Göttingen, F.R.G., 1986.

[11] SHELX76, program for crystal structure refinement, Sheldrick G. M., Univ. of Cambridge, England, 1976.